Geography of the Physical Environment

Jürgen Herget
Alessandro Fontana *Editors*

Palaeohydrology

Traces, Tracks and Trails of Extreme Events

Springer

Geography of the Physical Environment

The *Geography of the Physical Environment* book series provides a platform for scientific contributions in the field of Physical Geography and its sub-disciplines. It publishes a broad portfolio of scientific books covering case studies, theoretical and applied approaches as well as novel developments and techniques in the field. The scope is not limited to a certain spatial scale and can cover local and regional to continental and global facets. Books with strong regional focus should be well illustrated including significant maps and meaningful figures to be potentially used as field guides and standard references for the respective area.

The series appeals to scientists and students in the field of geography as well as regional scientists, landscape planners, policy makers, and everyone interested in wide-ranging aspects of modern Physical Geography. Peer-reviewed research monographs, edited volumes, advance and under-graduate level textbooks, and conference proceedings covering the major topics in Physical Geography are included in the series. Submissions to the Book Series are also invited on the theme 'The Physical Geography of…', with a relevant subtitle of the author's/editor's choice. Please contact the Publisher for further information and to receive a Book Proposal Form.

More information about this series at http://www.springer.com/series/15117

Jürgen Herget · Alessandro Fontana
Editors

Palaeohydrology

Traces, Tracks and Trails of Extreme Events

Springer

Editors
Jürgen Herget
Department of Geography
University of Bonn
Bonn, Germany

Alessandro Fontana
Dipartimento di Geoscienze
Università degli Studi di Padova
Padua, Italy

ISSN 2366-8865 ISSN 2366-8873 (electronic)
Geography of the Physical Environment
ISBN 978-3-030-23314-3 ISBN 978-3-030-23315-0 (eBook)
https://doi.org/10.1007/978-3-030-23315-0

This Springer imprint is published by the registered company Springer Nature Switzerland AG
The registered company address is: Gewerbestrasse 11, 6330 Cham, Switzerland

Preface

This book is written in the framework of the Focus Group "Palaeohydrology and Fluvial Archives—Extreme and Critical Events (HEX)" of the International Union for Quaternary Research (INQUA) and is edited by the coordinators of the group (Fig. 1). The idea for a temporal focus on extreme events in palaeohydrological research was developed during the conference "HEX 2014—Hydrological EXtreme events in historic and prehistoric times" which took place in Bonn, Germany, in June 2014. This group was active during the period 2015–2019 and continued the successful work of the previous INQUA commission on "GLobal COntinental PalaeoHydrology (GLOCOPH)" (Fig. 2).

Some of the chapters of this book deal with palaeohydrological extreme events, which also have been the main topic of the project "EX-AQUA", sustained by the Focus Group and sponsored by the TERPRO Commission of INQUA. The other branch of the Focus Group consists of the community of "FLAG", dealing with fluvial archives.

The aim of this book is to provide a review on the state of the art of palaeohydrological research, presenting recent progress, attractive new key studies of general interest, methodological updates, remaining challenges and promising perspectives in the early twenty-first century. The contributions to the book consist of invited review articles written by leading experts in the field. They were invited to share their knowledge and experiences with the readers or inspire them to initiate new projects such as the key studies they prepared and present here. The contributions provide a reliable state of the art on the individual topic as the authors are qualified to discuss and summarize different perspectives on their themes with related references to publications for further reading. Consequently, the compilation of the articles represents

Fig. 1 Logo of the INQUA Focus Group "Palaeohydrology and Fluvial Archives—Extreme and Critical Events"

Fig. 2 Logo of the previous INQUA commission "Global Continental Palaeohydrology"

an excellent introduction for non-experts and review material and references for the experienced reader. Such reference character of a publication cannot be achieved by a special issue of a journal focussing on innovation and the research frontier alone.

Both floods and droughts, as prominent extreme hydrological events, are topics here. Their traces, tracks and trails are followed and investigated. These terms have some similarities but differ in nuances. As illustrated by the key studies presented in this book, singular events tend to become periods on the longer timescale also due to decreasing temporal resolution. On the other hand, periods of time are characterized by events, e.g. the time of the temporary formation of exceptional large river meanders.

The book consists of three parts: I—Studies with Temporal Focus, II—Studies with Regional Focus and part III with contributions dealing with methodical and technical issues. Even with this broad structure, the book does not aim to be a manual of encyclopaedic character documenting the discipline completely, but provide inspiring views on a variety of topics.

All contributions were reviewed by colleagues who kindly found the time to provide some independent comments on the contributions of the book and therefore supported the clarity and balanced content of the manuscripts. As most of them preferred to remain anonymous, we are not able to acknowledge them individually. Last, but not least, we appreciate the efforts of Michael Leuchner who during his time as an editor at Springer contacted us with the invitation to preparation the book.

Bonn, Germany — Jürgen Herget
Padua, Italy — Alessandro Fontana
April 2019

Contents

Contributors

Victor R. Baker Department of Hydrology and Atmospheric Sciences, University of Arizona, Tucson, AZ, USA

Mariano Barriendos Department of History and Archaeology, University of Barcelona, Barcelona, Spain

Rudolf Brázdil Institute of Geography, Masaryk University, Brno, Czech Republic;
Global Change Research Institute, Czech Academy of Sciences, Brno, Czech Republic

Helmut Brückner Institute of Geography, University of Cologne, Cologne, Germany

Sébastien Castelltort Department of Earth Sciences, University of Geneva, Geneva, Switzerland

Kim M. Cohen Department of Physical Geography, Utrecht University, Utrecht, The Netherlands;
Department of Applied Geology and Geophysics, Deltares, Utrecht, The Netherlands

Max Engel Institute of Geography, University of Cologne, Cologne, Germany;
Geological Survey of Belgium, Royal Belgian Institute of Natural Science, Brussels, Belgium

Alessandro Fontana Department of Geosciences, University of Padova, Padua, Italy

Matteo Frassine Soprintendenza Archeologia, Belle Arti e Paesaggio per l'area Metropolitana di Venezia e le Province di Belluno, Padova e Treviso, Padua, Italy

Robert Giegengack Department of Earth and Environmental Science, University of Pennsylvania, Philadelphia, PA, USA

Lukas Gregori Department of Geography, Bonn University, Bonn, Germany

Jürgen Herget Department of Geography, Bonn University, Bonn, Germany

Andrea Kiss Institute for Hydraulic Engineering and Water Resources Management, Vienna University of Technology, Vienna, Austria;
Department of Historical Auxiliary Sciences, Institute of History, University of Szeged, Szeged, Hungary

Jörg Lang Leibniz Universität Hannover, Institut für Geologie, Hannover, Germany

Mark G. Macklin School of Geography and Lincoln Centre for Water and Planetary Health, University of Lincoln, Lincoln, UK;
Innovative River Solutions, Institute of Agriculture and Environment, Massey University, Palmerston North, New Zealand;
Centre for the Study of the Inland, La Trobe University, Melbourne, Australia

Samuel E. Munoz Department of Marine and Environmental Sciences, Northeastern University, Nahant, USA;
Department of Civil and Environmental Engineering, Northeastern University, Boston, USA

Ladislava Řezníčková Institute of Geography, Masaryk University, Brno, Czech Republic;
Global Change Research Institute, Czech Academy of Sciences, Brno, Czech Republic

Livio Ronchi Department of Geosciences, University of Padova, Padua, Italy

Aleksey Sidorchuk Geographical Faculty, Moscow State University, Moscow, Russia

Grace K. A. Skirrow Department of Geography and Planning, University of Liverpool, Liverpool, UK

Rachel K. Smedley Department of Geography and Planning, University of Liverpool, Liverpool, UK

Willem H. J. Toonen Egyptology Unit, Faculty of Arts, KU Leuven, Louvain, Belgium

Jef Vandenberghe Department of Earth Sciences, Vrije Universiteit, Amsterdam, The Netherlands

Jutta Winsemann Leibniz Universität Hannover, Institut für Geologie, Hannover, Germany

Abdallah S. Zaki Department of Earth Sciences, University of Geneva, Geneva, Switzerland

Part I
Studies with Temporal Focus

Global Megaflood Paleohydrology

1

Victor R. Baker

Abstract

After centuries of geological controversy, it is now well-established that the last major deglaciation of planet Earth involved huge fluxes of water from the wasting continental ice sheets, and that much of this water was delivered as floods of immense magnitude and relatively short duration. These late Quaternary megafloods had short-term peak flows comparable in discharge to the more prolonged fluxes of ocean currents. The discharges for both ocean currents and megafloods generally exceed a flow of one Sverdrup (Sv), or one million cubic meters per second, hence the prefix "mega." A global inventory of these phenomena includes more than 40 examples from Asia, Europe, North America, South America, and Iceland. Though there have been many advances in understanding the physical processes and geochronology of megaflooding, important controversies remain, including the nature of subglacial megaflooding, the details of the immense network of megaflood landscape features in Asia, and the causes of huge megaflood channels on the planet Mars. However, it is becoming increasing clear that immense outburst floods likely induced very rapid, short-term effects on the planetary environments on both Earth and Mars, greatly altering climates, drainage evolution, and the planetary patterns of water and sediment movement to lakes, seas, and oceans.

Keywords

Megafloods · Paleohydrology · Ice sheets · Uniformitarianism

1.1 Introduction

Centuries of geological controversy have surrounded the topic of very high-discharge flood flows, variously designated "catastrophic floods," cataclysmic floods," "superfloods," "megafloods," etc. Nevertheless, in recent decades, it has been well-established that the last major deglaciation of planet Earth involved huge fluxes of fresh water from the wasting continental ice sheets (Baker 1994, 2002a, 2009a), and that much of this water was delivered as floods of immense magnitude and relatively short duration (Baker 1997, 2002b). Baker (2013) documents more than 40 examples of late Pleistocene megaflood landscapes in North and South America, Europe, Asia, and Iceland. The central Asian region is particularly important, with recent studies revealing many megaflooding examples showing similarity to those originally recognized in the

V. R. Baker (✉)
Department of Hydrology and Atmospheric Sciences, University of Arizona, Tucson, AZ 85716-0816, USA
e-mail: baker@email.arizona.edu

J. Herget and A. Fontana (eds.), *Palaeohydrology*, Geography of the Physical Environment,
https://doi.org/10.1007/978-3-030-23315-0_1

northwestern USA (Baker et al. 1993; Komatsu et al. 2016). Many of the late Quaternary megafloods had short-term peak flows comparable in discharge to the more prolonged fluxes of ocean currents (Baker 2007, 2009b), which are measured in the unit "Sverdrup" (abbreviated "Sv")—a million cubic meters per second. This threshold of one Sv seems appropriate for defining the level associated with the prefix "mega," though the added modifier "high energy" seems appropriate (e.g., Baker 2002a) to distinguish these flows from low-velocity phenomena, such as ocean currents.

Neither modern hydrological instrumentation nor reliable human observation has documented high-energy megaflooding, defined as flooding achieving a peak discharge of one Sv. A possible candidate might be the 1918 jokulhaup (glacial outburst flood) from the ice cap overlying the Katla Volcano caldera in south-central Iceland (Tomasson 1996), but this estimate does not seem to be well documented. The Icelandic outburst floods derive from the presence of ice sheets over active volcanoes. During an eruption, melting of the ice produces a subglacial lake, the hydrostatic pressure of which facilitates flow beneath the glacier toward its margin, enlarging the flow path by melting and thereby draining the lake catastrophically.

Because megafloods are known through their past manifestations, they constitute a variety of paleoflood, such that their study is a subfield of the more general topic of paleoflood hydrology (Baker 2008a). The latter was originally defined for Holocene flooding of smaller magnitude (e.g., Baker et al. 1979; Kochel and Baker 1982), but methods of analysis are generally similar (Baker 1987) and comprise a part of broader approaches to fluvial paleohydrology (Baker 2014).

The association of so many examples of megaflooding with late Pleistocene glaciation (Baker 1997, 2013) derives from conditions that facilitated both the creation of large reservoirs for water storage and circumstances for the cataclysmic release of that water. In addition to the subglacial volcanism mechanism responsible for Icelandic jokulhlaups, there are also more regional factors that can lead to megaflooding. Continental ice sheets impose huge loads on the crust that deform the associated land surface. Because the ice sheets are warm-based, meltwater will form lakes in the depressions that develop between the ice sheets and the surrounding landscape bulges. Glacial ice can also block the lower courses of rivers, impounding flow, and even diverting it into adjacent drainage basins. Meltwater from glacial margins may also introduce huge discharges into land surface depressions that previously held much smaller lakes or were even dry prior to the glacial influence. These meltwater-swollen lakes can then fill to spill points, and the resulting outflow will erode deep spillways with cross sections that enlarge to accommodate the peak outflow discharges. Lakes formed in this way may also climatically alter water balances, promoting further glaciation through a positive feedback. Given that a variety of lakes can have the immense volumes needed to source megafloods, it seems appropriate to designate them as "megalakes" (Baker 2009c).

1.2 Historical and Philosophical Background

1.2.1 Earliest History of Megaflood Paleohydrology

With much of North America, Eurasia, and other regions experiencing huge inundations and diversions of drainage by glacial meltwater flooding during the period of major ice sheet decay in the late Pleistocene, it is not surprising that many human cultures developed narrative traditions involving "worldwide flooding." Certainly, "the world" for a local human society of 18–12,000 years ago involved a much smaller geographical extent than would be apparent to the global human society of today. Thus, it is likely that the most impressive events in the lives of many late ice age peoples would have been "worldwide flooding." The associated terrifying experience of surviving such events could initially have led to oral traditions passed down through the generations. Eventually, a few

thousand years ago written communications replaced oral traditions, leading to the recording of the many flood stories that developed during and after the late glacial flooding.

As science developed from the seventeenth century onward, the above experience likely provided an initial inspiration for understanding the surface features of the Earth. The Judeo-Christian tradition associated with Western science included the testimonial evidence of the Noachian debacle. This story provided an obvious starting point for explaining such features as the origin of valleys, the dispersal of erratic boulders, the large-scale scouring of valley floors, and huge accumulations of "diluvium." Contrary to many historical accounts, however, cataclysmic flooding commonly was not invoked simply for reasons of scriptural literalism. Rather, it was genuinely viewed as providing better causal explanations than alternatives for explaining key field observations. That there was also testimonial documentation of large-scale flooding from the biblical source was merely consistent with what could already be inferred from observing nature. Thus, there was a real sense that scientific understanding of cataclysmic megaflooding was advancing.

This all changed during geology's "axial age," the late eighteenth and early nineteenth centuries. First James Hutton and subsequently Sir Charles Lyell introduced what came to be known as "uniformitarianism". With his background as a lawyer, Lyell very effectively advocated that geology could not be done properly if geologists invoked hypotheses that ascribed past phenomena to types and magnitudes of river processes that they could not directly observe in operation today. This was Lyell's attempt to elevate geology to the same epistemological status of certitude as that of physics, for which Sir Isaac Newton had argued that true causes ("vera causae") formed a key element for successful scientific explanation (see Baker 1998).

Of course, strict application of Lyell's uniformitarian doctrine meant that very immense floods, being exceedingly rare on the timescales of human observation, had little chance of being directly observed, so they had to be excluded from consideration according to Lyell's uniformitarian doctrine. There was a more fundamental problem with this reasoning. Lyell's "uniformitarianism" had been both anticipated and soundly criticized on logical grounds by very author of the term, Lyell's contemporary, William Whewell (see Baker 1998). The existence of natural phenomena does not depend upon human observation, Whewell observed. It is not logically sound to exclude in advance from all consideration causes that might have real existence, especially when there is manifest evidence for those causes in various indicators of their past operation. When one excludes phenomena from study, then one can discover nothing about those phenomena.

Unfortunately, despite Whewell's efforts, most Earth scientists accepted Lyell's flawed reasoning, and uniformitarianism came to be enshrined as a fundamental principle of geology. Thus it was that progress in understanding cataclysmic flooding was retarded for about a century. It was not until the early 1920s that a renaissance began with studies of the cataclysmic flood origin of the Channeled Scabland region of the northwestern USA.

1.2.2 The Spokane Flood Controversy

In the early 1920s, Professor J Harlen Bretz developed the scientific hypothesis that during the last ice age, an immense flood, which he named the "Spokane Flood" (Bretz 1923), had emanated from the margins of the great ice sheet that then covered much of northwestern North America (Baker 1978a, 1981, 2008b; Baker and Nummedal 1978). Bretz was initially attracted to this problem by observing Potholes Coulee (Fig. 1.1), now known to be a cataract that developed as cataclysmic floodwater spilled from a large basin into the valley of the Columbia River. Subsequently, as a junior faculty member at the University of Chicago, Bretz worked with teams of advanced geology students (Fig. 1.2) doing studies of the area. He described the immense, dry valleys, termed "coulees" (Fig. 1.3) that comprised a great anastomosing

Fig. 1.1 Oblique aerial view of Potholes Cataract in the Channeled Scabland

Fig. 1.2 J Harlen Bretz (left) with University of Chicago graduate students at a cabin near Spokane, Washington, during fieldwork in the early 1920s. The photograph was provided by Brian Macdonald and was probably taken by Thomas Large, a high school teacher in Spokane, Washington, who aided with logistics for the 1920s fieldwork

Fig. 1.3 Moses Coulee, which is the westernmost tract of the Channeled Scabland. Note the hanging tributary valleys that were produced by the megaflood erosion of the floor of what was previously a normal fluvial valley (Hanson 1970)

complex of channel ways (Fig. 1.4) that had been carved through the relative soft Quaternary loess into the underlying Miocene basalt of the Columbia Plateau, such that preexisting valleys had been filled to levels that allowed the flood water to cross divides into adjacent valleys. Bretz (1923) named this remarkable region the "Channeled Scabland" and concluded, "It was a debacle which swept the Columbia Plateau" (Bretz 1923, p. 649).

Bretz's flood hypothesis was clearly a violation of uniformitarianism, and the geological community largely resisted the concept. This position continued for decades despite Bretz's eloquent arguments and marshaled field evidence in its favor (e.g., Bretz 1928, 1932). Opposition continued despite recognition by Pardee (1942) of a plausible source for the flooding: ice-dammed Pleistocene glacial Lake Missoula in northern Idaho and western Montana (Fig. 1.5) (see Baker 1995). However, evidence for the flood continued to accumulate, especially when Bretz et al. (1956) synthesized new data obtained during the course of the Columbia Basin Irrigation Project in the 1950s. Especially important for convincing flood skeptics was the discovery that giant current ripples (subfluvial gravel dunes) capping many of the scabland gravel mounds that Bretz had correctly interpreted in the 1920s to be flood bars (Fig. 1.6). As the field evidence for cataclysmic flooding became overwhelming, by the 1960s, Bretz's bold hypothesis came to be generally accepted (Bretz 1969). When quantitative understanding of the physical processes of cataclysmic flooding was shown to be completely consistent with that evidence (Baker 1973a, b), there was no longer any credible opposition.

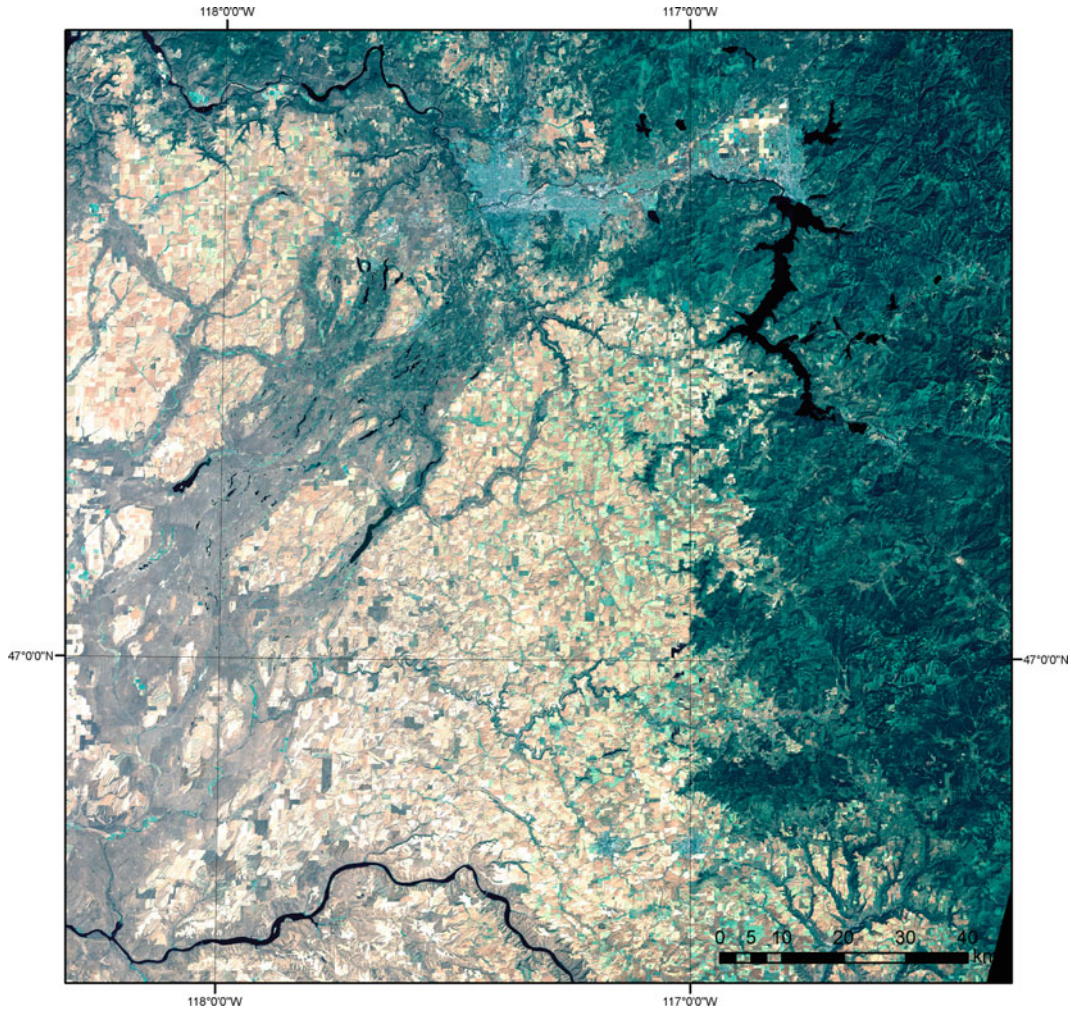

Fig. 1.4 This LANDSAT orbital spacecraft image shows the Cheney Palouse scabland tract (left half of image). The gray pattern of Miocene basalt bedrock exposed on channel floors contrasts with the yellow pattern of wheat fields developed on the Palouse loess-mantled uplands. Removal of the latter to a high-water level by the megaflooding was used to infer the paleo-water slope for the hydraulic calculations in Baker (1973a). Other features on the image include the dense forest cover (green) on the Idaho mountain areas (right portion of the image), the Spokane, Washington, urban area (bluish area to top center), and the Snake River (sinuous black line in lower left portion of the image)

1.3 Modern Methodologies

1.3.1 Paleohydraulics

Although Bretz (1925) published an estimate of the megaflood discharge for what he hypothesized to be the "Spokane Flood" and Pardee (1942) made an estimate for the outflow of glacial Lake Missoula, these calculations were based on a very crude use of the Chezy equation. Nevertheless, the results indicated the megaflood status of the Missoula Floods, including peak discharges of multiple Sverdrups and mean flow velocities of more than 10 m s^{-1}. Research begun in the late 1960s by Baker (1971, 1973a) greatly extended the hydraulic understanding of floods by employing systematic slope area

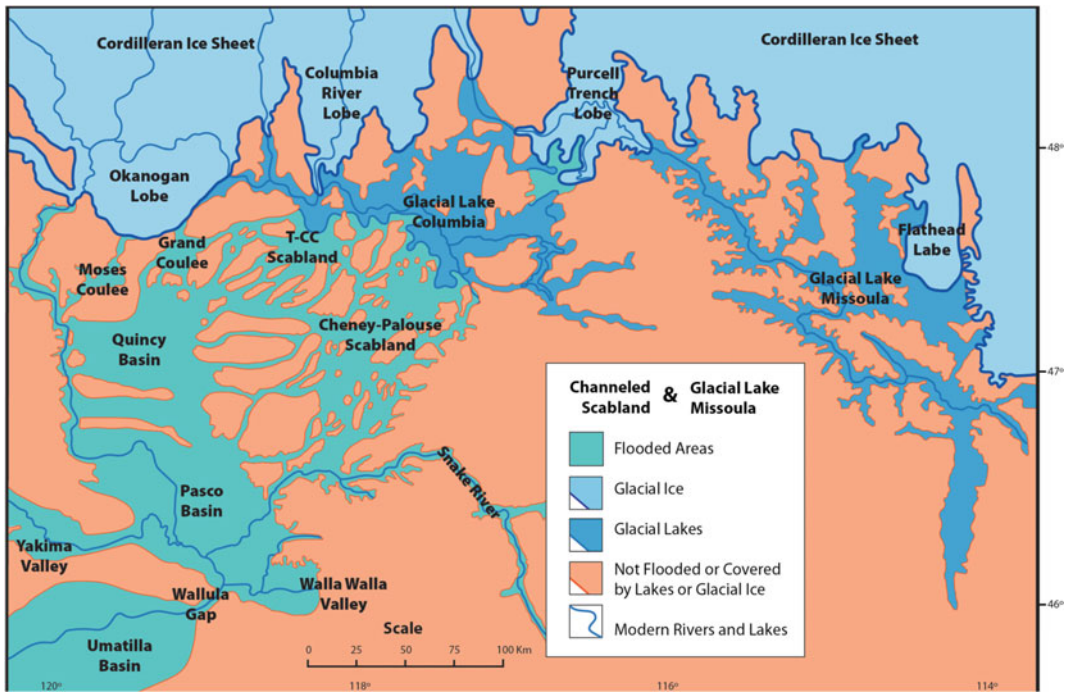

Fig. 1.5 General location of features related to the late Pleistocene megaflooding of the Channeled Scabland (left center) and the southern margin of the Cordilleran Ice Sheet (top). The glacial ice dam for glacial Lake Missoula is at the top center, where the Purcell Trench Lobe had its maximum extent. Another glacial lake (Columbia), 600 m lower in elevation than Lake Missoula, formed behind the Okanogan Lobe the west (upper left on the map). T-CC refers to the Telford–Crab Creek scabland tract, one of five major megaflood pathways that also include the upper Columbia River, the Grand Coulee, and the Cheney—Palouse tract

calculations that relied on megaflooding high-water-mark evidence that is exceptionally well-preserved throughout the Channeled Scabland and adjacent regions. This evidence constitutes what later has come to be known as the "paleostage indicators" (PSI) of the slack-water deposit/paleostage indicator (SWD-PSI) methodology of paleoflood hydrology (Baker 1987).

Examples of the paleostage indicators used for megaflood hydraulic analysis include ice-rafted boulders (Fig. 1.7), high-level flood deposits in slack-water zones (Fig. 1.8), and the upper levels of flood erosion (Fig. 1.4). The PSI data were combined with the extant channel morphology to produce the cross sections (Fig. 1.9) and water surface profiles needed for the flow calculations (Baker 1973a). The latter were then used to estimate the parameters necessary for understanding the basic hydraulics of the flood flows (Baker 1973a, 1978b) and their relationships to the scabland erosional and depositional features (Baker 1973a, b, 1978c, 2009b).

Advances in computer technology subsequently led to the use of 1D flow modeling that greatly improved upon earlier estimates. Methods originally applied to Holocene paleofloods (Ely and Baker 1985; Baker and Pickup 1987) were used for the Missoula Floods (O'Connor and Baker 1992; Benito 1997; Benito and O'Connor 2003). Collectively the hydraulics work explained the phenomenal sediment transport capability of the megaflooding, including the local entrainment of immense boulders. Komar (1980, 1998) and O'Connor (1993) had earlier found that at sustained bed shear stresses of 1000 N m^{-2}, particles as large as 10–20 cm can be transported in suspension, with coarse sand moving as washload. By extrapolating Komar's (1980, 1998) results, it can be inferred

Fig. 1.6 The Spirit Lake gravel dunes ("giant current ripples"), located in northern Idaho, close to the breakout point of glacial Lake Missoula from its ice dam. Note the partial cover of pine trees for scale. The mean dune spacing is about 85 m (Baker 1973a, Fig. 47)

that, at the phenomenally high bed shear stresses of 10^4–10^5 N m^{-2} achieved during the most energetic megaflooding (Baker and Costa 1987; Baker and Komar 1987; Baker 2002a), boulders up to several meters in diameter will move in suspension (Fig. 1.10).

The effects of high-energy megaflooding on bedrock erosion are no less impressive. Convention theory for bedrock channel erosion invokes the processes of abrasion (corrasion), corrosion, cavitation, fluid stressing, physical weathering, and plucking (Tinkler and Wohl 1998; Whipple et al. 2000; Richardson and Carling 2005). Plucking has long been considered to be the most important process for eroding the well-jointed basalt bedrock of the Channeled Scabland (Bretz 1924; Bretz et al. 1956; Baker 1973b, 1978b, 1979; Baker and Komar 1987). Benito (1997) showed that various measures of megaflood flow strength, including mean velocity, flow depth, and power per unit area of bed, correlated the scabland sequence of erosional forms.

Current paleohydraulic research makes use of 2D modeling. Early application to the Channeled Scabland by Craig (1987) was followed by the use of more advanced codes by Komatsu et al. (2000) and Miyamoto et al. (2006, 2007). Denlinger and O'Connell (2010) employed a high-resolution (250 m) 2D model to show that a less-than-maximum discharge output from glacial Lake Missoula generally matched high-water-mark indicators identified along the Missoula flooding pathways, though it failed to fill the Pasco Basin to the maximum level indicated by the field evidence. More recent 2D modeling results (Liu and Baker 2018) are presented in Fig. 1.11.

Fig. 1.7 Large granodiorite erratic boulder that was ice-rafted by Missoula Flood waters entering Badger Coulee, along the southwestern margin of the Pasco Basin (lower left portion of Fig. 1.5)

1.3.2 Geochronology

Paralleling advances in physical modeling, geochronology has likewise seen spectacular recent improvements in methodology. These improvements have followed the same trends as those for paleohydrology generally (Baker 2014), with radiocarbon dating and tephrochronology receiving much attention. However, both these and other techniques were limited in their application by the types of materials required for their analyses. New developments in two areas have greatly expanded the range of applications. These include terrestrial cosomogenic nuclide (TCN) (Gosse and Phillips 2001) and optically stimulated luminescence (OSL) dating (Rittenauor 2008). Ice-rafted boulders (Fig. 1.7) are particularly useful in establishing high-water

Fig. 1.8 High-level megaflood eddy bar along the valley of the Clark Fork River near Paradise, Montana. Note the pine trees for scale. These features were originally recognized by Pardee (1942) as evidence of the high-energy outflow of glacial Lake Missoula, later confirmed by the paleohydraulic modeling of Alho et al. (2010)

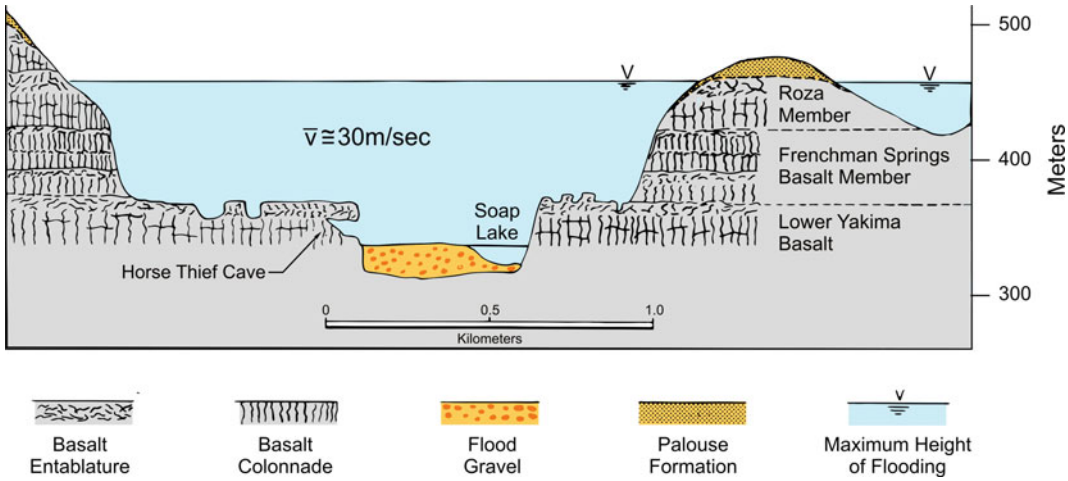

Fig. 1.9 Cross section of Lower Grand Coulee at Soap Lake, Washington, showing the scale of megaflood inundation and the mean flow velocity derived from paleohydraulic calculations (Baker 1973a). Also shown is the jointing pattern in the Columbia River Basalt, which controls the erosional topography of an inner channel (containing Soap Lake) and surrounding areas of butte-and-basin scabland (Baker 1973b, 1978b)

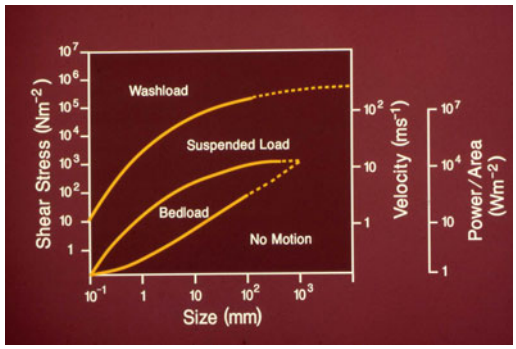

Fig. 1.10 Modes of sediment transport for different sediment particle sizes achieved over very broad ranges of flow strength: bed shear stress, mean flow velocity, and power per unit area of bed. Note that boulders are transported in suspension at levels of flow strength achieved in high-energy megaflooding

levels, and TCN dating has proven to be particularly effective for their geochronology (Balbas et al. 2017). TCN dating has also been applied to flood-scoured bedrock (e.g., Baynes et al. 2015), and OSL is now a technique receiving a wide application to fine-grained flood sediments.

1.4 More Controversies

1.4.1 Asian Megafloods

During the 1960s and 1970s, the late Mikhail G. Grosswald of the former Soviet Academy of Sciences promoted the hypothesis that the great ice sheets of Northern Eurasia formed on what are now shallow submarine continental shelf areas surrounding the Arctic Ocean. These ice sheets flowed from centers lying in what are now ocean areas southward on to the northern portions of Eurasia. In doing so, the great north-flowing Siberian Rivers, the Irtysh, Ob, and Yenisei, were blocked and impounded (Grosswald 1980). Moreover, immense amounts of meltwater were diverted to be diverted to the south-flowing Dneiper and Volga Rivers. The result was a complex pattern of huge proglacial lakes, and great spillways developed through the diversion of drainage (Fig. 1.12). Many of these

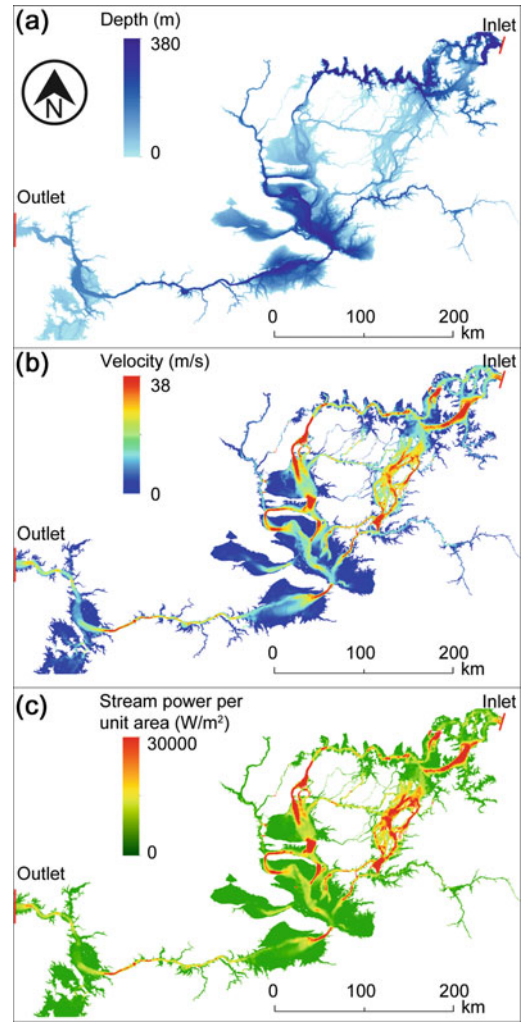

Fig. 1.11 2D paleohydraulic modeling results (Liu and Baker 2018). Flow depths (**a**), velocity (**b**), and stream power per unit area (**c**) were calculated from the modeling run on a 500-m computational mesh for the Channeled Scabland and surrounding regions

paleolakes and spillways had long been recognized, though their origins had not been linked into the genetic framework hypothesized by Grosswald (Fig. 1.13). Komatsu et al. (2016) provide a recent review of current thinking on this topic.

Grosswald's reconstructions became widely debated with time, resulting in considerable controversy. Some work (e.g., Mangerud et al.

Fig. 1.12 Generalized pattern of glaciation and megaflooding envisioned by Grosswald (1998). Flood pathways associated with mountain areas are shown as red arrows. Those associated with lowland areas are shown as yellow arrows. Various paleolakes are shown in violet. The extent of glaciation (dot pattern) is much more extensive than that envisioned by most contemporary researchers

2001) shows that field evidence is consistent with some the pattern, though not at the scale envisioned by Grosswald. Grosswald (1980) interpreted the river blockage to be late Weichselian in age (about 15,000–20,000 years ago). However, other work considers the event to have been early Weischselian (Arkhipov et al. 1995), about 90,000 years ago, when ice sheet growth was enhanced by the climatic influence of the ice-dammed lakes (Krinner et al. 2004). The review by Komatsu et al. (2016) provides more detail on the numerous hypotheses relating to late Pleistocene megaflooding in Northern Eurasia.

In his most comprehensive (and controversial) model for Asian glaciation and megaflooding, Grosswald (1999) proposed that much of central Russia was inundated in the late Quaternary by immense outbursts from the ice sheet margins to the north. He envisioned an ice cap covering nearly all the Arctic Ocean from which emanated colossal flows of water that entered what is now central Siberia from the north and turned

Fig. 1.13 Detailed compilation of spillways linked to glacially influenced megalakes (violet) and Pleistocene Ice Sheets (dot pattern), as envisioned by Grosswald (1998), and summarized in more detail by Komatsu et al. (2016). The numbers refer to spillways, as follows: 4—Keltma, 5—Manych, 6—Uzboi, 7—Turgai, 8—Kas-Ket, 9—Tanguska-Yensei, 10—Vilyuy-Tanguska. The letters refer to paleolakes, as follows E—Euxene, K—Knvarln, A—Aral, M—Mansi, Y—Yenisei, L—Lena, T—Tarim, J—Issyk-Kul, U—Darkat, S—Vadim, R—Amur

westward to follow the Turgai pass and other spillways, eventually reaching the Caspian and Black Sea basins by the routes noted above. The routing of the flooding was inferred through mapping from satellite imagery showing areas of large-scale streamlined topography and flow-like lineations that extend over immense regions. Much of this interpretation seems not yet to have been tested by detailed study on the ground.

Grosswald was also involved in studies of megaflood-related features in the mountain environments of southern Russia. His former Doctor of Science student, the late Alexei Rudoy spent many years arguing for a megaflood origin to features in the Altai Mountains of the south-central border region of the Siberian portion of the former Soviet Union. Rudoy's work met with considerable skepticism from his colleagues, despite his recognition of similarities to the megaflooding landscapes of the Channeled Scabland. In the early 1990s, however, this work received more recognition when it moved beyond the local debates among Russian scientists, receiving attention at international meetings

Fig. 1.14 Megaflood paleohydrologists at meeting of INQUA Commission on Global Continental Palaeohydrology, Toledo, Spain, September 1996. From left to right: V. R. Baker, M. G. Grosswald, and A. N. Rudoy

(Fig. 1.14) and publication in the international literature (Baker et al. 1993; Rudoy and Baker 1993; Grosswald and Rudoy 1996).

1.4.2 Subglacial Megafloods

For about 35 years or so a major debate in glacial geology has arisen involving the late John Shaw's (e.g., 1996, 2002) hypothesis for the generation of subglacial landforms. A broad variety of enigmatic landforms, involving erosion and deposition, formed beneath the Laurentide Ice Sheet and other late glacial continental ice sheets. Shaw (1983) originally formulated his hypothesis for drumlins, but it was subsequently extended to include a large assemblage of presumably genetically related landforms. These landforms include drumlins, Rogen moraines, large-scale bedrock erosional flutings and streamlining, gravel sheets in eskers, hummocky terrain, pendant bars, and tunnel channels (valleys). There are also a variety of erosional features developed in rock, including what have been termed "p-forms" (Dahl 1965). Though most commonly explained by subglacial ice and debris-layer deformational processes, the genesis of these features cannot be observed in modern glaciers that are much smaller in scale than their late Quaternary counterparts. Shaw (1996) explains the assemblage of landforms as part of an erosional/depositional sequence beneath continental ice sheets that precedes regional ice stagnation and esker formation with a phase of immense subglacial sheet floods at megaflood scale, which, in turn, follows a phase of ice sheet advance that terminates with surging, stagnation, and melt-out. Shaw calculates peak glacial outburst flood discharges of tens of Sv in his model. Munro-Stasiuk et al. (2009) provide a recent review of the subglacial megaflooding hypothesis.

There are similarities between the Shaw assemblage and the anastomosing channel complexes eroded by Pleistocene megaflooding into the basalt bedrock and overlying sediments of the Columbia Basin region of Eastern Washington State, USA, where the cataclysmic flooding produced the erosional and depositional macro-form and meso-form features of the Channeled Scabland.

The Laurentide Ice Sheet subglacial landforms are most commonly inferred to be the result of subglacial ice deformational processes (Benn and Evans 2010). Shaw's megaflood hypothesis for subglacial landscape development continues to be a source of considerable controversy among glacial geologists (Benn and Evans 2006), but it finds some support from both empirical and theoretical studies of the subglacial phenomena associated with large ice sheets (Lesemann and Brennand 2009; Livingstone et al. 2013).

1.5 Global Distribution of Megafloods

Evidence for ancient megaflooding is present on nearly all of the larger landmasses of planet Earth and even on the surface of Mars. Baker (2013) provides an inventory of various examples, and Fig. 1.15 shows locations for the northern hemisphere. The brief overview that follows is necessarily incomplete, but it will provide some sense of the scope of global megaflooding phenomena.

1.5.1 Iceland

Katla volcano with its Myrdalsökull ice cap has produced the largest historic jökulhlaups (glacial outburst floods) in Iceland. In 1918, a peak discharge may have achieved 1 Sv (Tomasson 1996). Earlier Holocene megafloods produced a scabland landscape along the path of the Jökulsá á Fjöllum River in northeastern Iceland (Carrivick et al. 2004). The responsible jökulhlaups emanated from what are now ice-filled calderas (Bararbunga and Kverkfjöll) beneath the Vatnajökull ice cap.

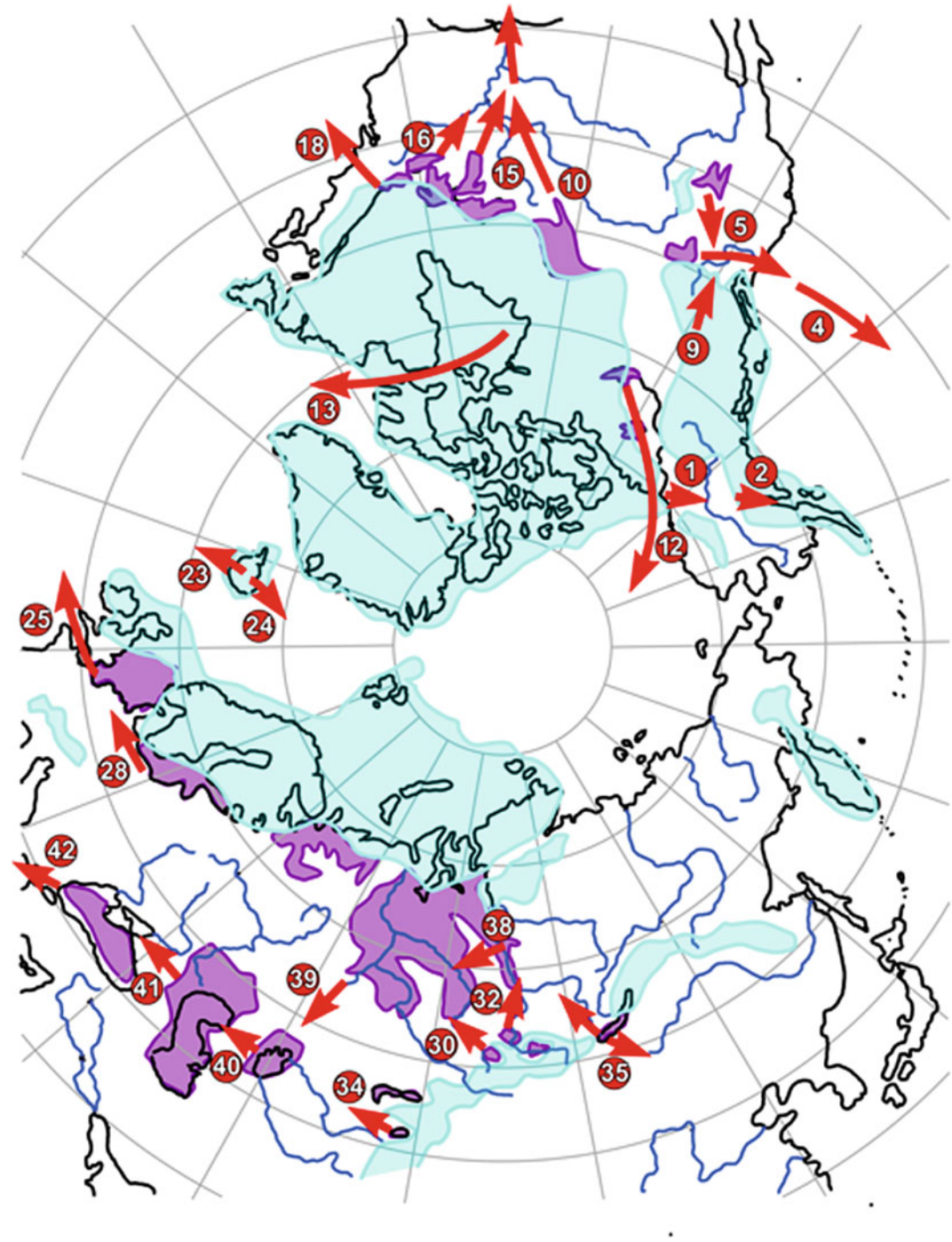

Fig. 1.15 Northern hemisphere locations of various hypothesized megaflood locations and pathways (red arrows) associated with late Pleistocene glaciation (light blue) and associated lakes (purple). Numbers refer to studies listed in Baker (2013, Table 2 and Fig. 2), some of which are also referenced in this paper. The pattern of glaciation and lacustrine extent are generalized from various compilations

1.5.2 Asia

In the mountain areas of central northern Asia, there were megaflood outbursts from the Issyk-Kul area, the Altai Mountains (upper Ob drainage), and the upper Yenisei River system. Less well understood is a much grander scale of possible megaflooding that includes a system of late glacial flood spillways extending over a distance of about 8000 km from northern and eastern Siberia to the Mediterranean (Baker 2007).

There has now been much research on megaflood landscapes in the mountain areas of central Asia. Much work has occurred in the Altai Mountains of south-central Siberia region (Baker et al. 1993; Carling et al. 2002; Herget 2005). The most extensive Altai megaflooding derived from the Chuja–Kuray ice-dammed lake, which held about 564 km^3 of water at a maximum depth of about 600 m (Carling et al. 2010). The Chuja and Katun River valleys, downstream of this lake, display immense gravel bars, up to 5 km long and 120 m in height. The bars were emplaced by flooding into various valley-side embayments (Herget 2005), and some of the bar surfaces and associated run-up layers of flood-transported gravel indicate maximum flow depths as great as 300 m. Flow modeling of the associated paleoflood discharges indicates a peak discharge of about 10 Sverdrups (Carling et al. 2010).

In the Tuva region, north of Mongolia, megafloods were generated from an ice-dammed lake in the Darkhat depression of north-central Mongolia (Grosswald and Rudoy 1996; Batbaatar and Gillespie 2016). This paleolake held about 200 km^3 of water with a depth of about 175 m at the ice dam. The paleoflooding impacted the upper Yenisei River, emplacing spectacular trains of giant current ripples (gravel dunes) near the Tuva capital city of Kyzyl (Komatsu et al. 2009).

Lake Issyk-Kul, Kirgizstan, was enlarged to an ice-dammed lake during the last glaciation, rising to 300 m above the present lake level (Grosswald et al. 1994). The paleolake failed by cataclysmic outburst flooding into its outlet, Boam Canyon, emplacing an enormous megafan that extends for 85 km from the canyon mouth. The immense Lake Baikal, with a current area of 31,500 km^2 and a volume of 23,000 km^3, also rose and fell during various cycles of Quaternary glaciation, releasing flooding through outlets, including that occupies by the modern Angara River. East of Baikal, glacial Lake Vitim formed in the headwater areas of the Vitim River, releasing an outburst megaflood of 3000 km^3 with mean flow depths of 120–150 m and a peak discharge of 4–6.5 Sverdrups, ultimately reaching the Arctic Ocean via the Lena River (Margold et al. 2018).

The largest of the flood-related lakes of central Asia occurred in tectonic depressions of the lowland plains. Largest of these was ice-dammed Lake Mansi of the west Siberian plain (M on Fig. 1.13), estimated by Mangerud et al. (2001) to have covered 600,000 km^2 at a surface elevation of 60 m. Both Arkhipov et al. (1995) and Grosswald (1980) infer that it was even larger, about 1.2 million km^2 in area, with a volume of about 75,000 km^3 at a surface elevation of 128 m. Mansi spilled southward, through the Turgai divide of north-central Kazakhstan (locality 7 on Fig. 1.13), to the basin of the modern Aral Sea (A on Fig. 1.13). The full-glacial Aral Sea rose to a surface elevation of 70 or 80 m, enlarging to a surface area of about 100,000 km^2. Grosswald proposed that this paleolake spilled southwestward through the Uzboi Channel at its southwestern end (locality 6 on Fig. 1.13) entering the basin of the modern Caspian Sea. The latter may have been enlarged by a glacially fed Volga River, though there remains controversy as to the timing for this (Panin et al. in press). In any case, the Caspian volume expanded to a Late Quaternary size over twice its modern extent. Known as the Khvalyn paleolake (K on Fig. 1.13), this megalake covered an area of 950,000 km^2, holding a volume of 135,000 km^3 at an elevation of 50 m. The Khvalyn megalake spilled westward through the Manych spillway (locality 5 on Fig. 1.13) into the Don River valley. The huge size of this spillway, up to 35 km wide, implies that it may have carried peak flows of 10 Sverdrups (Baker 1997), but this

interpretation remains controversial (see review by Panin et al. in press). Floodwater subsequently spilled into the Sea of Azov, through the Kerch Strait, and into to the Euxine Basin (E on Fig. 1.13), which presently holds the Black Sea.

1.5.3 Europe

The late Pleistocene of Europe was dominated by the Fennoscandian Ice Sheet, the maximum extent of which covered all of Scandinavia, extending across the Baltic to Estonia, Latvia, Lithuania, most of Poland, and northern Germany. During earlier glacial periods, it even extended across what is now the northern part of the North Sea, merging with the ice sheet that covered most of the British Isles. The very late Pleistocene retreat of the Fennoscandian Ice Sheet resulted in the formation of the Baltic Ice Lake in what is now the basin of the Baltic Sea. This megalake covered an area of 400,000 km^2, but it was relatively shallow resulting in a volume of about 9000 km^3. Because the ice sheet blocked what is now the connection of the Baltic to the North Sea, the late Pleistocene Baltic Ice Lake drained through a spillover across the Mt. Billingen area, southern Sweden (Bjorck 1995). Proglacial drainage from the southern margins of the Fennoscandian Ice Sheet was also conveyed via the Urstromtal valleys (east–west late Pleistocene ice marginal channels of northern Germany) to what is now the southern North Sea basin.

The southern part of the North Sea is separated from the Atlantic Ocean by a strait separating Britain from the rest of Europe. Known as "the Channel" to the English and "la Manche" to the French, it was hypothesized by Smith (1985) to represent a Quaternary-age breaching of the Chalk barrier at the site of the present-day Dover Strait at its eastern end. Toucanne et al. (2009) inferred from studies of a marine core from the Bay of Biscayne that the breaching of the Chalk barrier occurred during the Elsterian glaciation about 450,000 years ago. This breaching occurred by cataclysmic flooding, as documented by Gupta et al. (2007, 2017), who used naval sonar imagery to discover megaflood erosion features on the Channel's submarine floor.

1.5.4 North America

North American glacial megaflood landscapes are now recognized in the Columbia and Snake River drainages of the northwestern USA; in the spillway systems of the upper Mississippi Basin; near the Great Lakes and adjacent St. Lawrence Basin; the Hudson River Basin; the Mackenzie Basin; the Yukon Basin (Porcupine River); the Sustina and Copper River Basins (Alaska); and the Hudson Strait. Figure 1.16 provides the inventory of these and other North American megaflooding sites compiled by Baker (2013).

As the largest of North America's late Pleistocene ice sheets, the Laurentide of central and eastern Canada, retreated from its late Quaternary maximum extent, its southern and western margins contained immense meltwater lakes that developed in the glacio-isostatic troughs surrounding the ice mass. Rises of lake levels resulted in the carving of numerous spillways (into the drainages of the Mississippi, St. Lawrence, and Mackenzie Rivers) (Kehew and Teller 1994; Kehew et al. 2009). The initial retreat of the ice sheet produced relatively small lakes because of the regional river drainage to the south, away from the ice front. Surging and re-advancing led to a complex history for the basins that now contain the Great Lakes. After the ice sheet retreated north of this area, Lake Agassiz formed in the trough between the ice and drainage divides to the south and west, inundating parts of present-day North Dakota, Manitoba, and western Ontario. Agassiz was a megalake, and it seems to have been initiated close to the time of the Younger Dryas cooling event, which began about 12,700 calendar years ago. The cooling has been explained by diversion to the St Lawrence River of Laurentide meltwater that previously flowed to the Gulf of Mexico via the Mississippi. The resulting outflow of great quantities of freshwater into the North Atlantic then disrupted the salinity gradient that drives the thermohaline circulation by impeding deepwater

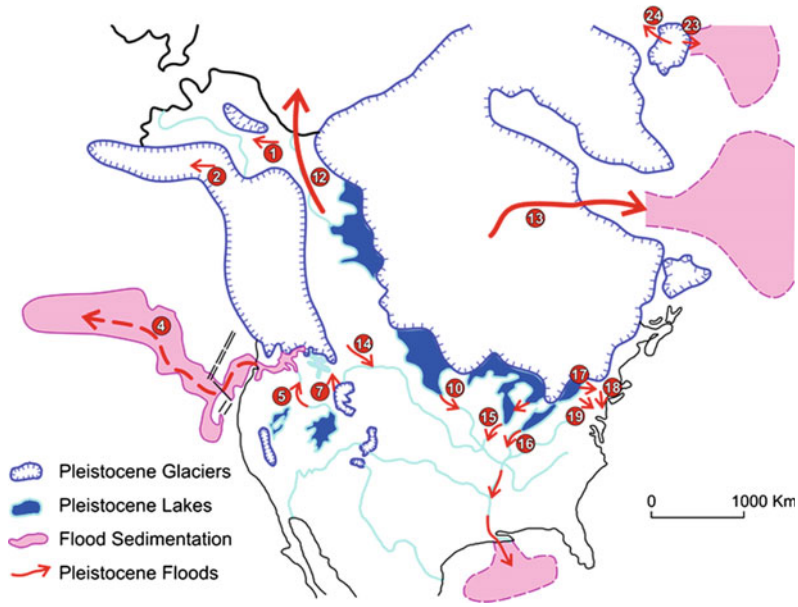

Fig. 1.16 Pattern of late Pleistocene megaflooding areas for North America. Numbers correspond to those in Fig. 1.15, and refer to studies listed in Baker (2013, Table 2 and Fig. 2), some of which are also referenced in this paper. Pink areas show possible extent of megaflood sedimentation on ocean floors

formation in the North Atlantic (Broecker and Denton 1989).

Over a period of about 5000 years, Laurentide lacustrine inundation at one time or other covered about 1.5 million km^2. The maximum one-time extent was achieved about 8400 years ago through a union between glacial Lake Agassiz and glacial Lake Ojibway in northern Ontario. This union produced a megalake covering about 840,000 km^2, holding about 160,000 km^3 of water (Leverington et al. 2002). This quantity is double the volume of the largest modern lake, the Caspian Sea. Because the megalake was dammed by remnants of the Laurentide Ice Sheet in present-day Hudson Bay, the system became highly unstable through the influx of marine water into Hudson Bay. This influx set up a massive subglacial outburst of the megalake water through Hudson Strait into the Labrador Sea that provided the probable trigger for an abrupt and widespread global climatic cooling event (Clarke et al. 2003). The maximum discharge for this event is estimated as 5 Sv (Clarke et al. 2004).

The Cordilleran Ice Sheet produced the Missoula flooding described above when its Purcell Lobe extended south from British Columbia to the basin of modern Pend Oreille Lake in northern Idaho (Fig. 1.5). The ice thereby impounded the Clark Fork River drainage to the east, forming a lake extending into western Montana with a water volume of about 2600 km^3 and a depth of 600 m at the dam (Smith 2006). Using 2D hydraulic modeling, Alho et al. (2010) found that the paleoflow conditions (velocities, bed shear stresses, and unit power values) that developed throughout the lake basin during the largest known draining(s) required a total failure of the ice dam. As recognized by Baker and Bunker (1985), the multiple outburst events were of greatly differing magnitudes. About 15 floods exceeded 3 Sverdrups, and at least one of these exceeded 10 Sverdrups in discharge (Benito and O'Connor 2003). The largest failure or failures probably involved a different source mechanism than the subglacial tunneling envisioned by Waitt (1985) because that mechanism yields discharges of only about 1–2 Sverdrups (Clarke et al. 1984).

Although the repeated outbursts from Lake Missoula have generally been inferred to have occurred between about 18,000 and 15,000 calendar years ago (Waitt 1985; Balbas et al. 2017), the total period for GLM flooding may have extended back to 23 or 24 thousand years ago (Benito and O'Connor 2003; Lopes and Mix 2009), and major glacial outburst flooding of the

Columbia continued until just after the time of Glacier Peak tephra emplacement, about 13,600 years ago (Waitt 2016). Other data on freshwater inputs to the northeast Pacific Ocean (Lopes and Mix 2009) and groundwater recharge in the Pasco Basin (Brown et al. 2010) indicate that flooding may have extended from about 31,000 to 16,000 calendar years ago.

The Columbia was also impacted by megaflooding down the Snake River. This flooding was generated by the spilling of Lake Bonneville, which was the ice age megalake predecessor to the modern Great Salt Lake. At its peak about 18,000 years ago, Bonneville covered a maximum area of 52,000 km^2 and held a volume of about 7500 km^3. The lake filled to the level of a spill point in south-central Idaho and then dropped 125 m as it eroded into the outlet at Red Rock Pass, releasing 5320 km^3 of water with a peak discharge of about 1 Sv (Abril-Hernández et al. 2018). This megaflood greatly impacted the Snake River valley all the way to its junction with the Columbia River (O'Connor 1993).

1.5.5 South America

South American megafloods in the Santa Cruz River system of southern Argentina emanated from the Patagonian Ice Sheet, and other Patagonian megaflooding are documented for the Baker River region of Chile (Dussaillant et al. 2010; Benito et al. 2014).

The Santa Cruz valley contains some flood bars that display giant current ripples (gravel dunes) (Pacifici 2009) similar to those that are common in the Channeled Scabland and in the central Asian megaflood landscapes.

1.5.6 Antarctica

Subglacial cataclysmic flooding is hypothesized to have occurred in the mid-Miocene when an early Antarctic Ice Sheet that overrode the Transantarctic Mountains (Denton and Sugden 2005; Lewis et al. 2006). The inferred megaflooding may have emanated from subglacial "catch lakes" that formed as the ice sheets evolved over preexisting water bodies. Numerous subglacial lakes exist under the modern Antarctic Ice Sheets, and the largest of these is Lake Vostok. Possible Quaternary megaflooding was hypothesized by Shaw et al. (2008), who based their interpretation on the morphology of troughs crossing the Antarctic continental shelf.

1.6 Research Frontiers

1.6.1 Marine Megafloods

The greatest megaflooding discharges for Earth were probably achieved during the Miocene, about 5.3 million years ago, when the Atlantic Ocean spilled into the then dry Mediterranean basin (Garcia-Castellanos et al. 2009). Known as the Zanclean Flood, this event also left distinctive megaflood features as it crossed from the western to eastern Mediterranean basins over a shelf to the south of what is now the island of Sicily (Micallef et al. 2018).

The classic Channeled Scabland region is now recognized as being but a small component of a source-to-sink system extending from ice marginal lacustrine (glacial lakes Columbia and Missoula) and possible subglacial sources beneath the Cordilleran Ice Sheet, through the Channeled Scabland intermediate zone, and on to sink relationships on the abyssal plain of the Pacific Ocean (Fig. 1.16). Upon reaching the Pacific Ocean, the Missoula floodwaters continued flowing down the continental slope as hyperpycnal flows and associated turbidity currents (Normark and Reid 2003). The sediment-charged floodwaters followed the Cascadia submarine channel into and through the Blanco Fracture Zone and out onto the abyssal plain of the Pacific (Griggs et al. 1970). As much as 5000 km^3 of sediment may have been carried and distributed as turbidites over a distance of 2000 km west of the Columbia River mouth. Locally, basins are filled with these turbidites, which have been cored and described by Brunner et al. (1999) and Zuffa et al. (2000).

During the last glaciation, the Black Sea was isolated from the Mediterranean Ocean, and it filled with fresh water derived from the great system of glacially augmented rivers entering it from the north. About 18,000 years ago, this phase, called the New Euxine, had a well-developed freshwater faunal facies, showing immense amounts of freshwater were entering from the glacially swollen Volga River as well as via the Caspian through spilling via the Manych spillway (Fig. 1.13). At times, so much freshwater entered that the New Euxine megalake spilled into the Sea of Marmara, which, in turn, spilled via the Hellespont into the Aegean and Mediterranean. During the transition to the Holocene, rising sea levels allowed the Mediterranean Sea water to spill catastrophically through the Turkish straits, Hellespont and Bosporus, about 9000 years ago (Ryan et al. 1997, 2003; Yanchilina et al. 2017).

1.6.2 Martian Megafloods

Cataclysmic flooding landscapes were discovered on the planet Mars through space probe imagery generated in the early 1970s (Baker and Milton 1974; Baker 1978a, 1982). The megaflooding occurred in episodes, extending back through more than 4 billon years of planetary history, to periods when Mars had abundant water (Baker 2001). The Martian megafloods are hypothesized to have induced the episodic formation of a water body covering the northern plains of the planet: "Oceanus Borealis" (Fig. 1.17). This water body seems to have been associated with contemporaneous volcanism, leading to relatively brief periods of enhanced hydrological cycling on the land surface (Baker et al. 1991; Baker 2001). The megaflood channel sizes for Mars are much greater than those of Earth, implying much greater discharges for their formation (Baker 2001). This topic continues to be a controversial one in regard to past climate change and the water inventory for the planet, as reviewed by Baker et al. (2015).

1.6.3 Megafloods and Planetary Change

It has now become clear that for both Earth and Mars, episodic megaflooding was likely a major factor in global climatic change (Baker 2009a). The Martian megafloods are even hypothesized to have induced the episodic formation of a northern plains "ocean," which, with contemporaneous volcanism, led to relatively brief periods of enhanced hydrological cycling on the land surface (Baker et al. 1991). For Earth, outbursts of meltwater into the Atlantic Ocean may have induced climate changes by influencing the thermohaline circulation of the North Atlantic Ocean (Teller et al. 2002).

1.7 Discussion and Conclusions

High-energy megaflooding is a planetary-scale phenomenon, associated with glacier outburst settings, megalake spillways, and large ice sheets. The peak discharges for these paleofloods, like those of ocean currents, are measured in millions of cubic meters per second. Ice marginal lakes sourced the largest, well-documented (and non-controversial) terrestrial glacial megafloods, and the best-studied example of these is glacial Lake Missoula, which was impounded by a lobe of the Cordilleran Ice Sheet of northwestern North America. Other examples are associated with the Laurentide Ice Sheet of central and eastern Canada, whose retreat from its late Quaternary maximum extent resulted in immense meltwater lakes filling troughs that had been created by ice loading of Earth's crust. Glacial megalakes also developed in Eurasia during the expansion and retreat of the huge Quaternary ice sheets that extended on to the continent from what are now shallow marine shelves around the Arctic Ocean. The resulting blockage of north-flowing rivers, notably the Ob, Irtysh and the Yenisei, produced a network of megaflood spillways that ultimately delivered meltwater to the Mediterranean.

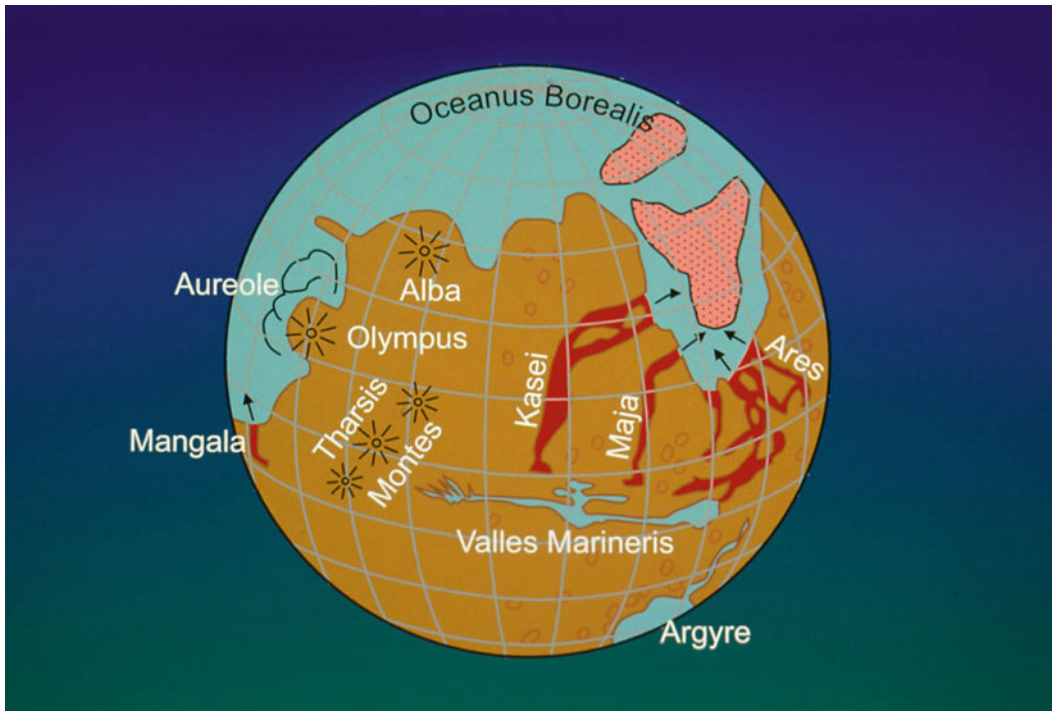

Fig. 1.17 Relation of cataclysmic flood channels on Mars (red) to highland terrains (brown) and ancient ponded water bodies (blue-green)

As noted in this review, many megaflooding concepts have been and continue to be highly controversial. Nevertheless, it is also true that many once controversial megaflooding hypotheses have proven to be very productive scientifically; if not in their original formulations, then commonly in modified versions that led to discoveries that were stimulated by research directed at resolving the controversies. Moreover, it is becoming clear that megaflooding is a process of profound planetary importance, not only impacting the patterns of drainage and river valleys, but also creating anomalous topography, inducting global environmental change, altering ocean currents, and influencing patterns of human migration and settlement. The pervasive influences of megaflooding during the last major glaciation on Earth could well have been responsible for some of near-ubiquitous flood stories in the mythological traditions of ancient peoples. Indeed, the collective subconscious memories of these phenomena may well have fostered the curiosity about them that later inspired their scientific study.

References

Abril-Hernández JM, Periáñez R, O'Connor JE et al (2018) Computational fluid dynamics of the Late Pleistocene Lake Bonneville Flood. J Hydrol 561:1–15

Alho P, Baker VR, Smith LN (2010) Paleohydraulic reconstruction of the largest Glacial Lake Missoula drainings. Quat Sci Rev 29:3067–3078

Arkhipov SA, Ehlers J, Johnson RG et al (1995) Glacial drainage towards the Mediterranean during the Middle and Late Pleistocene. Boreas 24:196–206

Baker VR (1971) Paleohydrology and sedimentology of Lake Missoula flooding in eastern Washington. PhD dissertation, University of Colorado

Baker VR (1973a) Paleohydrology and sedimentology of Lake Missoula flooding in eastern Washington. Geological Society of America Special Paper 144

Baker VR (1973b) Erosional forms and processes for the catastrophic Pleistocene Missoula floods in eastern Washington. In: Morisawa M (ed) Fluvial geomorphology. Allen and Unwin, London, pp 123–148

Baker VR (1978a) The Spokane flood controversy and the Martian outflow channels. Science 202:1249–1256
Baker VR (1978b) Paleohydraulics and hydrodynamics of scabland floods. In: Baker VR, Nummedal D (eds) The Channeled Scabland. National Aeronautics and Space Administration Planetary Geology Program, Washington DC, pp 59–79
Baker VR (1978c) Large-scale erosional and depositional features of the Channeled Scabland. In: Baker VR, Nummedal D, (eds) The Channeled Scabland. National Aeronautics and Space Administration Planetary Geology Program, Washington DC, pp 81–115
Baker VR (1979) Erosional processes in channelized water flows on Mars. J Geophys Res 84:7985–7993
Baker VR (ed) (1981) Catastrophic flooding: the origin of the Channeled Scabland. Hutchinson Ross, Stroudsburg/Pennsylvania
Baker VR (1982) The channels of Mars. University of Texas Press, Austin/Texas
Baker VR (1987) Paleoflood hydrology and extreme flood events. J Hydrol 96:79–99
Baker VR (1994) Glacial to modern changes in global river fluxes. In: Material fluxes on the surface of the Earth. National Academy Press, Washington DC, pp 86–98
Baker VR (1995) Joseph Thomas Pardee and the Spokane flood controversy. GSA Today 5:169–173
Baker VR (1997) Megafloods and glaciation. In: Martini IP (ed) Late glacial and post glacial environmental change. Oxford University Press, New York, pp 98–108
Baker VR (1998) Catastrophism and uniformitarianism: logical roots and current relevance. In: Blundell DJ, Scott, AC (eds) Lyell: the past is the key to the present. Geological Society (London) Special Publication 143, pp 171–18
Baker VR (2001) Water and the Martian landscape. Nature 412:228–236
Baker VR (2002a) High-energy megafloods: planetary settings and sedimentary dynamics. In: Martini IP, Baker VR, Garzon G (eds) Flood and megaflood processes and deposits: recent and ancient examples. International Association of Sedimentologists, Oxford, Special Publication 32, pp 3–15
Baker VR (2002b) The study of superfloods. Science 295:2379–2380
Baker VR (2007) Greatest floods—largest rivers. In: Gupta A (ed) Large rivers: geomorphology and management. Wiley, New York, pp 65–74
Baker VR (2008a) Paleoflood hydrology: origin, progress, prospects. Geomorphology 101:1–13
Baker VR (2008b) The Spokane flood debates: historical background and philosophical perspective. In: Grapes R, Oldroyd D, Grigelis A (eds) History of geomorphology and quaternary geology. Geological Society of London Special Publication 301, pp 33–50
Baker VR (2009a) Glacial megalakes. In: Gornitz V (ed) Encyclopedia of paleoclimatology and ancient environments. Springer, Dordrecht, pp 380–382
Baker VR (2009b) Megafloods and global paleoenvironmental change on Mars and Earth. In: Chapman MG, Kesthelyi L (eds) Preservation of random mega-scale events on Mars and Earth: influence on geologic history. The Geological Society of America Special Paper 453, pp 23–36
Baker VR (2009c) Overview of megaflooding: Earth and Mars. In: Burr DM, Carling PA, Baker VR (eds) Megaflooding on Earth and Mars. Cambridge University Press, Cambridge, pp 1–12
Baker VR (2013) Global late Quaternary fluvial paleohydrology with special emphasis paleofloods and megafloods. In: Shroder J (ed in chief), Wohl EE (ed) Treatise on geomorphology. Fluvial geomorphology, vol 9. Academic Press, San Diego, pp 511–527
Baker VR (2014) Paleohydrology. IAHS benchmark papers in hydrology 9. International Association of Hydrological Sciences Press, Wallingford, UK
Baker VR, Bunker RC (1985) Cataclysmic late Pleistocene flooding from glacial Lake Missoula: a review. Quat Sci Rev 4:1–41
Baker VR, Costa JE (1987) Flood power. In: Mayer L, Nash D (eds) Catastrophic flooding. Allen and Unwin, London, pp 1–24
Baker VR, Komar PD (1987) Cataclysmic flood processes and landforms. In: Graf WL (ed) Geomorphic systems of North America: Geological Society of America, The Geology of North America, Centennial Special Volume 2, pp 423–443
Baker VR, Milton DJ (1974) Erosion by catastrophic floods on Mars and Earth. Icarus 23:27–41
Baker VR, Nummedal D (eds) (1978) The Channeled Scabland: a guide to the geomorphology of the Columbia Basin, Washington. National Aeronautics and Space Administration Planetary Geology Program, Washington, D.C.
Baker VR, Pickup G (1987) Flood geomorphology of the Katherine Gorge, Northern Territory, Australia. Geol Soc Am Bull 98:635–646
Baker VR, Kochel RC, Patton PC (1979) Long-term flood-frequency analysis using geological data. International Association of Hydrological Sciences Publication 128, pp 3–9
Baker VR, Strom RG, Gulick VC et al (1991) Ancient oceans, ice sheets and the hydrological cycle on Mars. Nature 352:589–594
Baker VR, Benito G, Rudoy AN (1993) Paleohydrology of late Pleistocene superflooding, Altai mountains, Siberia. Science 259:348–350
Baker VR, Hamilton CW, Burr DM et al (2015) Fluvial geomorphology on Earth-like planetary surfaces: a review. Geomorphology 245:149–182
Balbas A, Barth AM, Clark PU et al (2017) ^{10}Be dating of late-Pleistocene megafloods and Cordilleran Ice Sheet retreat in the northwestern US. Geology 45:583–586
Batbaatar J, Gillespie AR (2016) Outburst floods of the Maly Yenisei, Part I. Int Geol Rev 58:1723–1752
Baynes ERC, Attal M, Niedermann S et al (2015) Erosion during extreme flood events dominates Holocene

canyon erosion in northeast Iceland. Proc Natl Acad Sci 112:2355–2360
Benito G (1997) Energy expenditure and geomorphic work of the cataclysmic Missoula flooding in the Columbia River Gorge, USA. Earth Surf Proc Land 22:457–472
Benito G, O'Connor JE (2003) Number and size of last-glacial Missoula floods in the Columbus River valley between Pasco Basin, Washington and Portland, Oregon. Geol Soc Am Bull 115:624–638
Benito G, Thorndycraft VR, Machado MJ et al (2014) Magnitude and timing of Holocene glacial lake outburst floods in the Baker River, Northern Patagonian Icefield, Chile. In: Avances de la Geomorfología en España 2012–2014. Libro de Actas de la XIII Reunión Nacional de Geomorfología. Sociedad Española de Geomorfología, Cáceres, Spain, pp 24–27
Benn D, Evans DJA (2006) Subglacial megafloods: outrageous hypothesis or just outrageous? In: Knight PG (ed) Glacier science and environmental change. Blackwell, Oxford, pp 42–46
Benn DI, Evans DJA (2010) Glaciers and glaciation. Hodder Education, London
Bjorck S (1995) A review of the history of the Baltic Sea, 13.0–8.0 ka BP. Quat Int 27:19–40
Bretz JH (1923) The Channeled Scabland of the Columbia Plateau. J Geol 31:617–649
Bretz JH (1924) The Dalles type of river channel. J Geol 32:139–149
Bretz JH (1925) The Spokane flood beyond the Channeled Scablands. J Geol 33(97–115):236–259
Bretz JH (1928) Channeled Scabland of eastern Washington. Geogr Rev 18:446–477
Bretz JH (1932) The Grand Coulee. American Geographical Society Special Publication 15
Bretz JH (1969) The Lake Missoula floods and the Channeled Scabland. J Geol 77:505
Bretz JH, Smith HTU, Neff GE (1956) Channeled Scabland of Washington: new data and interpretations. Geol Soc Am Bull 67:957–1049
Broecker WS, Denton GH (1989) The role of ocean–atmosphere reorganizations in glacial cycles. Geochim Cosmochim Acta 53:2465–2501
Brown K, McIntosh JC, Baker VR, Gosch D (2010) Isotopically-depleted late Pleistocene groundwater in Columbia River Basalt aquifers: evidence for recharge of Glacial Lake Missoula floodwaters? Geophys Res Lett 37:L21402. https://doi.org/10.1029/2010GL044992
Brunner CA, Normark WR, Zuffa GG et al (1999) Sedimentary record of late Wisconsin cataclysmic floods from the Columbia River. Geology 27:463–466
Carling PA, Kirkbride AD, Parnachov S et al (2002) Late Quaternary catastrophic flooding in the Altai Mountains of south-central Siberia: a synoptic overview and introduction to flood deposit sedimentology. In: Martini IP, Baker VR, Garzon G (eds) Flood and megaflood processes and deposits: recent and ancient examples. International Association of Sedimentologists Special Publication 32, Oxford, pp 17–35
Carling P, Villanueva I, Herget J et al (2010) Unsteady 1D and 2D hydraulic models with ice dam break for Quaternary megaflood, Altai Mountains, southern Siberia. Global Planet Change 70:24–34
Carrivick JL, Russell AJ, Tweed TS (2004) Geomorphological evidence for jokulhlaups from Kverkfjoll volcano, Iceland. Geomorphology 63:81–102
Clarke GKC, Mathews WH, Pack RT (1984) Outburst floods from glacial Lake Missoula. Quat Res 22: 289–299
Clarke G, Leverington D, Teller J, Dyke A (2003) Superlakes, megafloods, and abrupt climate change. Science 301:922–923
Clarke GKC, Leverington DW, Teller JT et al (2004) Paleohydraulics of the last outburst flood from Glacial Lake Agassiz and the 8200 BP cold event. Quat Sci Rev 23:389–407
Craig RG (1987) Dynamics of a Missoula flood. In: Mayer L, Nash D (eds) Catastrophic flooding. Allen and Unwin, London, pp 305–332
Dahl R (1965) Plastically sculptured detail forms on rock surfaces in northern Nordland, Norway. Geogr Ann 47:3–140
Denlinger RP, O'Connell DRH (2010) Simulations of cataclysmic outburst floods from Pleistocene glacial Lake Missoula. Geol Soc Am Bull 122:678–689
Denton GH, Sugden DE (2005) Meltwater features that suggest Miocene icesheet overriding of the Transantarctic Mountains in Victoria Land, Antarctica. Geogr Ann 87A:1–19
Dussaillant A, Benito G, Buytaert W et al (2010) Repeated glacial-lake outburst floods in Patagonia: an increasing hazard? Nat Hazards 54:469–481
Ely LL, Baker VR (1985) Reconstructing paleoflood hydrology with slackwater deposits: Verde River, Arizona. Phys Geogr 6:103–126
Garcia-Castellanos D, Estrada F, Jimenez-Munt I et al (2009) Catastrophic flood of the Mediterranean after the Messinian salinity crisis. Nature 462:778–781
Gosse JC, Phillips FM (2001) Terrestrial in situ cosmogenic nuclides: theory and application. Quat Sci Rev 20:1475–1560
Griggs GB, Kulm LD, Waters AC, Fowler GA (1970) Deep-sea gravels from Cascadia Channel. J Geol 78:611–619s, G.B
Grosswald MG (1980) Lake Weichselian Ice Sheet of northern Eurasia. Quat Res 13:1–32
Grosswald MG (1998) New approach to the ice age paleohydrology of northern Eurasia. In: Benito G, Baker VR, Gregory KJ (eds) Palaeohydrology and environmental change. Wiley, New York, pp 199–214
Grosswald MG (1999) Cataclysmic Megafloods in Eurasia and the polar ice sheets. Scientific World, Moscow (in Russian)
Grosswald MG, Rudoy AN (1996) Quaternary glacier dammed lakes in the mountains of Siberia. Polar Geogr 20:180–198
Grosswald MG, Kuhle M, Fastook JL (1994) Würm glaciation of Lake Issyk-Kul area, Tien Shan Mts:

a case study in glacial history of central Asia. GeoJournal 33:273–310
Gupta S, Collier JS, Palmer-Felgate A et al (2007) Catastrophic flooding origin of shelf valley systems in the English Channel. Nature 448:342–345
Gupta S, Collier JS, Garcia-Moreno D et al (2017) Two-stage opening of the Dover Strait and the origin of island Britain. Nat Commun. https://doi.org/10.1038/ncomms15101
Hanson LG (1970) The origin and development of Moses Coulee and other scabland features on the Waterville Plateau, Washington. PhD dissertation, University of Washington/Seattle
Herget J (2005) Reconstruction of Pleistocene ice-dammed lake outburst floods in the Altai Mountains, Siberia. Geological Society of America Special Paper 386
Kehew AE, Teller JT (1994) History of the late glacial runoff along the southwestern margin of the Laurentide Ice Sheet. Quat Sci Rev 13:859–877
Kehew AE, Lord M, Kozlowski A et al (2009) Proglacial megaflooding along the margins of the Laurentide Ice Sheet. In: Burr DM, Carling PA, Baker VR (eds) Megaflooding on Earth and Mars. Cambridge University Press, Cambridge, pp 104–127
Kochel RC, Baker VR (1982) Paleoflood hydrology. Science 215:353–361
Komar PD (1980) Modes of sediment transport in channelized flows with ramifications to the erosion of Martian outflow channels. Icarus 42:317–329
Komar PD (1998) Cataclysmic floods on Earth and Mars—morphology and hydraulic interpretations. In: Klingeman PC, Beschta RL, Komar PD, Bradley JB (eds) Gravel-Bed rivers in the environment. Water Resources Publications, Highlands Ranch, Colorado, pp 677–704
Komatsu G, Miyamoto H, Ito K, Tosaka H, Tokunaga T (2000) Back to Bretz? Comment. Geology 28:573–574
Komatsu G, Arzhannikov SG, Gillespie AR et al (2009) Quaternary paleolake formation and cataclysmic flooding along the upper Yenisei River. Geomorphology 104:143–164
Komatsu G, Baker VR, Arzhannikov SG et al (2016) Late Quaternary catastrophic flooding related to drainage reorganization and paleolake formation in northern Eurasia. A history of alternative hypotheses and indications for future research. Int Geol Rev 58:1693–1722
Krinner G, Mangerud J, Jakobsson M et al (2004) Enhanced ice sheet growth in Eurasia owing to adjacent ice-dammed lakes. Nature 427:429–432
Lesemann J-E, Brennand TA (2009) Regional reconstruction of subglacial hydrology and glaciodynamic behaviour along the southern margin of the Cordilleran Ice Sheet in British Columbia, Canada and northern Washington State, USA. Quat Sci Rev 28:2420–2444
Leverington D, Mann JD, Teller JT (2002) Changes in the bathymetry and volume of glacial Lake Agassiz between 9200 and 7700 14C yr BP. Quat Res 57:244–252
Lewis AR, Marchant DR, Kowalewski DE et al (2006) The age and origin of the Labyrinth, western Dry Valleys, Antarctica: evidence for extensive middle Miocene subglacial floods and freshwater discharge to the Southern Ocean. Geology 34:513–516
Liu T, Baker VR (2018) Hydraulic modeling of megaflooding using terrestrial and Martian DEMs. In: Geomorphometry conference proceedings, issue 27107v1, Boulder, Colorado. https://doi.org/10.7287/peerj.preprints
Livingstone SJ, Clark CD, Tarasov L (2013) Modelling North American palaeo-subglacial lake drainage pathways. Earth Planet Sci Lett 375:13–33
Lopes C, Mix AC (2009) Pleistocene megafloods in the northeast Pacific. Geology 37:79–92
Mangerud J, Astakhov V, Jakobsson M et al (2001) Huge ice-age lakes in Russia. J Quat Res 16:773–777
Margold M, Jansen JD, Codilean AT et al (2018) Repeated megafloods from the Eurasian interior to the Arctic Ocean over the past 60,000 years. Quat Sci Rev 187:41–61
Micallef A, Camerlenghi A, Garcia-Castellanos D et al (2018) Evidence of the Zanclean megaflood in the eastern Mediterranean Basin. Nat Sci Rep. https://doi.org/10.1038/s41598-018-19446-3
Miyamoto H, Itoh K, Komatsu G et al (2006) Numerical simulations of large-scale cataclysmic floodwater: a simple depth-averaged model and an illustrative application. Geomorphology 76:179–192
Miyamoto H, Komatsu G, Baker VR et al (2007) Cataclysmic scabland flooding: insights from a simple depth-averaged numerical model. Environ Model Softw 22(10):1400–1408
Munro-Stasiuk MJ, Shaw J, Sjorgren DB et al (2009) The morphology and sedimentology of landforms created by subglacial megafloods. In: Burr DM, Carling PA, Baker VR (eds) Megaflooding on Earth and Mars. Cambridge University Press, Cambridge, pp 78–103
Normark WR, Reid JA (2003) Extensive deposits on the Pacific Plate from late Pleistocene North-American glacial lake bursts. J Geol 111:617–637
O'Connor JE (1993) Hydrology, hydraulics and sediment transport of Pleistocene Lake Bonneville flooding on the Snake River, Idaho. Geological Society of America Special Paper 274
O'Connor JE, Baker VR (1992) Magnitudes and implications of peak discharges from glacial Lake Missoula. Geol Soc Am Bull 104:267–279
Pacifici A (2009) The Argentinean Patagonia and the Martian landscape. Planet Space Sci 57:571–578
Panin A, Astakhov V, Komatsu G et al (in press) Late Quaternary drainage diversions and outburst floods in North Eurasian plains. In: Carling PR, Baker VR, Herget J (eds) Megaflooding on Earth: a global perspective. Earth-Science Reviews Special Volume
Pardee JT (1942) Unusual currents in glacial Lake Missoula. Geol Soc Am Bull 53:1569–1600

Richardson K, Carling PA (2005) A typology of sculpted forms in open bedrock channels. Geological Society of America Special Paper 392

Rittenauor TM (2008) Luminescence dating of fluvial deposits: applications to geomorphic, palaeoseismic and archaeological research. Boreas 37:613–635

Rudoy AN, Baker VR (1993) Sedimentary effects of cataclysmic late Pleistocene glacial outburst flooding, Altay Mountains, Siberia. Sediment Geol 85:53–62

Ryan WBF, Pitman WC, Major CO et al (1997) Abrupt drowning of the Black Sea shelf. Marine Geol 138:119–126

Ryan WBF, Major CO, Lericolais G et al (2003) Catastrophic flooding of the Black Sea. Ann Rev Earth Planet Sci 31:525–554

Shaw J (1983) Drumlin formation related to inverted meltwater erosion marks. J Glaciol 29:461–479

Shaw J (1996) A meltwater model for Laurentide subglacial landscapes. In: McCann SB, Ford DC (eds) Geomorphology sans frontieres. Wiley, New York, pp 182–226

Shaw J (2002) The meltwater hypothesis for subglacial landforms. Quat Int 90:5–22

Shaw J, Pugin A, Young RR (2008) A meltwater origin for Antarctic shelf bedforms with special attention to megalineations. Geomorphology 102:364–375

Smith AJ (1985) A catastrophic origin for the palaeovalley system of the eastern English Channel. Marine Geol 64:65–75

Smith LN (2006) Stratigraphic evidence for multiple drainings of Glacial lake Missoula along the Clark Fork River, Montana, USA. Quat Res 66:311–322

Teller JT, Leverington DW, Mann JD (2002) Freshwater outbursts to the oceans from glacial Lake Agassiz and their role in climate change during the last deglaciation. Quat Sci Rev 21:879–887

Tinkler KJ, Wohl EE (eds) (1998) Rivers over rock: fluvial processes in bedrock channels. American Geophysical Union Monograph 107

Tomasson H (1996) The jökulhlaup from Katla in 1918. Ann Glaciol 22:249–254

Toucanne S, Zaragosi S, Bourillet JF et al (2009) A 1.2 Ma record of glaciation and fluvial discharge from the west European Atlantic margin. Quat Sci Rev 28:2974–2981

Waitt RB (1985) Case for periodic, colossal jÖkulhlaups from Pleistocene glacial Lake Missoula. Geol Soc Am Bull 96:1271–1286

Waitt RB (2016) Megafloods and the Clovis cache at Wenatchee, Washington. Quat Res 85:430–444

Whipple KX, Hancock GS, Anderson RS (2000) River incision into bedrock: mechanics and relative efficacy of plucking, abrasion and cavitation. Geol Soc Am Bull 112:490–503

Yanchilina AG, Bryan WBF, McManus JF et al (2017) Compilation of geophysical, geochronological, and geochemical evidence indicates a rapid Mediterranean-derived submergence of the Black Sea's shelf and subsequent substantial salinification in the early Holocene. Marine Geol 383:14–34

Zuffa GG, Normark WR, Serra F et al (2000) Turbidite megabeds in an oceanic rift valley recording jÖkulhlaups of late Pleistocene glacial lakes of the western U. S. J Geol 108:253–274

2 Flooding Northern Germany: Impacts and Magnitudes of Middle Pleistocene Glacial Lake-Outburst Floods

Jutta Winsemann and Jörg Lang

Abstract

The major objective of this study is to summarise the routing and impact of lake-outburst floods along the south-western margin of the Middle Pleistocene (Saalian) Fennoscandian ice sheet. We provide an overview about the spatial and temporal evolution and drainage history of ice-dammed lakes in northern Germany. The repeated drainage of these ice-dammed lakes contributed to the destabilisation of the ice margin and triggered ice-streaming and/or local re-advances. Major flood-related channels became part of the ice-marginal drainage system during the decay of the Saalian ice sheets. The most proximal lake-outburst flood drainage routes are characterised by deep plunge pools, channels, megaflutes, scour pools and streamlined hills cut into Pleistocene deposits and Cenozoic and Mesozoic bedrock. Depositional features include large sand and gravel bars and fields of sandy bedforms deposited by supercritical to subcritical flows. The clast composition of bars commonly indicates a strong reworking and redeposition of local fluvial and colluvial material, partly rich in mammoth bones. To quantify flow characteristics during glacial lake-outburst floods, 2D hydraulic simulations were conducted for different ice-margin configurations and flood hydrographs. Subsequently, the model outcomes were compared with the sedimentological and geomorphological evidence for the lake-drainage events in order to estimate the most likely flood pathways, the impact of the flood on erosion, sediment distribution and post-glacial landscape evolution.

Keywords

Northern Germany · Middle Pleistocene · Glacial lakes · Lake-outburst floods

2.1 Introduction

Glacial lake-outburst floods are commonly much larger than river floods and have the capacity to radically modify landscapes, including cutting deep channels and creating new fluvial drainage courses. Most of the described field examples of glacial lake-outburst floods are from the Late Pleistocene or Holocene, where flood-related landforms are still well preserved in the landscape and are not covered by thick younger

J. Winsemann (✉) · J. Lang
Leibniz Universität Hannover, Institut für Geologie, Callinstr. 30, 30167 Hannover, Germany
e-mail: winsemann@geowi.uni-hannover.de

J. Lang
e-mail: lang@geowi.uni-hannover.de

J. Herget and A. Fontana (eds.), *Palaeohydrology*, Geography of the Physical Environment,
https://doi.org/10.1007/978-3-030-23315-0_2

sediments. The best documented examples come from north-west America (Kehew and Lord 1986; Smith 1993; Teller et al. 2002; Baker 2009; Murton et al. 2010; Beeson et al. 2017; Smith 2017), Siberia (Rudoy 2002; Herget 2005; Carling et al. 2002, 2009c; Mangerud et al. 2004; Komatsu et al. 2009; Margold et al. 2011, 2018; Bohorquez et al. 2015), Iceland (Alho et al. 2005; Russell et al. 2006; Björnsson 2009; Carrivick 2007, 2009; Duller et al. 2008) and Greenland (Russell 2009).

In contrast, well-documented field examples from older Pleistocene glaciations are sparse. The longer-term post-glacial erosion and deposition often destroy the geomorphological evidence for large flood events, and older lake-outburst floods have to be reconstructed from marine bathymetric and seismic data (Gupta et al. 2007, 2017; Collier et al. 2015), borehole data (Meinsen et al. 2011) or depositional features that are preserved in sheltered areas along the flood pathways (Froese et al. 2003; Marren and Schuh 2009; Lang and Winsemann 2013; Winsemann et al. 2016; Lang et al. 2019).

Besides the enormous effects of glacial lake-outburst floods on the subsequent landscape and drainage evolution, ice-dammed lakes may exert an important control on ice-sheet dynamics by accelerating the ice flow and the loss of ice mass, causing a partial decoupling from climate trends (Stokes and Clark 2004; Winsborrow et al. 2010; Carrivick and Tweed 2013; Perkins and Brennand 2015; Sejrup et al. 2016). Ice streams may be triggered by the effects of proglacial lakes on glacier dynamics (Stokes and Clark 2003, 2004). The removal of large ice-masses during glacial lake-outburst floods will further destabilise the ice margin, trigger local re-advances and finally contribute to the decay of an ice sheet (Stokes and Clark 2004; Meinsen et al. 2011; Sejrup et al. 2016; Winsemann et al. 2011a, b, 2016; Lang et al. 2018). Furthermore, ice-dammed lakes within river valleys will raise the base level of the river and allow for the deposition of thick fluvial successions (Winsemann et al. 2015).

2.2 Middle Pleistocene Glaciations and Related Ice-Dammed Lakes in Northern Central Europe

During the Middle Pleistocene Elsterian and Saalian glaciations, several advances of the Fennoscandian ice sheets reached far into northern central Europe (Fig. 2.1). From the Elsterian glaciation, two major ice advances are known, which advanced to approximately the same maximum position and probably occurred during Marine Isotope Stages, MIS 12 and MIS 10 (Eissmann 2002; Gibbard and Cohen 2008; Litt et al. 2007; Ehlers et al. 2011; Marks 2011; Böse et al. 2012; Lang et al. 2012; Lee et al. 2012; Roskosch et al. 2015).

During the Saalian glaciation, three major ice advances occurred (Eissmann 2002; Litt et al. 2007; Ehlers et al. 2011; Marks 2011, 2018; Roskosch et al. 2015; Lang et al. 2018). The maximum extent of the Saalian ice cover in the Netherlands and Germany was reached during the older Saalian Drenthe glaciation, while the middle and younger Saalian Warthe glaciation had a lesser maximum extent (Ehlers et al. 2011; Laban and van der Meer 2011). Three substages can be distinguished for the older Saalian Drenthe glaciation, which differ in ice-flow direction and clast composition (Eissmann 2002; Skupin et al. 1993, 2003; Skupin and Zandstra 2010; Ehlers et al. 2011; Lang et al. 2018). In Poland, the Saalian maximum ice-sheet limit was similar or even less extensive than during the subsequent Saalian Warthe ice advances (Marks et al. 2018).

All these Saalian ice advances are commonly correlated with MIS 6 (Litt et al. 2007; Ehlers et al. 2011; Lang et al. 2018; Lauer and Weiss 2018). Luminescence ages from ice-marginal deposits of the older Saalian Drenthe advance range from 196 ± 19 to 157 ± 16 ka (Busschers et al. 2008; Roskosch et al. 2015; Winsemann et al. 2015; Lang et al. 2018) and from 155 ± 21 to 130 ± 17 ka for the middle and younger Saalian (Warthe) ice advances (Lüthgens et al. 2010; Kenzler et al. 2017). However, there is

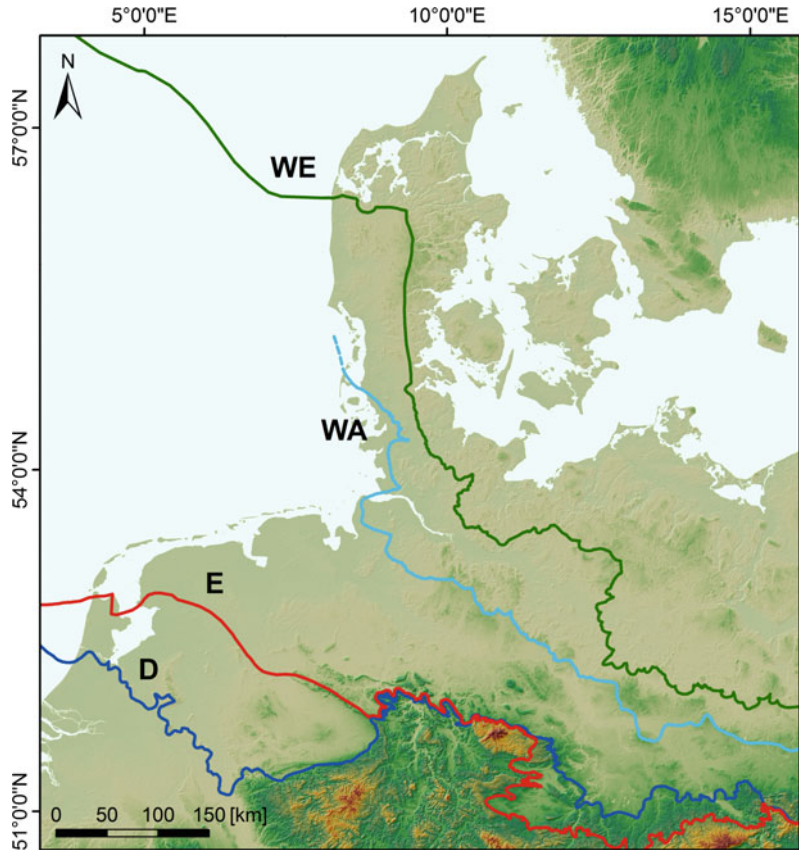

Fig. 2.1 Location of the study area in northern Germany, showing the maximum extent of the Middle Pleistocene Elsterian and Saalian ice sheets in Northern Central Europe. E: Elsterian ice margin. D: Saalian Drenthe ice margin. WA: Saalian Warthe ice margin. WE: Weichselian ice-margin. From Winsemann et al. (2011b)

also evidence of an extensive earlier Saalian ice advance that may have occurred during MIS 8 or early MIS 6 (Beets et al. 2005; Hall and Migoń 2010; Houmark-Nielsen 2011; Laban and van der Meer 2011; Marks 2011; Kars et al. 2012; Roskosch et al. 2015).

The blocking of the north-western river drainage led to the repeated formation of numerous ice-dammed lakes along the south-western margin of the Fennoscandian ice sheets. However, the existence and size of these glacial lakes have been controversially discussed for a long time, and various palaeogeographic reconstructions have been proposed. This long-term debate reflects problems recognising older Pleistocene lakes in steeper terrains. Although shoreline features have been reported from Late Pleistocene high-relief lake areas (e.g. Carling et al. 2002; Johnsen and Brennand 2006; Perkins and Brennand 2015; Rosenwinkel et al. 2017; Margold et al. 2018), shoreline features may be rapidly eroded by subsequent glacial, post-glacial and periglacial processes and later human modification (e.g. Colman et al. 1994; LaRoque et al. 2003). Therefore, the mapping of shoreline features does not work well in older lake systems. Lake reconstructions based on fine-grained lake-bottom sediments, which accumulate mainly in the deeper part of a lake basin, will commonly underestimate the size and volume of glacial lakes (e.g. Feldmann 2002; Eissmann 2002; Junge 1998; Junge et al. 1999). The extent and derivative lake-level curves of glacial lakes must therefore be reconstructed from lake-overspill channels and delta foreset–topset transitions, which together give the best estimates (e.g. Thome 1983; Herget 1998; LaRoque et al. 2003; Winsemann et al. 2007, 2011a, b, 2018; Perkins and Brennand 2015; Lang et al. 2018).

2.2.1 Palaeogeographic Reconstructions of Middle Pleistocene Ice-Dammed Lakes in Northern Germany and the Southern North Sea Basin

The best database exists for the ice-dammed lakes that formed along the older Saalian Drenthe ice sheet. Examples are documented from the southern North Sea Basin (Gibbard 2007; Busschers et al. 2008; Cohen et al. 2017), the Netherlands (Beets and Beets 2003; Busschers et al. 2008; Laban and van der Meer 2011), Germany (Eissmann 2002; Thome 1983; Klostermann 1992; Herget 1998; Junge 1998; Junge et al. 1999; Winsemann et al. 2007, 2009, 2011a, b, 2016; Meinsen et al. 2011; Roskosch et al. 2015; Lang et al. 2018), Czech Republic (Hanáček et al. 2018) and Poland (Marks 2011; Salamon et al. 2013; Marks et al. 2018). These glaciolacustrine deposits are commonly well dated and comprise fine-grained lake-bottom sediments, subaqueous ice-contact fans and (ice-marginal) deltas. Ground-penetrating radar and shear-wave seismic surveys allow for the reconstruction of the larger-scale depositional architecture of ice-marginal systems and the subsequent derivation of lake-level curves (e.g. Winsemann et al. 2009, 2011a, 2018; Roskosch et al. 2015).

At the north-western margin of the study area, the North Sea Lake (Fig. 2.2a) formed in the southern North Sea Basin between the ice margin and a palaeo-high in the Strait of Dover (Gibbard 2007; Peeters et al. 2015; De Clercq et al. 2018). This extensive lake had a lake level of ~5 m a.s.l. (Busschers et al. 2008; Cohen et al. 2017) and an extent of ~53,000 km^2. The exact water volume is not known but must have exceeded 250 km^3. In northern Germany, the maximum ice advance led to the storage of up to 265 km^3 of water in several lakes confined to river valleys (Meinsen et al. 2011; Winsemann et al. 2007, 2009, 2011a, b; Lang et al. 2018). The largest of these lakes were the Münsterland Lake, the Weser Lake, the Leine Lake and the Saale-Unstrut Lake, while numerous smaller lakes formed in river valleys along the ice margin in central and eastern Germany (Fig. 2.2a, b). Lake levels were controlled by the height of bedrock-overspill channels and commonly reached ~190–200 m a.s.l. Very high initial lake levels are recorded from the maximum ice advance in the Münsterland Embayment (~354–365 m a.s.l., Herget 1998; Meinsen et al. 2011) and at the northern margin of the Harz Mountains (300–360 m a.s.l., Pilger et al. 1991; Lang et al. 2018). The retreat of the ice margin changed the lake configuration and commonly led to an increase in lake area and volume and a connection of ice-dammed lakes via overspill channels (Meinsen et al. 2011; Winsemann et al. 2011b, 2016; Lang et al. 2018). During this stage, the lake levels ranged between ~115 and ~200 a.s.l. (Fig. 2.2b). The successive opening of lake-overspill channels eventually led to the westward and north-westward drainage of the lakes (Fig. 2.2b–d). Catastrophic lake-drainage events occurred when large overspills were suddenly opened (Meinsen et al. 2011; Winsemann et al. 2011a, 2016; Lang et al. 2018, 2019).

In contrast, the size and volume of Elsterian glacial lakes are less well constraint, and potential lake sediments are poorly dated. Examples of ice-dammed lakes are documented from the southern North Sea Basin and the Netherlands (Smith 1985; Gibbard 2007; Murton and Murton 2012; Cohen et al. 2014, 2017) and Germany (Thome 1983; Klostermann 1992; Junge 1998; Eissmann 2002; Roskosch et al. 2015). Thome (1998) proposed the existence of larger glacial lakes in the upper Weser and Leine Valleys. He argued that lake levels must have been up to 300 m a.s.l., controlled by the altitudes of potential outlet channels. However, in north-western Germany, the Elsterian ice margin most probably did not reach as far south-westward as the Saalian Drenthe ice sheet (Fig. 2.1). Therefore, it is not very likely that such large lakes were dammed in the upper Weser and Leine Valleys. There is evidence that the upper Leine Valley was dammed twice during the two Elsterian ice advances. Based on foreset-topset

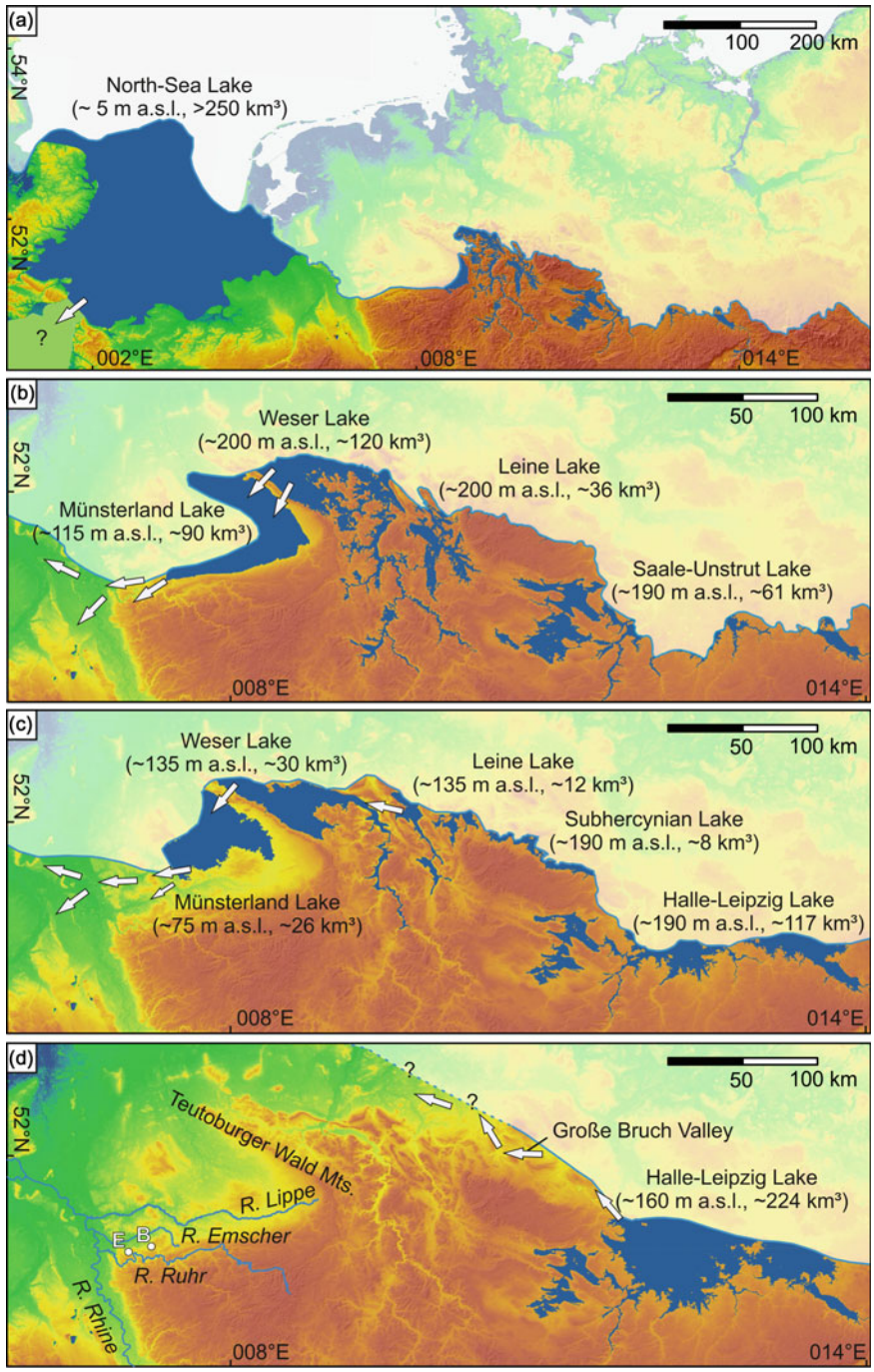

Fig. 2.2 Palaeogeographic reconstruction of ice-dammed lakes during the first older Saalian ice advance (compiled and modified from Busschers et al. 2008; Meinsen et al. 2011; Winsemann et al. 2007, 2009, 2011a, b, 2016; Cohen et al. 2017; Lang et al. 2018). **a** Maximum ice-sheet extent. Isolated lakes, restricted to river valleys, attain their maximum lake levels. **b** Early stage of ice-margin retreat. Opening of outlet channels in the Teutoburger Wald Mountains led to the first drainage event of the Weser Lake into the Münsterland Lake, which drained along the Ruhr and Emscher valleys into the Lower Rhine Embayment. **c** Further ice-margin retreat and opening of outlet channels led to the second drainage event of the Weser Lake into the Münsterland Lake. **d** Late stage of ice-margin retreat. While the lakes in the west have already drained, the large Halle-Leipzig Lake has formed in the east (E: Essen, B: Bochum)

transitions of an ice-marginal delta complex, the lake levels must have reached at least ~155 m a.s.l. (Roskosch et al. 2015).

The best evidence for Elsterian ice-dammed lakes comes from the eastern part of the study area. In the Halle-Leipzig area, these lakes probably reached lake levels between 140 and 190 m a.s.l. (Junge 1998; Eissmann 2002), similar to those of the Saalian glaciation (Lang et al. 2018). In the Elbe Valley, a lake-level highstand of up to 240 m a.s.l. may have been reached (Eissmann 2002).

2.3 Lake Drainage

2.3.1 Lake-Outburst Flood-Related Erosional and Depositional Features

Several depositional and erosional features in the Lower Rhine Embayment, the Ruhr Valley, the Lippe Valley, the Münsterland Embayment, the Weser Valley, the Harz Foreland area and Saale Valley indicate the passage of glacial lake-outburst floods, similar to those reported for other flood routes (e.g. Baker 1973; Lord and Kehew 1987; O'Connor 1993; Smith 1993; Manville et al. 1999; Duller et al. 2008; Marren and Schuh 2009; Kataoka 2011). These outburst-flood-related erosional and depositional features were described by Meinsen et al. (2011), Winsemann et al. (2011a), Lang and Winsemann (2013), Winsemann et al. (2016) and Lang et al. (2018, 2019).

The most proximal drainage routes are characterised by deep plunge pools, channels, megaflutes, scour pools and streamlined hills cut into Pleistocene deposits and Cenozoic and Mesozoic bedrock. Depositional features include large sand and gravel bars and fields of sandy bedforms deposited by supercritical to subcritical flows.

Plunge pools, channels, megaflutes, scour pools and streamlined hills

Plunge pools, channels, megaflutes, scour pools and streamlined hills have been identified in front of major overspill channels and along the major flood routes in the Lippe and Ruhr Valleys, the Münsterland Embayment, the Harz foreland area and in the Saale Valley (Fig. 2.3). Meinsen et al. (2011) reconstructed plunge pools, channels, megaflutes and streamlined hills in front of major overspill channels along the Teutoburger Wald Mountains by means of 3D subsurface modelling. Plunge pools are deeply incised into Mesozoic bedrock and are up to 780 m long, 400 m wide and 35 m deep. The expanding flows became rapidly channelised, carving out deep inner channels, and streamlined hills,

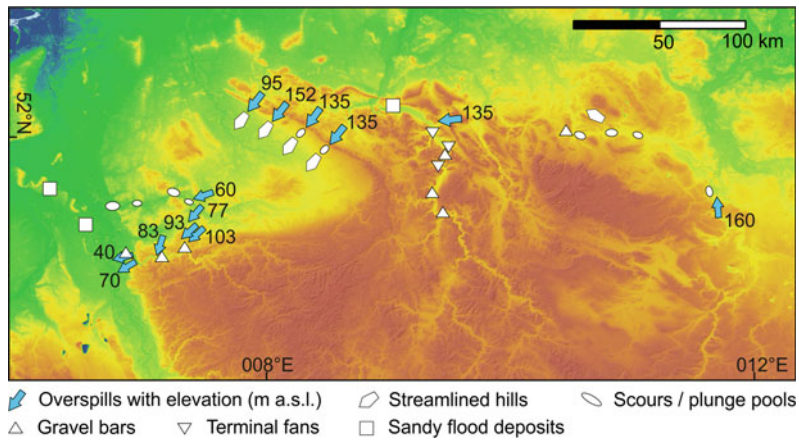

Fig. 2.3 Distribution of erosional and depositional features related to glacial-lake-outburst floods (compiled from Meinsen et al. 2011; Winsemann et al. 2016; Lang et al. 2019)

separated by a shallow channel network, formed in the outer zones. Downflow of major channels up to 4 km long and 12 m deep V-shaped megaflutes occur. The hills in the marginal zones formed under submerged to partly submerged flow conditions. They have quadrilateral to elongate, partly V-shaped chevron-like forms with an average aspect ratio of 1:3.3 and are similar to those described from the Channeled Scablands (Baker 2009) and the Northern Great Plains (Kehew and Lord 1986; Kehew et al. 2009). The fill of these lake-outburst-related channels commonly consists of fine-grained flood deposits, overlain by younger fluvial sediments. Coarse-grained lag deposits can be found at the bases of some large drainage channels (Meinsen et al. 2011), containing granites and cherts, mammal bones, oyster shells and belemnites (Bärtling and Breddin 1931; Jansen and Drozdzewski 1986), pointing to strong flood erosion and reworking of Pleistocene deposits and Cretaceous bedrock. Overspill zones from major flood routes may be indicated by (arrays of) shallow channels, which are 2–5 m deep, and are commonly filled with cross-stratified sand and gravel (Herget 1997, 1998; Grabert et al. 1980; Thome 1983; Winsemann et al. 2016). More elongate scours are 0.5–3.2 km long, 0.5–1.1 km wide, 5–30 m deep and are incised into bedrock or Cenozoic and Pleistocene sediments (Lang et al. 2019). These scours occur along the major flood pathway of the Halle-Leipzig Lake-outburst flood (Figs. 2.2d and 2.3), which most probably also carved out the Große Bruch Valley, an east–west-trending, 40 km long, 2–3 km wide and up to 20 m deep channel in the Harz foreland area, which is incised into Mesozoic bedrock, Palaeogene and Pleistocene deposits (Lang et al. 2018, 2019). The geometry and width-to-depth ratio matches the straight, trench-like valleys incised by glacial lake-outburst floods (cf. Baker 1973; Carling et al. 2009a, b; Curry et al. 2014).

Scour pools occur at the base and at the mouth of major drainage valleys (Fig. 2.3). The largest scour pools occur at the mouth of the drainage valleys in the areas of flow expansion where large-scale turbulence is expected to occur allowing for the intense erosion of bedrock and overlying poorly lithified Palaeogene to Pleistocene sediments. These scour pools are 30–80 m deep, 0.8–5 km wide and 10 km long (Winsemann et al. 2016; Lang et al. 2019) and similar to those reported from areas of rapid flow expansion (Hoyal et al. 2003; Pagliara et al. 2006). The fill of these scours may be coarse- or fine-grained (Winsemann et al. 2016; Lang et al. 2019). Broader erosional zones were mapped from the Emscher and Ruhr mouths where up to 10-km-wide and 5-m-deep scours merge into a southward-trending shallow channel-like feature, which is about 40 km long, 5 m deep and approximately 2–4 km wide (Bolsenkötter 1968).

Smaller-scale scour pools occur at the base of major drainage valleys (e.g. Lippe Valley, Emscher Valley, Große Bruch Valley). These local overdeepenings are commonly 5–20 m deep, approximately 250–400 m wide and 1000–2500 m long. They occur at major constrictions and valley bends. These smaller-sized scour pools have previously been interpreted as subglacial overdeepenings (Bolsenkötter and Hilden 1969; Hilden 1975; Jansen and Drozdzewski 1986; Speetzen 1990; Feldmann et al. 2001; Jansen 2001). However, more likely they represent pool-and-riffle sequences that formed during lake-outburst flooding (Winsemann et al. 2016; Lang et al. 2019). Especially valley bends or larger bedrock obstructions cause intense secondary flow circulations that lead to pool scouring (Carling et al. 2009b).

Gravel bars, terminal fans and deltas

Gravel bars, terminal fans and deltas attributed to glacial-lake-outburst floods have been identified in the Ruhr Valley, the southern Münsterland Embayment, the upper Weser Valley and Harz Foreland area (Fig. 2.3). Bars comprise pendant bars, expansion bars and longitudinal bars, similar to those described from major flood pathways (e.g. O'Connor 1993; Baker 2009; Carling et al. 2009b; Kehew et al. 2009; Marren and Schuh 2009; Kataoka 2011). They are commonly preserved at inner or outer valley bends and in

the lee of major bedrock highs that acted as obstacles. The internal facies architecture of these bars was exposed in some gravel pits, displaying different styles of deposition (Preuss 1975; Jansen 1980; Winsemann et al. 2015, 2016).

Bars are up to 5 km long, 500 m wide and 45 m thick and occur over altitude ranges from ~70 to ~215 m a.s.l. These flood-related bars have previously been interpreted as high fluvial terraces of Early Pleistocene age (Preuss 1975; Lepper 1976; Rohde 1989; Rohde and Thiem 1998) or end moraines, kames and deltas (Bärtling 1913; von der Brelie et al. 1956; Grabert et al. 1980; Jansen 1980; Thome 1983; Pieper 1990). However, these deposits strongly differ from the typical fluvial, meltwater or morainal sediments (Winsemann et al. 2015, 2016; Lang et al. 2018, 2019). They are planar or trough cross-stratified, commonly poorly sorted and contain large locally derived angular blocks, surrounded by a finer-grained matrix with better rounded pebbles or cobbles, indicating high suspension fall-out rates and ineffective sediment sorting during bedload transport (Lord and Kehew 1987; Marren and Schuh 2009; Carling 2013; Winsemann et al. 2016). The clast composition indicates reworking and redeposition of fluvial and colluvial deposits. Isolated erratic blocks with a Scandinavian provenance may have been dumped by icebergs (Winsemann et al. 2016) and/or indicate reworking of glacial deposits.

Flood-related terminal fans and deltas occur at the entrance to broad valley reaches and/or downflow of major lake-overspill channels. High sediment accumulations (20–70 m) at the entrance to broad valley reaches are interpreted as terminal fans or deltas, recording the deposition of upstream eroded sediments during rapid lake drainage (Winsemann et al. 2016). Similar terminal fans have been described from other main flood channels (Manville et al. 1999; Baker 2009; Kataoka 2011). Thick sediment bodies, representing accumulations downflow from major lake-overspill channels, in the Ruhr Valley are mainly preserved in abandoned meander bends. The up to 40-m-thick sediments consist of interbedded silt, sand and gravel with large isolated metre-sized erratic blocks (Jansen 1980; Stehn 1988; Thome 1983).

From two of these former outcrops (near Bochum-Langendreer and Essen-Werden), high concentrations of mammoth bones have been described (Bärtling 1913; Jansen 1980; Jansen and Drozdzewski 1986), pointing to strong reworking of older sediments, and subsequent hydraulic concentration and resedimentation of mammoth remain during the waning stage of flood (Winsemann et al. 2016).

Sandy bedforms

Lake-outburst flood-related sandy bedforms are developed on the Emme delta (Weser Valley). These bedforms have wavelengths of 60–90 m, amplitudes of ~3.8–5 m and were formed by supercritical flows during the second drainage event of the Weser Lake, when the lake level fell from ~135 to ~100 m a.s.l. (Fig. 2.2c). These longer wavelength bedforms may represent either deposits of large aggrading antidunes or net-depositional cyclic steps (Winsemann et al. 2011a, 2018) or transitional bedforms between antidunes and cyclic steps (Kostic 2014; Kostic et al. 2019). The estimated water depth during supercritical bedform formation was approximately 9–14 m (Winsemann et al. 2011a).

Smaller-scale sandy bedforms deposited by aggrading subcritical to supercritical flows in the lee of the Bönninghardt and Reichswald push-moraine ridges in the Lower Rhine Embayment (Fig. 2.3) have been interpreted to represent glacial lake-outburst flood deposits (Lang and Winsemann 2013; Winsemann et al. 2016). Deposits are up to 20 m thick and consist of climbing-ripple trough cross-laminated silt and fine-grained sand, overlain by medium-grained sand and pebbly sand. Bedforms of the coarser-grained sand and pebbly sand include cyclic steps, chutes-and-pools, breaking antidunes and humpback dunes. The frequent soft-sediment deformation structures indicate liquefaction and fluidisation processes, most likely caused by rapid depositional loading. Abundant kettle-hole fills (Klostermann 1992;

Winsemann et al. 2016) indicate the presence of ice blocks in the floodwater (Duller et al. 2008; Marren and Schuh 2009; Carling 2013).

2.3.2 Flood Magnitudes and Flood Simulations

In recent years, hydraulic simulations gave new insights into the flow dynamics of glacial-lake-outburst floods (Clarke et al. 2004; Miyamoto et al. 2006, 2007; Carrivick 2007, 2009; Alho et al. 2010; Carling et al. 2010; Denlinger and O'Connell 2010; Bohorquez et al. 2015; Margold et al. 2018). These modelling studies demonstrate that two-dimensional hydraulic simulations can be successfully utilised for the simulation of flood routing and hydrodynamic processes. However, the pre-flood topography is not entirely represented by a present-day DEM, and glacial lake-outburst floods may have huge erosion potential and sediment loads, which current two-dimensional hydraulic models are unable to simulate. Despite these limitations, two-dimensional simulations allow for coherent modelling of palaeo-flood flow behaviour that can be compared with the geomorphological and sedimentological field record (Miyamoto et al. 2006; Alho et al. 2010; Carling et al. 2010; Bohorquez et al. 2015).

Two previous modelling studies (2D hydraulic simulation, TUFLOW) have been conducted in the study area to reconstruct major flood pathways. Flood routings from the Weser/Münsterland lakes (Fig. 2.2b, c) were modelled by Winsemann et al. (2016). The study of Lang et al. (2019) reconstructs major pathways of the Halle-Leipzig Lake-outburst flood (Fig. 2.2d). The estimated peak discharges range between 183,000 and 338,000 $m^3\ s^{-1}$ (Münsterland Lake, ~60 km^3 drained volume) and 465,000 and 673,000 $m^3\ s^{-1}$(Halle-Leipzig Lake, ~200 km^3 drained volume).

The flow simulations of Winsemann et al. (2016) imply that parts of the Weser/Münsterland-Lake-outburst floods were routed through the Lippe and Emscher Valleys, creating an up to 50-m-high flood wave in the confined valley area. Maximum flow velocities (8–10 m s^{-1}) and bed-shear stress values (up to 1320 N m^{-2}) occurred along the valley constrictions and valley bends able to erode deep scours into poorly lithified Cretaceous and Tertiary bedrock (see also Sect. 2.3.1). When the flood entered the Lower Rhine Embayment, the flow rapidly spread out southwards and westwards, partly overtopping push-moraine ridges at the western Rhine Valley (Fig. 2.3). The flood then eventually flowed into the south-eastern Netherlands and the North Sea Lake.

The integration of these modelling results and field data explain the erosional and sedimentary record along the Lippe Valley (Münsterland Embayment) and the Lower Rhine Embayment (Fig. 2.3). However, the modelled flood wave was not high enough to produce significant overspill via the Emscher Valley into the Ruhr Valley, from where field evidence for a southward lake-outburst flood passage is given by deeply incised overspill channels (Thome 1983) and south- to south-westward-trending bar-like sediment bodies (Winsemann et al. 2016).

2.4 2D Hydraulic Simulation

To refine the understanding of the drainage of the Münsterland/Weser Lakes and close the gaps of the existing reconstructions (Meinsen et al. 2011; Winsemann et al. 2016), a new 2D hydraulic simulation (TUFLOW, Version 2018.03) was conducted. TUFLOW simulates flow over a regular grid of square elements and is based on solving the fully 2D depth-averaged, momentum and continuity equations for free-surface flow (Stelling 1984; TUFLOW 2017). Input parameters for the 2D hydraulic simulation are the basal topography, the flood hydrograph at the outlet and the ice margin. The simulation is based on the modern digital elevation model (EU-DEM; grid size: ~30 m, vertical accuracy: ~3 m) that has been aggregated to a 250 × 250-m-sized grid.

New ice-margin configuration and lake-drainage volume

The extent and volume of the ice-dammed lake, the overspill location and the proximal flood pathway were reconstructed based on the indicators for palaeo-lake levels, ice-marginal positions and flood-related features. The volume of the ice-dammed lake was then calculated based on the intersection of the palaeo-lake level and the modern topography (EU-DEM; grid: ~30 m; vertical accuracy: ~3 m). The exact ice-margin positions during the early stages of ice-margin retreat are poorly constrained and introduce considerable uncertainties concerning possible lake volumes and flood routes. During the first catastrophic outburst flood of the Weser Lake, approximately 90 km^3 of floodwater drained into the Münsterland Lake (Fig. 2.2b). Depending on the water volume of the Münsterland Lake (~50–90 km^3), which is not exactly known for this stage, ~50–90 km^3 of floodwater would have drained southwards into the Ruhr Valley. The overspill channels are located south-east of Bochum (Langendreer and Witten) and south of Essen over an altitude range of ~103 to ~83 m a.s.l. (Figs. 2.2d and 2.3; Thome 1983; Winsemann et al. 2016).

Calculation of the flood hydrographs

The flood hydrograph serves as the upstream boundary condition in the 2D hydraulic simulations, representing the temporal evolution of the flow at the outlet. The hydrographs of (ice) dam-break floods are commonly characterised by a very rapid rise and fall of the discharge, resulting in a triangular hydrograph (O'Connor and Baker 1992; Walder and Costa 1996; Alho et al. 2010; Carling 2013; Herget et al. 2015; Winsemann et al. 2016). In this study, we used a straightforward approach to estimate the flood hydrograph based on the peak discharge. The empirical regression-type formulations by Walder and Costa (1996) and Cenderelli (2000) were used for the calculation of the peak discharges. The estimated peak discharges range from 166,000 to 372,000 $m^3 s^{-1}$ and correspond to a drained lake volume of 50 or 90 km^3, respectively. The hydrographs are characterised by a steep linear rise, reaching the peak discharge after 30 h, and less steep linear fall, reaching zero discharge 100 h later (130 h total model time). Such asymmetrical hydrographs are consistent with the shapes of hydrographs derived from 1D numerical simulation (Denlinger and O'Connell 2010; Winsemann et al. 2016). Although this approach commonly provides a good correlation, the limitation is that flow unsteadiness (e.g. triggered by the complex failure dynamics of ice or earth dams) cannot be taken into account for (Herget et al. 2015). The unsteady flow behaviour of lake-outburst floods will affect the peak discharge and overall shape of the flood hydrograph (Herget et al. 2015; Winsemann et al. 2016), but is difficult to estimate for palaeo-floods. Tests of different hydrographs with different dam breach durations and peak discharges in modelling studies (e.g. Winsemann et al. 2016; Lang et al. 2019) show that the impact of the peak discharge on the maximum flood-water elevation surface is rather low, while the breach duration mainly impacts the arrival time of the maximum flood wave height at a certain location. However, the overall inundation pattern is not severely affected by the hydrograph shape. Noticeable effects on the flood-water elevation surface only occur in confined valley areas (Winsemann et al. 2016).

Reconstruction of the flow routing and hydraulic characteristics

Two simulations were conducted, testing the two different outlet hydrographs. Subsequently, the new model outcomes were compared with the sedimentological and geomorphological evidence for the lake-drainage events in the Ruhr Valley (e.g. Thome 1983; Meinsen et al. 2011; Lang and Winsemann 2013; Winsemann et al. 2016) in order to estimate the most likely flood pathways (Figs. 2.4, 2.5 and 2.6).

The new modelling results for the first Weser/Münsterland-Lake-outburst floods indicate that much of the lake water flowed westwards along the Ruhr Valley into the Lower Rhine

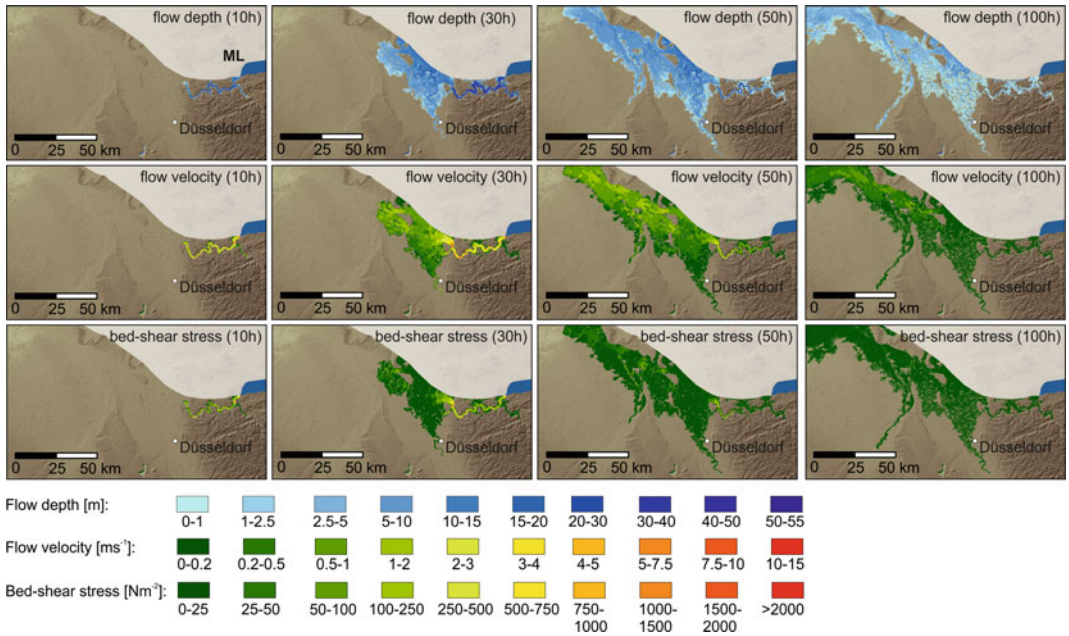

Fig. 2.4 Results of the 2D simulation of the outburst flood from the Weser/Münsterland Lakes (peak discharge is 372,000 m s^{-1}), showing the distribution of flow depth, flow velocity and bed-shear stress (ML: western margin of the Münsterland Lake)

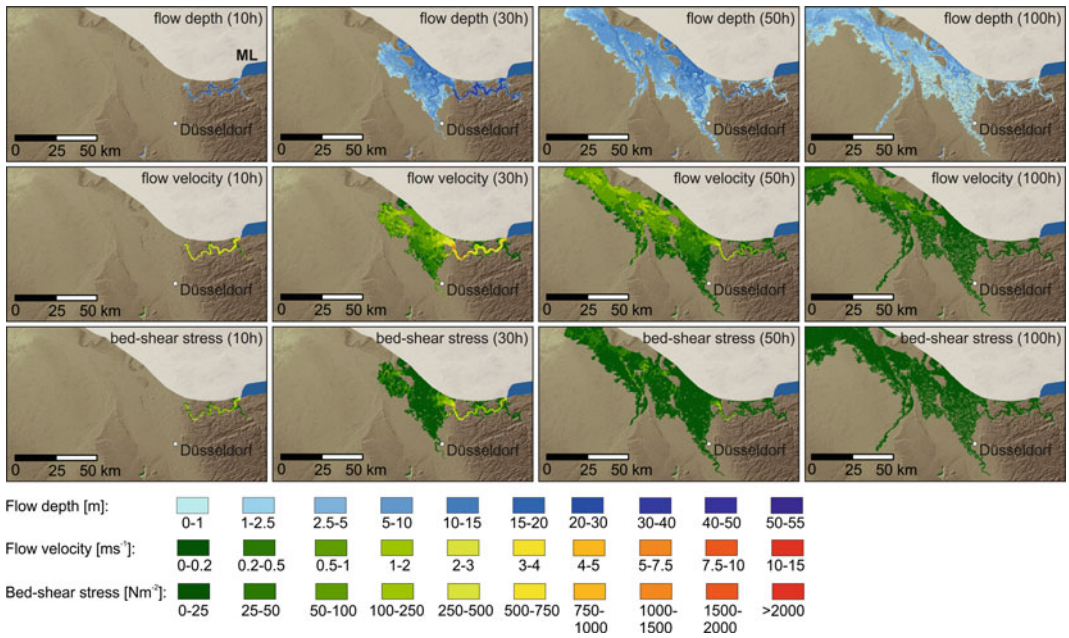

Fig. 2.5 Results of the 2D simulation of the outburst flood from the Weser/Münsterland lakes (peak discharge is 166,000 m s^{-1}), showing the distribution of flow depth, flow velocity and bed-shear stress (ML: western margin of the Münsterland Lake)

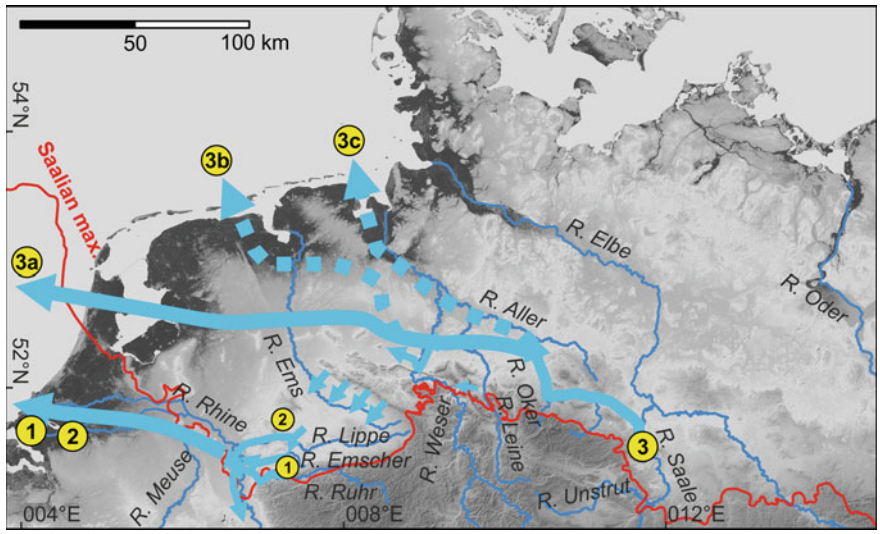

Fig. 2.6 Overview of the reconstructed drainage pathways of Middle Pleistocene glacial-lake-outburst floods. 1 and 2 indicate the drainage routes of successive floods from the Weser and Münsterland lakes. 3 indicates the drainage route of the flood from the Halle-Leipzig Lake. 3a indicates the most likely drainage route along a system of depressions and valleys across north-western Germany and the central Netherlands. 3b and 3c represent alternative (less likely) drainage routes (data are compiled and modified from Meinsen et al. 2011; Winsemann et al. 2016; Lang et al. 2019)

Embayment. Maximum water depths of the flood wave in the Ruhr Valley range from 35 to 52 m (large peak discharge) and 24 to 45 m (small peak discharge), corresponding to water-level elevations of 55–122 m a.s.l. Flow velocities in the narrow Ruhr Valley are generally high and range from 3 to 7 m s^{-1}, with peaks of 8–12 m s^{-1}. Peaks of the bed-shear stress occur at valley constrictions and at valley bends, attaining maximum values of 2000–4000 N m^{-2}, while typical values of the bed-shear stress are around 200–600 N m^{-2}. Near the mouth of the Ruhr Valley, very high values for the flow velocity and bed-shear stress occur, attaining velocities of 4–13 m s^{-1} for the large peak discharge and 4–10 m s^{-1} for the small peak discharge and bed-shear stresses of 800–2000 N m^{-2} for the large peak discharge and 800–1800 N m^{-2} for the small peak discharge. At the mouth of the Ruhr Valley, the outburst flood spreads into the Lower Rhine Embayment, resulting in a significant lowering of the maximum flow depth (6–18 m), velocity (0.5–2.5 m s^{-1}) and bed-shear stress (25–100 N m^{-2}) along the central flow path. Flow conditions are commonly Froude subcritical, because the large flow depths require very high velocities to attain Froude supercritical flow conditions.

Integration of modelling results and field data

The integration of modelling results and field data shows an overall good match, and both estimated discharges are consistent with much of the evidence for deposition along the modelled proximal flood pathway in the Ruhr Valley [e.g. flood-related deposits near Bochum (Witten, Langendreer) and Essen (Kupferdreh, Werden)]. South-west of Essen an array of south-westward-trending shallow channels has been mapped, which are incised into older Pleistocene fluvial and Tertiary deposits. These channels are filled with meltwater deposits, indicating widespread overflow from the Ruhr Valley into the Rhine Valley (Grabert et al. 1980; Thome 1983). The formation of these channels is not consistent with the modelling results. They most probably formed during a later stage of lake drainage, when further ice-margin retreat led to the opening of lower overspill channels located over an

altitude range of ~83 to ~40 m a.s.l. (Fig. 2.3; see also next section).

Near the mouth of the Ruhr Valley, very high values for the modelled bed-shear stress occur in a zone of valley constriction, where the River Ruhr is incised into Cretaceous and Carboniferous bedrock (Figs. 2.5 and 2.6). In this area, a ~10-m-deep scour is incised into the Carboniferous bedrock (Jansen and Drozdzewski 1986). This comparatively shallow depth (compared to the deep scours at the Lippe mouth, incised into unconsolidated Pleistocene and Tertiary deposits) may relate to the much higher resistance and low erodibility of the Carboniferous bedrock. The mapped wide (10 km) and shallow (5 m) erosional zones in front of the Ruhr and Emscher mouths (Bolsenkötter and Hilden 1969) are consistent with the modelling results, which imply a significant lowering of the flow velocity and bed-shear stress.

Lake drainage during further ice-margin retreat

During further ice-margin retreat, much of the floodwater (~20 km^3) was probably routed through the Emscher Valley. Near Essen-Dellwig, coarse-grained lag deposits, rich in granites, cherts, mammal bones, oyster shells and belemnites, occur at the base of the Emscher valley (Jansen and Drozdzewski 1986) and indicate strong flood erosion and reworking of older Pleistocene deposits and Cretaceous bedrock. These coarse-grained lag deposits are overlain by fine-grained sediments (Bärtling and Breddin 1931; Jansen and Drozdzewski 1986), probably deposited during the waning stage of flood (cf. Meinsen et al. 2011; Winsemann et al. 2016).

Approximately 26 km^3 of water remained in the Münsterland Lake (Fig. 2.2c). During the second drainage event of the Weser Lake, about 20 km^3 of water was released into the Münsterland Lake. This outburst event destabilised the Münsterland ice-lobe and triggered the opening of an overspill channel, located in the central Münsterland Embayment at an altitude of ~60 m a.s.l. (Fig. 2.2c). As a consequence, the Münsterland Lake completely drained through the Stever and Lippe Valleys towards the west, releasing approximately 50 km^3 of water (Winsemann et al. 2016). Evidence for a drainage through the Stever valley into the Lippe Valley is given by the presence of up to 30-m-deep scours along the Stever Valley (Bolsenkötter and Hilden 1969; Braun and Thiermann 1975) and (hanging) channels, which are incised into poorly lithified Upper Cretaceous marls and cannot be tied to a river system (Herget 1997; Winsemann et al. 2016). The subsequent redirection of the River Stever (Speetzen 1990) was probably a response to glacial lake-outburst flood erosion (Winsemann et al. 2016).

During this and the previous drainage event of the Münsterland/Weser lakes, the push-moraine ridges in the Lower Rhine Embayment were truncated and partly denudated (Meinsen et al. 2011; Winsemann et al. 2016).

2.5 Impact of Middle Pleistocene Lake-Outburst Floods on the Evolution of Ice-Marginal Valleys and Post-glacial Fluvial Systems

The repeated lake-outburst floods from the Middle Pleistocene Elsterian and Saalian ice-dammed lakes most probably impacted the meltwater-drainage systems and the post-glacial fluvial evolution. Along the proximal flood pathways, deep channels (e.g. Große Bruch Valley) were carved out and valley meander bends (Ruhr Valley, Lippe Valley, Weser Valley) were cut off, which partly led to a post-glacial redirection of tributary rivers (e.g. River Stever, River Saale).

However, these effects are difficult to estimate for the distal flood pathways, where the flood waves rapidly spread out and the use of the present-day DEM for the flow simulations might affect the modelled flood routing and inundation area, because it does not entirely represent the pre-flood topography.

It is likely that in the south-eastern Netherlands, the Weser and Münsterland-Lake-outburst floods were concentrated along the older Saalian Valley of the River Rhine (Busschers et al. 2008; Meinsen et al. 2011; Winsemann et al. 2016). During further ice-margin retreat, the drainage pathways changed and the more eastward-located

glacial lakes drained north-westwards via northern Germany and/or the central Netherlands into the North Sea Lake (Lang et al. 2019). Depending on the ice-margin position and the former regional topography, two alternative drainage routes are likely (Fig. 2.6). The most likely pathway follows an approximately east–west to south-east-to-north-west-trending route through topographic depressions between plateaus of older Saalian till (Lang et al. 2019). These depressions form part of a system of deep glaciotectonic basins, which were excavated during the first Saalian ice-sheet advance (Van den Berg and Beets 1987). Assuming an ice-margin position further north-east, the major flood wave would have followed a more north-westerly pathway. Eventually, the flood entered the ice-dammed lake in the southern North Sea Basin, where the added volume of water may have contributed to the overspill and drainage of the North Sea Lake via the Strait of Dover (cf., Gupta et al. 2017; Lang et al. 2019).

All lake-outburst floods probably initiated channels, which became a crucial part of the ice-marginal drainage system during the decay of the older Saalian ice sheet and subsequent middle and late Saalian re-advances (van den Berg and Beets 1987; Ehlers et al. 2011; Meinsen et al. 2011; Peeters et al. 2016; Winsemann et al. 2016; Lang et al. 2019). However, in general, the meltwater-drainage system during the older Saalian glaciation is poorly constrained and some reconstructions are disputed (Meyer 1983; Speetzen and Zandstra 2009). Potential meltwater-drainage channels occur at the surface and in the subsurface of the Münsterland Embayment, north-western Germany and the central and northern Netherlands and trend E-W to SSE-NNW (Fig. 2.6). Common features of these channels are a large size (width: 10–25 km; depth: 10–70 m), a coarse-grained basal infill, including gravel lags and bone beds, and the dissection of the older Saalian till. The upper channel fills commonly comprise finer-grained flood deposits and fluvial deposits of late Saalian to Holocene age (Ruegg 1983; Ter Wee 1983; Speetzen and Zandstra 2009; Meinsen et al. 2011; Peeters et al. 2015, 2016; Winsemann et al. 2016). However, it is not known to which extent local entrenchment and valley widening occurred during outburst flood passage and to which extent later glaciofluvial/ fluvial erosion modified the valley cross-sectional areas.

2.6 Summary

During the Middle Pleistocene Elsterian and Saalian glaciations, ice-dammed lakes repeatedly formed along the south-western margin of the Fennoscandian ice sheets. These ice-dammed lakes stored more than 500 km^3 of water during the respective maximum ice advances.

Although these ice-dammed lakes were comparatively small, the lakes and glacial lake-outburst floods considerably impacted the stability of the ice margin, the progress of the deglaciation and the post-glacial landscape evolution.

During ice-margin retreat, the lakes successively drained westwards and north-westwards. The individual drainage volumes range between ~20 and ~200 km^3; the estimated peak discharges between 166,000 and 673,000 $m^3\ s^{-1}$.

The repeated drainage of these lakes left a distinctive array of depositional and erosional features. Plunge pools, channels, megaflutes, scour pools, streamlined hills and bar complexes can be found along the major flood routes, and many of these features are similar to those left by the huge Late Pleistocene floods in Northern America and Siberia, although the scale is smaller. The flood-related channel systems subsequently became a crucial part of the ice-marginal drainage system during the decay of the older Saalian ice sheet and subsequent re-advances.

Coarse-grained expansion bars, longitudinal bars and pendant bars are mostly located at the transition between steep and confined segments and wider reaches of the main flood channels. Bar deposits commonly comprise a very large proportion of clasts characteristic for the regional colluvial and fluvial deposits, indicating strong reworking and redeposition of local material. Therefore, these flood-related bars previously

have partly been interpreted as older Pleistocene fluvial terrace deposits. The presence of isolated large erratic blocks points to dumping by icebergs and/or reworking of glacial deposits.

Acknowledgements Parts of this study were funded in the framework of the "Wege in die Forschung" programme by Leibniz Universität Hannover (project title: "Mittelpleistozäne Megafluten in Norddeutschland: Auswirkungen und Magnituden"; Grant No. II-05-2014-05) and by MWK Niedersachsen Project (11.2-76202-17-7/08). Hill-shaded relief maps were produced using Copernicus data and information funded by the European Union (EU-DEM layers).We thank LBEG (Niedersächsisches Landesamt für Bergbau, Energie und Geologie) and GD NRW for providing borehole data and unpublished subsurface maps and Fugro Consult GmbH for providing GeODin software for data management. The manuscript benefited from the discussion with A. Lenz and M. Dölling. Constructive comments by J. Herget and an anonymous reviewer are highly appreciated and helped to improve the manuscript. Many thanks are also due to the owners of the open-pits for permitting us to work on their properties.

References

Alho P, Russell AJ, Carrivick JL et al (2005) Reconstruction of the largest Holocene jökulhlaup within Jökulsá á Fjöllum, NE Iceland. Quat Sci Rev 24:2319–2334

Alho P, Baker VR, Smith LN (2010) Paleohydraulic reconstruction of the largest Glacial Lake Missoula draining(s). Quat Sci Rev 29:3067–3078

Bärtling R (1913) Geologisches Wanderbuch für den Niederrheinisch-Westfälischen Industriebezirk, umfassend das Gebiet vom nördlichen Teil des Rheinischen Schiefergebirges bis zur holländischen Grenze. Enke, Stuttgart

Bärtling R, Breddin H (1931) Erläuterungen zur geologischen Karte von Preußen und benachbarter deutscher Länder 1:25000, Blatt Mühlheim (Ruhr) Nr. 2575. Preußische Geologische Landesanstalt, Berlin

Baker VR (1973) Paleohydrology and sedimentology of Lake Missoula flooding in eastern Washington. Boulder, CO. Geological Society of America Special Paper 144, pp 1–7

Baker VR (2009) Channeled Scabland morphology. In: Burr DM, Carling PA, Baker VR (eds) Megaflooding on Earth and Mars. Cambridge University Press, Cambridge, pp 65–77

Beeson JW, Goldfinger C, Fortin WF (2017) Large-scale modification of submarine geomorphic features on the Cascadia accretionary wedge caused by catastrophic flooding events. Geosphere 13:1713–1728

Beets CJ, Beets DJ (2003) A high resolution stable isotope record of the penultimate deglaciation in lake sediments below the city of Amsterdam, The Netherlands. Quat Sci Rev 22:195–207

Beets DJ, Meijer T, Beets CJ et al (2005) Evidence for a Middle Pleistocene glaciation of MIS 8 age in the southern North Sea. Quat Int 133–134:7–19

Björnsson H (2009) Jökulhlaups in Iceland: sources, release and drainage. In: Burr DM, Carling PA, Baker VR (eds) Megaflooding on Earth and Mars. Cambridge University Press, Cambridge, pp 50–64

Böse M, Lüthgens C, Lee JR et al (2012) Quaternary glaciations of northern Europe. Quat Sci Rev 44:1–25

Bolsenkötter H (1968) Die Quartärbasis der Niederrheinischen Bucht von Düsseldorf bis zur Landesgrenze. Fortsch Geol Rheinland und Westfalen 16, pp 333–338

Bolsenkötter H, Hilden HD (1969) Ein Beitrag zur Talgeschichte der Stever und der unteren Lippe. Fortsch Geol Rheinland und Westfalen 17, pp 47–54

Bohorquez P, Carling PA, Herget J (2015) Dynamic simulation of catastrophic late Pleistocene glacial-lake drainage, Altai Mountains, central Asia. Int Geol Rev 58:1795–1817

Braun FJ, Thiermann A (1975) Erläuterungen zur geologischen Karte von Nordrhein-Westfalen 100000, Blatt C4306 Recklinghausen. Geologisches Landesamt Nordrhein-Westfalen, Krefeld

Busschers FS, Van Balen RT, Cohen KM et al (2008) Response of the Rhine-Meuse fluvial system to Saalian ice-sheet dynamics. Boreas 37:377–398

Carling PA (2013) Freshwater megaflood sedimentation: what can we learn about generic processes? Earth-Sci Rev 125:87–113

Carling PA, Kirkbride, AD, Parnachov S et al (2002) Late Quaternary catastrophic flooding in the Altai mountains of south–central Siberia: a synoptic overview and an introduction to flood deposit sedimentology. In: Martini PI, Baker VR, Garzon G (eds) Flood and megaflood processes and deposits: recent and ancient examples. Special Publication International Association of Sedimentology, vol 32. Blackwell Science, Oxford, pp 17–35

Carling PA, Burr DM, Johnsen TF et al (2009a) A review of open-channel megaflood depositional landforms on Earth and Mars. In: Burr DM, Carling PA, Baker VR (eds) Megaflooding on Earth and Mars. Cambridge University Press, Cambridge, pp 33–49

Carling PA, Herget J, Lanz JK et al (2009b) Channel-scale erosional bedforms in bedrock and in loose granular material: character, processes and implications. In: Burr DM, Carling PA, Baker VR (eds) Megaflooding on Earth and Mars. Cambridge University Press, Cambridge, pp 13–32

Carling PA, Martini IP, Herget J et al (2009c) Megaflood sedimentary valley fill: Altai Mountains, Siberia. In: Burr DM, Carling PA, Baker VR (eds) Megaflooding

on Earth and Mars. Cambridge University Press, Cambridge, pp 243–264

Carling P, Villanueva I, Herget J et al (2010) Unsteady 1-D and 2-D hydraulic models with ice-dam break for Quaternary megafloods, Altai Mountains, southern Siberia. Global Planet Change 70:24–34

Carrivick JL (2007) Hydrodynamics and geomorphic work of jökulhlaups (glacial outburst floods) from Kverkfjöll volcano, Iceland. Hydrol Process 21:725–740

Carrivick JL (2009) Jökulhlaups from Kverkfjöll volcano, Iceland: modelling transient hydraulic phenomena. In: Burr DM, Carling PA, Baker VR (eds) Megaflooding on Earth and Mars. Cambridge University Press, Cambridge, pp 273–289

Carrivick JL, Tweed FS (2013) Proglacial lakes: character, behaviour and geological importance. Quat Sci Rev 78:34–52

Cenderelli DA (2000) Floods from natural and artificial dam failures. In: Wohl EE (ed) Inland flood hazards: human, riparian, and aquatic communities. Cambridge University Press, Cambridge, pp 73–103

Clarke GKC, Leverington DW, Teller JT et al (2004) Paleohydraulics of the last outburst flood from glacial Lake Agassiz and the 8200 BP cold event. Quat Sci Rev 23:389–407

Cohen KM, Gibbard PL, Weerts HJT (2014) North Sea palaeogeographical reconstructions for the last 1 Ma. Neth J Geosci 93:7–29

Cohen KM, Westley K, Erkens G et al (2017) The North Sea. In: Flemming NC, Harff J, Moura D, Burgess A, Bailey GN (eds) Submerged landscapes of the European continental shelf: quaternary palaeoenvironments. Wiley, Chichester, pp 147–186

Collier JS, Oggioni F, Gupta S et al (2015) Streamlined islands and the English Channel megaflood hypothesis. Global Planet Change 135:190–206

Colman SM, Clark JA, Clayton L et al (1994) Deglaciation, lake levels, and meltwater discharge in the Lake Michigan Basin. Quat Sci Rev 13:879–890

Curry BB, Hajic ER, Clark JA et al (2014) The Kankakee torrent and other large meltwater flooding events during the last deglaciation, Illinois, USA. Quat Sci Rev 90:22–36

Denlinger RP, O'Connell DRH (2010) Simulations of cataclysmic outburst floods from Pleistocene Glacial Lake Missoula. Geol Soc Am Bull 122:678–689

De Clercq M, Missiaen T, Wallinga J et al (2018) A well-preserved Eemian incised-valley fill in the southern North Sea Basin, Belgian Continental Shelf-Coastal Plain: Implications for northwest European landscape evolution. Earth Surf Process Land 43:1913–1942

Duller RA, Mountney NP, Russell AJ et al (2008) Architectural analysis of a volcaniclastic jökulhlaup deposit, southern Iceland: sedimentary evidence for supercritical flow. Sedimentology 55:939–964

Eissmann L (2002) Quaternary geology of eastern Germany (Saxony, Saxon-Anhalt, South Brandenburg, Thuringia), type area of Elsterian and Saalian Stages in Europe. Quat Sci Rev 21:1275–1346

Ehlers J, Grube A, Stephan HJ et al (2011) Pleistocene glaciations of North Germany—new results. In: Ehlers J, Gibbard PL, Hughes PD (eds) Quaternary glaciations—extent and chronology: a closer look. Developments in quaternary science, vol 15. Elsevier, Amsterdam, pp 149–162

Feldmann L (2002) Das Quartär zwischen Harz und Allertal mit einem Beitrag zur Landschaftsgeschichte im Tertiär. Clausth Geowiss 1, pp 1–149

Feldmann L, Groetzner JP, Weymann HJ (2001) Zur pleistozänen Geschichte des "Großen Bruch" im nördlichen Harzvorland. Geol Beitr Hannover 2, pp 127–137

Froese DG, Smith DG, Westgate JA et al (2003) Recurring middle Pleistocene outburst floods in east-central Alaska. Quat Res 60:50–62

Gibbard PL (2007) Palaeogeography: Europe cut adrift. Nature 448:259–260

Gibbard P, Cohen KM (2008) Global chronostratigraphical correlation table for the last 2.7 million years. Episodes 31:243–247

Grabert H, Jansen F, Pieper B et al (1980) Erläuterungen zur geologischen Karte 1:100000, Blatt C4706 Düsseldorf-Essen. Geologisches Landesamt Nordrhein-Westfalen, Krefeld

Gupta S, Collier JS, Palmer-Felgate A et al (2007) Catastrophic flooding origin of shelf valley systems in the English Channel. Nature 448:342–346

Gupta S, Collier JS, Garcia-Moreno D et al (2017) Two-stage opening of the Dover Strait and the origin of island Britain. Nat Commun 8:15101

Hall AM, Migoń P (2010) The first stages of erosion by ice sheets: evidence from central Europe. Geomorphology 123:349–363

Hanáček M, Nýlt D, Skácelová Z et al (2018) Sedimentary evidence for an ice-sheet dammed lake in a mountain valley of the Eastern Sudetes, Czechia. Acta Geol Pol 68:107–134

Herget J (1997) Die Flußentwicklung des Lippetals. Bochumer Geograph Arb 62, pp 1–132

Herget J (1998) Temporäre Entwässerungsbahnen am Südrand der Westfälischen Tieflandsbucht – ein Szenario. In: Glatthaar D, Herget J (eds) Physische Geographie und Landeskunde – Festschrift für Herbert Liedtke. Bochumer Geograph Arb Sonderreihe 13, pp 23–30

Herget J (2005) Reconstruction of Pleistocene ice-dammed lake outburst floods in the Altai-Mountains, Siberia. Geological Society of America Special Paper 386, pp 1–118

Herget J, Schütte F, Klosterhalfen A (2015) Empirical modelling of outburst flood hydrographs. Z Geomorphol Supplementary Issues 59:177–198

Hilden HD (1975) Erläuterungen zur hydrogeologischen Karte von Nordrhein-Westfalen 1:100000, Blatt C4306 Recklinghausen. Geologisches Landesamt Nordrhein-Westfalen, Krefeld

Houmark-Nielsen M (2011) Pleistocene glaciations in Denmark: a closer look at chronology, ice dynamics and landforms. In: Ehlers J, Gibbard PL, Hughes PD (eds) Quaternary glaciations—extent and chronology: a closer look. Developments in quaternary science, vol 15. Elsevier, Amsterdam, pp 47–58

Hoyal DCJD, Van Wagoner JC, Adair NL et al (2003) Sedimentation from jets: a depositional model for clastic deposits of all scales and environments. Search and Discovery Article #40082

Jansen F (1980) Erläuterungen zur geologischen Karte von Nordrhein-Westfalen, 1:25000, Blatt 4510 Witten. Geologisches Landesamt Nordrhein-Westfalen, Krefeld

Jansen F (2001) Erläuterungen zur geologischen Karte von Nordrhein-Westfalen 1:25000, Blatt 4305 Wesel. Geologischer Dienst Nordrhein-Westfalen, Krefeld

Jansen F, Drozdzewski G (1986) Erläuterungen zur geologischen Karte von Nordrhein-Westfalen 1:25000, Blatt 4307 Mühlheim an der Ruhr. Geologischer Dienst Nordrhein-Westfalen, Krefeld

Johnsen TF, Brennand TA (2006) The environment in and around ice-dammed lakes in the moderately high relief setting of the southern Canadian Cordillera. Boreas 35:106–125

Junge FW (1998) Die Bändertone Mitteldeutschlands und angrenzender Gebiete. Altenb Naturwiss Forsch 9:1–210

Junge FW, Böttger T, Siegert C (1999) Die Stauseesedimente des Bruckdorfer Horizontes: Ergebnis der Eisrandoszillation des saaleglazialen skandinavischen Inlandeises in Mitteldeutschland. Mauritiana 17:257–276

Kars RH, Busschers FS, Wallinga J (2012) Validating post IR-IRSL dating on K-feldspars through comparison with quartz OSL ages. Quat Geochronol 12:74–86

Kataoka KS (2011) Geomorphic and sedimentary evidence of a gigantic outburst flood from Towada caldera after the 15 ka Towada-Hachinohe ignimbrite eruption, northeast Japan. Geomorphology 125:11–26

Kehew AE, Lord ML (1986) Origin and large-scale erosional features of glacial-lake spillways in the northern Great Plains. Geol Soc Am Bull 97:162–177

Kehew AE, Lord ML, Kozlowski AL et al (2009) Proglacial megaflooding along the margins of the Laurentide Ice Sheet. In: Burr DM, Carling PA, Baker VR (eds) Megaflooding on Earth and Mars. Cambridge University Press, Cambridge, pp 104–127

Kenzler M, Tsukamoto S, Meng S et al (2017) New age constraints from the SW Baltic Sea area–implications for Scandinavian Ice Sheet dynamics and palaeo-environmental conditions during MIS 3 and early MIS 2. Boreas 46:34–52

Komatsu G, Arzhannikov SG, Gillespie AR et al (2009) Quaternary paleolake formation and cataclysmic flooding along the upper Yenisei River. Geomorphology 104:143–164

Kostic S (2014) Upper flow regime bedforms on levees and continental slopes: turbidity current flow dynamics in response to fine-grained sediment waves. Geosphere 10:1094–1103

Kostic S, Casalbore D, Chiocci F et al (2019) Role of upper-flow-regime bedforms emplaced by sediment gravity flows in the evolution of deltas. J Mar Sci Eng 7(1):5

Klostermann J (1992) Das Quartär der Niederrheinischen Bucht - Ablagerungen der letzten Eiszeit am Niederrhein. Geologisches Landesamt Nordrhein-Westfalen, Krefeld

Laban C, van der Meer JJ (2011) Pleistocene glaciation in the Netherlands. In: Ehlers J, Gibbard PL, Hughes PD (eds) Quaternary glaciations—extent and chronology: a closer look. Developments in quaternary science, vol 15. Elsevier, Amsterdam, pp 247–260

Lang J, Winsemann J (2013) Lateral and vertical facies relationships of bedforms deposited by aggrading supercritical flows: from cyclic steps to humpback dunes. Sediment Geol 296:36–54

Lang J, Winsemann J, Steinmetz D et al (2012) The Pleistocene of Schöningen, Germany: a complex tunnel valley fill revealed from 3D subsurface modelling and shear wave seismics. Quat Sci Rev 39:86–105

Lang J, Lauer T, Winsemann J (2018) New age constraints for the Saalian glaciation in northern central Europe: implications for the extent of ice sheets and related proglacial lake systems. Quat Sci Rev 180:240–259

Lang J, Alho P, Kasvi E et al (2019) Impact of Middle Pleistocene (Saalian) glacial lake-outburst floods on the drainage pathways in northern central Europe: Insights from 2D numerical flood simulation. Quat Sci Rev 209:82–99

Lauer T, Weiss M (2018) Timing of the Saalian-and Elsterian glacial cycles and the implications for Middle-Pleistocene hominin presence in central Europe. Sci Rep 8:5111

Lee JR, Busschers FS, Sejrup HP (2012) Pre-Weichselian Quaternary glaciations of the British Isles, The Netherlands, Norway and adjacent marine areas south of 68°N: implications for long-term ice sheet development in northern Europe. Quat Sci Rev 44:213–228

LaRoque A, Dubois JMM, Leblon B (2003) A methodology to reconstruct small and short-lived ice-dammed lakes in the Appalachians of Southern Québec. Quat Int 99–100:59–71

Lepper J (1976) Erläuterungen zur geologischen Karte von Nordrhein-Westfalen 1:25000, Blatt Karlshafen 4322. Geologisches Landesamt Nordrhein-Westfalen, Krefeld

Litt T, Behre KE, Meyer KD, Stephan HJ, Wansa S (2007) Stratigraphische Begriffe für das Quartär des norddeutschen Vereisungsgebietes. E&G Quat Sci J 56:7–65

Lüthgens C, Böse M, Krbetschek M (2010) On the age of the young morainic morphology in the area ascribed to the maximum extent of the Weichselian glaciation in north-eastern Germany. Quat Int 222:72–79

Lord ML, Kehew AE (1987) Sedimentology and paleohydrology of glacial-lake outburst deposits in southeastern Saskatchewan and northwestern North Dakota. Geol Soc Am Bull 99:663–673

Manville V, White JDL, Houghton BF et al (1999) Paleohydrology and sedimentology of a post-1.8 ka breakout flood from intracaldera Lake Taupo, North Island, New Zealand. Geol Soc Am Bull 111:1435–1447

Mangerud J, Jakobsson M, Alexanderson H et al (2004) Ice-dammed lakes and rerouting of the drainage of northern Eurasia during the Last Glaciation. Quat Sci Rev 23:1313–1332

Margold M, Jansson KN, Stroeven AP et al (2011) Glacial Lake Vitim, a 3000-km^3 outburst flood from Siberia to the Arctic Ocean. Quat Res 76:393–396

Margold M, Jansen JD, Codilean AT et al (2018) Repeated megafloods from glacial Lake Vitim, Siberia, to the Arctic Ocean over the past 60,000 years. Quat Sci Rev 187:41–61

Marks L (2011) Quaternary glaciations in Poland. In: Ehlers J, Gibbard PL, Hughes PD (eds) Quaternary glaciations—extent and chronology: a closer look. Developments in quaternary science, vol 15. Elsevier, Amsterdam, pp 299–303

Marks L, Karabanov A, Nitychoruk J et al (2018) Revised limit of the Saalian ice sheet in central Europe. Quat Int 478:59–74

Marren PM, Schuh M (2009) Criteria for identifying jökulhlaups deposits in the sedimentary record. In: Burr DM, Carling PA, Baker VR (eds) Megaflooding on Earth and Mars. Cambridge University Press, Cambridge, pp 225–242

Meinsen J, Winsemann J, Weitkamp A et al (2011) Middle Pleistocene (Saalian) lake outburst floods in the Münsterland Embayment (NW Germany): impacts and magnitudes. Quat Sci Rev 30:2597–2625

Meyer KD (1983) Zur Anlage der Urstromtäler in Niedersachsen. Z Geomorphol NF 27:147–160

Miyamoto H, Ito K, Komatsu G et al (2006) Numerical simulations of large-scale cataclysmic floodwater: a simple depth-averaged model and an illustrative application. Geomorphology 76:179–192

Miyamoto H, Komatsu G, Baker VR et al (2007) Cataclysmic scabland flooding: insights from a simple depth-averaged numerical model. Environ Model Softw 22:1400–1408

Murton DK, Murton JB (2012) Middle and Late Pleistocene glacial lakes of lowland Britain and the southern North Sea Basin. Quat Int 260:115–142

Murton JB, Bateman MD, Dallimore SR et al (2010) Identification of Younger Dryas outburst flood path from Lake Agassiz to the Arctic Ocean. Nature 464:740–743

O'Connor JE (1993) Hydrology, hydraulics, and geomorphology of the Bonneville Flood. Geological Society of America Special Paper 274, pp 1–83

O'Connor JE, Baker VR (1992) Magnitudes and implications of peak discharges from glacial Lake Missoula. Geol Soc Am Bull 104:267–279

Pagliara S, Hager WH, Minor HE (2006) Hydraulics of plane plunge pool scour. J Hydraul Eng 132:450–461

Peeters J, Busschers FS, Stouthamer E (2015) Fluvial evolution of the Rhine during the last interglacial-glacial cycle in the southern North Sea basin: a review and look forward. Quat Int 357:176–188

Peeters J, Busschers FS, Stouthamer E et al (2016) Sedimentary architecture and chronostratigraphy of a late Quaternary incised-valley fill: a case study of the late Middle and Late Pleistocene Rhine system in the Netherlands. Quat Sci Rev 131:211–236

Perkins AJ, Brennand TA (2015) Refining the pattern and style of Cordilleran Ice Sheet retreat: palaeogeography, evolution and implications of lateglacial ice-dammed lake systems on the southern Fraser Plateau, British Columbia, Canada. Boreas 44:319–342

Pieper B (1990) Erläuterungen zur geologischen Karte von Nordrhein-Westfalen 1:25000, Blatt 4508 Essen. Geologisches Landesamt Nordrhein-Westfalen, Krefeld

Pilger A, Mocha P, Petzold B et al (1991) Die nordischen Gletscher am nordwestlichen Harzrand und ihre Stauseen. Clausth Geol Abh 48:1–159

Preuss H (1975) Gliederung und Zusammensetzung der Weserterrassen bei Bodenfelde (mit einer geologischen Kartierung). Mitt Geol Inst Techn Univ Hannover 12, pp 5–49

Rohde P, Thiem W (1998) Die eiszeitliche Weser im heutigen Weser- und Leinetal. In: Feldmann L, Meyer KD (eds) Quartär in Niedersachsen. Exkursionsführer zur Jubiläums-Hauptversammlung der Deutschen Quartärvereinigung in Hannover, Exkursion C. DEUQUA, Hannover, pp 89–153

Rohde P (1989) Elf pleistozäne Sand-Kies-Terrassen der Weser: Erläuterungen eines Gliederungsschemas für das obere Wesertal. Eiszeit Gegenw 39:42–56

Rosenwinkel S, Landgraf A, Schwanghart W et al (2017) Late Pleistocene outburst floods from Issyk Kul, Kyrgyzstan? Earth Surf Process Land 42:1535–1548

Roskosch J, Winsemann J, Polom U et al (2015) Luminescence dating of ice-marginal deposits in northern Germany: evidence for repeated glaciations during the Middle Pleistocene (MIS 12 to MIS 6). Boreas 44:103–126

Russell AJ (2009) Jökulhlaup (ice-dammed lake outburst flood) impact within a valley-confined sandur subject to backwater conditions, Kangerlussuaq, West Greenland. Sediment Geol 215:33–49

Russell AJ, Roberts MJ, Fay H et al (2006) Icelandic jökulhlaup impacts: implications for ice-sheet hydrology, sediment transfer and geomorphology. Geomorphology 75:33–64

Rudoy AN (2002) Glacier-dammed lakes and geological work of glacial superfloods in the Late Pleistocene, Southern Siberia, Altai Mountains. Quat Int 87:119–140

Ruegg GHJ (1983) Glaciofluvial and glaciolacustrine deposits in the Netherlands. In: Ehlers J (ed) Glacial deposits in North-West Europe. AA Balkema, Rotterdam, pp 379–392

Salamon T, Krzyszkowski D, Kowalska A (2013) Development of Pleistocene glaciomarginal lake in the foreland of the Sudetes (SW Poland). Geomorphology 190:1–15

Sejrup HP, Clark CD, Hjelstuen BO (2016) Rapid ice sheet retreat triggered by ice stream debuttressing: evidence from the North Sea. Geology 44:355–358

Skupin K, Zandstra JG (2010) Gletscher der Saale-Kaltzeit am Niederrhein. Untersuchungen zur Petrographie und Leitgeschiebeführung der Stauchmoränen des Niederrheins und deren Anbindung an die Moränen des Münsterlandes. Geologischer Dienst Nordrhein-Westfalen, Krefeld

Skupin K, Speetzen E, Zandstra JG (1993) Die Eiszeit in Nordwestdeutschland. Zur Vereisung der Westfälischen Bucht und angrenzender Gebiete. Geologisches Landesamt Nordrhein-Westfalen, Krefeld

Skupin K, Speetzen E, Zandstra JG (2003) Die Eiszeit in Nordost-Westfalen und angrenzenden Gebieten Niedersachsens. Geologischer Dienst NRW, Krefeld

Smith AJ (1985) A catastrophic origin for the palaeovalley system of the eastern English Channel. Mar Geol 64:65–75

Smith GA (1993) Missoula flood dynamics and magnitudes inferred from sedimentology of slack-water deposits on the Columbia Plateau, Washington. Geol Soc Am Bull 105:77–100

Smith LN (2017) Repeated sedimentation and exposure of glacial Lake Missoula sediments: a lake-level history at Garden Gulch, Montana, USA. Quat Sci Rev 155:114–126

Speetzen E (1990) Die Entwicklung der Flußsysteme in der Westfälischen Bucht (NW-Deutschland) während des Känozoikums. Geol Paläont Westfalen 16:7–25

Speetzen E, Zandstra JG (2009) Elster-und Saale-Vereisung im Weser-Ems-Gebiet und ihre kristallinen Leitgeschiebegesellschaften. Münstersche Forsch Geol Paläont 103, pp 1–113

Stehn O (1988) Erläuterungen zur geologischen Karte von Nordrhein-Westfalen, 1:25000, Blatt 4509 Bochum. Geologisches Landesamt Nordrhein-Westfalen, Krefeld

Stelling GS (1984) On the construction of computational methods for shallow water flow problems. Rijkswaterstaat Com 35, pp 1–226

Stokes CR, Clark CD (2003) The Dubawnt Lake palaeo-ice stream: evidence for dynamic ice sheet behaviour on the Canadian Shield and insights regarding the controls on ice-stream location and vigour. Boreas 32:263–279

Stokes CR, Clark CD (2004) Evolution of late glacial ice-marginal lakes on the northwestern Canadian Shield and their influence on the location of the Dubawnt Lake palaeo-ice stream. Palaeogeogr Palaeoclimatol Palaeoecol 215:155–171

Teller JT, Leverington DW, Mann JD (2002) Freshwater outbursts to the oceans from glacial Lake Agassiz and their role in climatic change during the last deglaciation. Quat Sci Rev 21:879–887

Ter Wee MW (1983) The Saalian glaciation in the northern Netherlands. In: Ehlers J (ed) Glacial deposits in North-West Europe. AA Balkema, Rotterdam, pp 405–412

Thome KN (1983) Gletschererosion und –akkumulation im Münsterland und angrenzenden Gebieten. N Jb Geol Paläont Abh 166:116–138

Thome KN (1998) Einführung in das Quartär: das Zeitalter der Gletscher. Spinger, Berlin

TUFLOW (2017) TUFLOW User Manual. BMT, Brisbane.

Van den Berg MW, Beets DJ (1987) Saalian glacial deposits and morphology in the Netherlands. In: Van der Meer JJM (ed) Tills and glaciotectonics. Balkema, Rotterdam, pp 235–251

Von der Brelie G, Rein U, Klusemann H et al (1956) Pleistozän-profile im Essener Raum. N Jb Geol Paläont Mh 113–132

Walder JS, Costa JE (1996) Outburst floods from glacier-dammed lakes: the effect of mode of lake drainage on flood magnitude. Earth Surf Process Land 21:701–723

Winsborrow MC, Clark CD, Stokes CR (2010) What controls the location of ice streams? Earth-Sci Rev 103:45–59

Winsemann J, Asprion U, Meyer T et al (2007) Facies characteristics of Middle Pleistocene (Saalian) ice-margin subaqueous fan and delta deposits, glacial Lake Leine, NW Germany. Sediment Geol 193:105–129

Winsemann J, Hornung JJ, Meinsen JC et al (2009) Anatomy of a subaqueous ice-contact fan and delta complex, Middle Pleistocene, NW Germany. Sedimentology 56:1041–1076

Winsemann J, Brandes C, Polom U (2011a) Response of a proglacial delta to rapid high-amplitude lake level change: an integration of outcrop data and high resolution shear-wave seismic. Basin Res 23:22–52

Winsemann J, Brandes C, Polom U et al (2011b) Depositional architecture and palaeogeographic significance of Middle Pleistocene glaciolacustrine ice marginal deposits in northwestern Germany: a synoptic overview. E&G Quat Sci J 60:212–235

Winsemann J, Lang J, Roskosch J et al (2015) Terrace styles and timing of terrace formation in the Weser and Leine valleys, northern Germany: response of a fluvial system to climate change and glaciation. Quat Sci Rev 123:31–57

Winsemann J, Alho P, Laamanen L et al (2016) Flow dynamics, sedimentation and erosion of glacial lake outburst floods along the Middle Pleistocene Scandinavian ice sheet (northern Central Europe). Boreas 45:260–283

Winsemann J, Lang J, Polom U et al (2018) Ice-marginal forced-regressive deltas in glacial lake basins: geomorphology, facies variability and large-scale depositional architecture. Boreas 47:973–1002

3 Outburst Flood from Möhne Reservoir in May 1943 After Aerial Bombing

Jürgen Herget and Lukas Gregori

Abstract

Among the widespread phenomenon of outburst floods, a luckily unique event was the one artificially triggered by a bombardment during World War II. Among other reservoirs, the British Royal Air Force bombed the Möhne Reservoir located in the headwaters of the River Ruhr to interrupt drinking water supply for the Ruhr District, the armoury of Germany in those days. By this operation "Chastise", the dam wall of the Möhne Reservoir was destroyed. Based on analysis of historical documents, eyewitnesses reports and flood marks along the pathway of the outburst flood its frontal wave velocity and flood levels are reconstructed. Based on the flood levels, the peak discharge in different sections along the valley of the River Ruhr could be modelled. As mentioned in the historic reports, the outburst flood could be significantly buffered in lakes long valley. By these measures, the peak discharge was significantly reduced and further damage avoided. The release of water from the lakes downstream of the destroyed dam wall confused flood chronologies in previous publications. The findings presented here are based on discussions of plausibility and consistency of the historic records and reports and could consider previously not known unpublished historic gauge data including newly modelled discharge estimations.

Keywords

Outburst flood · Man-made flood · Dam failure · Flood weapon · Strategic flooding · Warfare

3.1 Introduction

Outburst floods are an exceptional kind of flood as analysed and illustrated in several key and case studies including resulting reviews in recent years (e.g. Costa and Schuster 1988, 1991; Cenderelli 2000; Manville 2001; O'Connor et al. 2002; Korup and Tweed 2007; O'Connor and Beebee 2009; Herget 2012; Carrivick and Tweed 2016). They occur by an uncontrolled release of water stored in lakes which naturally were generated by dams of earthen material (e.g. landslides, rockfalls, glacial moraines), solid rock (e.g. volcanic lava) or ice. Such events might occur independent from meteorological dynamics and therefore in many cases are unexpected. Artificial dams and reservoirs are carefully protected against dam failure and outburst flood release by technical measures and constructions with a variety of safety regulations. Even though,

J. Herget (✉) · L. Gregori
Department of Geography, Bonn University,
Meckenheimer Allee 166, 53115 Bonn, Germany
e-mail: herget@giub.uni-bonn.de

J. Herget and A. Fontana (eds.), *Palaeohydrology*, Geography of the Physical Environment,
https://doi.org/10.1007/978-3-030-23315-0_3

several dam failures with resulting outburst floods had to be recorded (e.g. Jansen 1980; Singh 1996; O'Connor and Beebee 2009; Herget 2012). A luckily unique event was the successful raid of the British Royal Air Force against drinking water reservoirs in Germany in May 1943 which exemplifies that catastrophic outburst floods are also triggered intentionally.

During World War II, it was an obvious strategic target by the Allies to destroy weapon production in Germany, e.g. in the Ruhr District. The reservoirs in headwater catchments became localized targets as both the outburst flood after a successful raid and the missing water supply were assumed to reduce Nazi-German abilities to continue the war significantly. So a human-initiated flood was planned to be used as a weapon against the enemy. Such strategy was carried out before, e.g. during wars in China, respectively, the Netherlands and coastal Flanders where dams and natural levees were opened to inundate vast regions to slow the march of invasive forces (Dutch 2009; de Kraker 2015) and even successful bombing and sabotage has occurred in more recent times (Jansen 1980, 111f). The operation "Chastise", which was the code word of the assault by the British Royal Air Force carried out on the reservoirs in the headwaters of the River Ruhr in May 1943, reached an unseen level of effort to allow airborne bombers to successfully approach the water supply system of the industrial heart of Nazi-Germany, the Ruhr District.

The final successful assault became popular news on both sides, the British for the defiant strike against the Nazis and from the German perspective the local catastrophe it caused to the local population. Consequently, numerous reviews and descriptions were prepared during previous decades since the assault took place with different foci by British and German authors. Up-to-date reviews of convincing scientific standard are valuable due to reference to numerous facsimiles of historic documents. Sweetman (2004) focuses on the historic background and the perception of the event from a British perspective while Blank (2013) analyses the perspective of the war and the influence of the specific raid for the German population. Falconer (2010), Euler (2007) and Ziegler (1983) tend to a more popular style of presentation but illustrate their reviews from the different perceptions with numerous illustrations and historic documents. A valuable review including a bibliography of the historic records was presented by Sweetman (2004).

From the point of view of natural sciences, it is surprising that so far no updates on the first estimations of the discharge of the outburst flood itself have been produced. In the meantime, in several palaeohydrological studies useful tools to estimate hydrological and hydraulic parameters of previous floods were developed (e.g. reviews by House et al. 2002; Benito and Thorndycraft 2004; Herget 2012 or Baker 2014). Recently, Gregori (2014) carried out a compilation of flood level and timing indicators for the Ruhr raid based on various sources both in the field and in different archives. After a careful analysis and discussing numerous contradictory data and reports by eyewitnesses and data in previous publications, he significantly improved knowledge and understanding of the dynamics of the outburst flood.

In this paper, the exceptional hydrological extreme event of the outburst flood from the Möhne Reservoir is presented in focusing on the hydrological parameters of peak discharge along its pathway and the dynamics of the flood wave as it can be reconstructed from historic sources. First, the context of the operation "Chastise" is presented by illustrating the importance of the Ruhr District for the weapon production of Nazi-Germany in 1943. The focus is given on its water supply and the way this was attacked by bombing the Möhne Reservoir. Introduced by a brief review on the applied methods, the results of the reconstruction of the outburst flood are

documented, the destruction it caused illustrated, and finally put into perspective by presenting conclusions derived so far.

3.2 The Ruhr District of 1943 and Its Water Supply

Based on the local coal mining, the Ruhr District became an industrial centre of global importance (Wiel 1970; Weber 1982; Blank 2013). The Ruhr District was the dominating area of coal mining, which was essential for steal production, the power of steam locomotives of the railway system, and heating in winter times. Coal production reached an even increased importance during the war by the production of synthetic fuel, e.g. in Gelsenkirchen and synthetic rubber in Marl, both products of coal chemistry. The steal plants of Krupp located in Essen became famous for their nickel steel which was exceptional solid and therefore used for tanks and battleships. Already in the nineteenth century, the plants became famous for the number and quality of cannon tubes produced resulting in the nickname "Kanonenkönig" (king of cannons) for the founder of the company Alfred Krupp. Even though there are some ongoing debates about it among historians, the reputation of the Ruhr District as armoury of Germany was generally acknowledged (Blank 2013, 40f). The distribution of these products predominately occurred by railway, which resulted in a railway network in Central Europe, which was orientated to the region.

Both the industrial plants and the population of about 4.5 million in the 1940s depend on reliable water supply. Due to the extreme rapid growing and agglomeration of settlements and industrial plants hygienic problems became serious and culminated in extremely poor water quality (Brüggemeier and Rommelspacher 1992, 89ff). By the beginning of the twentieth century, a decision was made for a systematic and consequent functional differentiation of the three rivers flowing through the Ruhr District east to west (Heinrichsbauer 1936) (Fig. 3.1).

The River Emscher draining the central parts was used as central waste water canal with a single sewage plant right before the confluence with the River Rhine. While the main function of the River Lippe on the northern boundary of the Ruhr was the supply of process water, the function of the River Ruhr was the supply of drinking water. In the headwaters of the River Ruhr catchment area, the annual precipitation is >1200 mm and was stored in several reservoirs to guarantee a steady minimum discharge throughout the year (Link 1932; Timmermann 1951). Numerous water supply facilities along the valley bottom transferred the water taken and cleaned out of the channel by bank filtration towards the demanding areas also beyond the catchment area boundaries.

The River Möhne is a tributary of the River Ruhr located in the north-eastern margin of the catchment (Fig. 3.1). The size of the catchment is 468 km^2 with a length of the river channel of 65 km (Ruhrverband 2018). The source of the river is located at an elevation of 565 m a.s.l. and the mouth into the River Ruhr at 151 m a.s.l. The discharge is significantly modified by the Möhne Reservoir, but given as 0.9 m^3/s for mean low water discharge, 6.4 m^3/s for mean discharge and 37.5 m^3/s for mean flood discharge.

The Möhne Reservoir was built 1908–1913 and has a storage capacity of 134.5 million m^3 (Ruhrverband and Ruhrtalsperrenverein 1988; Ruhrverband 2012). The dam was constructed as gravity dam with a minor arch shape and consists of a quarry stone dam wall with a length of 650 m, a maximum height of 40.3 m and a thickness of up to 34.2 m at the bottom and 6.25 m on the top. Not visible as located deep below the water level within the reservoir is the frontal Intze-Wedge of earthen material. Its function was to provide additional support to the dam itself in the sections of the highest water pressure. Two units of gatehouses with two pipes each were located in towers within the dam wall (Fig. 3.2).

In March 1943, the British Bomber Command and later also the US Air Force started the "Battle of the Ruhr" as the first systematic air offensive

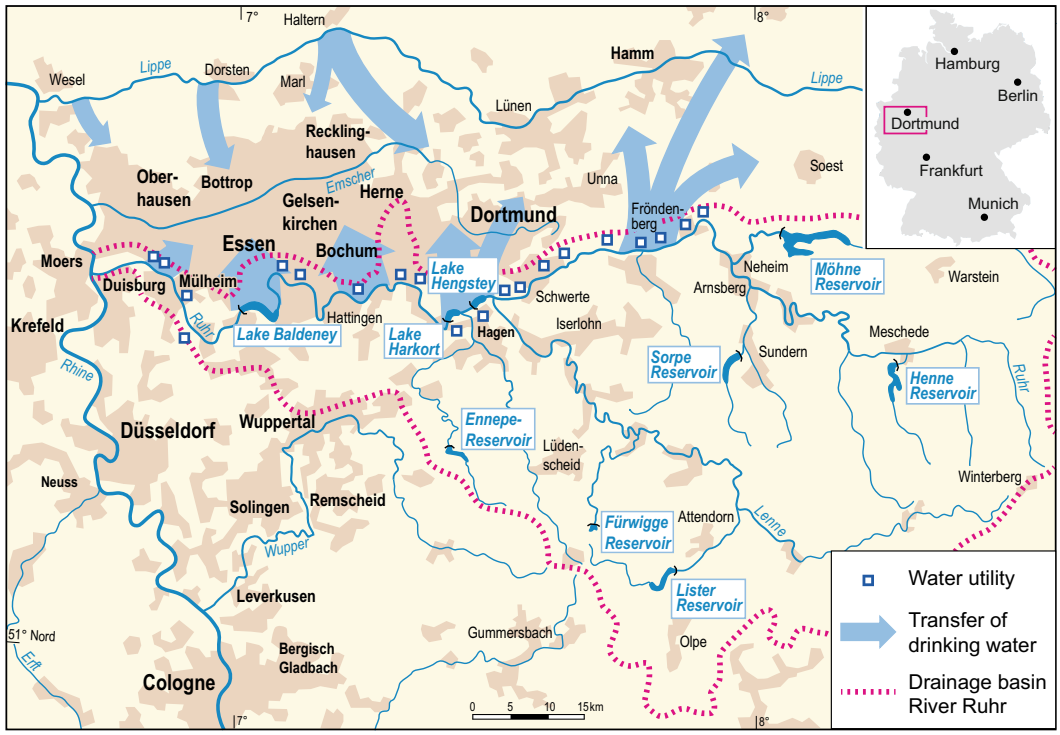

Fig. 3.1 Drainage basin of the River Ruhr with reservoirs and generalized locations of water utilities in May 1943

Fig. 3.2 Air side of the recent dam wall of the Möhne Reservoir; the visible water surface is a compensation basin on the downstream side of the dam wall

against an industrial area (Blank 2013). The declared aim was the systematic destruction of industrial and traffic infrastructure, including population centres. Based on the steel production, the Ruhr District was well known as the armoury of the Nazi regime and consequently a

top priority target. The water supply infrastructure of the region was one of the central components because of its obvious function as the source of both drinking water and industrial water and its function to extinguish fires inflamed by firebomb assaults.

3.3 Weapon Technology and the Attack in May 1943

The reservoirs of Möhne and Sorpe were identified as tactical targets already by 1937 and different concepts were developed while technical limitations hindered an attack until 1943 (cf. Blank 2013; Cockell 2002; Euler 2007; Falconer 2010; Sweetman 2004, for further details). Theoretical concepts were based on super-heavy explosive bombs or high-energy torpedoes while no aircraft capable to transport the estimated 10 tons bomb was available. The reservoirs' surfaces were too small to launch a torpedo from an aircraft. By December 1942, Barnes Wallis, chief designer of Vickers Aircraft Cooperation, concluded plans on the development of a bouncing bomb that should be able to cross the installed dam wall protection facilities. These facilities consisted of double-lined torpedo nets on the water side, camouflage and tree cover on the wall itself to camouflage its signature and steel nets and mats on the air side to avoid contact of explosive bombs with the wall in addition to anti-aircraft guns in the surrounding area. The bouncing bomb of 1.6 m length and 1.3 m in diameter had a weight of 4.2 t and was filled with 2.6 t of explosives. Before the drop, the bomb was put in rotation and from a height of 18 m and for a flight speed of 350 km/h, it should be able to bounce over the torpedo nets to reach the dam wall. Along the wall, it should sink down into the water until the water pressure triggers the explosion at a depth of 9 m. To fulfil the high precision requirements of the bomber's approach, two spotlights were installed below the airplane set at a specific angle that merge to a single spot at the required height over the water surface. To drop the bomb at the right distance from the wall, the bombardier had a mechanical sighting device that is related to the distance of the aircraft to the turrets on the dam walls. According to calculations, experiments on models and simulations on reservoirs in Scotland and Wales, none of the dams in River Ruhr catchment should be able to withstand an assault.

On the night of 16/17 of May 1943, 19 British Lancaster bombers of No. 671 squadron started the operation "Chastise", an assault against five reservoirs in the headwaters of the River Ruhr including the Eder Reservoir east of it. While the attacks on the Sorpe, Lister and Ennepe Reservoirs were not successful, both the dam walls of Möhne and Eder Reservoirs were destroyed.

The first formation targeted the Möhne Reservoir and reached it by 00.20 h. Only six anti-aircraft guns were installed around the dam as the demand for them in the Ruhr District area itself was more serious. The bombers started their assault by 00.28 h. and by 00.49 h. during the sixth approach the wall broke. The exact time could be fixed by seismic records caused by the bomb drops and the final explosion (Sweetman 2004, 228). Before the burst, one bouncing bomb jumped over the dam wall and destroyed the local power plant below, while another one exploded on the wall with minor effect. Even though one aircraft was shot down and another one damaged, the remaining planes continued towards Eder Reservoir as originally planned as further bombs were left to be deployed. The dam wall was destroyed by 01.52 h after several approaches.

Of the second formation, only one bomber reached the Sorpe Reservoir. By 00.46 h, one bomb was dropped and hit the dam. Due to the strong construction of earthen material, the surface was significantly damaged, but the dam itself did not fail. Another aircraft of the third formation, which has started by midnight, dropped a second rotating bomb on the dam of the Sorpe Reservoir with the same minor effect: the dam remained in working order. The run-up on the Lister Reservoir was not successful as all aircraft were shot down before they could reach the target area. Anyhow, the assault generally was successful and the Royal Air Force 617 Squadron chose the motto "Après moi le déluge"

("After me, the flood") with a badge illustrating a broken dam and was deployed for other special approaches in World War II until recent days (Royal Air Force 2017).

The offence on the Möhne Reservoir was most significant and momentous so a focus on further details of the ensuring flood is warranted.

3.4 Applied Methods

Gregori (2014) reviewed and discussed numerous source texts like eyewitness interviews, documentary data, photographs and documents including previous publications for a compilation of hydrological data of the outburst flood along the valleys of the Rivers Möhne and Ruhr downstream of the reservoir. Data contradictory to previous publications (e.g. Kirschmer 1949) presented in the table of the results (Table 3.1) are based on plausibility analysis and discussion by Gregori (2014).

For the downstream valley sections, only qualitative descriptions, individual local flood marks and semi-quantitative estimations are have been published to describe the outburst characteristics (e.g. Rumpf 1954; Gantenberg 1993; Euler 2007; Blank 2013). More detailed local

Table 3.1 Hydrological characteristics of the outburst flood on 17 May 1943 along its pathway compiled from various sources

Location (distance from dam)	Time flood started	Peak discharge: time	Peak discharge: max water elevation	Peak discharge: (range of uncertainty)	Gauge data$^{(W)}$: Mean discharge Mean flood discharge
Dam wall (0 km)	00.45 h$^{(A)(K)}$ 00.49 h$^{(*)}$	–	–	8800 m^3/s$^{(K)}$	7 m^3/s 39 m^3/s
Neheim (13 km)	01.20 h$^{(A)(K)}$	~01.30 h$^{(*)}$ 01.40 h$^{(A)(K)}$	157.20 m$^{(B)}$	~7200 m^3/s$^{(K)}$ 7100 m^3/s (4800–8000 m^3/s)$^{(*)}$	27 m^3/s 196 m^3/s
Fröndenberg (29 km)	~02.20 h$^{(K)}$ 02.45 h$^{(*)}$	~03.40 h$^{(K)}$	124.30 m$^{(B)}$ 127.30 m$^{(*)}$	~5500 m^3/s$^{(K)}$ 5000 m^3/s (4300–6100 m^3/s)$^{(*)}$	27 m^3/s 172 m^3/s
Schwerte/Villigst (44 km)	03.45 h$^{(A)(K)}$	05.45 h$^{(A)(K)}$	108.30 m$^{(B)}$	~4500 m^3/s$^{(K)}$ 4800 m^3/s (4100–5800 m^3/s)$^{(*)}$	29 m^3/s 239 m^3/s
Lake Hengstey (54 km)	<04.40 h$^{(A)}$ 06.30 h$^{(K)}$	<09.15 h$^{(A)}$	97.85 m$^{(B)}$	~3700 m^3/s$^{(K)}$ <4000 m^3/s (<3500–4700 m^3/s)$^{(*)}$	<67 m^3/s <533 m^3/s
Hattingen (94 km)	08.00 h$^{(*)}$ 08.30 h$^{(K)}$ 09.30 h$^{(A)}$	14.00 h$^{(A)(C)(K)}$	67.95 m$^{(B)}$	~2800 m^3/s$^{(K)}$ 2600 m^3/s$^{(C)}$ 2000 m^3/s (1800–2300 m^3/s)$^{(*)}$	70 m^3/s 562 m^3/s
Lake Baldeney (121 km)	>10.45 h$^{(A)}$ 13.30 h$^{(K)}$	>17.00 h$^{(A)}$ 19.45 h$^{(K)}$ 20.00 h$^{(C)}$	51.80 m$^{(B)(C)}$	~2300 m^3/s$^{(C)(K)}$	75 m^3/s 582 m^3/s
Duisburg (150 km)	19.00 h$^{(K)}$	01.10 h$^{(K)}$	21.53 m$^{(B)}$	1840 m^3/s$^{(K)}$	>74 m^3/s >654 m^3/s

Sources A—Table Wasserwirtschaftsamt Hagen 1.6.1943 (archive RP Arnsberg, unpubl.); B—Table without date and place (archive RP Arnsberg, unpubl.); C—written communication Ruhrschiffahrts-Verwaltung Duisburg to RP Arnsberg 22.5.1943 (archive RP Arnsberg, unpubl.); *—own investigations; K—Kirschmer (1949); W—http://www.tlz-ruhr.de

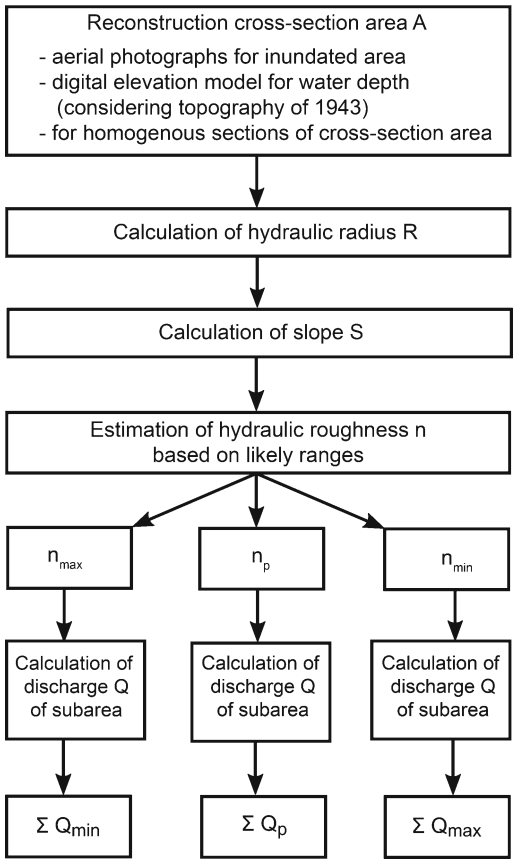

Fig. 3.3 Scheme for the estimation of peak discharge of the outburst flood along the River Ruhr (modified according to Herget et al. 2014)

hydrographs of the water level during the passing outburst as in Hattingen (Gantenberg 1993) are a rare exception.

The new estimations of peak discharge Q presented here are based on the approach given by Herget et al. (2014) for estimation for historic flood events (Fig. 3.3). The factors of the equation of continuity $Q = v \times A$ were calculated by the Manning Equation for the mean velocity at peak discharge v and cross-section area A was calculated by indicators of the historic flood levels. Based on the compiled data of flood levels from the historic sources and air photographs taken by the Royal Air Force on 17 of May 1943 (Sweetman 2004; Euler 2007), the depth of flow and width of the inundated floodplain were determined. Using topographic data from a digital elevation model, the cross-section area A was calculated considering the topography in 1943 given in the photographs. The hydraulic radius R and the slope S, required for the calculation of the mean flow velocity $v = R^{2/3} S^{1/2} n^{-1}$, were also derived from the historic palaeostage indicators. The coefficient of the hydraulic roughness n was estimated by the local conditions of the floodplain by summing roughness components consisting of surface roughness, vegetation, channel irregularity, channel alignment, obstructions, and the degree of meandering. As the values of the roughness elements can only be determined as likely estimated ranges so the ranges for the resulting discharge are determined. Based on a plausible n-value given as the mean value within the data range, a mean discharge can be estimated. The final step is to add up the discharges of the homogeneous subareas of the cross-section area (e.g. river channel, floodplain with agricultural use, settled areas, etc…) to the cumulated discharge.

3.5 Reconstruction of the Outburst Flood Along the River Ruhr Valley

As documented by photographs (Euler 2007, 67) and lake level records (cf. below), the Möhne Reservoir was filled to its maximum level during the time of the attack. There are different reports about the formation of the gap in the dam wall after the bomb detonation: some of the British pilots reported leaking gaps already caused by the earlier bombs immediately after returning to their home-base (Rumpf 1954, 235; Euler 2007, 106) while Blank (2013, 179) generalizes that an initial small crack increased rapidly to the final maximal dimension of 77 m in width and 22.2 m in depth (Fig. 3.4) as documented by historic surveys before the rebuilding of the dam wall (Euler 2007, 222). During the rebuilt, it was found that cracks within the wall extended up to 105 m in width and 26 m depth (Quast 1949, 138). Euler (ibid.) concludes by the rectangular shape of the final gap and eyewitness reports a practically instantaneous gap developed

Fig. 3.4 Destroyed dam wall of the Möhne Reservoir, 17 May 1943 (Bundesarchiv 101I-637-4192-23/Schalber—reprinted by permission of the publisher)

equivalent to the final dimension. The contradictory reports on this detail cannot be resolved as plausible reports of water columns reaching tens of metre height and overtopping the dam wall crest indicate confusing conditions during the night assault (Sweetman 2004, 166).

A characteristic of an abrupt dam failure is an hydrograph with an extremely steep rising part and a more gentle decay of the falling limb (e.g. Walder and Costa 1996; Cenderelli 2000; Herget et al. 2015). The hydrograph for the dam location is reconstructed based on the record of the reducing lake level in the Möhne Reservoir (Kirschmer 1949) which indicates the changes in the drained volumes through time (Fig. 3.5).

The outburst flood lasted for approximately 10 h at the dam area with some water remaining in the reservoir as the gap in the dam wall did not

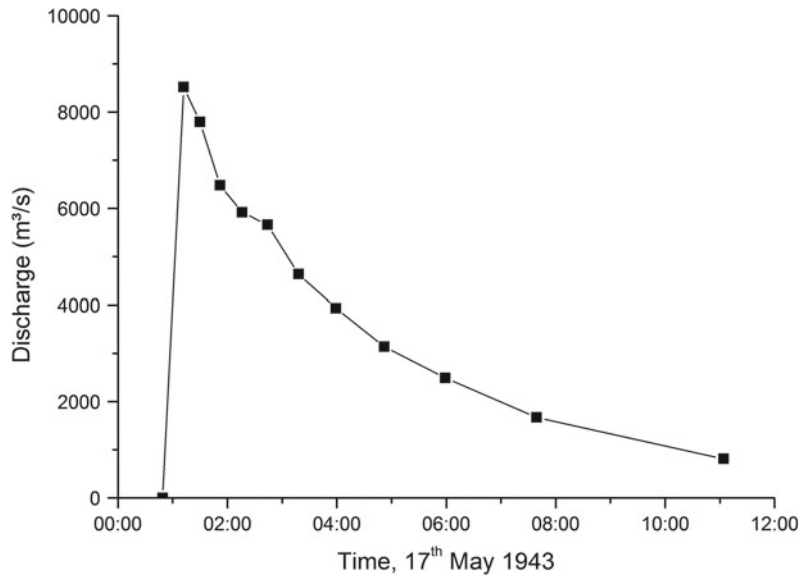

Fig. 3.5 Hydrograph of the outburst flood at the dam location based on the reservoir level and remaining impounded volume (based on data from Kirschmer 1949)

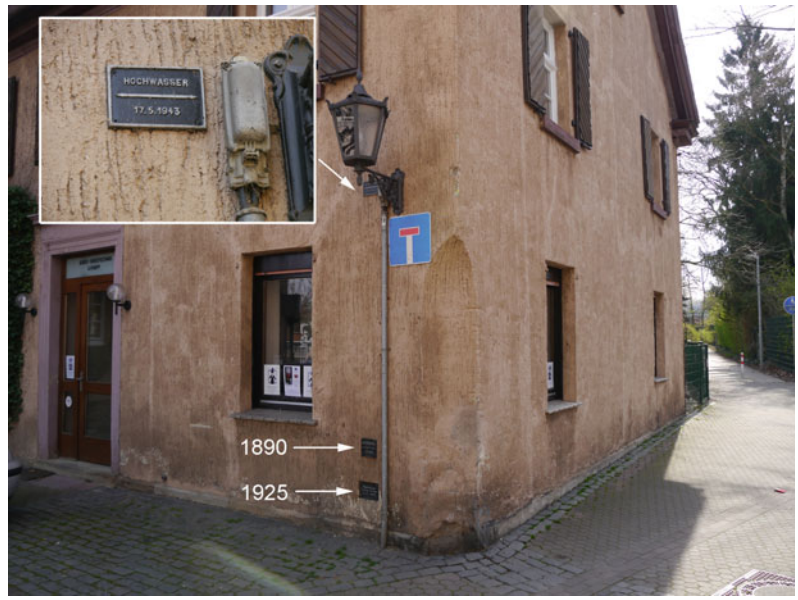

Fig. 3.6 Dam-break flood level on 17th of May 1943 in comparison with previous natural flood levels as shown by flood markers on a building in Schwerte

reach the bottom level of the entire construction (Fig. 3.4) which consisted of the Intze-Wedge of earthen material (cf. Euler 2007, 222). The peak discharge at the dam area was >8000 m^3/s which is larger by three orders of magnitude than the recent anthropogenic-influenced mean discharge of 7 m^3/s (mean low discharge 0.8 m^3/s, mean flood discharge 39 m^3/s; Ruhrverband 2018) downstream of the reservoir. Rumpf (1954, 236) summarizes, that the entire drainage lasted for 36 h with 10×10^6 m^3 of the initially 132×10^6 m^3 remaining still in the reservoir.

The outburst flood initiated at 00.49 h at the dam wall and reached the confluence of Möhne and Ruhr Rivers at Neheim (cf. Fig. 3.1) within half an hour by 01.20 h. Peak discharge was not reduced significantly at this location compared to the initial discharge peak. By 03.00 h, the wavefront had reached the water supply facilities at Fröndenberg and by sunrise the small town of Schwerte was reached. There, the flood level was significantly higher than the largest flood levels in the historic natural flow record from November 1890 and December 1925 (Fig. 3.6).

Downstream, the reconstruction becomes complicated as unpublished records of the gauge at Wetter indicate two minor flood waves interpreted as generated by a enforced separate drainage of Lake Hengstey and Lake Harkort before the outburst flood reached the area (Gregori 2014, 178). The questionable identification of the frontal outburst flood of water from the Möhne Reservoir might explain contradictory accounts of the timing and the discharge of the outburst flood wave in the region downstream of the two lakes (cf. e.g. Gantenberg 1993 for the hydrograph at Hattingen; extrapolations given by Kirschmer 1949). According to unpublished historic correspondence archived at RP Arnsberg, at the small town of Wetter located downstream of Lake Harkort, two separated minor rises of the water level within the river were observed before the outburst flood had reached the area. Lake Baldeney, located approximately 120 km downstream of the reservoir was drained at the time and provided storage capacity for large parts of the remaining outburst flood volume reaching the downstream part of

River Ruhr valley. Downstream of Lake Baldeney, the flood level remained below the flood level for the record natural flood of 1890. At the confluence of the Rivers Ruhr and Rhine at Duisburg, the flood level was not significant.

3.6 Damage, Psychological Effects and Political Consequences Caused by the Outburst Flood

The damage caused by the outburst flood was devastating on the entire valley bottom of the Rivers Möhne and Ruhr down to the area around Hattingen (Blank 2013, 183). Since the outburst flood occurred, several collections of historic documents and descriptions have been compiled (e.g. Ziegler 1983; Gantenberg and Wührl 1993; Euler 1999, 2007) which detail the destruction and its consequences in addition to the brief summary compiled here.

Destruction occurred by both the energy of the initial outburst flood wave front impacting houses and bridges, while the height of the peak water level reached far beyond the natural floodplain level especially in the upper reaches. A third component was the extensive and thick coverage of the terrain by fine sediments which blanketed fields, traffic routes and especially infiltration basins of water supply facilities. Due to backwater effects at obstacles like settlements and bridges, the water level varied significantly which, in combination with the stressful situation for the population as the flood wave passed, might explain numerous contradictory statements in the reports of eyewitnesses who made their observations in the night-time. Rumpf (1954) mentions values of a mean depth of the flood of 7 m with maximum values reaching up to 10 m; according to our own data compilation for discharge estimations (cf. above) these values tend to be too high but depend also on the local reference level selected (Gregori 2014) (cf. Fig. 3.6). Rumpf (1954) summarized the damage caused by the outburst flood along Möhne and Ruhr Valley in a list (further details are given by Euler 2007, 203):

List of damage along River Möhne and Ruhr by the outburst flood (Rumpf 1954):

- 3 power plant destroyed;
- 12 power plants damaged or out of order;
- 7 weirs destroyed or seriously damaged;
- 25 water supply utilities out of order or seriously damaged;
- 3 waste water treatment facilities out of order;
- 4 railway bridges out of order or destroyed;
- 30 km of railway track incl. 2 stations destroyed;
- 11 road bridges destroyed, 5 seriously damaged;
- 10 factories destroyed, others limited in capacity;
- 60 residence destroyed;
- 20 km of road damaged;
- estimated loss of 50,000,000 Goldmark (∼190.000.000 €) by crop damage.

Subsequent to the event, water supply was limited for one month until it was brought back to the previous level. Consequently, especially in Dortmund, Hagen and Bochum, weapon production capacities were reduced while coal mining, coke and steel production in the central parts of the Ruhr District were not effected (Blank 2013, 185).

Literally fatal for many parts of the population was the warning given similar to those for air alerts which resulted in the people seeking shelter underground. According to official registrations >1579 deaths were recorded, >1020 of them were prisoners of war and foreign forced labourers (Blank 2013, 174), many of them were located in a fenced camp on the inundated floodplain at Neheim (Euler 2007, 150f).

The Nazi regime immediately started the reconstruction of the dam wall. Paramilitary forces of the Organisation Todt were drafted to

the Möhne Reservoir and into the Ruhr valley to support reconstructions. By 28 May 1943, the rebuilding began and up to 2192 workers were deployed daily, which illustrates the severity for this measure (Euler 2007, 204f). The rebuilding was finished on 24 September 1943, and the refill of the reservoir was initiated.

In the meantime, historical analysis on both sides British (e.g. Sweetman 2004, 224ff, 281ff) and German (e.g. Blank 2013, 180f) concluded, that beyond the disastrous destructions on the floodplain of the Möhne and upper Ruhr Valley, the raid was mainly a political success and had significant psychological impact on several leaders of the Nazi regime.

From the British perspective, Air Chief Marshall Arthur Harris commented that the assault had only minor effect and was not as significant as promised, while Prime Minister Winston Churchill interpreted it politically as an indicator of a revival in British strength. Of course, the report of the successful raid was on the front cover page of most British and American newspapers with propagandistic capital main of the raid.

The aim to break the support and identification with the Nazi regime of the population of the Ruhr District was only partly reached. Supported by insufficient shelter infrastructure in the densely settled region and a less effective civil administration, the local population seriously feared the continuous bombardments. The continuous assaults by the US Air Force during the daytime and the British Air Force in the nights physically tired the population. On the other hand, a supportive presence of political organizations of the regime supported the perpetuation of the trust in the system within the Ruhr District that only weaken by the end of 1944 (Mommsen 2013). A significant trigger was the fact that hundreds of thousands people lost their homes and especially children were evacuated and grew up far away from their parents, which definitely broke morale. Personal notes by leaders of the Nazi regime like Josef Goebbels (Minister of Public Enlightenment and Propaganda) or Albert Speer (Minister of Armaments and War Production) document the shock effect of the successful assault on the German reservoirs beyond any statement given officially.

3.7 Context and Conclusion

Considering the volume of the released water and the dimension of the gap in the dam wall, the magnitude of the outburst flood from the destroyed Möhne Reservoir is in the range of similar outburst flood events (e.g. Costa and Schuster 1988, 1991; Cenderelli 2000; O'Connor and Beebee 2009; Herget 2012). Even the unique event of the outburst flood triggered by bombardment can be estimated by magnitude as outburst floods from man-made dams by constructional or dimensioning mistakes are considered in the reviews. Applying the empirical relationships derived by Cenderelli (2000, Table 3.4 therein) results in estimated peak discharges between 4700 and 11,500 m^3/s while that the Möhne Reservoir 8800 m^3/s were reached directly below the wall. With an estimated discharge of 8000 m^3/s, the regression approach considering potential energy as product of height of the gap, volume of water and its specific weight by Costa and Schuster (1988, Table 3.6) fits very well to the observed discharge.

Due to limited space, the outburst flood from Eder Reservoir is not considered in detail above. Reviews and documents are given, e.g. by Euler (1999, 2007), Falconer (2010), Kirschmer (1949), Pörtge and Deutsch (2012), Quast (1949), Rumpf (1954), Seemann (1950) and Seidenfaden (2003). A peak discharge of 8500 m^3/s was estimated after the event and water depths of up to 9 m had to be observed. Theoretical analysis by Frank (1951) results in significantly lower values in the magnitude of less than the half of the previous estimation. Except immediately downstream the reservoir, water levels along the River Weser remained below the highest water levels of flood records in historic times (Seemann 1950; Pörtge and Deutsch 2012).

So far, the sedimentary respectively erosional traces of the outburst flood along the valley

bottoms of the Rivers Möhne and Ruhr are not investigated systematically. Recent investigations by Kasielke (pers. communication 7 March 2018) revealed a layer of fine sands with artificial components like brick debris of 0.4–1 m downstream the confluence of the River Möhne and Ruhr. This layer is located above the widespread silts and clays in the floodplain. Locally found channels within the floodplain are generated previous of the outburst flood in May 1943.

From the engineering perspective, Kirschmer (1949, 302) concluded, among other technical details, that dams build by earthen materials provide higher safety levels against violent destructions in war times. In case of urgent danger, water levels in the reservoirs should be lowered by a few metres while the entire released of the water in advance is not necessary. A significant reduction in the magnitude of an outburst flood is possible in wide valleys and especially with the support of lowered water levels at impoundments downstream.

Fortunately, a comparable event has not occurred in more recent time, even though conclusions were made for military planning early (e.g. Boniface 1950). A partly comparable assault was carried out in June 1952 during the Korean War by the US Air Force on the Sui-ho Dam in North Korea, but the main targets were the related power plants, not the dam itself (Futrell 1983). In the meantime, Article 56 from 1977 of the Protocol I amendment to the Geneva Conventions, outlawed attacks on dams.

By the reconstruction of the main hydrological parameters of the outburst flood resulting from the bombing of the Möhne Reservoir, a new perspective has been provided on the historic event which did and still does receive a lot of attention as is evident, e.g. during the anniversaries of the raid.

Acknowledgements The authors appreciate logistical and intellectual support by numerous persons and organizations, amongst others, Anica Althoff, Paul Carling, Jürgen Dodt (†), Uwe Jansen, Till Kasielke, Daniel Koch, Oskar Kroll, Hans Middelkoop and Lioba Wachter should be named individually. The topic was presented and discussed during the workshop EX-AQUA 2016 "Palaeohydrological extreme events—evidence and archives" in Padova/Italy which was kindly supported by the INQUA commission on Terrestrial Processes, Deposits and History TERPRO.

References

Baker VR (2014) Palaeohydrology. IAHS benchmark papers in hydrology series 9. International Association of Hydrological Sciences, Wallingford

Benito G, Thorndycraft VR (eds) (2004) Systematic, palaeoflood and historical data for the improvement of flood risk estimation—methodological guidelines. Centro de Ciencias Medioambientales, Madrid

Boniface A (1950) La destruction du barrage de la Möhne. Revue Militaire Suisse 95(4):145–162

Blank R (2013) Ruhrschlacht – das Ruhrgebiet im Kriegsjahr 1943. Klartext, Essen

Brüggemeier F-J, Rommelspacher T (1992) Blauer Himmel über der Ruhr - Geschichte der Umwelt im Ruhrgebiet 1840–1990. Klartext, Essen

Carrivick JL, Tweed FS (2016) A global assessment of the societal impacts of glacier outburst floods. Glob Planet Chang 144:1–16

Cenderelli DA (2000) Floods from natural and artificial dam failures. In: Wohl EE (ed) Inland flood hazards. Cambridge University Press, Cambridge, pp 73–103

Cockell CS (2002) The science and scientific legacy of Operation Chastise. Interdisc Sci Rev 27:278–286

Costa JE, Schuster RL (1988) The formation and failure of natural dams. Geol Soc Am Bull 100(7):1054–1068

Costa JE, Schuster RL (1991) Documented historical landslide dams from around the world. US Geological Survey Open-File Report 91-239

de Kraker AMJ (2015) Flooding events as man-made disasters—special flooding events in coastal Flanders and the inlets of the SW Netherlands 1400–1600. Zeitschrift für Geomorphologie 59(Suppl 3):111–125

Dutch SI (2009) The largest act of environmental warfare in history. Environ Eng Geosci 15:287–297

Euler H (1999) Als Deutschlands Dämme brachen. Motorbuch, Stuttgart

Euler H (2007) Wasserkrieg – 17. Mai 1943 Rollbomben gegen die Möhne-, Eder- Sorpestaudämme. Motorbuch, Stuttgart

Falconer J (2010) The dam busters—breaking the great dams of Germany, 16–17 May 1943. Haynes, Sparkfort

Frank J (1951) Betrachtungen über den Ausfluss beim Bruch von Stauwänden. Schweizerische Bauzeitung 69(29):401–406

Futrell RF (1983) The United States Air Force in Korea, 1950–1953. Office of Air Force History United States Air Force, Washington

Gantenberg WE (1993) Was konnte die Bevölkerung im Ruhrgebiet im Mai 1943 über die Flutwelle in den Zeitungen lesen? – Ergebnisse von Untersuchungen in verschiedenen Zeitungsarchiven. In: Gantenberg WE,

Wührl E (eds) (1993) Die Bombardierung der Möhnetalsperre am 16./17. Mai 1943 und ihre Auswirkungen am Bochum-Dahlhausen im mittleren Ruhrtal. Heimatkundliche Schriften über das mittlere Ruhrtal und den Stadtbezirk Bochum-Südwest 1/1993, pp 43–52

Gantenberg WE, Wührl E (eds) (1993) Die Bombardierung der Möhnetalsperre am 16./17. Mai 1943 und ihre Auswirkungen am Bochum-Dahlhausen im mittleren Ruhrtal. Heimatkundliche Schriften über das mittlere Ruhrtal und den Stadtbezirk Bochum-Südwest 1/1993

Gregori L (2014) Modellierung der Ausbruchsflutwelle des Möhnesees nach seiner Bombardierung im Mai 1943. Master thesis Dept. of Geography Bonn University

Heinrichsbauer A (1936) Die Wasserwirtschaft im Rheinisch-Westfälischen Industriegebiet. Glückauf, Essen

Herget J (2012) Am Anfang war die Sintflut - Hochwasserkatastrophen in der Geschichte. Primus, Darmstadt

Herget J, Schütte F, Klosterhalfen A (2015) Empirical modelling of outburst flood hydrographs. Zeitschrift für Geomorphologie 59(Suppl 3):177–198

Herget J, Roggenkamp T, Krell M (2014) Estimation of peak discharges of historical floods. Hydrol Earth Syst Sci 18:4029–4037

House PK, Webb RH, Baker VR, Levish DR (eds) (2002) Ancient floods, modern hazards—principles and applications of paleoflood hydrology. Water science and application 5. American Geophysical Union, Washington

Jansen RB (1980) Dams and public safety—a water resources technical publication. US Government Printing Office, Denver

Kirschmer O (1949) Zerstörung und Schutz von Talsperren und Dämmen. Schweizerische Bauzeitung 67:277–281, 300–303

Korup O, Tweed F (2007) Ice, moraine, and landslide dams in mountainous terrain. Quatern Sci Rev 26:3406–3422

Link E (1932) Talsperren und ihre Einwirkung auf die Wasserversorgung an der Ruhr. Das Gas- und Wasserfach 75:601–607

Manville V (2001) Techniques for evaluating the size of potential dam-break floods from natural dams. Science Report 2100/28. Institute of Geological & Nuclear Science, Lower Hutt

Mommsen H (2013) Zum Geleit. In: Blank R (ed) Ruhrschlacht – das Ruhrgebiet im Kriegsjahr 1943. Klartext, Essen, pp 9–10

O'Connor JE, Beebee RA (2009) Floods from natural rock-material dams. In: Burr DM, Carling PA, Baker VR (eds) Megaflooding on Earth and Mars. Cambridge University Press, Cambridge, pp 128–171

O'Connor JE, Grant GE, Costa JE (2002) The geology and geography of floods. In: House PK, Webb RH, Baker VR, Levish DR (eds) Ancient floods, modern hazards—principles and applications of palaeoflood hydrology. American Geophysical Union, Washington, pp 359–385

Pörtge KH, Deutsch M (2012) Hochwasserereignisse und sie beeinflussende Faktoren - am Beispiel Weser. Cottbuser Studien zur Geschichte von Technik Arbeit und Umwelt 38:119–131

Quast H (1949) Zerstörung und Wiederaufbau der Möhne- und Eder-Talsperre. Wasser- und Energiewirtschaft 11:135–139, 12:149–154

Royal Air Force (ed) (2017) 617 squadron. https://www.raf.mod.uk/our-organisation/squadrons/617-squadron/. Accessed 22 Nov 2018

Ruhrverband (ed) (2012) Möhnetalsperre. Ruhrverband, Essen

Ruhrverband (ed) (2018) Characteristics of River Möhne catchment. http://www.ruhrverband.de/fluesse-seen/fluesse-baeche/moehne/. Accessed 13 Nov 2018

Ruhrverband, Ruhrtalsperrenverein (ed) (1988) 75 Jahre im Dienst für die Ruhr. Ruhrverband, Essen

Rumpf H (1954) Die Luftangriffe auf die Möhne-, Eder- und Sorpetalsperren 16/17 Mai 1943 und ihre Wirkungen. Ziviler Luftschutz 10:233–237

Seemann D (1950) Die Kriegsbeschädigungen der Edertalsperrmauer, die Wiederherstellungsarbeiten und die angestellten Untersuchungen über die Standfestigkeit der Mauer. Die Wasserwirtschaft 41(1):1–7, 49–55

Seidenfaden H (ed) (2003) Die Nacht, als die Flut kam - die Bombardierung der Edertalsperre 1943. Wartberg, Gudensberg-Gleichen

Singh VP (1996) Dam breach modelling technology. Kluwer, Dortrecht

Sweetman J (2004) The dambusters raid. Cassell, London

Timmermann R (1951) Die Talsperren am Nordrande des Rheinischen Schiefergebirges. Forschungen zur Deutschen Landeskunde 53

Walder JS, Costa JE (1996) Outburst floods from glacier-dammed lakes—the effect of mode of lake drainage on flood magnitude. Earth Surf Proc Land 21:701–723

Weber W (1982) Industriealisierung - Das Ruhrgebiet. Westermann, Braunschweig

Wiel P (1970) Wirtschaftsgeschichte des Ruhrgebietes - Tatsachen und Zahlen. Siedlungsverband Ruhrgebiet, Essen

Ziegler JW (ed) (1983) Die Sintflut im Ruhrtal - eine Bilddokumentation zur Möhne-Katastrophe. Meinerzhagener Druck- und Verlaghaus, Meinerzhagen

Part II
Studies with Regional Focus

4 Droughts in Historical Times in Europe, as Derived from Documentary Evidence

Rudolf Brázdil, Andrea Kiss, Ladislava Řezníčková and Mariano Barriendos

Abstract

Documentary evidence can provide high-resolution data pertaining to past droughts. This may include a wide range of sources, among them: narratives (annals, chronicles, memoirs); diaries kept by persons specifically interested in the weather; accountancy and economic-administrative archives; legal-administrative records; religious observances; letters; songs; newspapers and magazines; paintings and pictographic evidence; chronograms; epigraphic evidence; early instrumental meteorological observations; society and professional reports; and weather compilations. Most of these are generally available for many European countries. Such a variety of documentary information is sufficient to distinguish between the basic types of drought (meteorological, agricultural, hydrological and socio-economic) and reconstruct hydroclimatic conditions in the form of series of precipitation totals, drought frequencies and drought indices. This paper presents a European overview of existing documentary-based drought studies for the Mediterranean, western, central and eastern areas of Europe. Examples of outstanding European droughts are drawn from events of 1361, 1616 and 1718–1719 CE. The descriptions of European droughts and of human responses to them, pay particular attention to impacts on society, to perceptions of drought and to spiritual and ritual responses, as well as to the institutional/legal-administrative decisions and changes droughts have brought about. Perspectives for future research into historical droughts in Europe are also presented.

Keywords

Drought · Documentary data · Long-term variability · Impacts · Human responses · Europe

R. Brázdil (✉) · L. Řezníčková
Institute of Geography, Masaryk University, Brno, Czech Republic
e-mail: brazdil@sci.muni.cz

R. Brázdil · L. Řezníčková
Global Change Research Institute, Czech Academy of Sciences, Brno, Czech Republic

A. Kiss
Institute for Hydraulic Engineering and Water Resources Management, Vienna University of Technology, Vienna, Austria

A. Kiss
Department of Historical Auxiliary Sciences, Institute of History, University of Szeged, Szeged, Hungary

M. Barriendos
Department of History and Archaeology, University of Barcelona, Barcelona, Spain

J. Herget and A. Fontana (eds.), *Palaeohydrology*, Geography of the Physical Environment,
https://doi.org/10.1007/978-3-030-23315-0_4

4.1 Introduction

Droughts, together with floods, are one of the most extreme phases of the hydrologic cycle. However, "floods" may be clearly defined, while it is far more difficult to refer to "droughts" in a succinct and unambiguous way; a generally accepted definition of drought simply does not exist. They cannot be viewed as merely physical phenomena, but rather as "*the result of interplay between the natural event and the demand placed on a water supply by human-use systems*" (Wilhite and Pulwarty 2018, p. 18). Van Loon et al. (2016a, b, p. 3631) consider drought the result of "*complex interactions between meteorological anomalies, land surface processes, and human inflows, outflows, and* [water] *storage changes*". According to Svoboda and Fuchs (2018), drought is a normal, recurrent feature of climate that occurs in virtually all climatic zones.

A primary reason for drought is a reduction of precipitation in the given area compared to its "mean" or "normal" precipitation totals. This situation may occur in any place and at any time and lasts from weeks to months. Such "meteorological drought" may be enhanced by high temperatures, low relative humidity and higher wind speeds. Lack of precipitation may lead to shortages of water for growing plants, which is known as "agricultural drought". Similar effects and scale of influence may also occur in forests, be they ornamental, conservation sites or commercial. After extended meteorological drought, the deficiency in precipitation may be reflected in lack of water in streams, rivers, water reservoirs and any underground waters; such a situation constitutes "hydrological drought" (Mishra and Singh 2010 also reported in terms of "underground water drought"). The impacts of these droughts on society, and human responses to drought, may appear after some time in economic, social and political life, thus identified as "socio-economic drought" (Heim 2002; Wilhite and Pulwarty 2018).

A plethora of drought indices have been developed in order to describe droughts and their various environmental effects (e.g. Heim 2000, 2002; Svoboda and Fuchs 2018). Among them, the Standardised Precipitation Index (SPI) (McKee et al. 1993), Standardised Precipitation Evapotranspiration Index (SPEI) (Vicente-Serrano et al. 2010; Beguería et al. 2014) and the Palmer Drought Severity Index (PDSI) (Palmer 1965; Dai 2011) are the most frequently used. Since they are calculated from instrumental meteorological measurements of air temperature and precipitation, series of them for Europe may benefit from the relatively large number of long-term meteorological observations that have been made (e.g. Camuffo and Jones 2002; van der Schrier et al. 2007; Todd et al. 2013; Haslinger and Blöschl 2017).

There exist several different types of proxies that may serve to extend our knowledge of drought into the pre-instrumental period (see PAGES Hydro2k Consortium 2017). Documentary evidence is one of them, used as the basic source of data in historical climatology (Brázdil et al. 2005, 2010; White et al. 2018), and it plays an important role. Such information is derived from a range of written sources that offer high-resolution qualitative or quantitative data, concerning droughts and their impacts. These sources have been used to create long-term drought chronologies (e.g. Lyakhov 1984; Martín-Vide and Barriendos Vallvé 1995; Piervitali and Colacino 2001; Domínguez-Castro et al. 2008; Tejedor et al. 2018), sometimes combined with droughts from the instrumental period (e.g. Brázdil et al. 2013, 2016; Noone et al. 2017), and to investigate certain important past drought events in detail, including their human impacts and responses to them (e.g. Munzar 2004; Wetter et al. 2014; Kiss and Nikolić 2015; Roggenkamp and Herget 2015; Kiss 2017, 2019; Brázdil et al. 2019).

This chapter of the book presents the state-of-the-art in the study of the spatiotemporal variability of droughts, their impacts and responses to them in Europe (for the worldwide scale, *see* Brázdil et al. 2018). It describes the types of documentary sources that relate to droughts, the methods of drought reconstruction and long-term drought variability, providing examples of outstanding droughts, drought impacts and human responses. It gleans what can be

learned from historical droughts and applied to recent and future droughts, and finally formulates perspectives for future research into historical droughts.

4.2 Documentary Evidence

Documentary evidence consists of any material object that bears or contains any man-made information contemporaneous with the culture of its time (e.g. chronicle, manuscript, financial accounts, "books of memory") and structural records (on bridges, commemorative stones, etc.). Many such records may also contain information about the weather or related phenomena, including droughts. The main individual types of documentary sources are listed below. Each type is generally characterised with respect to the data within it, by references addressing such types of data, and finally by example(s) of records that serve to gather more a detailed idea of the context in which the information came into existence. The following main types of documentary evidence may be used for the study of droughts in Europe:

(i) **narrative sources**

Droughts and their impacts are among the climatic phenomena that appear in several types of narrative source (annals, chronicles, "books of memory" and inscriptions among them). Together, they constitute some of the main sources of documentary data in historical climatology. Records were kept to preserve memories of outstanding events or phenomena, particularly those that involved loss of human lives, material damage and possible socio-economic effects on society in general.

Examples The first annals of Novgorod (Russia) (*Novgorodskaya pervaya letopis starshego i mladshego izvoda*) reported a drought in AD 1471 (Shmakin et al. 2013, p. 53): "*So it was that in Novgorod District no droplet of rain fell out of the sky to the earth for the whole summer from the month of May to September, and* [from] *the heat of the sun all the earth and marshes dried up*. […] [The river] *Lovat' dried out because drought and doom were massive in that year*." The Congregational Church Book of Guestwick in the English county of Norfolk includes a drought in its record for 26 August 1719 (Kington 1980, p. 125): "[…] *sometime was set apart for prayer to seek God on account of the great heat and extreme drought. Such a summer for heat in the months of May, June, July and August was hardly known in the memory of any man living – the pastures scorched, the pits and ponds dried up, the poor beasts of the fields pining for want of water* […] *the season is very threatening for man and beast.* […] *Fevers and deaths* [have been] *many*".

(ii) **diaries**

Personal and private records often include some accounts of the weather, recorded by their keepers for a variety of reasons in ephemerides, calendars, work-related and personal diaries. Weather diaries were also kept, containing more-or-less systematic daily visual weather records (e.g. Symons 1891). These may be supplemented by detailed descriptions of certain weather extremes or by monthly or annual weather summaries in which, as well as short notes related to dry weather on individual days, longer drought episodes may be described.

Examples Gregorio Susanna, in his diary for 1760–1761 in Catanzaro (Italy) used his end-of-year record for 31 December 1760 to summarise drought impacts for that year (Diodato and Bellocchi 2011, p. 192): "*Food supplies have been very low because of the great drought that never seems to stop. Decimating all fruits, with grapes also destined to perish, and very little must and wheat and oil* […] *Drought has occurred because there has been no rain up to late December, the countryside is arid and bare of grass, and almost all the cattle are dead. Starvation threatens; much prayer is in order.* […]". The diary of Nicoll (1836, p. 138), a Scot living in Edinburgh, described the great summer

drought of 1654 (see also Dawson 2009): "*All this summer and harvest, in the year of Our Lord 1654, there occurred an exceedingly great drought though all parts of* [the region of] *Lothian, but especially around Edinburgh, where all the wells dried out, to the extent that the inhabitants could not get enough to process their food, and water could not be found. Despite this, all the west of the country, from Glasgow to the Rhinns of Galloway had rain and wet as usual, or more. All this time, and since, great drought* [has] *continued in all the wells of Edinburgh, and throughout the land of Lothian, so much so that the people of Edinburgh have been forced to venture out for a* [Scottish] *mile* [1.8 km] *before they can get any clean water, either for the brewing of ale or beer, or for cooking food in a pot*".

(iii) **financial and economic-administrative records**

Particular documents (mainly accountancy sheets and letters of application) prepared at various levels of governmental or state administration, which may obtain some drought-related information, are important financial and economic-administrative sources. One type of example may be found in documents related to the rebate of taxes, when agricultural production had been significantly damaged by hydro-meteorological extremes (e.g. Brázdil et al. 2012b), or requests for postponement of debt payment, tax exemption or financial support. Severe droughts could give rise to all of these.

Example The accounts covering the incomes of the bishop of Eger (Hungary) report the 1507 drought in these terms (Kovács 1992, p. 233): "*On the given date* [15 July 1507] *the above-mentioned tithes of the citizens of Heperyes* [Prešov, Slovakia] *were to be sold and leased for 84 fl.* [florins]*, as in this year a great drought destroyed their harvest* etc.*; from this* [sum] *they now render 42 fl., and the other 42 fl. is bound over to be rendered by the forthcoming St. Nicolas day* [6 December]".

(iv) **legal-administrative evidence**

Documentary sources recording the flow of "application–decision" between the various levels of public administration show a range of responses to the stresses produced by drought, exploring technical, legal alternatives to improve water resources.

Examples The Duke of Dalmatia gave permission to the Morlachs (the Black Vlach pastoral community) to stay within the territory of Trogir town until 24 April 1362 "[…] *because great drought and difficult times are now so threatening, and because of the tenderness of the lambs of the Morlachs, who are at present living at a great distance from their homeland, in order to avoid enormous loss* […]" (Smičiklas et al. 1915, p. 211). Another typical example comes from Spain. In Catalonia, after a long drought period, the Barcelona City Council authorities sent an official communication to the Kingdom Council on 28 August 1627 requesting authorisation to build a channel for river transfer from the River Llobregat to the Barcelona area to alleviate and diminish drought "*especially in times when heaven threatens the secrets of God with such droughts on earth*" (Dietari de l'Antic Consell Barceloní, vol. 10, p. 181).

(v) **religious sources**

Prayer and processions of religious entreaty are widespread and traditional religious responses to drought events. Typical of the Roman Catholic Church, they were organised to beseech God for rain (*pro pluvia* rogations) or for Him to stop wet/stormy periods (*pro serenitate* rogations), in order to avoid damage to agricultural crops. These processions were often mentioned in the records of local governments (Fig. 4.1). Particularly in the regions that were part of the

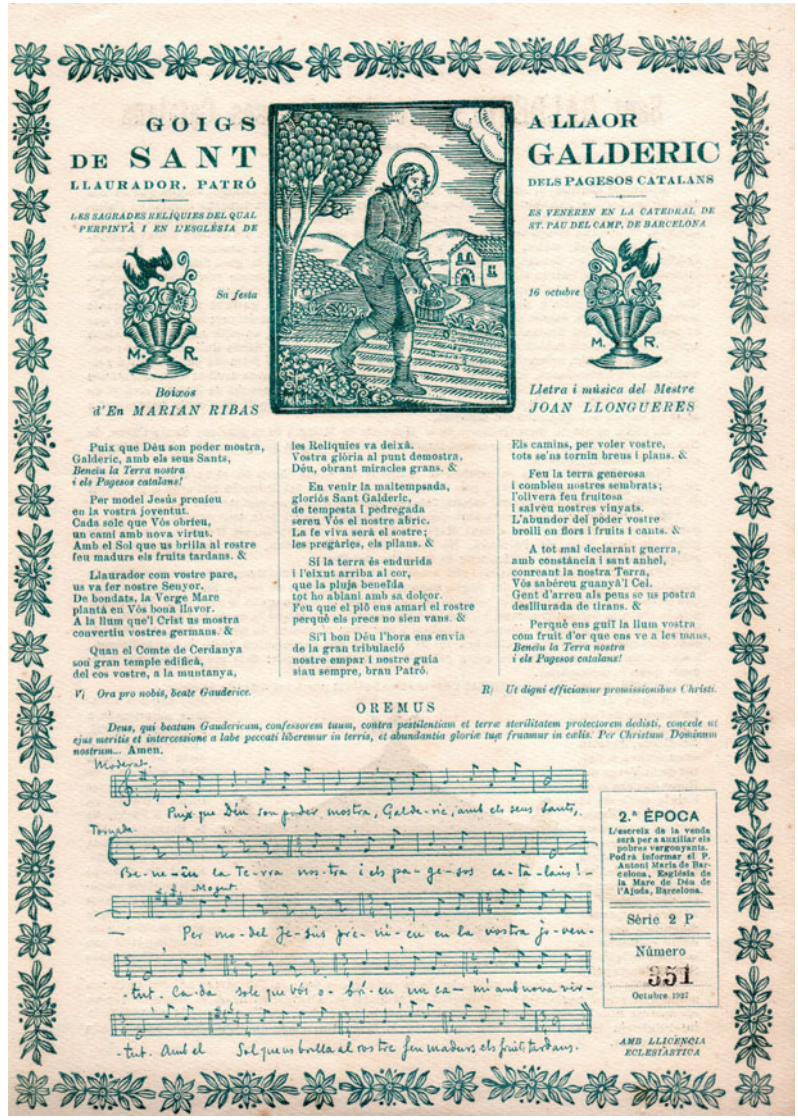
GOIGS
DE SANT
LLAURADOR, PATRÓ
LES SAGRADES RELÍQUIES DEL QUAL PERPINYÀ I EN L'ESGLÉSIA DE
Sa festa
Boixos d'En MARIAN RIBAS
A LLAOR
GALDERIC
DELS PAGESOS CATALANS
ES VENEREN EN LA CATEDRAL DE ST. PAU DEL CAMP, DE BARCELONA
16 octubre
Lletra i música del Mestre JOAN LLONGUERES
Puix que Déu son poder mostra, Galderic, amb els seus Sants, Beneïu la Terra nostra i els Pagesos catalans!
Per model Jesús prenieu en la vostra joventut. Cada sole que Vós obrieu, un camí amb nova virtut. Amb el Sol que us brilla al rostre feu madurs els fruits tardans. &
Llaurador com vostre pare, us va fer nostre Senyor. De bondats, la Verge Mare plantà en Vós bona llavor. A la llum que'l Crist us mostra convertiu vostres germans. &
Quan el Comte de Cerdanya sos gran temple edificà, del cos vostre, a la muntanya, les Relíquies va deixà. Vostra glòria al punt demostra, Déu, obrant miracles grans. &
En venir la maltempsada, gloriós Sant Galderic, de tempesta i pedregada sereu Vós el nostre abric. La fe viva serà el sostre; les pregàries, els pilans. &
Si la terra és endurida i l'eixut arriba al cor, que la pluja benaïda tot ho ablani amb sa dolçor. Feu que el plò ens amari el rostre perquè els precs no sien vans. &
Si'l bon Déu l'hora ens envia de la gran tribulació nostre empar i nostre guia siau sempre, brau Patró. Els camins, per voler vostre, tots se'ns tornin breus i plans. &
Feu la terra generosa i combleu nostres sembrats; l'olivera feu fruitosa i salveu nostres vinyats. L'abundor del poder vostre broilli en flors i fruits i cants. &
A tot mal declarant guerra, amb constància i sant anhel, conreant la nostra Terra, Vós sabéreu guanyar'l Cel. Gent d'arreu als peus se us postra deslliurada de tirans. &
Perquè ens guiï la llum vostra com fruit d'or que ens ve a les mans, Beneïu la Terra nostra i els Pagesos catalans!
V/ Ora pro nobis, beate Gauderice.
R/ Ut digni efficiamur promissionibus Christi.
OREMUS
Deus, qui beatum Gaudericum, confessorem tuum, contra pestilentiam et terræ sterilitatem protectorem dedisti, concede ut ejus meritis et intercessione a labe peccati liberemur in terris, et abundantia gloriæ tuæ fruamur in cælis. Per Christum Dominum nostrum... Amen.
Moderato.
Puix que Déu son poder mostra, Galde-ric, amb els seus Sants,
Tornada.
Be-ne-ïu la Te-rra nos-tra i els pa-ge-sos ca-ta-lans!
Mogut.
Per mo-del Je-sús pre-nì-eu en la vostra jo-ven-
-tut. Ca-da sole que Vós o-bri-eu un ca-mí amb nova vir-
-tut. Amb el Sol que us brilla al rostre feu madurs els fruits tardans.
2.ª ÈPOCA
L'escreix de la venda serà per a auxiliar els pobres vergonyants. Podrà informar el P. Antoni Maria de Barcelona, Església de la Mare de Déu de l'Ajuda, Barcelona.
Sèrie 2 P
Número
351
Octubre 1927
AMB LLICÈNCIA ECLESIÀSTICA

Fig. 4.1 "Goig" of St. Galderic the Farmer (1846 edition). St. Galderic was patron to Catalan farmers, with special focus on drought events in northern Catalonia (Spain). A "Goig" is a text for songs and prayers during rogation ceremonies. A public assistant took this sheet to ensure that the various songs and prayers appropriate to the ceremony were performed perfectly, to the letter (Anonymous 1927)

Hispanic Kingdom, such rogations have proven very useful proxies for droughts events (e.g. Martín-Vide and Barriendos Vallvé 1995; Barriendos 1997, 2005; Domínguez-Castro et al. 2008, 2010, 2012; Tejedor et al. 2018).

Example Barcelona City Council sent an official request to the Cathedral Chapter on 8 November 1715 to start drought rogation ceremonies: "*This day, the City Council of Barcelona sends the deputy of present House with a message to Most Illustrious Chapter of the Cathedral, pleading that, in view of the need for water for the farmland at the present time, an order be served to perform the usual rogations to obtain from God the grace to give us the water we need: And during the 10th day of the aforementioned month the Most Illustrious Chapter came to the present House, confirming to the Board of Illustrious*

Administrators that the Illustrious Chapter had accepted the request, and a 'Collecta pro pluvia' would be convoked and displayed, which is the first step usually taken by the Church" (Dietari de l'Antic Consell Barceloní, vol. 44, fol. 26).

(vi) letters

Letters of a private or institutional character contain information on droughts if a corresponding dry episode concerned the writer in some way. Such communications may contain not only information related to dry weather, but also already-observed impacts of droughts as well as a broader perspective and anticipated socio-economic consequences. An example of the systematic use of private correspondence for climate reconstruction is a paper made by Rodrigo et al. (1998), using Jesuit letters exchanged in Castille (Spain) in the 1634–1648 period, or precipitation reconstruction for Zafra (Spain) by Fernández-Fernández et al. (2015) based on weekly letters from 1750 to 1840.

Example Martin Škvorecký, an administrator at Pacov (Czech Republic), reported to Lady Zuzana Černínová in a letter dated 16 May 1638: "*God's* [harvest] *of winter rye and wheat becoming burned due to extremely hot and dry weather, spring grain similarly. If this continues* [any] *longer, everything in the fields will mature without profit. The grass also appears bad and cannot grow due to great drought*." (Teplý 1928, p. 105).

(vii) songs

Hydro-meteorological events involving loss of lives and great damage, as in the case of floods or flash floods, became themes for the folk songs and broadsheets of the marketplace and shopkeepers. Although drought is a phenomenon without such direct dramatic impacts and consequences, dry episodes also appeared in song form. For example, the severe drought of 1678 in Bohemia inspired the song "A Key to the Rain, or a New Song for a Time of Drought" (*Klíč od deště aneb Nová píseň v čas sucha*) by Václav Šťastný František Rambek, first published in Prague in 1678 and in a second edition a year later (Brázdil and Trnka 2015).

Example "A Song for Want of Rain" (*Píseň za déšť potřebný*), from a manuscript of Antonín Štěpán, a wealthy citizen of Pelhřimov (Czech Republic), consists of 28 verses and is of a supplicatory character. It related to a severe drought in 1790 (Martínková 2005). The second verse of the song provides an insight into its nature (ibid., p. 142): "*For the sake of Your thirst on your cross, have mercy, /Oh Lord, /Water the earth, because* [it] *is thirsty, for it has become cracked /And parched. /Due to this all the crops of the earth /For want of rainwater /*[they] *vanish and perish. /May God grant that* [they] *die not*".

(viii) newspapers and magazines

Weather and climatic extremes appear frequently in newspapers and magazines. Reports of droughts usually take the form of descriptions of the human hardships arising out of lack of water for various aspects of everyday life (reduced water sources, crop failure or bad harvest increases in prices, famine, etc.) or by expression of anticipated negative impacts in the near future. An example of the use of newspaper reports for creation of climate proxies appears as a paper by Gallego et al. (2008), and for compilation of droughts for the island of Ireland as a paper by Murphy et al. (2017).

Examples The French newspaper/journal *Mercure* (1615, pp. 414–415) published an article under the title "*Cold weather, hot weather, drought, and fire ruins this year* [1615] *in Germany & Hungary*". The Austrian newspaper *Wiener Zeitung* (No. 59, 24 July 1748, non-paginated) reported from a Poznań (Poland) correspondent, for 10 July 1748: "*The drought continues even further; it has not rained at all for four weeks, and the cereals of the ground in various areas are completely scorched.*" In 1790 in Vienna (Austria), "*After an almost three-month-long drought, on the 25th* [June] *a great thunderstorm occurred at 5 o'clock in the morning and the fertile but cold rain continued*

Fig. 4.2 A '*pro pluvia'* rogation procession in Paris during the drought of 1694 (Bibliothèque nationale de France, 62 C 2000L; see also Garnier et al. 2015)

for two days …" (*Wiener Zeitung*, No. 52, 30 June 1790, p. 1703).

(ix) **paintings and pictographic evidence**

Compared to the floods, windstorms and severe winters that usually attracted great public attention, droughts and their effects only seldom appear in paintings and pictographic evidence.

Examples Although pictures of processions appear quite often, those related directly to drought are very scarce. One of them is an image of a *pro pluvia* procession from Paris (France) related to drought in 1694 (Fig. 4.2). Another such rare example is a painting titled "Prayer in Time of Drought" by the Russian artist Grigoryi Grigorievich Myasoyedov (1834–1911), dated to between 1878 and 1881, which shows poor people praying for rain, one of the traditional responses to drought (see Fig. 4.8 in Brázdil et al. 2018).

(x) **chronograms**

Chronograms consist of records painted or carved into stone statues, walls or the timber of buildings, but also recorded in chronicles or other narrative sources, that commemorate any significant event (e.g. flood, drought) or years during which people have been heavily affected (e.g., loss of lives, damage). They were quite common in eighteenth-century western and central Europe and were frequently written in Latin or German verse. In a chronogram, selected letters are interpreted as Roman figures (in capital letters or in bold), indicating the year of an event.

Example Hieronymus Haura, a member of the Augustinian order in Brno (Czech Republic),

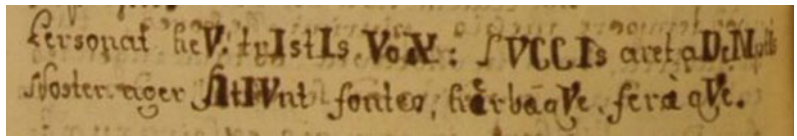

Fig. 4.3 Cut-out of chronogram related to drought in 1746 in the Czech Lands, from the chronicle of Hieronymus Haura

reported a drought of 1746 in his chronicle thus (Fig. 4.3): "Personat he**V**! tu**I**st**I**s **V**o**X**: S**V**C**C**I**s** aret a**D**e**M**pt**I**s /Noster ager s**I**t**IV**nt fontes, herbaeq**V**e, feraeq**V**e." (i.e. It resounds! Oh, woe betide, such a voice: The drought desiccated, it eats up our fields, the springs are thirsty, the plants and animals, too.) The year 1746 follows from the sum of the highlighted Roman figures: V + I + I + V + X + V + C + C + I + D + M + I + I + I + V + V + V (5 + 1 + 1 + 5 + 10 + 5 + 100 + 100 + 1 + 500 + 1000 + 1 + 1 + 1 + 5 + 5 + 5 = 1746) (Brázdil and Trnka 2015).

(xi) epigraphic evidence

Protrusions of bedrock located in river beds have been used as indicators of low-water levels, shown by corresponding year-marks (although the reliability of the marks has to be proved). As signs of long-term hydrological drought, often accompanied by bad harvests and subsequent shortages, they are also known as "hunger stones". Such stones have been reported, for example, for the River Elbe at Děčín (Brázdil and Kotyza 1995), for other places on this river (Elleder 2016) and for the River Danube at Budapest (Palotay et al. 2012).

Example Low-water levels in the River Rhine were recorded on the "Laufenstein" stone in Laufenburg (Germany/Switzerland) (Fig. 4.4a). Walter (1901) reports, as well as visible marks for the years 1541, 1750, 1823, 1858, 1891 and 1893 (Fig. 4.4b), a further four uncertain years: 1692, 1764, 1797 and 1848 (Pfister et al. 2006 consider three of them as correct, with a one-digit correction each: 1672 instead of 1692, 1714 instead of 1764, and 1767 instead of 1797).

(xii) early instrumental observations

Those instrumental meteorological observations that began before the establishment of national meteorological institutes to organise systematic

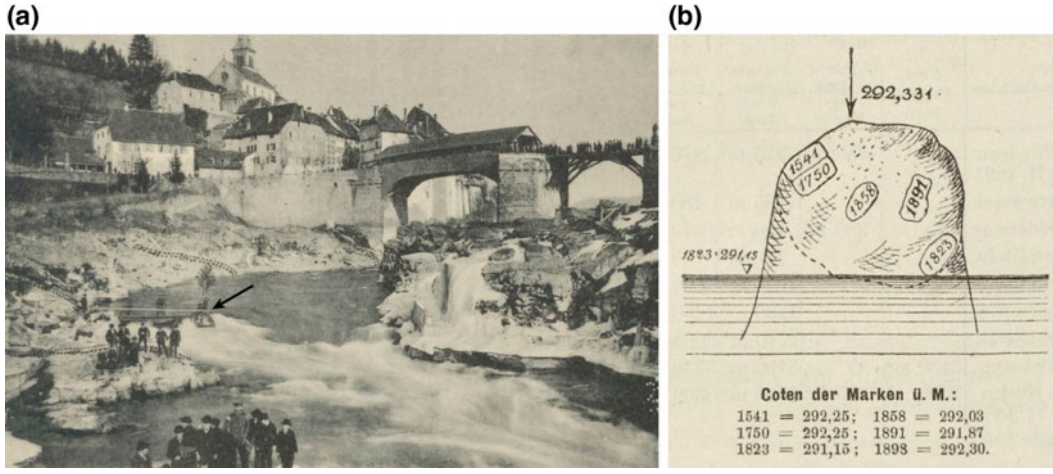

Fig. 4.4 **a** The "Laufenstein" stone (identified by arrow) on the River Rhine at Laufenburg (January 1891); **b** the water marks on "Laufenstein": heights in m asl (Walter 1901)

Sammlung
Von
Natur- und Medicin-
Wie auch
hierzu gehörigen Kunst- und Literatur-.
Geschichten,
So sich
An. 1717. in den 3. Sommer-Monaten
In Schlesien und andern Ländern begeben.
Welcher Gestalt nemlich:
1) Die Veränderung des Gewitters von Tage zu Tage und von Zeit zu Zeit. 2) Land- und Witterungs-Seuchen, von Monat zu Monat, nach dem Einfluß Lufft und Wetters. 3) Zu- und Mißwachs von Feld-Wald- und Garten-Früchten, auch allerhand animalischem Proventu, in allerley Ländern Europens von einer Jahrs-Zeit zur andern bemercket worden: Wie nicht weniger 4) was vor einzelne eclatante natürliche Begebenheiten am Firmament, in der Lufft, auf und unter der Erde, im Wasser, an Menschen und Vieh: auch 5) was vor neue physicalische und medicinische Erfindungen diese Zeit über hervorgebracht und bekant worden: und denn 6) was in re literaria Physico-Medica veränderliches vorgefallen.
Alles in ordentlicher Connexion und mit allerley Reflexions
Aus vielfältiger Correspondenz, und andern Relationibus, so wie grossen Theils aus eigener Erfahrung zusammen gelesen;
Und
Als ein Versuch ans Licht gestellet
Von
Einigen Breßlauischen Medicis.
Sommer-Quartal 1717.
Breßlau,
Bey Michael Hubert, M DCC XVIII.

Fig. 4.5 Title page of the first volume of the Breslau network series with meteorological observations for the summer quarter of 1717

observations in established formal station networks are generally considered "early instrumental observations". At the pan-European level, they arose out of the personal interests of certain individuals [e.g. the Medici Network organised by Grand Duke Ferdinand II de'Medici and his brother Prince Leopold in Italy, with measurements from 1654 to 1670 (Camuffo and Bertolin 2012), and the Breslau Network organised by the physician Johann Kanold in Breslau, recently Polish Wrocław, with published meteorological measurements in 1717–1730 (Fig. 4.5; e.g. Lüdecke 2010)] or some institutes or societies [e.g. *Societas Meteorologica Palatina*, organised by the German Scientific Society at Mannheim, with published meteorological measurements from 1781 to 1792 (Kington 1974)]. Early instrumental observations have been systematically elaborated, for example, for Poland (Przybylak 2010), the Czech Republic (Brázdil et al.

2012a), Portugal (Alcoforado et al. 2012) and Spain (Domínguez-Castro et al. 2014b). As well as measured temperatures and precipitation totals, they may also contain remarks or descriptions concerning dry weather or droughts.

Example With reference to the drought of 1718, reported from Budapest (Hungary) as one of places covered by the Breslau Network (Kanold 1719, p. 1162): "[…] *from the 14th of June, it was reported that, because of the great heat, misery was greatly aggravated there, and the fields and meadows were heavily distressed, so that the marshes and swamps dried out.* […] *because of the lack of water, people were obliged, with their cattle, to move partly to the* [River] *Danube and partly the* [River] *Tisza so that* [the animals] *would not die of thirst* […]."

(xiii) society and professional reports

Droughts and their impacts may also appear in the reports/publications of various learned and other societies engaged in agricultural and forestry production. Such publications became particularly widespread in Europe in the eighteenth–nineteenth centuries. For example, the I. R. Patriotic-Economic Society in Bohemia organised its own network of meteorological and phenological stations and published observations and annual reports of agricultural production (1822–1845), including forestry management reports as well from 1828 onwards (Brázdil et al. 2011; Bělínová and Brázdil 2012). Among individual professional reports, the paper "A note concerning the physical-meteorological causes of constant droughts in Murcia and Almería" by Manuel Rico Sinobas, published in Madrid in 1851, is one example of a professional report, possibly the first scientific approach to drought in Spain, considering not only atmospheric processes, but also deforestation impacting on soil moisture, land use changes, etc.

Example A recent drought is reflected in a report of the French "*Société royale de medicine*" in Paris for 18 September 1781 (Réflexions 1781, p. 1): "*Diseases have occurred in the capital and its surroundings which, although not an epidemic proper, have nevertheless acquired a somewhat general character, which must be attributed to the heat and excessive drought that have made this season remarkable especially for* [we] *"Medics" whose role is to compare the phenomena that nature presents to us with the changes which these phenomena produce,* [and] *present to us in our system*".

(xiv) weather compilations

Although such compilations cannot be treated as a separate source type, their widespread application renders as it is necessary to mention such data and text collections in some detail. There exists quite a long tradition of collecting and publishing weather-related (including drought-related) reports in Europe. Particularly worthy of mention are the compilations by Weikinn (1958–2002) for Europe and by Buisman (1995–2006) for the Low countries. Because these compilations gather data from historical sources of varying quality, usually without critical evaluation of sources, their practical use may be biased, producing misleading or even erroneous results (for criticisms of compilations see e.g. Bell and Ogilvie 1978). Even compilations prepared with a source-critical approach (e.g. Malewicz 1980; Alexandre 1987) may require additional source analysis.

In order to preserve documentary data, usually collected at national levels, then prepare them for the analysis using computers, as well as to make them accessible to further researchers, some databases (also containing drought-related information) have been created in Europe. Among the foremost are the Euro-Climhist database, started by C. Pfister in Bern (Switzerland) (http://www.euroclimhist.unibe.ch) and the Tambora database, started by R. Glaser in Freiburg (Germany) (https://www.tambora.org; Riemann et al. 2015).

4.3 Methods of Drought Reconstruction

4.3.1 Interpretation of Droughts from Documentary Data

As partly follows from examples of reporting drought in documentary sources (see Sect. 4.2), the following indicators of individual types of drought may be found in documentary evidence (see also Brázdil et al. 2018):

(i) **meteorological drought**

Meteorological drought is indicated by reports describing, for example, a lack of rain, drought, dry weather, hot and dry weather, periods without rain, "rain that hardly moistened the soil", "rain needed", drought "beyond living memory" and dust on the roads.

(ii) **agricultural drought**

The occurrence of agricultural drought is made evident, for example, by information related to complete failure of crops or bad harvests, lack of seed, lack of feed for livestock, cracked earth, dried-out pastures, limited availability of straw, conditions impossible for soil cultivation or sowing (Fig. 4.6), tearing grain by hand rather than reaping, the occurrence of outbreaks of caterpillars, mice and other pests or damage to crops.

(iii) **hydrological drought**

The occurrence of hydrological drought can be derived, for example, from information reporting low-water levels in rivers and the appearance of hunger stones, standing and/or green water in rivers, crossing large rivers "barefoot" or with wagons, springs, wells, fountains, brooks, streams and fish cultivation ponds drying out, lack of water for people and animals, sale of water, watermills out of operation, cessation of river transport or lack of water for extinguishing fires.

(iv) **socio-economic drought**

Among the indicators of socio-economic drought that may appear in documentary evidence are, for example, information concerning bad harvests, food shortages, price rises (grain and other

Fig. 4.6 Drought had a negative influence not only on the growth of field crops, but also on soil cultivation (ploughing, sowing): a ploughman by Matouš Ornys z Linperka in the Třebenice hymn book, 1577–1578 (*Photo* O. Kotyza archive)

crops), poverty, debt, distress, famine, requests for tax reduction, administrative measures, raised awareness of alleged witchcraft and other rain-related ritual practices, human mortality, disease, epidemics, emigration, fires consuming both buildings and forests and the sale of livestock at well below normal market prices. However, because of the intrinsic complication of this suite of effects, the triggers of drought and its role in socio-economic processes or phenomena have to be clearly indicated or proved.

The overview of basic drought-related documentary sources in Sect. 4.2 makes it clear that work with such evidence requires a careful and critical approach to the collection, interpretation and elaboration of drought information from prevailingly qualitative data. The following steps appear the most important: (i) use of information about drought-related events experienced by the author of the records (primary sources); (ii) a critical approach to documentary sources with respect to their origin (contemporary or non-contemporary; local or foreign) and the contemporaneous socio-economic situation; (iii) temporal and spatial cross-checking of various data; (iv) careful meteorological interpretation and analysis of the evidence available, supported by knowledge of recent climatic patterns in the area studied (for more details see, for example, Brázdil et al. 2005, 2010).

4.3.2 Drought Reconstructions

A range of statistical approaches to quantitative climatic reconstruction (particularly for temperatures and precipitation) have been applied in historical climatology in recent decades. For some time, these were targets for a degree of criticism from scientists not involved in the historical-climatological community. This changed when standard palaeoclimatological methods of climate reconstruction began to be applied to historical-climatological research (see e.g. Leijonhufvud et al. 2008, 2010; Dobrovolný et al. 2009, 2010).

Three types of documentary-based reconstructions of dry patterns, drought characteristics and drought indices may be categorised:

(i) **series of precipitation indices**

Series of precipitation indices may be employed to analyse drier and wetter periods. Depending on the density and quality of the documentary evidence, appropriate precipitation indices may be created. For example, a 3-degree scale may classify months as dry (−1), normal (0) or wet (1), while a 7-degree scale may break down as extremely dry (−3), very dry (−2), dry (−1), normal (0), wet (1), very wet (2) and extremely wet (3). Seasonal (winter DJF, spring MAM, summer JJA, autumn SON) or annual values are obtained as sums of indices for the corresponding months (e.g. Pfister 1992). Applying standard palaeoclimatological methods, series of precipitation indices may then be used for reconstruction of precipitation totals (e.g. Dobrovolný et al. 2015).

(ii) **series of drought frequency or drought proxies**

Various approaches have been used to create series of drought frequencies and drought proxies:

- combination of several consecutive months classified as dry, very dry or extremely dry (e.g. at least two such consecutive months were considered as a drought episode by Brázdil et al. 2013)
- Drought Rogation Index, taking into account the five levels of drought intensity/duration according to the hierarchical system of religious rogation ceremonies (e.g. Martín-Vide and Barriendos Vallvé 1995; Barriendos 1997)
- Drought Index (DI): DI = 1 for meteorological drought associated with agricultural drought in at least in two places (central-southern Italy), otherwise DI = 0; if at least three successive months could be classified as DI = 1, this is considered a drought year (Diodato and Bellocchi 2011).

(iii) **series of drought indices**

Reconstructed monthly series of mean temperatures and precipitation totals for the same area can be further used for calculations of series of drought indices. Temperature series for central Europe (Dobrovolný et al. 2010) and precipitation series for the Czech Lands (Dobrovolný et al. 2015) were used to calculate series of seasonal, summer half-year and annual SPI, SPEI, Z-index and PDSI from AD 1501 onwards for the Czech Lands by Brázdil et al. (2016). Further, phenological series sensitive to drought can be used for calculation of drought indices, as has been demonstrated for April–August SPEI reconstructed from grape harvest dates for the Bohemian wine-growing region from AD 1499 onwards by Možný et al. (2016).

4.4 Droughts in Historical Times in Europe

4.4.1 Spatiotemporal Overview of the Long-Term Variability of Droughts

The results of long-term spatiotemporal variability of droughts, based either fully or partly on documentary evidence, are summarised below by European region. The northern Europe region is not included due to a current absence of documentary-based, long-term drought series.

4.4.1.1 The Mediterranean

Although several series of precipitation indices or precipitation totals have been reconstructed for the Mediterranean (Rodrigo et al. 1995, 1999; Diodato 2007; Rodrigo 2008; Rodrigo and Barriendos 2008), *pro pluvia* rogations remain the basic source of information for Spain (e.g. Tejedor et al. 2018) and also, in part, for Portugal (Fragoso et al. 2018) and Italy (Piervitali and Colacino 2001). Drought fluctuations in the Mediterranean may be described in terms of different types of documentary-based, drought-related series:

(a) annual values of the weighted Drought Rogation Index for the Catalonian coast of north-eastern Iberia, 1501–1860 (Martín--Vide and Barriendos Vallvé 1995; Oliva et al. 2018)
(b) annual Drought Weighted Index Sums (DWISs) for central-southern Italy, 1501–2000 (Diodato and Bellocchi 2011)
(c) a series of 50 *pro pluvia* processions in Erice, Western Sicily, 1565–1915 (Piervitali and Colacino 2001).

It follows from Fig. 4.7 that it is difficult to find any common features in the series of decadal fluctuations of Mediterranean droughts employed, a factor reflected in statistically insignificant correlation coefficients among all three series. Some coherence is apparent for the driest decades between 1541 and 1570 in Spain, based on rogation indices (Fig. 4.7a) and Italian DWISs; in Italian series, the decades 1541–1550 and 1791–1800 were the driest (Fig. 4.7b). On the other hand, four *pro pluvia* processions occurred in Western Sicily in 1661–1670, while in the other decades, their frequency was between zero and three (Fig. 4.7c).

The drought information appearing in Fig. 4.7 may be extended back to before AD 1500 by surviving Byzantine documentary sources for the eastern Mediterranean and the Middle East. Based on these, Telelis (2008) detected a higher frequency of droughts (at least two dry events of extended duration per decade as inclusion criterion) in AD 360–390, 530–580, 690–720 and 1090–1200 for the temperate semi-arid regions, in AD 320–340, 390–420, 450–480, 510–560, 600–630, 740–770, 1040–1070, 1130–1200 and 1290–1320 for the desert region, and in AD 560–590, 740–790, 1020–1050, 1070–1110 and 1140–1160 for the Mediterranean regions. Domínguez-Castro et al. (2014a), analysing 11 Islamic chronicles with high temporal and spatial resolution for Iberia in the AD 711–1010 period, identified three severe droughts in 748–754 (drought reported each year), 812–823 (droughts with long famines) and 867–879 (droughts with references to famine).

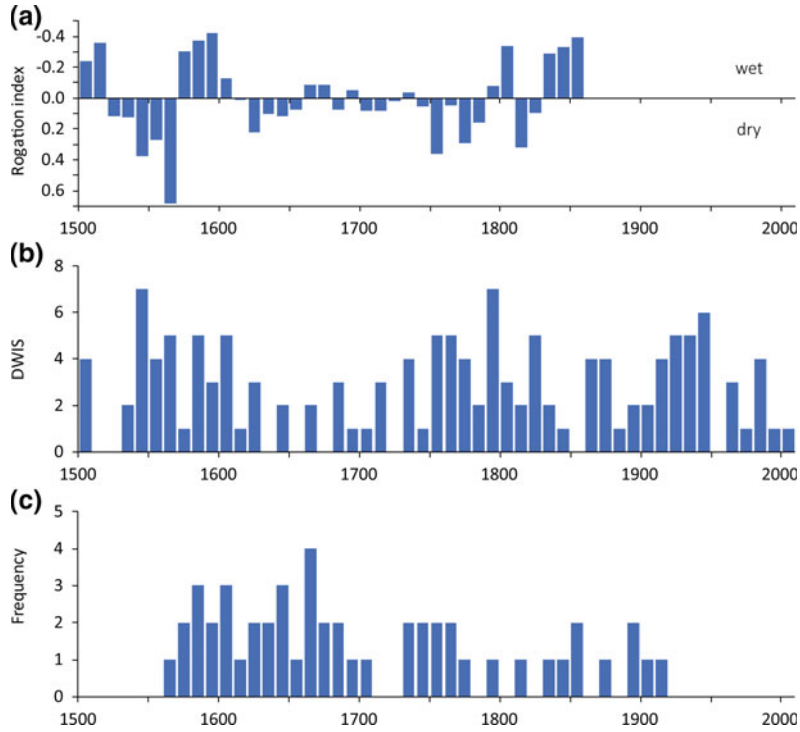

Fig. 4.7 Fluctuations in decadal values of drought-related series in the Mediterranean: **a** means of the weighted Drought Rogation Index for the Catalonian coast of north-eastern Iberia, 1501–1860 (Martín-Vide and Barriendos Vallvé 1995; Oliva et al. 2018); **b** Drought Weighted Index Sums (DWISs) for central-southern Italy, 1501–2000 (Diodato and Bellocchi 2011); **c** frequency of *pro pluvia* processions in Erice, Western Sicily, 1565–1915 (Piervitali and Colacino 2001)

4.4.1.2 Western Europe

Drought patterns for the past millennium in western Europe are covered by a number of types of documentary-based, drought-related series:

(i) annual frequencies of unusually dry JJA months in western Europe derived from various chronicle sources, 1000–1419 (Alexandre 1987)

(ii) "precipitation scores"—dry patterns identified for England by monthly scores of −2 (slightly more dry than normal) and −3 (particularly dry), although with many missing data (June and July are the most complete), 1200–1439 (Ogilvie and Farmer 1997)

(iii) a series of 40 droughts for the UK and 68 droughts for the Ile-de-France region (Paris and surroundings), 1500–2014, with severity classified according to the Historical Severity Drought Scale (HSDS), graded from 1 to 5 (Garnier 2019)

(iv) a drought catalogue for the island of Ireland represented by SPI-12 values (based on documentary data before 1850), 1765–2015 (Noone et al. 2017).

As Fig. 4.8a–b indicate, each of the three decades with the highest frequencies of dry JJA months in series for western Europe and England agree in 1371–1380 and 1411–1420 and differ in 1241–1250 (only western Europe) and 1301–1310 (only England). While frequencies of droughts in the UK from AD 1500 fluctuate only between zero and two (Fig. 4.8c), droughts for the Ile-de-France region indicate a very distinct peak between 1691 and 1740 (with five droughts in 1701–1710 and four in the following decade), but no such events are apparent in the subsequent 30 years after 1740 (Fig. 4.8d). SPI-12 values for the island of Ireland (Fig. 4.8e) indicate that the 1801–1810 decade was the driest, followed by another drier period between 1831 and 1860. Correlation coefficients among all the five series analysed are statistically non-significant.

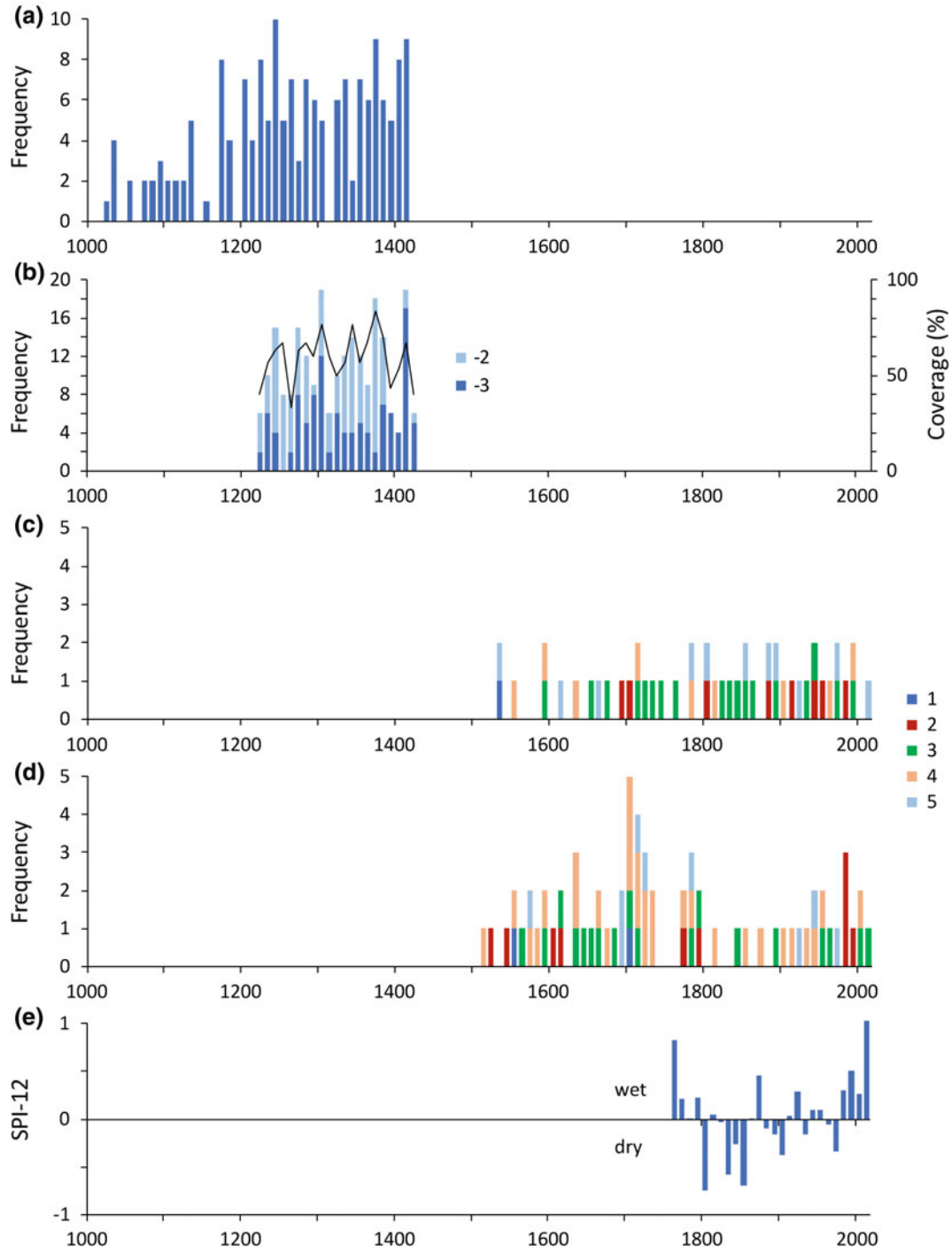

Fig. 4.8 Fluctuations in decadal values of drought-related series in western Europe during the past millennium: **a** frequencies of unusually dry JJA months, western Europe, 1000–1419 (Alexandre 1987); **b** frequencies of months with "scores" −2 and −3 corresponding to dry patterns (columns), UK, 1221–1430 (Ogilvie and Farmer 1997) with percentage coverage of totally interpreted months (line); **c** frequency of droughts with respect to their severity according to HSDS (1: absence of rainfall, 2: locally low waters, 3: general low waters, 4: severe low-water marks and 5: exceptional drought), UK, 1500–2014 (data derived from Garnier 2019); **d** the same, Ile-de-France region, France, 1500–2014 (data derived from Garnier 2019); **e** means of SPI-12, Ireland, 1765–2015 (Noone et al. 2017)

4.4.1.3 Central Europe

Drought patterns for the past 500 years in central Europe may be covered by several types of drought-related series:

(i) monthly precipitation indices series derived from documentary data for Germany, 1501–1850, and reconstructed seasonal and annual precipitation totals since AD 1501 (Glaser 2001, 2008)
(ii) monthly precipitation indices series derived from documentary and instrumental data for Switzerland, 1550–2003 (Pfister 1999, extended)
(iii) seasonal, summer half-year and annual series of drought indices (SPI, SPEI, Z-index and PDSI) for the Czech Lands, AD 1501–2017 (Brázdil et al. 2016, extended)
(iv) April–August SPEI series for the Bohemian wine-growing region, Czech Lands, 1499–2012 (Možný et al. 2016).

Documentary-based, drought-related series in central Europe, represented by reconstructions for Germany, Switzerland and Czech Lands (Fig. 4.9), show slight coherence, expressed by statistically significant correlation coefficients only between German and Czech summer half-year SPEI ($r = -0.34$) and the two Czech series ($r = 0.58$). The decade of 1811–1820, with the highest frequency of precipitation indices indicating dry patterns (from dry to extremely dry) in Germany (Fig. 4.9a) also exhibits the highest frequency for Switzerland (Fig. 4.9b), where 1661–1670 also appears with the same frequency. However, two subsequent decades with higher frequencies in Germany (1771–1780, 1791–1800) disagree with those in Switzerland (1661–1670, 1821–1830). Droughts expressed by SPEI for the Czech Lands dominate in the pre-instrumental period in 1721–1730 for the Czech summer half-year (Fig. 4.9c), while for April–August SPEI in Bohemia, the equivalent period is 1531–1540. Droughts in both decades also appear in other Czech (Bohemian) series, but are less intense. A higher frequency of droughts in the last decades of the eighteenth century and at the beginning of the nineteenth century in Germany corresponds to drier patterns expressed by SPEI in the both Czech series.

4.4.1.4 Eastern Europe

The non-chernozem European part of the former Soviet Union was addressed by Lyakhov (1984), who presented frequency of extremely dry and wet MAM–JJA seasons for 30-year intervals from the thirteenth century to 1980. Nine extremely dry seasons appeared in 1351–1380, 1831–1860 and 1891–1920, eight in 1201–1230 and seven in 1411–1440, 1801–1830 and 1951–1980. In contrast, only one extremely dry season each was recorded for the 1231–1260 and 1771–1800 periods (Fig. 4.10a). A compilation containing a thousand-year history of unusual natural events in the Russian Lands and western Europe from Russian written sources by Borisenkov and Pasetskiy (1988) appeared after Lyakhov's paper, later extended back to the fifth century BC (Borisenkov and Pasetskiy 2002). But lack of territorial focus in listed drought events (*zasucha*) complicates critical use of their presented drought chronology. More recently, Shmakin et al. (2013) presented documentary-based droughts over the Eastern European Plain during the eleventh–nineteenth centuries, classifying them into three categories, with 29 droughts in category 1 (local droughts without described impacts), 31 droughts in category 2 (regional droughts with described impacts) and 16 droughts in category 3 (drought in several regions with described heavy impacts). The highest frequency of droughts was found in 1861–1890 with seven dry episodes. Several 30-year periods without any drought or with one–two droughts may reflect insufficient density of documentary sources available (Fig. 4.10b). Besides significantly smaller number of droughts in Shmakin et al (2013) compared to Lyakhov (1984), both series are not statistically significant correlated.

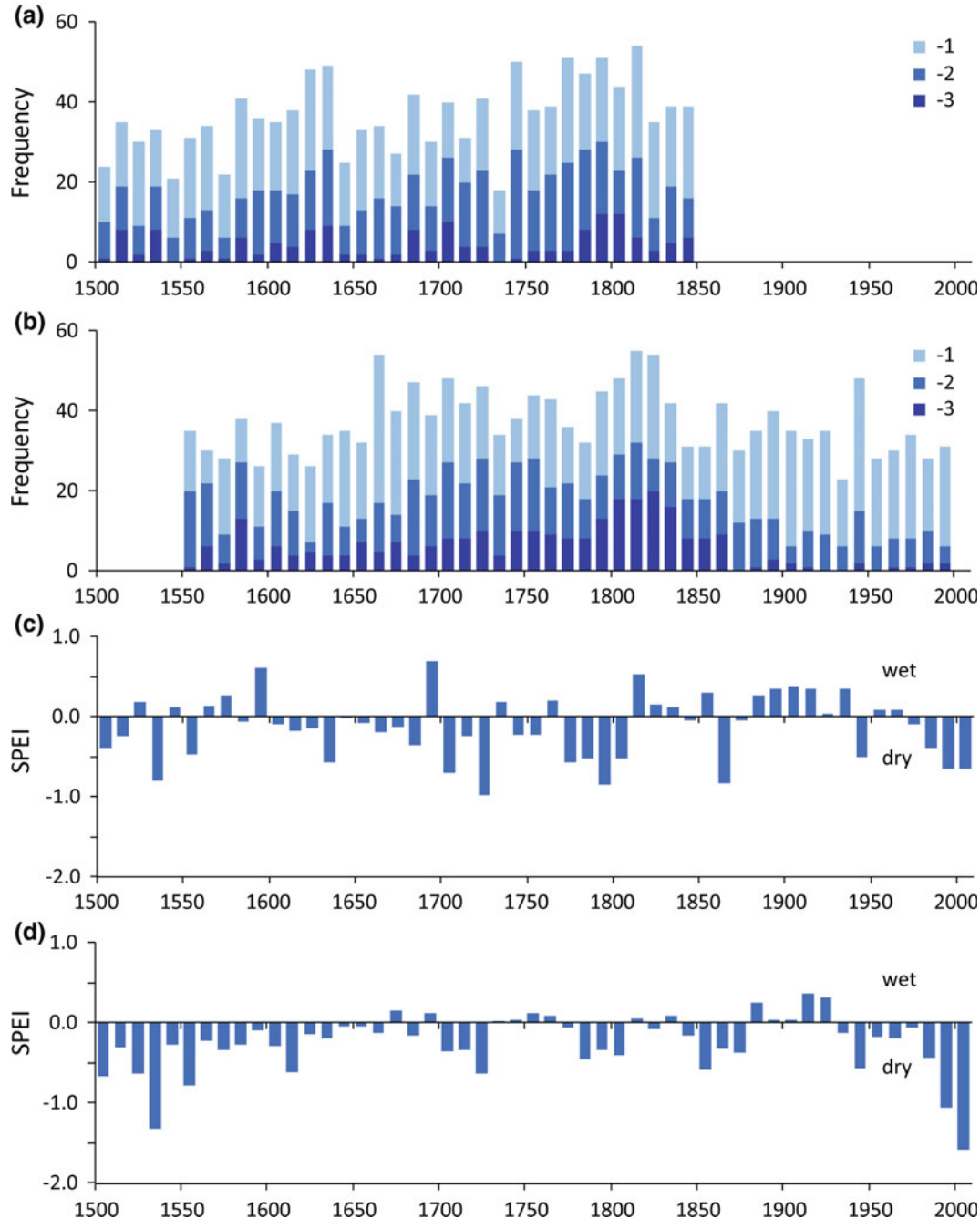

Fig. 4.9 Fluctuations in decadal values of drought-related series in central Europe during the past 500 years: **a** frequency of precipitation indices expressing dry patterns (−1 dry, −2 very dry, −3 extremely dry), Germany, 1501–1850 (Glaser 2001, 2008); **b** same as (**a**) for Switzerland, 1551–2000 (Pfister 1999); **c** means of summer half-year SPEI in the Czech Lands, 1501–2010 (Brázdil et al. 2016); **d** means of April–August SPEI in Bohemia, Czech Lands, 1501–2010 (Možný et al. 2016)

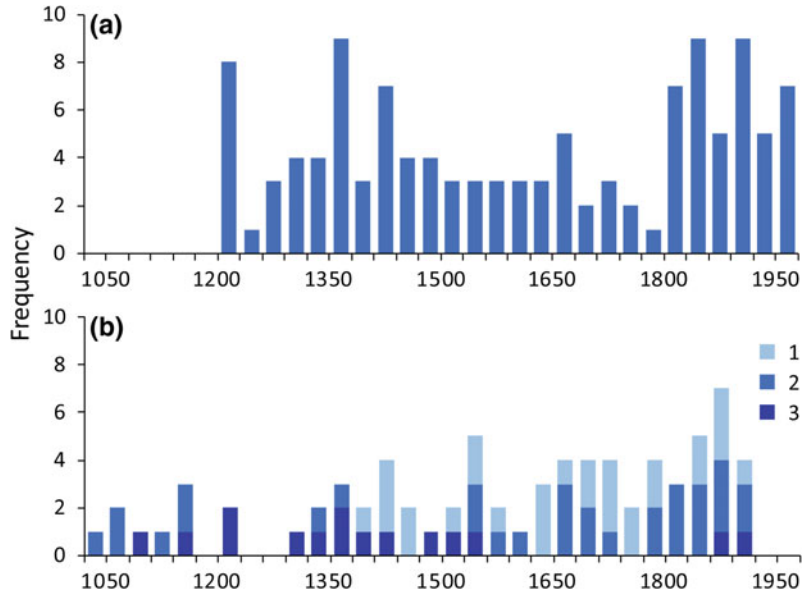

Fig. 4.10 Fluctuation of 30-year frequency of droughts in eastern Europe during the past millennium: **a** Non-chernozem European part of the former Soviet Union, 1201–1980 (Lyakhov 1984); **b** Eastern European Plain, eleventh–nineteenth century, the last column only 1891–1900 (Shmakin et al. 2013). Key: 1—local droughts without described impacts, 2—regional droughts with described impacts, 3—drought in several regions with descriptions of severe impacts

4.4.2 Examples of Outstanding European Droughts in the Past

Using documentary evidence, and judging by their meteorological character and impacts, many past drought events have been identified as extreme or outstanding at national levels. On the European scale, this is especially true of the year 1540, which Wetter et al. (2014) used to coin the term "megadrought" for long and intense dry patterns deducible from rich documentary evidence in western and central Europe. Also, identified as a very warm year (Wetter and Pfister 2013), it has been compared with the patterns of a far more recent extreme year in 2003 (e.g. Orth et al. 2016; Pfister 2018). The year 1473 was also described as an outstandingly warm and dry year by Camenisch et al. (2019). Without repeating the facts related to these events, some further examples of outstanding European droughts are described in brief below.

4.4.2.1 Drought in 1361

Although 1360 and 1362 might have been to some extent dry, the most important drought occurred in England in 1361 (Pribyl 2017). In Liège (Belgium), the year 1361 was characterised by a great drought, although the wine vintage was good (but heat and dry weather had already been reported there in 1360). A good wine vintage was also noted for Fosses in northern France. Early ripening of fruit and grapes, as well as an early vintage took place in France (e.g. Bordeaux, Metz), Germany (e.g. Konstanz) and also northern Italy (e.g. Bologna). In the southern German areas, Austria, Poland, Silesia and Hungary, great heat and drought resulted in moderately bad cereal harvests. The excessive summer heat also reached the Baltic Sea area (e.g. Bremen) in 1361, followed by abundant rainy spells later (Alexandre 1987).

Several contemporary sources reported a major drought event for 1361 in central Europe. A hot and dry summer occurred in Silesia and

Poland, where drought together with frequent thunderstorms and frost in June combined to produce a bad harvest. Quite bad grain harvests caused by drought were also reported from Austria, Bohemia and Hungary, with increases in prices. This situation caused particular difficulties in the food supply as, for example, in Vienna (Malewicz 1980; Brázdil and Kotyza 1995; Rohr 2007; Kiss and Nikolić 2015; Kiss 2017). These factors contributed to shortages and famine continuing through to 1362; these resulted, for example, in an instruction from the Czech king and Emperor Charles IV to collect any excess of grain into community granaries in Bohemia (but rather for military purposes), and even to the prohibition of grain export from the Hungarian and Croatian kingdoms (Brázdil and Kotyza 1995; Kiss and Nikolić 2015). In central Dalmatia, significant confrontation had to be resolved in March 1362, when the Morlachs, far from their homelands, received—rather exceptionally—permission from the Duke of Dalmatia to use the lands of Trogir town, in view of the great drought (see Sect. 4.2, point (iv)). Similarly, excessive drought-related problems were mentioned along the French Mediterranean coastline, where religious processions of entreaty for rain were organised in mid-April and early May at Nimes (see Alexandre 1987; Kiss and Nikolić 2015).

4.4.2.2 Drought in 1616

In the Netherlands, JJA of 1616 was described as much hotter and drier than usual; in some areas with devastating hail at the end of June and with destructive fires in, among other places, Amsterdam (Buisman 2000). In Germany, a dry episode started in mid-April of 1616 and continued over JJA; this drought led to a very bad haymaking season and an inferior harvest of cereals. Phenological phases started much earlier than usual (e.g. the vintage was a month early) and the wine was very good. Many fires broke out (e.g. Buisman 2000; Glaser 2008, 2013). Glaser (2008) classified MAM as mild and dry, JJA as very hot and extremely dry and SON as dry. No rain fell between 6 June and 30 July in Switzerland and the grass perished; Pfister (1999) classified both these months as extremely warm and extremely dry.

Dry patterns also prevailed in the Czech Lands (Brázdil et al. 2019). For example, no rain was recorded between 3 April and 31 July in Louny in north-western Bohemia and the drought continued into SON. Documentary sources reported significant drought impacts: shortages of water; lack of water to drive watermills, which forced people to travel great distances to grind their grain; very bad grain harvests; great heat; dried-up rivers and the River Vltava "stinking" at Prague and more. Extreme drought in 1616 in the Czech Lands is commemorated by a low-water mark on the 'hunger stone' in the River Elbe at Děčín, while a printed sermon by the Reverend Daniel Philomates the Elder spoke of a 100-year drought (Fig. 4.11). Similarly, JJA in Hungary was long and very hot, with great drought. Apart from a significant drop in water levels, frequent thunderstorms and fire events, the cereal harvests and the haymaking were very bad, but vine and fruit harvests were better. Mice and starlings appeared in abundance, while many people died of dysentery (e.g. Kovács 1995).

Of only a general character is information about the 1616 JJA drought in Latvia (Tarand et al. 2013) and of intense heat and severe droughts in Istria, where many people fell ill and livestock died (Ogrin 2002). A great drought followed by famine also occurred in the European part of Russia (Shmakin et al. 2013; Yurchenkov 2014). Droughts in 1616, as in 1615, also occurred in the various parts of England, but it appears that their severity did not reach the level of the intense drought of 1612 (Jones et al. 1984; Pribyl and Cornes 2019). Significant drought, which destroyed harvests, has already been mentioned regarding Germany and Hungary in 1615 (*Mercure*, 1615, pp. 414–415).

4.4.2.3 Drought in 1718–1719

In the Netherlands, August 1718, as well as the entire JJA period (as in 1719) were among the hottest and driest for many years (Buisman 2006). Drought and low-water levels were also reported in France (again, as in 1719); a great

Fig. 4.11 Two surviving records of the extreme severity of the 1616 drought in the Czech Lands: **a** a mark on the hunger stone located in the River Elbe at Děčín-Podmokly, 1904 (*Photo* O. Kotyza archive); **b** a printed sermon by the Reverend Daniel Philomates the Elder related to the 1616 drought (Collection of the National Museum, Prague)

(accidental) fire broke out in late April along the River Seine in Paris (Kanold 1719). In 1718, very warm and dry weather set in as early as April–May in eastern Austria. In JJA, with extended sweltering weather, crops perished, the earth was cracked, forest fires occurred, and wells, springs, rivers, brooks and lakes dried up (Strömmer 2003). Records from Germany speak of a hot and very dry JJA with damaging consequences, making particular mention of the soil cracking. Warm weather continued into September; the wine was considered good (Glaser 2008). According to documentary evidence from the Czech Lands, MAM and JJA were very dry, leading to considerable consequences. For example, the grain harvest was very bad, resulting in shortages and increases in prices; low-water levels, even rivers drying out, put some watermills out of operation, forcing people to go great distances to mill (Brázdil and Kirchner 2007). In Switzerland, a warm and dry period started on 20 May and continued, with a degree of interruption in the last third of October, until the end of November. However, Pfister (1999) classified only July as very dry and September as extremely dry. In Slovenia, the year of 1718 was described as hot and dry with shortages in the coastal zone (the Piran area). Agricultural crops, grapes and olives perished due to dry weather, leading to causing heavy losses (Ogrin 2002). Great heat and drought were also reported from Volhynia (today's south-eastern Poland, south-western Belarus, and western Ukraine), Podolia (today's west-central and south-western Ukraine and north-eastern Moldova) as well as the southern Romanian principality Valachia (Kanold 1718). In the southern part of the Carpathian Basin, in the Temesvár/Timişoara (SW Romania) the rivers and swamps dried up, and the excessive heat and drought reportedly continued until early November in the area of present-day Slovakia (Kanold 1720). Severe heat and drought were reported also in Italy. Excessive heat and drought also prevailed in JJA and early SON in Scandinavia (Kanold 1720).

Great heats and extreme droughts in 1719 from May to August were mentioned in the Norfolk county in England with scorched pastures, dried-up pits and ponds and lack of water for livestock (see Sect. 4.2, point (i); Kington 1980). In eastern Austria, MAM and JJA of this year were characterised by very warm weather and great drought. Grass and cereals perished utterly, summer crops were very bad, the grapes were harvested extraordinarily early and trees blossomed two or three times in some places (Strömmer 2003). Outstanding periods of heat and drought prevailed in JJA in Germany. In Brandenburg, for example, no rain fell in the

eight weeks leading up to 20 August; rivers such as the Oder had ran very low indeed; forest fires broke out; an already poor bad grain harvest was exacerbated by an overabundance of mice in the fields. Warm and dry weather continued during SON (Glaser 2008). In Switzerland, only scant precipitation fell from mid-March to 20 June, not even enough to moisten the soil. April, May and June were classified as very dry. Periods of heat in July were broken by thunderstorms, but August was again interpreted as very warm and extremely dry. Wells dried up and people were forced to travel great distances for water and milling (Pfister 1999).

Reports for 1719 from the Czech Lands speak of great periods of heat and drought in JJA, with serious consequences: problems with milling due to lack of water, bad harvests of grains and flax, dry grass in the pastures, etc. Matters were serious enough at the end of August for processions of entreaty for rain to be organised in Uherské Hradiště (Brázdil and Kirchner 2007). In Hungary, very dry and hot weather prevailed from April (at the latest) throughout JJA, with devastating hailstorms reported all over the country in June. While low waters were already occurring in some areas in MAM, many large bodies of water dried up in SON, leading to shortages, although the period was already wetter in certain areas. The cereal harvest was scant or completely lost. The drought, and its consequent food shortages, hunger and even famine, was at its worst in Transylvania (e.g. Csáki 2010) and in the southern part of the Carpathian Basin, but similar drought-related problems were also reported from Croatia and Serbia (Kanold 1719). Due to an exceptionally poor hay harvest, people moved, together with their cattle to the great rivers, i.e. the Danube and the Tisza. An infamous witchcraft trial, directly associated with the great drought, started in Szeged in the same year (Kanold 1719; Petrovics 2005). In Latvia, the drought was so extraordinary that bushes and tussocks dried out to their very roots and the water in the River Daugava was so low that it was possible to drive carts through it in many places (Tarand et al. 2013).

4.5 Drought Impacts and Societal Responses

Because many impacts and responses of droughts were already generally reported in Sects. 4.3.1 and 4.4.2, this section concentrates particularly on the major topics: in which ways drought affected society and how society responded on the effects of this major natural hazards in the mediaeval and early modern period.

4.5.1 Impacts of Drought on Society

Apart from the primary shortage or lack of appropriate drinking water for human consumption and for domestic animals, probably the most important problems arose in agricultural activities. It was particularly the lack of (appropriate) rainwater in the periods crucial for the vegetation growth. Further, intriguing factors for the agriculture during drought were heat waves and the higher frequency and intensity of destructive convective events (thunderstorms, hails, torrential rains, heavy winds). The negative effects of drought could be different under various climatic conditions. While in central and eastern Europe or the Mediterranean, a drought usually meant bad cereal harvest (wheat, barley, rye, oat) and played an important role in the development of dearth and famine, for example, in England, it was mainly the oat and barley that suffered, whereas wheat yields were usually above average, and a drought year typically did not mean a famine year (e.g. Jones et al. 1984; Brázdil and Kotyza 1995; Ogrin 2002; Glaser 2013; Pribyl 2017). However, all over Europe, droughts were accompanied by weaker legume harvests and bad hay harvests. In western and west-central Europe drought was usually followed by good quality and good or normal quantity grapevine and fruit; towards the east, also depending on the conditions of the preceding period, droughts were accompanied by low quantity of wine and fruit (e.g. Brázdil and Kotyza 1995; Glaser 2013; Camenisch 2015). Apart from bad harvest, dried-up soils were more difficult to plough.

Trees during drought also dried up in increasing numbers that sometimes concerned also fruit trees (e.g. Ogrin 2002; Pribyl 2017). The negative impact of bad harvest due to drought was in some cases strengthened by inflexible taxation, for example, by the special food taxes for the army as in 1717 in Transylvania (Csáki 2010).

Drought also resulted in great problems in animal husbandry and pastoral communities: the lack of drinking water in parallel to the bad hay harvest and the dried-up pastures caused a great stress for domestic animals, especially for the young ones, all over Europe. Drought years were often accompanied by the mass losses of domestic animals caused partly by the lack of appropriate water and fodder, but also due to the easily spreading diseases what the underfed, weakened animals were much more prone to than in normal years (e.g. Ogilvie 1990; Bellon 1996; Ogrin 2002; Kiss 2009; Cullen 2010; Gómez-Baggethun et al. 2012; Kiss and Nikolić 2015; Pribyl 2017; Fragoso et al. 2018). The lack of water and excessive heat not only affected the animals themselves, but generally also dairy production, i.e. milk and milk products (e.g. Gómez-Baggethun et al. 2012; Gerrard and Petley 2013). When referring to domestic animals, less obvious cases also have to be taken into consideration. For example, excessive heats and droughts negatively affected bees and bee-products, but regarding cultivated vegetation the same is true for some of the important drought-sensitive vegetables such as cabbage which, in a preserved form, was usually a main source of vitamin supply in wintertime (Kiss 2019).

Animal invasions during and after the drought period often increased the stress caused by drought, mainly affecting the anyway bad harvests. Although locusts (Fig. 4.12) are usually associated with drought, apart from areas where locusts stayed and nested for years (e.g. in Hungary—Kiss 2009), their invasion usually occurred in the affected parts of Europe after grain harvest time, and their impact was spatially restricted (Rohr 2007; Brázdil et al. 2014). Additionally, other pests such as birds, caterpillars, mice and hamsters (e.g. Brázdil et al. 2008, 2018; Pribyl 2017; see also Sect. 4.4.2.2) might have also accompanied drought events that further decreased harvest outcomes.

The shortage of drinking water, lack of cereals and other drought-related circumstances resulted in high prices, malnutrition, higher child mortality, dearth and famine in human population, and favoured the renewed occurrence, spread and increase of certain diseases such as dysentery or plague (e.g. Behringer 1999; Xoplaki et al. 2001; Ogrin 2002; Telelis 2008; Glaser 2013; Yurchenkov 2014; Noone et al. 2017; Fragoso et al. 2018). However, drought years were usually not followed by food shortage and famine in England (Pribyl 2017).

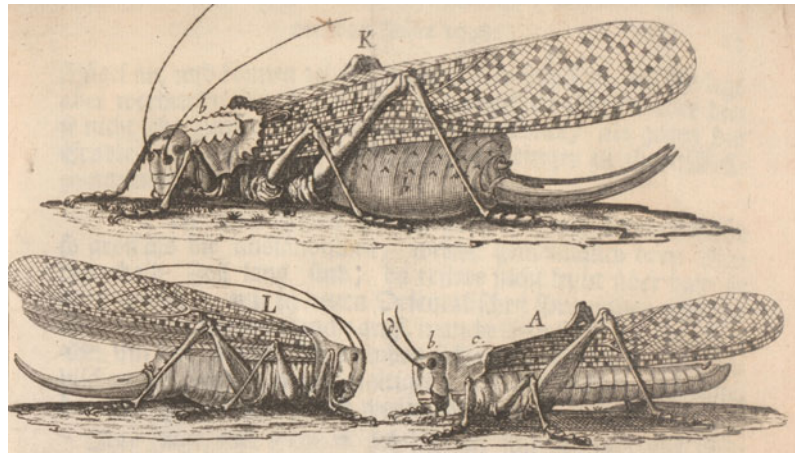

Fig. 4.12 Historical illustration of locusts showing female and male adults migratory locusts (section from a figure in Kundmann 1748)

Drought strongly affected energy production: due to lack of water, mills could not grin that further increased the high prices of flavour and bread. Not only bad or very bad harvests, but also the transport of heavy bulk food (grain) became more difficult as the rivers were hardly navigable due to low-water levels (e.g. Brázdil and Kotyza 1995; Garnier 2010; Glaser 2013; Garnier et al. 2015; Kiss and Nikolić 2015). During the most severe droughts, large rivers became passable on foot that greatly weakened the natural defence of fortifications and country borders; as a consequence, military conflict zones were more prone to violent conflicts, swift raids over large areas, military campaigns and wars (Kiss and Nikolić 2015; Kiss 2017). Furthermore, drought led to unemployment, social unrest and conflicts, and frequent legal disputes over water resources and land boundaries (e.g. Kiss 2005; Gómez-Baggethun et al. 2012; Grau-Satorras et al. 2016).

Prolonged droughts and heats were often accompanied by accidental fire events. Although most reports are usually related to the fires in settlements with special emphasis on towns, wildfires were also recorded on numerous occasions. While in the famous drought years such as 1473 and 1540 forest fires were widespread in large regions of central Europe, bushfire near Antwerp and "soil" fire in Poland were also reported from time to time (e.g. Ogrin 2002; Gerrard and Petley 2013; Wetter et al. 2014; Brázdil et al. 2018; Camenisch et al. 2019). Especially in urban areas, the most typical house building material was partly or entirely wood; only the rich could afford to build houses mainly of stone (or brick). During droughts, the occurrence of devastating fire had a much higher probability that could threaten large part of a town (e.g. London fire in 1666—Garrioch 2016). However, even before the development of systematic fire protection in cities, certain fire prevention measures were often taken in account to avoid fire. For example, in Hamburg, a certain amount of water had to be stored between houses for the case of incidental fire during the 1718 or 1719 drought (Kanold 1719).

Migration was a further important, indirect consequence of severe droughts, either talking about short- or long-term leave or emigration. The migration of pastoral communities, due to the lack of water and fodder were forced temporarily to drive their animals towards areas that were less prone to water shortage, namely to large water bodies, rivers or lakes, is a typical example. During prolonged drought, this was also a practice among individuals with large herds of animals, who usually returned home when vegetation revived after drought (e.g. Kanold 1719; Kiss and Nikolić 2015; Grau-Satorras et al. 2016). Another, much more severe type of migration took place when people, urged by hunger, after selling all their valuable properties for buying food, were forced to leave their homes and try to find food and living elsewhere (e.g. Kanold 1719; Bellon 1996; Csáki 2010; Noone et al. 2017; Fragoso et al. 2018).

4.5.2 Social Responses

4.5.2.1 Perception, Spiritual and Ritual Approaches

Although drought was also understood as a natural/environmental phenomenon in pre-industrial societies, spiritual causative believes were, in parallel, associated with destructive drought phenomena. Drought, similar to other destructive natural hazards, was often considered, especially in the Middle Ages, as the scourge of God for the sins of humans. And although the practice of public prayers, rogations, processions, pilgrimages in times of drought, asking God and the intervention of specific saints are known also from some other parts of Europe (e.g. Brázdil and Kotyza 1995; Gómez-Baggethun et al. 2012; Gerrard and Petley 2013; Camenisch 2015; Kiss and Nikolić 2015; Williams 2016; Fragoso et al. 2018; Mrgic 2018), the most systematic contemporary documentation and recent scientific analyses of these events are known in particular from Spain and Italy (e.g. Martín-Vide and Barriendos Vallvé 1995; Barriendos 1997, 2005; Piervitali and Colacino 2001; Domínguez-Castro et al. 2008, 2010, 2012; Tejedor et al. 2018). Among other significant natural hazards affecting human

societies, drought also influenced long-term spiritual responses, for example, the development of regular prayers and processions, change of the local patron saint or establishment of new parishes (e.g. Grau-Satorras et al. 2016). For example, in France, Saint Godeberta of Noyon, Saint Honorius of Amiens, Saint Angadrisma of Beauvais, Saint Solange of Bourges and Saint Trophimus of Arles were specific saints to pray to avoid drought (Gerrard and Petley 2013).

On the other hand, in mediaeval, but especially in early modern times, drought was also believed to be related to demonic forces. These believes, especially in times of high socio-economic and political vulnerability, more often led to the accusation of people for drought-related magic and witchcraft. Whereas the main period of witch-hunting in western and central Europe was in the sixteenth–seventeenth centuries and weather-related accusations were much more rare in the Middle Ages, the importance of droughts and related extremes in the accusation of witches (as weather-makers) was already notable in mediaeval eastern Europe (e.g. Russia or Ukraine) (Zgutam 1977; Worobec 1995; Behringer 1999; Pfister 2007; Levack 2016). In most other parts of Europe witch accusations (Fig. 4.13) intensified from the sixteenth century onwards, when harvest failure due to weather effects formed connection between agricultural crisis and witchcraft (e.g. Behringer 1997, 1999; Pfister 2007). The theories reflecting the intervention of supernatural powers existed parallel in time: for example, during a witch accusation of 1718 in Hungary, drought was mentioned by some of the trial witnesses as the God's scourge, while others gave the testimony that witches took away the rain or dew and/or sold it to Turkish witches (Reizner 1899). Frequency of witch accusations was intensified particularly during political and socio-economic instability and it was related not only to drought or other weather-related extremes (e.g. Behringer 1999; Petrovics 2005; Pfister 2007).

Fig. 4.13 Execution of three witches on 4 November 1585 in Baden (Switzerland) (Zentralbibliothek Zürich, Collection of Johann Jakob Wick, Ms F 33, fol. 277r)

4.5.2.2 Institutional/Legal-Administrative Decisions and Changes

Numerous methods were applied to solve immediately the shortage of (drinking) water: one solution was to allocate and utilise new water supplies, for example, deepen the existing wells or dig new (deeper) wells in time of drought, while often the transportation of freshwater to a greater distance was, to some extent, another feasible solution (e.g. Brázdil and Kotyza 1995; Dawson 2009; Glaser 2013; Grau-Satorras et al. 2016). In times of water shortage and low-water levels, the utilisation of wetlands and inundation areas intensified: these areas could still provide fodder for the animals even in times when very bad hay harvests caused by drought made significant problems. Additionally, wet pastures were sometimes ploughed and temporarily turned into arable land (e.g. Kiss 2005).

As for the solution of short-term food shortage and dearth, increased cereal import might provide some auxiliary help (e.g. Rohr 2007; Keene 2011). Charity was another, broadly applied immediate reaction of individuals and communities that gained special importance in the time of scarcity, often induced by drought throughout mediaeval and early modern period, until modern times (e.g. McRee 1993; Boa 2012; Gerrard and Petley 2013). In most cases, however, documentary evidence reports mainly administrative decisions. A widespread form of easing the drought-driven stress was tax reduction and/or partly or entirely postponing tax payment for later times, or release tax depths for more public works (e.g. Gerrard and Petley 2013; Brázdil et al. 2018; Fragoso et al. 2018; Kiss 2019).

Some legal-administrative provisions were organised on the state level: the prohibition of cereal (legume, vegetable) export abroad was used especially in the Middle Ages as an important tool to decrease the negative effects of (threatening) food shortage, partly or mainly caused by drought. Public granaries, usually ordered and maintained by the sovereign, on a local–regional level further served the purpose of grain distribution to the locals in need (e.g. seed for sowing). Although granaries were most widespread from the eighteenth century, for example, in France, Portugal, Prussia and the countries of the Habsburg Empire, in some cases, they were already mentioned in the Middle Ages, too (Black 1990; Brázdil and Kotyza 1995; Domínguez-Castro et al. 2012; Gómez-Baggethun et al. 2012; Glaser 2013; Kiss 2017).

Apart from short-term administrative responses, beyond the above-mentioned response types, several long-term changes and developments served to decrease social vulnerability towards drought on community level. Among these long-term solutions, for example, the selection of drought-resistant main cultivated plants was one of the many important issues. However, drought-related legal decisions, water access rights, new water reservoirs and water diversions, the development and maintenance of irrigation systems particularly in the Mediterranean, organised and maintained by the local and municipal administration, also played a crucial role on community level. Another problem to be solved on the community level during droughts was water quality, regular maintenance and monitoring (e.g. Grau-Satorras et al. 2016).

4.6 Perspectives for Future Research into Historical Droughts in Europe

Dai (2013) reported a possible future increase in the frequency and severity of drought episodes attributable to recent global warming. Naumann et al. (2018) analysed future drought conditions corresponding to global warming of 1.5, 2 and 3 °C compared to pre-industrial times: they pointed out a progressive and significant increase in drought frequency, particularly in the Mediterranean, most of Africa, western and southern Asia, Central America and Oceania, even five or even ten times higher than at present. Drought projections for the twenty-first century indicate that the Mediterranean, a consistent drought-prone region of Europe, is one of the most endangered areas (e.g. García-Ruiz et al. 2011; Seager et al. 2014). However, indications from other parts of Europe signal that drought may also become a serious natural extreme on a far wider scale (Spinoni et al. 2018).

Because future estimates of droughts are primarily based on projections of climate models, it would appear quite important to possess detailed knowledge of droughts from the past, i.e. from the pre-instrumental as well as instrumental periods. A wealth of documentary evidence related to droughts in Europe has facilitated the collation of much important information concerning the spatiotemporal variability and impacts of historical droughts, from which we may learn much that is relevant to recent droughts as well as their future projections in the context of anthropogenically enhanced global warming. Recent and projected future droughts can be confronted in terms of their frequency, severity, spatial extent, human impacts and responses in times of clearly prevailing natural forcing. The study in hand demonstrates the importance of studying drought frequency and severity with respect to regional differences in Europe. As well as events of broad territorial extent, there are also episodes at regional and sub-regional scales that may have impacts just as severe.

Brázdil et al. (2018), giving a worldwide overview of drought studies from documentary sources, indicated certain key points for future drought research which remain valid, with some of them also extending to Europe:

(i) Compilation of long-term drought series combining documentary and instrumental data for the study of the long-term spatiotemporal variability of droughts, a particularly pressing matter in countries currently lacking drought series, or for which these are only incomplete.
(ii) Use of documentary data for the reconstruction of series of generally used drought indices based on reconstructed temperatures and precipitation or documentary-based biophysical series.
(iii) Comprehensive analysis of past major droughts in order to estimate the potential impacts of extreme droughts for current and future societies.
(iv) Comparison of documentary-based droughts with those derived from other high-resolution proxies to improve understanding of past drought episodes.
(v) Communication with climate modellers as to way in which to use knowledge of documentary-based droughts in past model simulations and in future drought projections.
(vi) Interdisciplinary cooperation with scientists in a wider range of fields to establish what lessons may be learnt from drought management practices in the past, with the future in mind.

These points are also related to, or may be supplemented by, the topical questions raised by multidisciplinary drought research for the first quarter of the twenty-first century, as formulated by Trnka et al. (2018). The present contribution strongly indicates that the use of documentary data has great potential for the study of historical droughts with important and relevant implications for the better understanding of recent and future droughts in Europe.

Acknowledgements Rudolf Brázdil acknowledges the support of Czech Science Foundation, project ref. 17-10026S. Andrea Kiss acknowledges financial support from the Austrian Science Funds, project ref. I 3174. Ladislava Řezníčková was supported by "SustES – Adaptation strategies for sustainable ecosystem services and food security under adverse environmental conditions" project ref. CZ.02.1.01/0.0/0.0/16_019/0000797. Mariano Barriendos acknowledges support from the Spanish Ministry of Economy and Competition, programme I + D + i, funding project CLIMED, ref. CGL2015-69985-R. We would like to thank the following individuals and institutions: for provision of data, N. Diodato (Benevento), C. Murphy and S. Noone (Kildare), C. Pfister (Bern) and V. V. Popova (Moscow); for providing us with figures and permission with their publication—Fig. 4.2, Bibliothèque nationale de France, Paris, Figs. 4.6 and 4.11a, O. Kotyza (Litoměřice), Fig. 4.11b, the National Museum, Prague and Fig. 4.13, Zentralbibliothek, Zürich; for further assistance with this manuscript, Jaak Jaagus (Tartu), Neil Macdonald (Liverpool) and Kathleen Pribyl (Norwich). Tony Long (Svinošice) helped work up the English. We also thank anonymous referee for valuable critical comments.

References

Alcoforado MJ, Vaquero JM, Trigo RM, Taborda JP (2012) Early Portuguese meteorological measurements (18th century). Clim Past 8:353–371. https://doi.org/10.5194/cp-8-353-2012

Alexandre P (1987) Le climat en Europe au Moyen Âge. Contribution à l'histoire des variations climatiques de 1000 à 1425, d'après les sources narratives de l'Europe occidentale. Éditions de l'École des Hautes Études en Sciences Sociales, Paris

Anonymous (1927) Goigs a llaor de Sant Galderic llaurador, patró dels pagesos Catalans (Prayers and songs in honour of Saint Galderic the Farmer, patron of all Catalan farmers). Arnau-Ors i Bartrés, Barcelona

Barriendos M (1997) Climatic variations in the Iberian Peninsula during the late Maunder Minimum (AD 1675–1715): an analysis of data from rogation ceremonies. Holocene 7:105–111. https://doi.org/10.1177/095968369700700110

Barriendos M (2005) Climate and culture in Spain. Religious responses to extreme climatic events in the Hispanic Kingdoms (16th–19th century). In: Behringer W, Lehmann H, Pfister C (eds) Kulturelle Konsequenzen der "Kleine Eiszeit" – Cultural Consequences of the "Little Ice Age". Vandenhoeck & Ruprecht, Göttingen, pp 379–414

Beguería S, Vicente-Serrano SM, Reig F, Latorre B (2014) Standardized precipitation evapotranspiration index (SPEI) revisited: parameter fitting, evapotranspiration models, tools, datasets and drought monitoring. Int J Climatol 34:3001–3023. https://doi.org/10.1002/joc.3887

Behringer W (1997) Witchcraft persecutions in Bavaria. Popular magic, religious zealotry and reason of state in early modern Europe. Cambridge University Press, Cambridge

Behringer W (1999) Climatic change and witch-hunting: the impact of the Little Ice Age on mentalities. Clim Change 43:335–351. https://doi.org/10.1023/A:1005554519604

Bělínová M, Brázdil R (2012) Meteorologická pozorování c. k. Vlastenecko-hospodářské společnosti v Čechách v letech 1817–1847 (Meteorological observations of I. R. Patriotic-Economic Society in Bohemia in the years 1817–1847). Meteorol Zpr 65:13–22

Bell WT, Ogilvie AEJ (1978) Weather compilations as a source of data for the reconstruction of European climate during the medieval period. Clim Change 1:331–348. https://doi.org/10.1007/BF00135154

Bellon T (1996) Beklen. A nagykunsági mezővárosok állattartó gazdálkodása a XVIII-XIX. században (Beklen. Animal husbandry of the towns in Greater Cumania in the 18–19th centuries). Karcag Város Önkormányzata, Karcag

Black J (1990) History of Europe. Eighteenth century Europe 1700–1789. Macmillan, New York

Boa K (2012) Az 1863–1864. évi aszály és ínség Békés megyében (The 1863–1864 drought and dearth in Békés County). Fons 19:161–199

Borisenkov YP, Pasetskiy VM (1988) Tysyatcheletnaya letopis neobytchaynykh yavleniy prirody (A thousand-year history of unusual natural events). Mysl, Moskva

Borisenkov YP, Pasetskiy VM (2002) Letopis neobytchaynikh yavleniy prirody za 2.5 tysyatcheletiya (V v. do n.e.–XX v. n.e.) (A chronicle of unusual natural events for 2.5 millennia (5th century BC–20th century AD)). Gidrometeoizdat, Saint-Petersburg

Brázdil R, Kirchner K (eds) (2007): Vybrané přírodní extrémy a jejich dopady na Moravě a ve Slezsku (Selected natural extremes and their impacts in Moravia and Silesia). Masarykova univerzita, Český hydrometeorologický ústav, Ústav geoniky Akademie věd České republiky, v.v.i., Brno, Praha, Ostrava

Brázdil R, Kotyza O (1995) History of weather and climate in the Czech Lands I. Period 1000–1500. Zürcher Geographische Schriften 62. ETH Zürich, Zürich

Brázdil R, Trnka M (eds) (2015) Sucho v českých zemích: minulost, současnost, budoucnost (Droughts in the Czech Lands: Past, present and future). Centrum výzkumu globální změny Akademie věd České republiky, v.v.i., Brno

Brázdil R, Pfister C, Wanner H et al (2005) Historical climatology in Europe—the state of the art. Clim Change 70:363–430. https://doi.org/10.1007/s10584-005-5924-1

Brázdil R, Kiss A, Luterbacher J, Valášek H (2008) Weather patterns in eastern Slovakia 1717–1730, based on records from Breslau meteorological network. Int J Climatol 28:1639–1651. https://doi.org/10.1002/joc.1667

Brázdil R, Dobrovolný P, Luterbacher J et al (2010) European climate of the past 500 years: new challenges for historical climatology. Clim Change 101:7–40. https://doi.org/10.1007/s10584-009-9783-z

Brázdil R, Bělínová M, Rožnovský J (2011) Phenological observations made by the I. R. Bohemian Patriotic-Economic Society, 1828–1847. Theor Appl Climatol 105:71–81. https://doi.org/10.1007/s00704-010-0373-9

Brázdil R, Bělínová M, Dobrovolný P et al (2012a) Temperature and precipitation fluctuations in the Czech Lands during the instrumental period. Masaryk University, Brno

Brázdil R, Chromá K, Valášek H, Dolák L (2012b) Hydrometeorological extremes derived from taxation records for south-eastern Moravia, Czech Republic, 1751–1900 AD. Clim Past 8:467–481. https://doi.org/10.5194/cp-8-467-2012

Brázdil R, Dobrovolný P, Trnka M et al (2013) Droughts in the Czech Lands, 1090–2012 AD. Clim Past 9:1985–2002. https://doi.org/10.5194/cp-9-1985-2013

Brázdil R, Řezníčková L, Valášek H et al (2014) Past locust outbreaks in the Czech Lands: do they indicate particular climatic patterns? Theor Appl Climatol 116:343–357. https://doi.org/10.1007/s00704-013-0950-9

Brázdil R, Dobrovolný P, Trnka M et al (2016) Documentary and instrumental-based drought indices for the Czech Lands back to AD 1501. Clim Res 70:103–117. https://doi.org/10.3354/cr01380

Brázdil R, Kiss A, Luterbacher J et al (2018) Documentary data and the study of past droughts: a global state of the art. Clim Past 14:1915–1960. https://doi.org/10.5194/cp-14-1915-2018

Brázdil R, Dobrovolný P, Trnka M et al (2019) Extreme droughts and human responses to them: the Czech Lands in the pre-instrumental period. Clim Past 15:1–24. https://doi.org/10.5194/cp-15-1-2019

Buisman J (1995–2006) Duizend Jaar Weer, Wind en Water in de Lage Landen. Vol. 1, to 1300 (1995); Vol. 2, 1300–1450 (1996); Vol. 3, 1450–1575 (1998); Vol. 4, 1575–1675 (2000); Vol. 5, 1675–1750 (2006). Uitgegeverij Van Wijnen, Franeker

Camenisch C (2015) Endlose Kälte. Witterungsverlauf und Getreidepreise in dem Burgundischen Niederlanden im 15. Jahrhundert. Schwabe, Basel

Camenisch C, Brázdil R, Kiss A et al (2019) Extreme heats and droughts of 1473 and their impacts in Europe in context of the early 1470s. Reg Environ Change, in review

Camuffo D, Bertolin C (2012) The earliest temperature observations in the world: the Medici Network (1654–1670). Clim Change 111:335–363. https://doi.org/10.1007/s10584-011-0142-5

Camuffo D, Jones P (eds) (2002) Improved understanding of past climatic variability from early daily European instrumental sources. Kluwer Academic Publishers, Dordrecht

Csáki Á (2010) Szárazság és pestis Háromszéken 1717–1720-ban (Drought and plague in Háromszék [Hargita county, Romania] in 1717–1720). Acta Siculica 2010:277–287

Cullen JK (2010) Famine in Scotland: The 'Ill Years' of the 1690s. Scottish Historical Review Monograph, Edinburgh University Press

Dai A (2011) Characteristics and trends in various forms of the Palmer Drought Severity Index (PDSI) during 1900–2008. J Geophys Res 116:D12115. https://doi.org/10.1029/2010JD015541

Dai A (2013) Increasing drought under global warming in observations and models. Nat Clim Change 3:52–58. https://doi.org/10.1038/nclimate1633

Dawson A (2009) Do foul and fair a day. A history of Scotland's weather and climate. Birlinn, Edinburgh

Diodato N (2007) Climatic fluctuations in southern Italy since the 17th century: reconstruction with precipitation records at Benevento. Clim Change 80:411–431. https://doi.org/10.1007/s10584-006-9119-1

Diodato N, Bellocchi G (2011) Historical perspective of drought response in central-southern Italy. Clim Res 49:189–200. https://doi.org/10.3354/cr01020

Dobrovolný P, Brázdil R, Valášek H et al (2009) A standard paleoclimatological approach to temperature reconstruction in historical climatology: an example from the Czech Republic, A.D. 1718–2007. Int J Climatol 29:1478–1492. https://doi.org/10.1002/joc.1789

Dobrovolný P, Moberg A, Brázdil R et al (2010) Monthly and seasonal temperature reconstructions for Central Europe derived from documentary evidence and instrumental records since AD 1500. Clim Change 101:69–107. https://doi.org/10.1007/s10584-009-9724-x

Dobrovolný P, Brázdil R, Trnka M et al (2015) Precipitation reconstruction for the Czech Lands, AD 1501–2010. Int J Climatol 35:1–14. https://doi.org/10.1002/joc.3957

Domínguez-Castro F, Santisteban JI, Barriendos M, Mediavilla R (2008) Reconstruction of drought episodes for central Spain from rogation ceremonies recorded at the Toledo Cathedral from 1506 to 1900: a methodological approach. Glob Plan Change 63:230–242. https://doi.org/10.1016/j.gloplacha2008.06.002

Domínguez-Castro F, García-Herrera R, Ribera P, Barriendos M (2010) A shift in the spatial pattern of Iberian droughts during the 17th century. Clim Past 6:553–563. https://doi.org/10.5194/cp-6-553-2010

Domínguez-Castro F, Ribera P, García-Herrera R et al (2012) Assessing extreme droughts in Spain during 1750–1850 from rogation ceremonies. Clim Past 8:705–722. https://doi.org/10.5194/cp-8-705-2012

Domínguez-Castro F, de Miguel JC, Vaquero JM et al (2014a) Climatic potential of Islamic Chronicles in Iberia: extreme droughts (AD 711–1010). Holocene 24:370–374. https://doi.org/10.1177/0959683613518591

Domínguez-Castro F, Vaquero JM, Rodrigo FS et al (2014b) Early Spanish meteorological records (1780–1850). Int J Climatol 34:593–603. https://doi.org/10.1002/joc.3709

Elleder L (2016) The Hunger stones: a new source for more objective identification of historical droughts. EGU General Assembly, Vienna, Austria, 17–22 Apr 2016, EGU2016-14986

Fernández-Fernández MI, Gallego MC, Domínguez-Castro F et al (2015) The climate in Zafra from 1750 to 1840: precipitation. Clim Change 129:267–280. https://doi.org/10.1007/s10584-014-1315-9

Fragoso M, Carraça MGD, Alcoforado MJ (2018) Droughts in Portugal in the 18th century—a study based on newly found documentary data. Int J Climatol 38:5522–5541. https://doi.org/10.1002/joc.5745

Gallego D, García-Herrera R, Prieto R, Peña-Ortiz C (2008) On the quality of climate proxies derived from newspaper reports—a case study. Clim Past 4:11–18. https://doi.org/10.5194/cp-4-11-2008

García-Ruiz JM, López-Moreno JI, Vicente-Serrano SM et al (2011) Mediterranean water resources in a global change scenario. Earth Sci Rev 105:121–139. https://doi.org/10.1016/j.earscirev.2011.01.006

Garnier E (2010) Bassesses extraordinaires et grandes chaleurs. 500 and de sécheresses et de chaleurs en France et dans lespays limitrophes. La Huille Blanche 4:1–17. https://doi.org/10.1051/lhb/2010039

Garnier E (2019) Historic drought from archives: beyond the instrumental record. In: Iglesias A, Assimacopoulos D, Van Lanen HAJ (eds) Drought. Science and policy. Wiley, Hoboken, pp 45–67

Garnier E, Assimacopoulos D, van Lanen HAJ (2015) Historic droughts beyond the modern instrumental records: an analysis of cases in United Kingdom, France, Rhine and Syros. DROUGHT-R&SPI, Technical Report No. 35

Garrioch D (2016) 1666 and London's fire history: a re-evaluation. Hist J 59:319–338. https://doi.org/10.1017/S0018246X15000382

Gerrard CM, Petley DN (2013) A risk society? Environmental hazards, risk and resilience in the later Middle Ages in Europe. Nat Hazards 69:1051–1079. https://doi.org/10.1007/s11069-013-0750-7

Glaser R (2001) Klimageschichte Mitteleuropas. 1000 Jahre Wetter, Klima, Katastrophen. Primus Verlag, Darmstadt

Glaser R (2008) Klimageschichte Mitteleuropas. 1200 Jahre Wetter, Klima, Katastrophen. 2. Auflage. Primus Verlag, Darmstadt

Glaser R (2013) Klimageschichte Mitteleuropas. 1200 Jahre Wetter, Klima, Katastrophen. 3. Auflage. Primus Verlag, Darmstadt

Gómez-Baggethun E, Reyes-García V, Olsson P, Montes C (2012) Traditional ecological knowledge and community resilience to environmental extremes: a case study in Doñana, SW Spain. Glob Environ Change 22:640–650. https://doi.org/10.1016/j.gloenvcha.2012.02.005

Grau-Satorras M, Otero I, Gómez-Baggethun E, Reyes-García V (2016) Long-term community responses to droughts in the early modern period: the case study of Terrassa, Spain. Ecol Soc 21:33. https://doi.org/10.5751/ES-08232-210233

Haslinger K, Blöschl G (2017) Space-time patterns of meteorological drought events in the European Greater Alpine Region over the past 210 year. Water Resour Res 53:9807–9823. https://doi.org/10.1002/2017WR020797

Heim RR (2000) Drought indices. A review. In: Wilhite DA (ed) Drought: a global assessment. Hazards Disaster Series, vol I. Routledge, New York, pp 159–167

Heim RR (2002) A review of twentieth-century drought indices used in the United States. Bull Am Met Soc 83:1149–1165. https://doi.org/10.1175/1520-0477-83.8.1149

Jones PD, Ogilvie AEJ, Wigley TML (1984) Riverflow data for the United Kingdom: reconstructed data back to 1844 and historical data back to 1556. CRURP 8. Climate Research Unit, Norwich

Kanold J (1718–1720) Sammlung von Natur- und Medicin-, wie auch hierzu gehörigen Kunst- und Literatur-Geschichten. Michael Hubert, Breslau

Keene D (2011) Crisis management in London's food supply, 1250–1500. In: Dodds B, Liddy CD (eds) Commercial activity, markets and entrepreneurs in the Middle Ages: essays in honour of Richard Britnell. Boydell & Brewer, pp 45–62

Kington J (1974) The Societas Meteorologica Palatina: an eighteenth-century meteorological society. Weather 29:416–426. https://doi.org/10.1002/j.1477-8696.1974.tb04330.x

Kington B (1980) Searches for historical weather data: appeals and responses. Weather 35:124–134. https://doi.org/10.1002/j.1477-8696.1980.tb04731.x

Kiss A (2005) Utilization of the inundation area at Lake Fertő before regulation works: example of Sarród and its surroundings. Acta Geographica 38:39–49

Kiss A (2009) Historical climatology in Hungary: role of documentary evidence in the study of past climates and hydrometeorological extremes. Időjárás 113:315–339

Kiss A (2017) Droughts and low water levels in late Medieval Hungary II: 1361, 1439, 1443–4, 1455, 1473, 1480, 1482(?), 1502–3, 1506: documentary versus tree-ring (OWDA) evidence. J Environ Geogr 10:43–56. https://doi.org/10.1515/jengeo-2017-0012

Kiss A (2019) Anatomy of a great drought in late medieval Hungary. the drought of (1506–)1507 and its multiannual socio-economic consequences in a Central-European context. Reg Environ Change, in review

Kiss A, Nikolić Z (2015) Droughts, dry spells and low water levels in Medieval Hungary (and Croatia) I: the great droughts of 1362, 1474, 1479, 1494 and 1507. J Environ Geogr 8:11–22. https://doi.org/10.1515/jengeo-2015-0002

Kovács PE (1992) Estei Hippolit püspök egri számadáskönyvei 1500–1508 (The Account Books of the Bishop of Eger, Ippolito d'Este). Heves Megyei Levéltár, Eger

Kovács JL (1995) Faut Márk és Klein Menyhért krónikája. – Die Chronik des Marx Faut und Melchior Klein. 1526–1616. Sopron város történeti forrásai – Quellen zur Geschichte der Stadt Ödenburg. C sorozat 1. kötet – Reihe C Band 1. Soproni Levéltár – Burgenländischen Landesregierung, Sopron – Eisenstadt

Kundmann JC (1748) Anmerckungen über die Heuschrecken in Schlesien von dem Jahre 1748. Johann Jacob Korn, Breßlau

Leijonhufvud L, Wilson R, Moberg A (2008) Documentary data provide evidence of Stockholm average winter to spring temperatures in the eighteenth and nineteenth centuries. Holocene 18:333–343. https://doi.org/10.1177/0959683607086770

Leijonhufvud L, Wilson R, Moberg A et al (2010) Five centuries of Stockholm winter/spring temperatures reconstructed from documentary evidence and instrumental observations. Clim Change 101:109–141. https://doi.org/10.1007/s10584-009-9650-y

Levack BP (2016) The witch-hunt in early modern Europe, 4th edn. Routledge, London

Lüdecke C (2010) Von der Kanoldsammlung (1717–1730) zu den Ephemeriden der Societas Meteorologica Palatina (1781–1792). Meteorologische Quellen zur Umweltgeschichte des 18. Jahrhunderts. In: Popplow M (ed) Landschaften agrarisch-ökonomischen Wissens: Strategien innovativer Ressourcennutzung in Zeitschriften und Sozietäten des 18. Jahrhunderts. Waxmann, pp 97–119

Lyakhov ME (1984) Klimatitcheskiye extremumy v tsentralnoy tchasti yevropeyskoy territorii SSSR v XIII–XX vv (Climatic extremes in the central part of the European USSR in the 13th to the 20th centuries). Izvestiya Akad Nauk SSSR – Ser Geogr 6:68–74

Malewicz HM (1980) Zjawiska przyrodnicze w relacjach dziejopisarzy polskiego średniowiecza (Natural events in reports by the historians of Medieval Poland). Ossolineum, Wrocław

Martínková L (2005) Paměti pelhřimovských měšťanů z přelomu 18. a 19. století. Filip Ignác Dremsa & Antonín Štěpán (Memoirs of the burghers of Pelhřimov from the end of the 18th century and the start of the 19th. Filip Ignác Dremsa & Antonín Štěpán). Moravský zemský archiv v Brně – Státní okresní archiv v Pelhřimově, Pelhřimov

Martín-Vide J, Barriendos Vallvé M (1995) The use of rogation ceremony records in climatic reconstruction: a case study from Catalonia (Spain). Clim Change 30:201–221. https://doi.org/10.1007/BF01091842

McKee TB, Doesken NJ, Kleist J (1993) The relationship of drought frequency and duration to time steps. In: Preprints, 8th Conference on Applied Climatology. Anaheim, 17–22 Jan 1993, pp 179–184

McRee BR (1993) Charity and gild solidarity in late Medieval England. J British Studies 32:195–225. https://doi.org/10.1086/386030

Mishra AK, Singh VP (2010) A review of drought concepts. J Hydrol 391:202–216. https://doi.org/10.1016/j.jhydrol.2010.07.012

Možný M, Brázdil R, Dobrovolný P et al (2016) Drought reconstruction based on grape harvest dates for the Czech Lands, 1499–2012. Clim Res 70:119–132. https://doi.org/10.3354/cr01423

Mrgic J (2018) Intemperate weather in violent times—narratives from the Western Balkans during the Little Ice Age (17–18th centuries). Cuadernos de Investigación Geográfica 44:137–169

Munzar J (2004) Extreme droughts in Central Europe in the preinstrumental period. Morav Geogr Rep 12:13–23

Murphy C, Noone S, Duffy C et al (2017) Irish droughts in newspaper archives: rediscovering forgotten hazards? Weather 72:151–155. https://doi.org/10.1002/wea.2904

Naumann G, Alfieri L, Wyser K et al (2018) Global changes in drought conditions under different levels of warming. Geophys Res Lett 45:3285–3296. https://doi.org/10.1002/2017gl076521

Nicoll J (1836) A diary of public transactions and other occurrences, chiefly in Scotland from January 1650 to June 1667. T. Constable, Edinburgh

Noone S, Broderick C, Duffy C et al (2017) A 250-year drought catalogue for the island of Ireland (1765–2015). Int J Climatol 37:239–254. https://doi.org/10.1002/joc.4999

Ogilvie AEJ (1990) Climatic changes in Iceland A.D. c. 865 to 1598. Acta Archaeologica 61:233–251

Ogilvie A, Farmer G (1997) Documenting the medieval climate. In: Hulme M, Barrow E (eds) Climates of the British Isles. Present, past and future. Routledge, London, pp 112–133

Ogrin D (2002) Dry and wet years in submediterranean Slovenia from the 14th to the mid-19th century. Acta Univ Palacki Olomuc, Fac Rer Nat – Geographica 37:55–62

Oliva M, Ruiz-Fernández J, Barriendos M et al (2018) The Little Ice Age in Iberian mountains. Earth-Sci Rev 177:175–208. https://doi.org/10.1016/j.earscirev.2017.11.010

Orth R, Vogel MM, Luterbacher J et al (2016) Did European temperatures in 1540 exceed present-day records? Environ Res Lett 11:114021. https://doi.org/10.1088/1748-9326/11/1/114021

PAGES Hydro2k Consortium (2017) Comparing proxy and model estimates of hydroclimate variability and change over the Common Era. Clim Past 13:1851–1900. https://doi.org/10.5194/cp-13-1851-2017

Palmer WC (1965) Meteorological drought. Office of climatology research paper 45. U.S. Weather Bureau, Washington

Palotay M, Mindszenty A, Kopecskó K, Poros Z (2012) Az Ínség-kő geológiája (Geology of the dearth-stone). Földtani Közlöny 142:243–250

Petrovics I (2005) Witch-hunt in Szeged in the early eighteenth century. In: Szeghyová B (ed) The role of magic in the past. Learned and popular magic, popular beliefs and diversity of attitudes. Pro Historia, Bratislava, pp 108–116

Pfister C (1992) Monthly temperature and precipitation in central Europe 1525–1979: quantifying documentary evidence on weather and its effects. In: Bradley RS, Jones PD (eds) Climate since A.D. 1500. Routledge, London, pp 118–142

Pfister C (1999) Wetternachhersage. 500 Jahre Klimavariationen und Naturkatastrophen (1496–1995). Paul Haupt, Bern

Pfister C (2007) Climatic extremes, recurrent crises and witch hunts: strategies of European societes in coping with exogenous shocks in the late sixteenth and early seventeenth centuries. Medieval Hist J 10:33–73. https://doi.org/10.1177/097194580701000202

Pfister C (2018) The "Black Swan" of 1540. Aspects of a European megadrought. In: Leggewie K, Mauelshagen F (eds) Climatic change and cultural transition in Europe. Leiden, Brill, pp 156–194

Pfister C, Weingartner R, Luterbacher J (2006) Hydrological winter droughts over the last 450 years in the Upper Rhine basin: a methodological approach. Hydrol Sci J 51:966–985. https://doi.org/10.1623/hysj.51.5.966

Piervitali E, Colacino M (2001) Evidence of drought in Western Sicily during the period 1565–1915 from liturgical offices. Clim Change 49:225–238. https://doi.org/10.1023/A:1010746612289

Pribyl K (2017) Farming, Famine and Plague. The impact of climate in late Medieval England. Springer, Cham

Pribyl K, Cornes R (2019) Droughts in medieval and early modern England. Part 2: Impacts. Weather (in press)

Przybylak R (2010) Instrumental observations. In: Przybylak R, Majorowicz J, Brázdil R, Kejna M (eds) The Polish climate in the European context: an historical overview. Springer Science + Business Media B.V., pp 129–166

Réflexions lues dans la séance tenue au Louvre, par la société royale de médecine, le 18 septembre 1781: sur la nature de la Constitution de cette année, & le traitement des maladies qu'elle a occasionnées à la fin. Ph.-D. Pierres, Impr., Paris, 1781

Reizner J (1899) Szeged története (History of Szeged), vol 4: Chartulary, Szeged Szabad Királyi Város közönsége, Szeged

Riemann D, Glaser R, Kahle M, Vogt S (2015) The CRE tambora.org—new data and tools for collaborative research in climate and environmental history. Geosci Data J 2:63–77. https://doi.org/10.1002/gdj3.30

Rodrigo FS (2008) A new method to reconstruct low-frequency climatic variability from documentary sources: application to winter rainfall series in Andalusia (Southern Spain) from 1501 to 2000. Clim Change 87:471–487. https://doi.org/10.1007/s10584-007-9312-x

Rodrigo FS, Barriendos M (2008) Reconstruction of seasonal and annual rainfall variability in the Iberian peninsula (16th–20th centuries). Glob Plan Change 63:243–257. https://doi.org/10.1016/j.gloplacha.2007.09.004

Rodrigo FS, Esteban Parra MJ, Castro DY (1995) Reconstruction of total annual rainfall in Andalusia (Southern Spain) during the 16th and 17th centuries from documentary sources. Theor Appl Climatol 52:207–218. https://doi.org/10.1007/BF00864044

Rodrigo FS, Esteban Parra MJ, Castro-Diez Y (1998) On the use of the Jesuit order private correspondence records in climate reconstructions: a case study from Castille (Spain) for 1634–1648 A.D. Clim Change 40:625–645. https://doi.org/10.1023/A:1005316118817

Rodrigo FS, Esteban-Parra MJ, Pozo-Vazquez D, Castro-Díez Y (1999) A 500-year precipitation record in Southern Spain. Int J Climatol 19:1233–1253. https://doi.org/10.1002/(SICI)1097-0088(199909)19:11%3c1233:AID-JOC413%3e3.0.CO;2-L

Roggenkamp T, Herget J (2015) An extreme drought in the year 69 AD on Lower Rhine. A quantitative reconstruction. Z Geomorph 59(Suppl 3):99–109. https://doi.org/10.1127/zfg_suppl/2015/S-59205

Rohr C (2007) Extreme Naturereignisse im Ostalpen. Naturerfahrung im Spätmittelalter und am Beginn der Neuzeit. Böhlau Verlag, Köln

Seager R, Liu H, Henderson N et al (2014) Causes of increasing aridification of the Mediterranean region in response to rising greenhouse gases. J Clim 27:4655–4676. https://doi.org/10.1175/JCLI-D-13-00446.1

Shmakin AB, Chernavskaya MM, Popova VV (2013) "Velikaya" zasucha 2010 g. na Vostochno-Evropeyskoy Ravnine: istoricheskiye analogi, cirkulyacionnyye mekhanismy (The Great drought of 2010 in the eastern European plain: historical analogues, circulation mechanisms). Izvestiya RAN – Ser Geogr 6:41–57

Smičiklas T, Kostrenčić M, Laszowski E (1915) Codex Diplomaticus Regni Croatiae, Dalmatiae et Slavoniae – Diplomatički zbornik Kraljevine Hrvatske, Dalmacije i Slavonije, vol 13. Tisak Dioničke Tiskare, Zagreb

Spinoni J, Vogt JV, Naumann G et al (2018) Will drought events become more frequent and severe in Europe? Int J Climatol 38:1718–1736. https://doi.org/10.1002/joc.5291

Strömmer E (2003) Klima-Geschichte. Methoden der Rekonstruktion und historische Perspektive. Ostösterreich 1700 bis 1830. Franz Deuticke, Wien

Svoboda MD, Fuchs BA (2018) Handbook of drought indicators and indices. In: Wilhite DA, Pulwarty RS (eds) Drought and water crises. Integrating science, management, and policy. CRC Press, Taylor & Francis Group, Boca Bayton, pp 155–207

Symons GJ (1891) Merle's MS. Considerationes temperiei pro 7 annis. Per Magistrum Willelmum Merle, socium domus de Merton. The earliest known journal of the weather. Kept by The Rev. William Merle, rector of Driby, Lincolnshire. 1377–1344. E. Stanford, London

Tarand A, Jaagus J, Kallis A (2013) Eesti kliima minevikus ja tänapäeval (Estonian climate: past and present). Tartu Ülikool, Kirjastus

Tejedor E, de Luis M, Barriendos M et al (2018) Rogation ceremonies: a key to understand past drought variability in northeastern Spain since 1650. Clim Past Discuss. https://www.clim-past-discuss.net/cp-2018-67/

Telelis I (2008) Climatic fluctuations in the Eastern Mediterranean and the Middle East AD 300–1500 from Byzantine documentary and proxy physical paleoclimatic evidence—a comparison. Jahrbuch der Österreichischen Byzantinistik 58:167–208. https://doi.org/10.1553/joeb58s167

Teplý F (1928) Martina Škvoreckého, úředníka na Pacově, hospodářská korespondence z dob války třicetileté (1630–1642) (Financial correspondence of Martin Škvorecký, a clerk at Pacov, from the time of the Thirty Years' War, 1630–1642). Nákladem Ministerstva zemědělství Republiky československé, Praha

Todd B, Macdonald N, Chiverrell RC et al (2013) Severity, duration and frequency of drought in SE England from 1697 to 2011. Clim Change 121:673–687. https://doi.org/10.1007/s10584-013-0970-6

Trnka M, Hayes M, Jurečka F et al (2018) Priority questions in multidisciplinary drought research. Clim Res 75:241–260. https://doi.org/10.3354/cr01509

van der Schrier G, Efthymiadis D, Briffa KR, Jones PD (2007) European Alpine moisture variability 1800–2003. Int J Climatol 27:415–427. https://doi.org/10.1002/joc.1411

Van Loon AF, Gleeson T, Clark J et al (2016a) Drought in the anthropocene. Nat Geosci 9:89–91. https://doi.org/10.1038/ngeo2646

Van Loon AF, Stahl K, Di Baldassarre J et al (2016b) Drought in a human-modified world: reframing drought definitions, understanding, and analysis approaches. Hydrol Earth Syst Sci 20:3631–3650. https://doi.org/10.5194/hess-20-3631-2016

Vicente-Serrano SM, Beguería S, López-Moreno JI (2010) A multi-scalar drought index sensitive to global warming: the standardized precipitation evapotranspiration index—SPEI. J Clim 23:1696–1718. https://doi.org/10.1175/2009JCLI2909.1

Walter H (1901) Ueber die Stromschnelle von Laufenburg. Vierteljahrsschrift d. naturf. Ges. Zürich 46:232–263 (see also: Inaugural-Dissertation, Zürich)

Weikinn C (1958–2002) Quellentexte zur Witterungsgeschichte Europas von der Zeitwende bis zum Jahre 1850. Hydrographie. Teil 1 (Zeitwende–1500), Teil 2 (1501–1600), Teil 3 (1601–1700), Teil 4 (1701–1750), Teil 5 (1751–1800), Teil 6 (1801–1850). Akademie-Verlag, Berlin

Wetter O, Pfister C (2013) An underestimated record breaking event. Why summer 1540 was likely warmer than 2003. Clim Past 9:41–56. https://doi.org/10.5194/cp-9-41-2013

Wetter O, Pfister C, Werner JP et al (2014) The year-long unprecedented European heat and drought of 1540—a worst case. Clim Change 125:349–363. https://doi.org/10.1007/s10584-014-1184-2

White S, Pfister C, Mauelshagen F (eds) (2018) The Palgrave handbook of climate history. Palgrave Macmillan, London

Wilhite DA, Pulwarty RS (2018) Drought as hazard: understanding the natural and social context. In: Wilhite DA, Pulwarty RS (eds) Drought and water crises. Integrating science, management, and policy. CRC Press, Taylor & Francis Group, Boca Bayton, pp 3–20

Williams H (2016) Saint Geneviève's miracles: art and religion in eighteenth-century Paris. French Hist 30:322–353. https://doi.org/10.1093/fh/crv076

Worobec CD (1995) Witchcraft beliefs and practices in prerevolutionary Russian and Ukrainian villages. Russ Rev 54:165–187. https://doi.org/10.2307/130913

Xoplaki E, Maheras P, Luterbacher J (2001) Variability of climate in meridional Balkans during the periods 1675–1715 and 1780–1830 and its impact on human life. Clim Change 48:581–614. https://doi.org/10.1023/A:1005616424463

Yurchenkov V (2014) Impact of natural conditions on the regional historical development (based on the example of the Mordovian Land of the XVIIth century). In: Božić S (ed) History and geography: meetings and permations. Geography Institute Jovan Cvijić (SASA), Institute of Recent History of Serbia, Institute of Slavic Studies (RAS), Belgrade, pp 583–594

Zgutam R (1977) Witchcraft trials in seventeenth-century Russia. Amer Hist Rev 82:1187–1207

5 Geomorphological and Geoarchaeological Evidence of the *Medieval Deluge* in the Tagliamento River (NE Italy)

Alessandro Fontana, Matteo Frassine and Livio Ronchi

Abstract

Between the second part of the sixth century and the seventh century, many regions of Europe have been characterized by dramatic changes in the hydrographic setting, probably related to a strong cooling phase. In northern Italy, the chronicle of a huge flood event referred by the Lombard historian Paul the Deacon to the autumn of 589 AD has achieved a major importance and induced many researchers to attribute to this "deluge" episode many of the floods occurred during early Middle Age. In this paper, we consider the alluvial system of Tagliamento, which is one of the main rivers fed by south-eastern Alps and experienced a strong avulsion phase between the sixth and eleventh centuries. In that period, the river activated up to three branches and the hydrographical changes strongly influenced the human activity. This work critically reanalyses both published data and new stratigraphic and archaeologic evidence in order to assess and quantify the times and modes of this instability phase. The data suggest the occurrence of an extreme flood event at the end of the sixth century, which was also responsible for the burial of the ancient city of Concordia Sagittaria. The geochronological constraints suggest the possibility that this catastrophic episode occurred in 589 AD, thus confirming the Medieval Chronicle. Anyhow, other alluvial events occurred in the distal plain of Tagliamento River slightly before and after that moment.

Keywords

Extreme floods · Avulsions · Geoarchaeology · Radiocarbon dating · Venetian–Friulian Plain · Concordia Sagittaria

5.1 Introduction

The dramatic environmental alterations predicted for the near future (e.g. IPCC 2014) have drawn an increasing attention on the effects exerted by past climate changes on ancient human groups as possible analogues for the ongoing situation and the potential societal and economic crisis. In particular, several papers considered a time interval within the first millennium AD, when Europe was shocked by the collapse of the classical world and the migration period. This period of instability, described in many areas with the term "Dark Ages" since nineteenth

A. Fontana (✉) · L. Ronchi
Department of Geosciences, University of Padova, Via Gradenigo 6, 35131 Padua, Italy
e-mail: alessandro.fontana@unipd.it

M. Frassine
Soprintendenza Archeologia, Belle Arti e Paesaggio per l'area Metropolitana di Venezia e le Province di Belluno, Padova e Treviso, Via Aquileia 7, 35139 Padua, Italy

J. Herget and A. Fontana (eds.), *Palaeohydrology*, Geography of the Physical Environment,
https://doi.org/10.1007/978-3-030-23315-0_5

Table 5.1 Passage of the *Historia Langobardorum*, written around the end of the eighth century AD by Paul the Deacon (Liber III, 23), in which the author describes the deluge event referred to 23 October 589 AD

"Eo tempore fuit aquae diluvium in finibus Veneciarum et Liguriae, seu ceteris regionibus Italiae, quae post Noe tempus creditur non fuisse. Factae sunt lavinae possessionum seu villarum, hominumque pariter et animantium magnus interitus. Destructa sunt itinera, dissipatae viae, tantumtuncque Atesis fluvius crevit, ut circa basilicam Beati Zenonis martyris, quae extra Veronensis urbis muros sita est, usque ad superiores fenestras aqua pertingeret, licet, sicut et beatus Gregorius post papa scripsi, in eadem basilicam aqua minime introierit. Urbis quoque eiusdem Veronensis muri ex parte aliqua eadem sunt inundatione subruti. Facta est autem haec inundatio sexto decimo Kalenda Novembris"	"At that time, there was a deluge in the territories of Venice, Liguria and other Italian regions, which is believed to have had no equals since the days of Noah. Fields and villages were greatly damaged and many people and animals died. Paths were swept away and roads were destroyed. The level of the Adige River rose to reach the upper windows of the basilica of S. Zeno, which is located outside of the city walls of Verona. Nevertheless, as written by the future Pope St. Gregory, no water entered the church, while the city walls were partly destroyed by the flood. This flood occurred on October 23rd, AD 589"

century (cf. Lamb 1995 and previous versions), lasted between the fifth and the eighth centuries. According to recent reviews (Büntgen et al. 2016; Helama et al. 2017), the Dark Ages in Europe are generally characterized by the development of a rather cold and humid phase between 410 and 775 AD. Moreover, an interval of significant cooler condition has been evidenced in Europe between 536 and 660 AD and has been called by some authors the "Late Antique Little Ice Age" for its similarities with the Little Ice Age of the fourteenth–nineteenth centuries (Büntgen et al. 2016).

While the main researches attempted to reconstruct paleoemperature and paleoprecipitation through the analysis of climate proxies (e.g. dendrochronology, ice cores, speleothems), the archives of the phenomena related to the climatic variations, such as landslides, floods and coastal changes, are still largely unexplored. In particular, paleoflood research, in combination with archaeological investigations, has proven to be largely effective in reconstructing the relations between ancient societies and environmental variations (e.g. Brown 1997). Paleoflood archives are still not fully exploited in some regions of Europe and large sectors of Italy are included in this list (for a review, see Benito et al. 2015 and reference therein).

Several places in northern Italy show evidence of archaeological sites that have been affected by extreme floods and some of the major examples occurred during the early Middle Ages (e.g. Marcello and Comel 1963; Cremaschi and Gasperi 1989; Calzolari 1996; Dall'Aglio 1997; Castiglioni 2001; Bondesan and Meneghel 2004; Stefani and Vincenzi 2005; Fontana 2006; Cremonini et al. 2013; Mozzi et al. in press). On several of these sites, a burden in the interpretation of the evidence has been represented by a short passage of the *Historia Langobardorum* (Table 5.1), written around the end of the eighth century AD by Paul the Deacon (Liber III, 23). The chronicle was written 200 years after the described event and the manuscript mentions in detail the facts occurred in the city of Verona; nevertheless, this source obtained an extraordinary success within the archaeological scientific community and created a kind of myth of the so-called Deluge of the sixth century or Deluge of Paulus Diaconus. As clearly evidenced by Squatriti (2010), actually Paul the Deacon reported in a slightly different way the facts originally described by Pope Gregorius Magnus (560–604 AD) in his *Dialogues*, where he cited for 589 AD also the severe flood of Rome, which is completely neglected by the Lombard historian. Sometimes the effects of this event have been exported in most of the sites where archaeological structures dating to Late Antiquity and early Middle Age have been affected by alluvial deposition, often without a clear constraining chronology.

Recently, Cremonini et al. (2013) carried out an important work integrating geoarchaeological

evidence and historical sources at the scale of the central portion of the southern Po Plain, considering the stratigraphic and archaeological traces with a full interdisciplinary approach. The authors demonstrated that in the area between Bologna and Modena the period of fluvial instability and alluvial deposition experienced significant episodes before the sixth century, already since third century, and deposition was rather continuous until the eighth century. Notwithstanding, in that area the importance and magnitude of the floods occurred between the end of the sixth and the seventh centuries were very important, but it is not possible to constrain the absolute age and the number of the alluvial episodes.

In this work, we considered the alluvial plain of Tagliamento River that was strongly transformed during the early Middle Age by an avulsion phase which led to the abandonment of the former channel belt that had been active during Roman Age and Late Antiquity, in favour of the present direction (Fontana 2006; Fontana et al. 2014). This period of hydrographic transformation formed some important sedimentary units in the whole distal plain of Tagliamento, where the deposits have been dated with a number of radiocarbon dates and through the cross-correlation with archaeological structures. In particular, as already recognized by scholars since the nineteenth century (e.g. Bertolini 1877; Marcello and Comel 1963; Favero 1991; Valle and Vercesi 1996), evident traces of flooding are documented in the ancient city of Concordia Sagittaria (#S in Fig. 5.1), where the archaeological remains had been buried by flood deposits at the end of the sixth century (Croce Da Villa and Di Filippo Balestrazzi 2001).

In this paper, we analyse the stratigraphic, geochronological, archaeological and historical data that are available in Concordia and in other key sites to look for a precise chronology of the flood deposits of Tagliamento River during the first millennium AD. One of the aims is to check if the evidence is compatible with a catastrophic fluvial event in 589 AD. For this purpose, we want to investigate if in the study area it is possible to recognize a single extreme episode rather than a cluster of events and, eventually, to assess their magnitude in comparison with the major floods of last centuries. Tagliamento could represent a good case history for paleohydrology reconstruction as it is one of the major rivers in NE Italy and the large dimensions of its mountain catchment allow to limit the influence of local factors in the formation of the flood, which can be prevailing in small mountain basins.

Moreover, this case study offers the possibility to investigate the times and modes of the avulsion process that brought Tagliamento River to its present direction and to check if the hydrographic changes occurred in a short time interval or they have been produced during a rather long period. As documented in the Rhine Delta, the duration of the avulsion process which took place in that region during the early Middle Age shifting the active path of the Rhine River played an important role in conditioning the human activity in the area and the development of the settlement network (van Dinter et al. 2017).

5.2 Geomorphological and Archaeological Setting

The mountain basin of Tagliamento extends over an area of 2580 km^2 in the Carnic and Julian Alps, with a mean annual precipitation of ca. 2000 mm/a and phases of maxima occurring in autumn and, secondarily, in spring. This region is generally affected by western cells passing south of the Alps that often create significant rainfall events along the pre-Alps where, in some sectors, the daily rainfall can exceed 400 mm (Cicogna, 2008). The sediment and water discharge of Tagliamento are fed almost entirely by its mountain catchment, while in the alluvial plain, downstream of Pinzano, the river does not receive significant contributions (Fig. 5.1). This river has a flash pluvio-nival regime, with a mean flow of 81 m^3/s and a peak of 4050 m^3/s, measured about 20 km upstream of Pinzano (Venzone gouging station) in the period 1932–1973 (Surian et al. 2009). The last major floods, occurred in 1966, 1965, 1920, 1882, 1851, 1770,

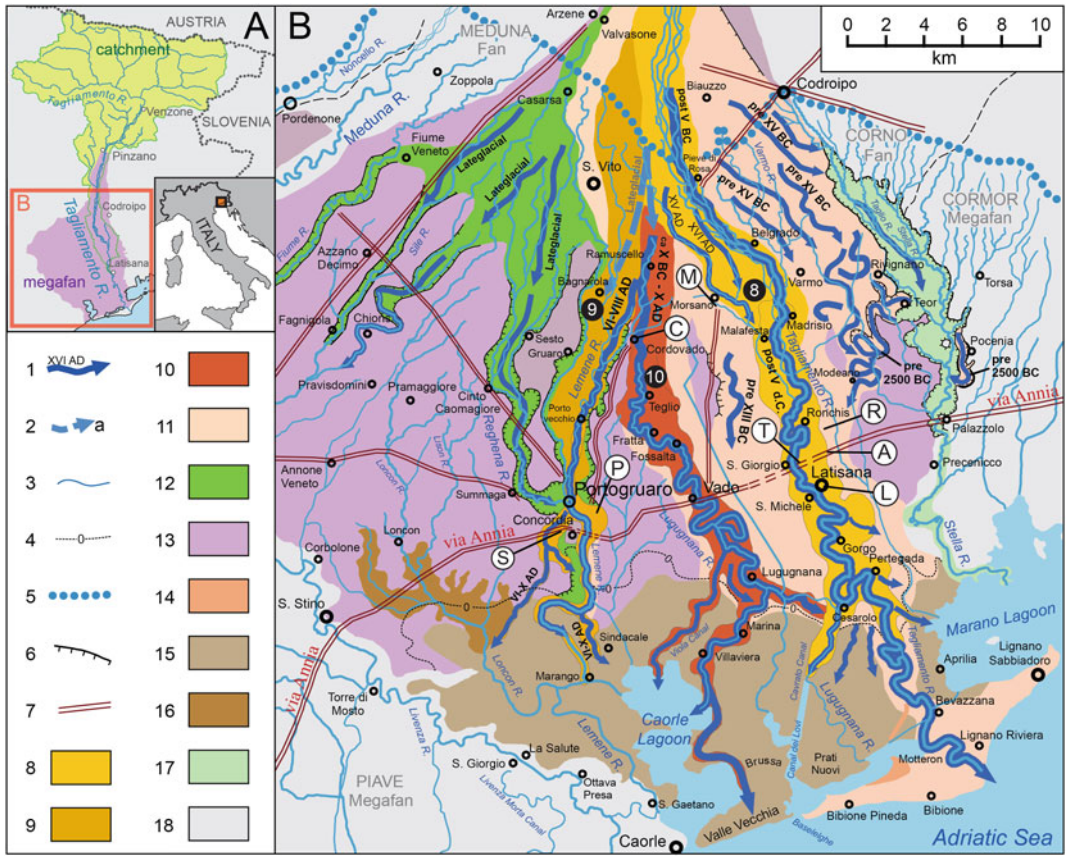

Fig. 5.1 Simplified scheme of the distal sector of the Tagliamento River megafan (modified after Fontana 2006). Legend 1 channel belt, with indication of the period of activity, 2 buried channel belt, 3 rivers and streams, 4 isoline 0 m a.s.l., 5 upper limit of the spring belt, 6 fluvial scarp, 5 trace of via Annia, 8 present Tagliamento (Latisana unit), 9 Concordia Sagittaria unit, 10 unit of *Tiliaventum Maius* (Roman Tagliamento), 11 undifferentiated Holocene deposits, 12 late glacial and early Holocene incised valley, 13 LGM alluvial deposits, 14 pre-Roman coastal sand ridges, 15 Holocene lagoon deposits, 16 Paludal deposits, 17 incision of Stella, 18 deposits of other fluvial systems

1692 and 1596, only affected the area downstream of Arzene (Fig. 5.1), while upstream of this location the channel bed is entrenched and the external alluvial plain is inactive (Castellarin 1990). The channel bed is characterized by a spectacular gravelly braided morphology up to Belgrado, while downstream it displays a transitional channel and it has a clearly meandering style from Ronchis down to the river mouth (Fig. 5.1).

The depositional activity of the Tagliamento formed an alluvial megafan in the Friulian Plain, which was mainly built during the Last Glacial Maximum (LGM, 29–19 ka BP; Fontana et al. 2014), when the river was a major outwash of the glacier hosted in the mountain catchment (Monegato et al. 2007). In the post-LGM (last 19 ka), the Tagliamento River activated several channel belts and changed directions downstream of a main avulsion node, located near the city of San Vito (Fig. 5.1), which corresponds to the transition from the steep gravelly apical sector of the megafan to the distal one that has a gentler gradient and is dominated by silty sediments (Fontana 2006). This lower portion is also characterized by a belt of springs that originate a dense network of minor groundwater-fed streams (Fontana et al. 2014).

During the Lateglacial and early Holocene, the Tagliamento system experienced a phase of sedimentary starvation which led the river to entrench in the LGM alluvial plain, along few narrow incised valleys (Fontana et al. 2014). Two major examples of such features, now filled and almost completely buried, have been documented below the present course of Lemene River (Fig. 5.1) and below the channel belt of the *Tiliaventum Maius* (#10 in Fig. 5.1; Fontana 2006; Fontana et al. 2012).

Since about 7.5 ka BP, the sea reached a level few metres below the present and favoured the formation of lagoon and estuarine environments in the distal plain and within the incised valleys. This setting led the Tagliamento to start a new phase of alluvial deposition, which was almost completely confined within the incised valleys until about 3.5 ka BP (Fontana et al 2014). After this moment, the channel belts activated by Tagliamento have been characterized by fluvial ridges along their final tract (#8, 9 and 10 in Fig. 5.1).

The first direction corresponds to the one active during the Roman Age, which was described as the *Tiliaventum Maius* by the geographer Plinio the Elder in his *Naturalis Historia* (liber III, XVIII, V, 126) in the first century AD and likely had the mouth in the coast of Valle Vecchia. This source cites also the *Tiliaventum minus* that was a minor branch which can be probably identified as the distributive channel separating from the main channel belt of *Tiliaventum Maius* near Lugugnana and headed towards SSE (Bondesan and Meneghel 2004; Fontana 2006). Some authors supposed that the *Tiliaventum minus* coincided with the present direction of Latisana, but the stratigraphic data demonstrate that during the Roman period only a groundwater-fed river was flowing along this path, reoccupying an incised channel abandoned by Tagliamento around 1500 BC (Fontana 2006).

During early Middle Age, an avulsion phase led to the progressive abandonment of the *Tiliaventum Maius* and the coeval activation of both directions towards Concordia and Latisana. After the tenth century, an avulsion near San Vito led to the definitive abandonment of the *Tiliaventum Maius* branch, which was not silted and was instead rapidly occupied in a parasitic way by the groundwater of the Lugugnana stream (Bondesan and Meneghel 2004; Fontana 2006). Since that period, only the Tagliamento branch of Latisana remained active.

In the study area a, rather complex settlement system already existed during the late Bronze Age, when sites were diffused in the distal plain and also within the lagoon environment (Fontana et al. 2017). Concordia was one of the major sites and achieved a main role in the area especially during Iron Age (Bianchin Citton 1996). Since the first part of the second century BC, the whole NE Italy entered in the direct influence of the Romans that settled a colony of veterans in the city of Aquileia and occupied almost completely the alluvial plain east of Tagliamento, building the classical agricultural division system of the *centuriatio* (Prenc 2002). The via Annia was the major road connecting the main cities along the coastal plain, such as Altinum, Concordia and Aquileia (Rosada et al. 2010; Uggeri 2013) and it was built after 153 BC (Figs. 5.1, 5.2).

Concordia became the Roman colony of *Iulia Concordia* in 42 or 41 BC and a widespread *centuriatio* characterized the alluvial plain north of the city (Croce Da Villa and Di Filippo Balestrazzi 2001). The study area experienced a major phase of prosperity between first century BC and the beginning of second century AD, while a significant economic crisis hit the whole NE Italy during the third century AD. This phase probably led to a re-arrangement of the agricultural system, which caused a progressive abandonment of part of the former territorial management, as documented by the need to restore several swamped tracts of the via Annia in the fourth century (Rosada et al. 2010). This phase of progressive decline since the beginning of the fifth century has been punctuated by significant episodes related to the barbarian invasions, for instance the Visigoths in 410 AD and the Huns of Attila in 452 AD (Christie 2006). Attila is intimately related to the complete collapse of the main cities in the plains of NE Italy as he induced the inhabitants of the region to seek shelter in the lagoon areas. This process increased after the end of the sixth century, when

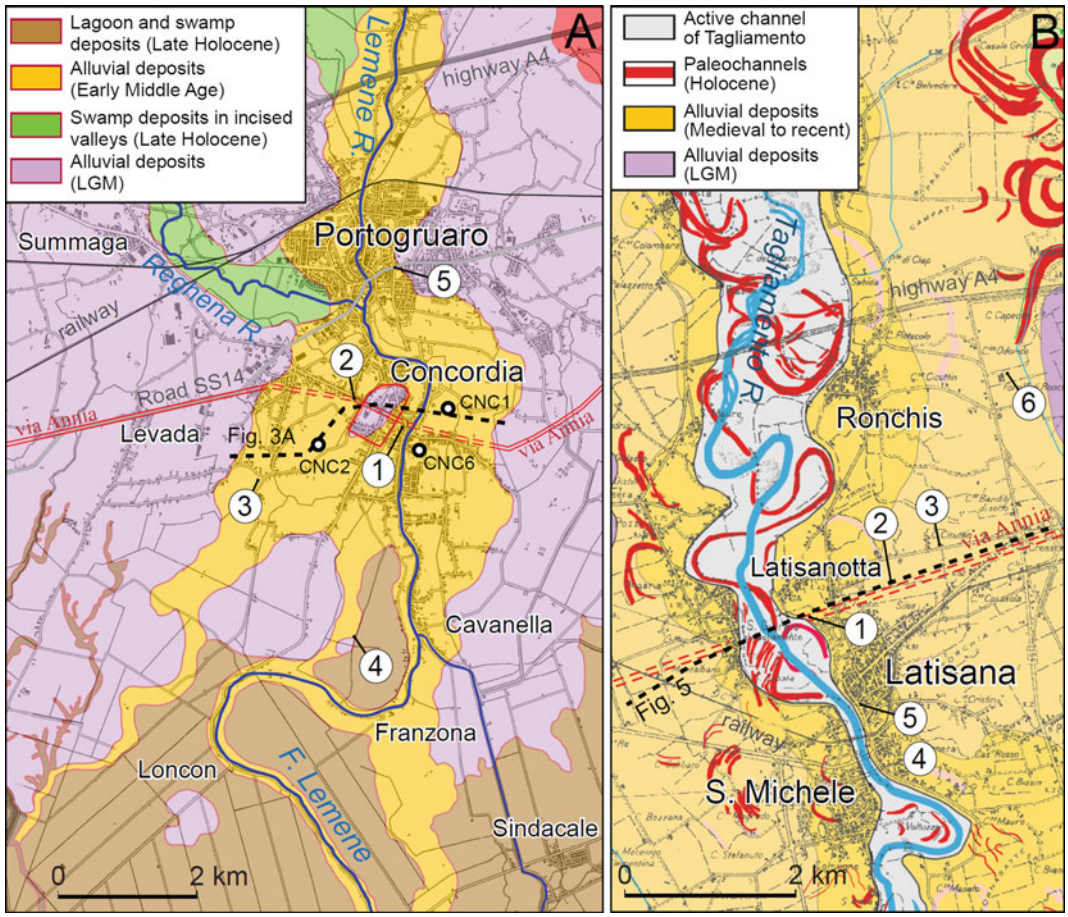

Fig. 5.2 **a** Simplified geological map with indication of the sites described in the text: area near Portogruaro and Concordia: 1 basilica, 2 via S. Pietro, 3 via 25 aprile, 4 Fossariola canal, 5 Portogruaro viale Isonzo; **b** area along the Tagliamento River between Varmo and Latisana: 1

the Lombards occupied northern Italy and only the lagoon and coastal zones remained under the Byzantine domain. These facts progressively prompted the importance of lagoon settlements as in the area of Venice, Jesolo, Caorle and Grado, while the alluvial plain was largely abandoned (Christie 2006).

Even after the collapse of the administrative system and the floods occurred in the early Middle Age, Concordia maintained its cultural role because of the siege of the bishop and the importance of the religious buildings. Notwithstanding, since the eleventh century the cities of Portogruaro and Latisana achieved a significant economic role in the area as they became important fluvial harbours settled on the Lemene and Tagliamento rivers, respectively. Nevertheless, all the area of the distal plain suffered from the difficulties in managing the surface waters and only when the area entered in the direct influence of the Republic of Venice, since the fifteenth century, some major hydraulic interventions started and improved the control of the territory.

A major phase in shaping the present landscape took place since the end of the nineteenth

century and particularly in the first half of the twentieth century, when all the coastal plain and large sectors of the Lagoon of Caorle and Marano-Grado have been reclaimed through the construction of a dense network of ditches, canals, dikes and a number of pumping stations (Fontana 2006; Bondesan and Furlanetto 2012 and references therein).

5.3 Methods

This research was designed as review aimed at the use of multidisciplinary information obtained by complementary sources, such as remote sensing, high-resolution digital elevation models (DTMs), description of sedimentary cores and stratigraphic sections, radiocarbon dating, archaeological excavations and analysis of written sources. In the recent years, the area has been surveyed for the geological (Fontana et al. 2012), geomorphological (Bondesan et al. 2004; Fontana 2006) and pedological mapping (Ragazzi and Zamarchi 2008; Michelutti et al. 2003) leading to both general and detailed survey of the distal plain. Moreover, the area was investigated by a detailed geoarchaeological research which checked the sites for their geochronological and paleoflood meaning (Fontana 2006), while some more recent work has been carried out in some of the selected sites, as described in the specific session (Sect. 5.4).

A major aspect of this work is represented by the analysis of the available geochronological dates which can constrain the alluvial evolution. The ages of frequentation of the site were obtained through the analysis of the typology of the pottery or other artefacts and are based on the specific published literature. The measured ^{14}C ages were then calibrated by using OxCal software, version 4.2.3 (Bronk Ramsey 2009), with the IntCal-13 atmospheric calibration curves (Reimer et al. 2013). Calendar ages presented hereafter correspond to the 2σ confidence level (Table 5.2).

5.4 Results

5.4.1 Area of Concordia Sagittaria and Portogruaro

The Roman city of *Julia Concordia* was built on a pre-existing settlement over a remnant terrace of LGM plain, isolated inside the incised valley (Figs. 5.2a and 5.3a). The city walls fenced this elevated area, while the suburbs expanded also in the depressed areas around the centre, especially in the eastern side, where in Late Antiquity the paleo-Christian basilica was constructed. The infill of the valley is characterized by the presence of an organic-rich/peaty interval with a thickness of 40–90 cm; this is generally found at a depth between 1 and 6 m from the ground and is not documented in the elevated areas (Fig. 5.3a, b). This organic unit formed in a freshwater marsh environment, with episodes of lagoon ingression (Favaretto and Sostizzo 2006), and had been generally accumulating from the first millennium BC but is covered by Medieval alluvial deposits (Fontana 2006). Thus, this horizon includes also the Roman period and represents a powerful stratigraphic marker, easily recognizable in cores and trenches, which allows geometric correlations over long distance along the incised valley, from Portogruaro to Sindacale (Fig. 5.2a). In 2017, the renovation of a major drainage canal directly exposed the peat layer for about 2.5 km (Fig. 5.3b).

Important details for reconstructing the evolution of the area were provided by excavation of the paleo-Christian basilica (b in Figs. 5.2a and 5.3a), where the restoration of the mosaic floor was carried out around the mid part of the sixth century and this ground was later covered by the debris related to the collapse of the building with the occurrence of traces of a fire (Croce Da Villa and Di Filippo Balestrazzi 2001). This layer is covered by alternations of sandy silts, silts and very fine sands that have a maximum thickness of 3–4 m and, below the present church, they can be separated in seven layers (Fig. 5.4a, b; Croce Da

Table 5.2 Available radiocarbon dates related to the evolution of the Tagliamento River between the Roman period and the early Middle Age

Sample name	Lab code	Location	Core/section	Location	Material	^{14}C age a BP	Calib. 1σ	Calib. 2σ	Stratigraphic meaning	Ref.
RIV02	Ua-37044	Ronchis Rivis di Mies	Section Archaeology	45° 48′ 26.40″ N 13° 1′ 12.18″E	Organic silt	1645 ± 30	380–426 AD	333–434 AD	Terminus post-quem for alluvial deposition	1
LAT-TRC	LTL-4963A	Latisanotta Selve di Sopra	Section Archaeology	45° 47′ 32.57″ N 13° 0′ 43.88″E	Trunk	1194 ± 40	774–881 AD	763–902 AD	Flood event	1
LAT-ARG	LTL-4965A	Latisanotta dyke Via Giardini	Core	45° 47′ 5.44″N 12° 59′ 13.08″ E	Plant macroremain	1579 ± 50	481–536 AD	387–593 AD	Terminus post-quem for alluvial deposition	1
LAT-FOR	Ua-37043	Latisana Piazza Indipendenza	Section Archaeology	45° 46′ 35.28″ N 12° 59′ 40.37″E	Charcoal	865 ± 25	1162–1211 AD	1150–1225 AD	Terminus ante-quem for fluvial ridge formation	1
CND A2 1	Beta-173013	Sepolcreto Concordia	Core	45° 45′ 24″'N 12° 51′ 12″E	Peat	1800 ± 70	131–260 AD	75–387 AD	Terminus post-quem for alluvial deposition	2
CNCPal554	Beta-184249	Paludetto Concordia	Core	45° 45′ 20″N 12° 49′ 46″E	Organic sediment	1920 ± 60	2–139 AD	43 BC–233 AD	Terminus post-quem for alluvial deposition	2
CNC6493400	Beta-184395	City hall Concordia	Core	45° 45′ 11.00″ N 12° 50′ 51.72″E	Peat	1910 ± 90	4–219 AD	112 BC–333 AD	Terminus post-quem for alluvial deposition	1
CORD-RIV	MAMS-15857	CordovadoVia Rivis	Section Archaeology	45° 50′ 35.34″ N 12° 52′ 45.99″E	Quercus sp. sez. Robur	1492 ± 20	558–600 AD	541–618 AD	Flood event	3
MORS_MFM 12	LTL-12800A	Morsano Moro	Section Archaeology	45° 51′ 14.14″ N 12° 55′ 55.82″E	Peach seed	1244 ± 35	680–860 AD	680–880 AD	Terminus post-quem for alluvial deposition	3

The column of references refers to: 1 this study, 2 Fontana (2006), 3 Frassine et al. (2014)

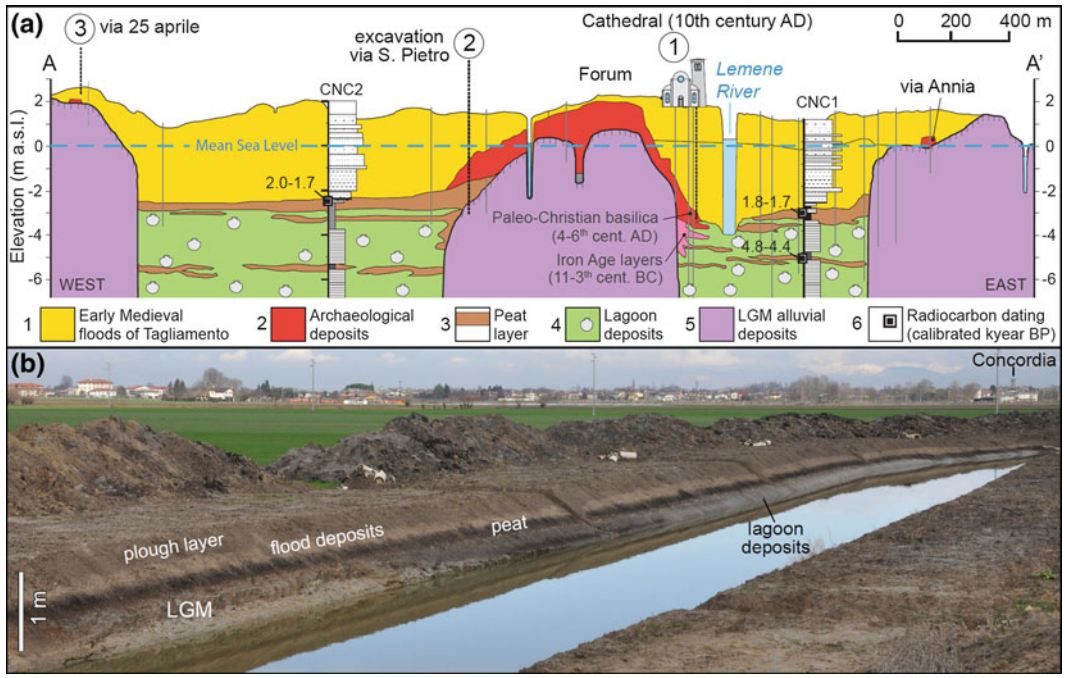

Fig. 5.3 **a** Simplified stratigraphic section of the area of Concordia Sagittaria (modified from Fontana 2006; Fontana et al 2014). The trace of the section is indicated in Fig. 5.2a. **b** Stratigraphic section exposed along the slope of Fossariola canal (#4 in Fig. 5.2a) in which is clearly visible the dark peaty layer; this rests on top of lagoon sediments of the first millennium BC and is buried by the yellowish silt of the Medieval floods

Villa and Di Filippo Balestrazzi 2001). The basal layer consists only of silt and is very different from the following ones as it testifies clear traces of activity related to the rework and spoliation of the building material covered by this first alluvial deposit. During this earliest phase of the floods, the religious functions were still going on in the buildings along the southern side of the basilica that had a slightly elevated position. The rest of the overlaying alluvial layers are very homogeneous and characterized by an evident draping geometry over the archaeological remains. These layers can be separated for the presence of flow structures, as ripples, with different orientation and dimensions. Anyhow, important erosive features or traces of significant depositional *hiata*, such as surfaces with indications of pedogenetic processes (i.e. entisols), are missing. This evidence suggests that their deposition can be associated with a single event characterized by several pulsations or, eventually, with different episodes occurred within a limited interval of time.

A remarkable indication of the power of the flood is supported by the four logs of populous tree found in the area of the basilica during the excavation of 1959, which were torn at 50–90 cm from the former ground and presented traces of torsion induced by the water flow (Marcello and Comel 1963). According to the description of the authors, the trees had been planted after the first flood episodes and lived for less than 20 years.

On top of the alluvial deposits, the remains of a wooden house and this building are dated to the eighth–ninth centuries, but possibly even since the end of the seventh century (Croce Da Villa and Di Filippo Balestrazzi 2001). In the same period a new church had been built over the former one but, slightly after, in the tenth–eleventh centuries, the construction of the present cathedral has already started.

In the area of via San Pietro (#S in Figs. 5.2a and 5.3a), on the western margin of the city, where the via Annia was passing from the incised

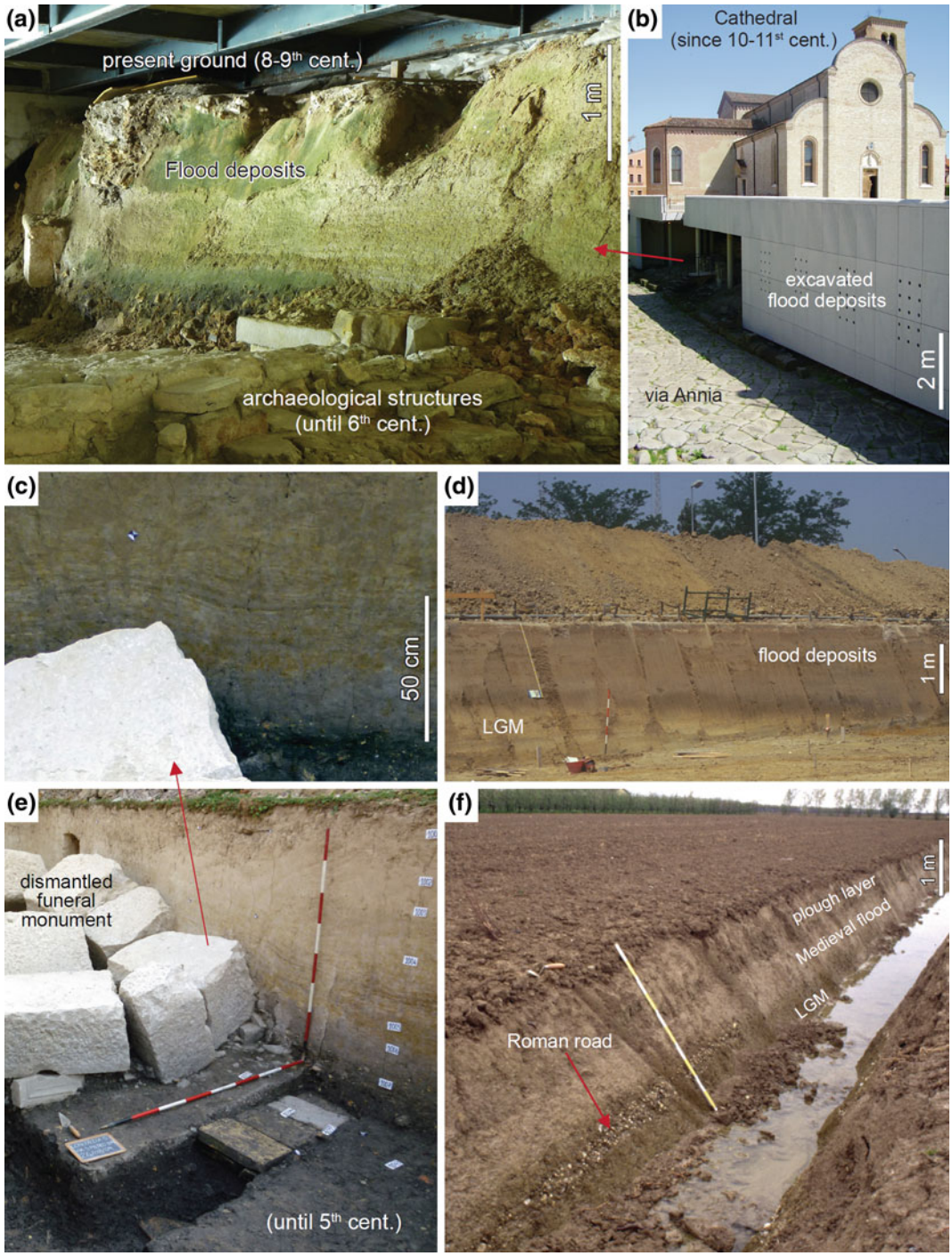

Fig. 5.4 Compilation of significant pictures for documenting the boundary between pre-Roman and post-Roman deposits in the area of Concordia and Portogruaro. **a** Stratigraphic section of the alluvial deposits burying the paleo-Christian basilica and covered by the present cathedral, **b** the area of the cathedral of Concordia with the path of the via Annia, **c** and **e** Concordia via San Pietro (#5 in Fig. 5.2a), stratigraphic section of the flood deposits covering a dismantled funerary monument and detailed picture (**c**) of the draping deposits (modified from Rinaldi and Vigoni 2015), **d** Portogruaro viale Isonzo (#5 in Fig. 5.2a), the dark brown layer represents the top of the LGM alluvial plain covered by the flood deposits of early Middle Age, **f** Concordia via 25 aprile (#3 in Fig. 5.2a), a minor roman road resting over the LGM alluvial plain and covered by alluvial silts

valley to the slope of the terrace of Concordia, the investigations documented the presence of the road and several tombs and funeral monuments. The ancient structures were dating between the first century BC and the fourth century AD, but clear traces documented the activity of spoliation of the funeral monuments at least until the fifth century AD (Rinaldi and Vigoni 2015). In this site the last layer of frequentation is a mix of debris of the dismantling activity and organic material, testifying the swamp environment (Fig. 5.4c, e). The alluvial deposits burying the area are 1.5 m thick and they are rather homogeneous, but a clear draping layering, sometimes even slightly laminated, is visible (Fig. 5.4c). The detailed description of the alluvial sequence recognized up to three different layers, distinguished on the bases of grain size and diverse pattern of planar lamination. Also in this site, as in the area of the basilica, the evidence suggests that the deposition of the sediments occurred in a single event with different pulses or as the product of very close episodes. Here a layer marking a first phase of post-Roman flooding was not recognized.

Almost in the centre of the depression located west of Concordia, the core CNC2-Paludetto intercepted the peat layer at a depth of 5.54 m and the top was radiocarbon dated to 42 BC–233 AD (Fig. 5.2a; Table 5.2). A similar age was obtained in core CNC6493400 (CNC6 in Fig. 5.2a), in the centre of the incised valley on the eastern side of the city (91 BC–260 AD), where the peat layer was found at a depth of 4 m; slightly north of this point the top of the peat is at the same depth, but it gave a slightly younger result (75–387 AD). All these geochronological data highlight that in the centre of the incised valley the accumulation of organic material had already stopped during the Roman period.

The counter part of the paleohydrologic evolution of Concordia is represented by the history of Portogruaro, a city founded on top of the fluvial ridge built by Tagliamento during the flooding period that sealed the Roman city (#5 in Fig. 5.2a). According to recent archaeological and historical reconstructions, Portogruaro was already existing in the tenth century and is mentioned as an important centre in 1140 AD (Sandron 2013).

5.4.2 Cordovado via Rivis

An excavation in the city of Cordovado (#C in Fig. 5.1) exposed the gravelly braided channel deposits of Tagliamento River, evidencing the presence of several trunks with length of 5–10 m at a depth of 3.5–4.0 m from the ground (Fig. 5.5c). This area is located nearby the avulsion point that separates the branch of Concordia from the *Tiliaventum Maius*, and in the last century, several trunks, almost complete, had been found at a depth of 2 m in the gravel pits just south of the village. Two samples of different trunks were analysed (trunk 8 and DD1) for dendrochronology by Olivia Pignatelli and one of them was also radiocarbon dated (Frassine et al. 2014; Frassine 2017). Sample 8 has 77 rings while sample DD1 76, but they died at the same time and, according to radiocarbon dating on trunk 8, this occurred between 541 and 618 AD (Fig. 5.5d; Table 5.2), which is exactly matching with the end of sixth century.

The name "Cordovado" derives from the contraction of *Curtis ad vadum* (the court near the ford), indicating that the settlement was close to the passage over the large river. A similar name is presented also by the village of "Vado" (derived from *vadum*), 8 km downstream that was located at the passage of the via *Annia* over the Tagliamento River during the Roman period. As these toponyms are already related to the post-Roman tradition, they probably testify that the branch of *Tiliaventum Maius* was still active during Late Antiquity and part of the early Middle Age. Moreover, another proof of the rather important activity of this branch until the eighth century is the so-called *Donatio Sextenses*, which is a document describing the goods and properties donated in 762 AD by Lombard princes to the monastery of Sesto al Reghena

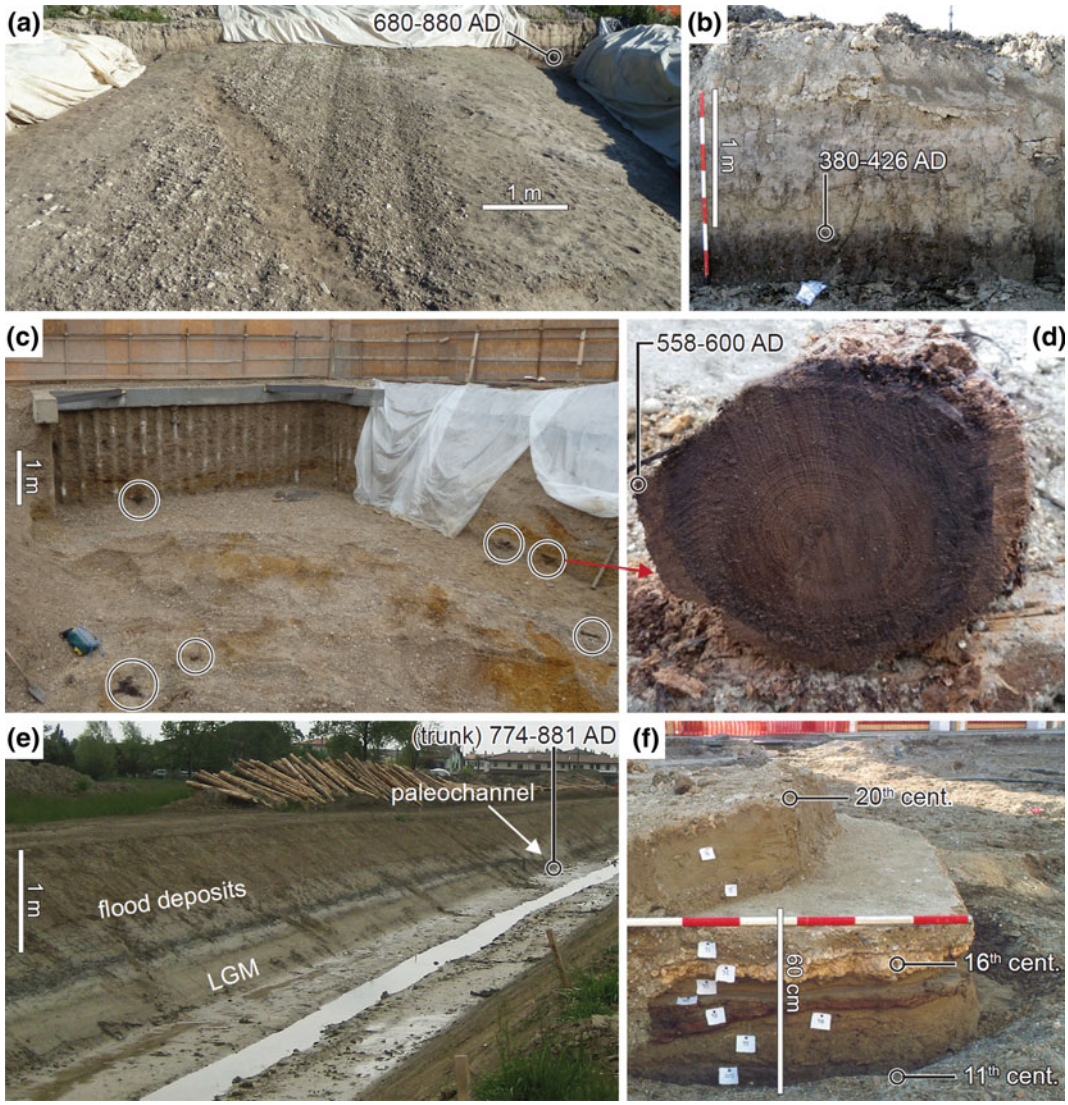

Fig. 5.5 Compilation of pictures of sites with key indications about the evolution of Tagliamento between Roman period and Middle Age; radiocarbon dates are indicated with 1σ. **a** Morsano, top surface of a Roman road with traces of carriage wheels (#M in Fig. 5.1), **b** Ronchis Rivis di Mies (#1 in Fig. 5.2b) alluvial deposits covering the organic layer with debris of Roman bricks, **c** Excavation in Cordovado (#C in Fig. 5.1) with evidenced some of the wood logs amalgamated in the gravelly deposits of Tagliamento, **d** sliced section of the radiocarbon dated trunk **d** found in Cordovado and radiocarbon dated to the end of the sixth century, **e** Latisanotta aqueduct (#2 in Fig. 5.2b), stratigraphic section in which the alluvial deposits cover an organic-rich layer with trunks dating to the ninth century, **f** Latisana Piazza Indipendenza (#4 in Fig. 5.2b), archaeological succession corresponding to the period between the tenth century and present day

(Fig. 5.1). In this document, the village of Ramuscello, that is 4 km north of Cordovado, is described as standing on the eastern side of Tagliamento (… *trans fluvio Tiliamento casa Ramoscello* …; cf. Destefanis 1999), while now it is over 2 km west of the active channel and

was already in this position around 1200 AD. In fact, another document, written by Pope Urbanus III, states that in 1186 AD the river avulsed and passed east of Cordovado and the near village of Saletto.

5.4.3 Morsano

South of the village of Morsano in 2012–2013, a Roman road with SSW–NNE direction was excavated (#M in Fig. 5.1). The road, built in 1–2 AD and gravelly paved and with a width of 12 m, was buried by only 50 cm of alluvial silt (Frassine et al. 2014 and reference therein). The archaeological structure was exposed at least until the end of the eighth century, as demonstrated by some Middle Age potsherds, and a seed of peach found in the western ditch of the road and radiocarbon dated to 680–880 AD (Fig. 5.5a; Table 5.2). The road surface is characterized by several well-preserved tracks of carriages and, considering the lack of gullies or other erosive features, it is likely that the path had been covered in a single event that also brought to abandon it, allowing its preservation.

Until the fifteenth century, the right bank of Tagliamento was located just east of Morsano and the excavated site was only 300 m apart. In the following centuries, the river channel progressively shifted eastwards through some local avulsions (Fontana 2006), but this process does not seem to have left sedimentary traces on the site.

5.4.4 Area of Latisana

The early Medieval avulsion phase of Tagliamento activated its current channel belt along the direction of Madrisio, Ronchis, Latisana and Bevazzana and led to the formation of the present delta (Fig. 5.1). South of Madrisio, the river built a huge fluvial ridge that is up to 4 m higher than the related floodplain and which sealed with its sediments the previous landscape. In particular, the alluvial deposits buried the remains of several Late Antiquity settlements and in the area north of Latisana also the trace of the via Annia for a length of over 2 km (Fig. 5.6). The Roman road has been used as a marker to separate pre-Roman and the post-Roman alluvial deposits, checking the stratigraphic position and the chronology through a number of boreholes and few selected archaeological investigations.

North of Latisana, close to the artificial dyke of Tagliamento in Latisanotta (#1 in Figs. 5.2b and 5.6), the gravels forming the pavement of the via Annia are found at a depth of about 3 m and the northern ditch running along the road was filled by an organic-rich deposit (Ventura et al. 2011). The top portion of these sediments has been radiocarbon dated to 380–600 AD (Table 5.2), and this age represents a *terminus*

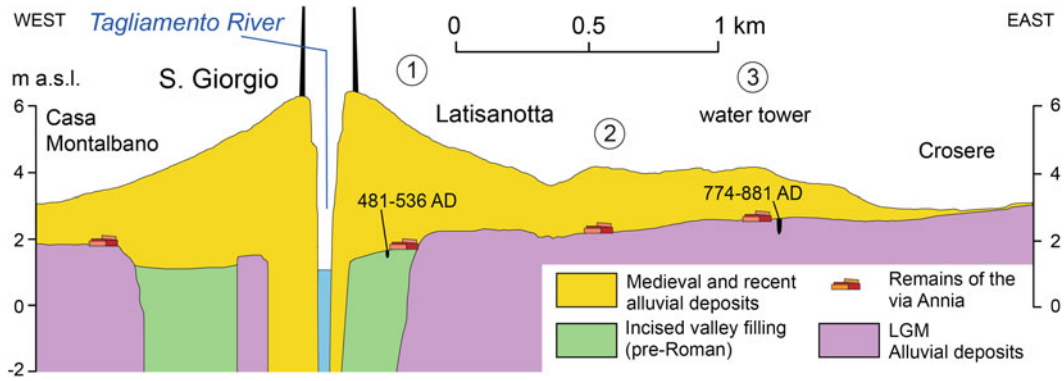

Fig. 5.6 Schematic stratigraphic section of the current fluvial ridge of Tagliamento, north of Latisana (modified from Fontana 2006). The trace of the section is indicated in Fig. 5.2b

post-quem for the beginning of the alluvial deposition connected to the branch of Latisana.

East of the village of Latisanotta (#2 in Figs. 5.2b and 5.6), several archaeological remains have been documented along the road and this zone probably corresponds to the ancient settlement of *Apicilia*, which is cited in the so-called *itinerarium Burdigalensis* of the fifth century AD (Ventura et al. 2011 and reference therein). The buried structures directly rest on top of the LGM plain, testifying that a very long period of non-deposition occurred before the Medieval phase of deposition. The thickness of the alluvial cover progressively thins towards east, up to 2 km far from Tagliamento, where the LGM sediments crop out.

In the area of the water tower of Latisana (#3 in Fig. 5.2b and Fig. 5.6), near the via Annia, the investigations documented the ancient presence of a small local stream with the channel infill characterized by organic-rich and peaty sediments (Fig. 5.5e). Several trunks were present on the top part of it, buried by 1.5 m of alluvial silts of Tagliamento, and they were aligned along the direction of the flow. The bark of one of them, with about 40 rings, has been dated to 760–900 AD, and this age is considered a *terminus post-quem* for the arrival of the distal deposits of the Tagliamento. It is worth noting that after a first phase of flood, on the surface of via Annia some traces of limited restoration activity were detected, documenting that even after the tenth century the road was partly in use (Ventura et al. 2011).

Traces of Roman settlements have been found also at depth of 1.7 m in the subsurface of the hospital of Latisana (#4 in Fig. 5.2b), while in the centre of the city (#5 in Fig. 5.3c), where the Medieval village was settled, the archaeological excavation detected several ground floors of the houses and workshop activities dating since the eleventh–twelfth centuries AD (Fig. 5.5f; Fontana 2006). An oven structure corresponding to one of the first phases of the village has been radiocarbon dated to 1147–1218 AD. These archaeological remains were found at 1 m of depth, sealed by the younger anthropogenic structures related to the lower Medieval, Renaissance and modern activity, documenting that the alluvial sedimentation was rather limited or lacking. As for Portogruaro, also the early Medieval settlement of Latisana was a village of new foundation that was built over the top portion of the fluvial ridge formed by the early Medieval flood deposits. The community of Latisana settled on the bank of the active channel of Tagliamento, with the function of a fluvial harbour. At that time, the place was the northern point of influence of the tidal backwater effect, allowing the boats to reach Latisana and descent along the river.

5.4.5 Ronchis A4 Rivis di Mies

In this area (#6 in Fig. 5.2b), a Roman furnace was found at a depth of 0.5–1.5 m from surface, covered by alluvial deposits connected to the present channel belt of Tagliamento. The building had been built along the southern bank of an incised paleochannel of Tagliamento, which had been abandoned around 2500 BC and has been after characterized by a swampy environment with accumulation of organic material (Fontana 2006). The top portion of the organic sediments filling the residual channel is marked by the abundant presence of bricks and other Roman artefacts (Fig. 5.5b), which are partly related to the spoliation and reworking of the site in Late Antiquity that was already abandoned in the fourth century (Cividini and Ventura 2007). The radiocarbon dating of a sample from the real top of the organic unit gave an age of 348–431 AD and this could be considered a *terminus post-quem* for the beginning of the alluvial sedimentation transported along the present direction of the river.

5.5 Discussions and Conclusions

In the lower sector of the alluvial megafan of Tagliamento, the information collected from different independent and complementary sources allows to attempt a detailed reconstruction of the alluvial events which occurred in the area during the early Middle Age and to seek for

similarities and differences existing among the data supported by historical chronicles, archaeological investigations and geological research.

The available radiocarbon dates of the samples collected near the dyke of Tagliamento in Latisanotta (#1 in Fig. 5.6) and in the archaeological site of Ronchis Rivis di Mies (Fig. 5.5b) allow to hypothesize that the alluvial sedimentation along the present direction of Tagliamento had already started between the fifth and the sixth centuries AD. This situation suggests that the avulsion process which led the river to change its active channel belt from that of the *Tiliventum Maius* (#10 in Fig. 5.1) to the one of Latisana (#8 in Fig. 5.1) had already started before the end of the sixth century. Also near Concordia Sagittaria, a significant environmental change is documented already during the Roman period, when in the first and second centuries AD the accumulation of plant remains in the incised valleys surrounding the city stopped and some very limited sedimentation occurred. Anyhow, this variation in the paleo-ecological setting is documented only through the stratigraphic cores collected in the lower areas (CNC1, CNC2, CNC6 in Fig. 5.2a) and they are compatible with the important changes of land use which affected even the most depressed zones around the Roman city. It is likely that part of the marshes that occupied the incised valleys had been reclaimed for agricultural and productive purposes and, moreover, one of the major necropolises expanded along via Annia in the eastern depression (i.e. near CNC1; cf. Croce Da Villa and Di Filippo Balestrazzi 2001).

Notwithstanding, the alluvial deposition in the zone of the paleo-Christian basilica of Concordia is documented only since the second half of the sixth century, when part of the religious complex had already collapsed. After a first flood episode, the local community still maintained some religious functions in this depressed area and tried to recover part of the construction materials from the ruined buildings but, few years later, the most significant alluvial deposition took place. This latter twisted and ripped away the trees planted in the area of the basilica, as described by Marcello and Comel (1963), and according to the age of the plants, it is likely that about 20 years have passed from the first flood. The evidence suggests that this was a catastrophic single episode with several pulsations or a clustering of events, very close in time and with similar characteristics. A wooden house was built at the top of the alluvial sequence in eighth–ninth centuries and also a new church was built in the same period, testifying that the flood phase had ended before, most probably already during the seventh century.

Because of the homogeneous aspect of the flood deposits documented around the basilica, but also in many other places inside the incised valleys all around the city of Concordia (Figs. 5.3b and 5.5), we advance the hypothesis that a major extreme event occurred in the area. In particular, this is suggested by the lack of erosive features and of surfaces with evidence of pedogenetic processes or plant activity within the stratigraphy. The flooding phase filled the incised valleys with up to 4 m of sandy silts and silty sands and, along the channels used by Tagliamento River, some fluvial ridges have been built (Fig. 5.2a). The major one has been after occupied by the Lemene River, while one is documented in the area of Franzona and another has a SW direction, from Concordia towards Loncon.

The trunks found in Cordovado testify that an important flood event occurred along the direction of *Tiliaventum Maius* in the last decades of the sixth century (558–660 AD). This is the only direct and chronologically rather well-constrained proof that a hydrological extreme event likely occurred around 589 AD (Fig. 5.7). In fact, the other chronological markers found in the study area correspond to *termina post-quem* or *ante-quem* indicators in relation to the floods, while it is likely that the trunks of Cordovado have been uprooted by the same flood which also transported them. In the river system of Tagliamento, the evidence related to the possible synchronicity between the alluvial deposition in Concordia, the flood in Cordovado and the catastrophic deluge reported by Paul the Deacon is significant. Thus, the hypothesis that the main flood in Concordia occurred in 589 AD is plausible. Notwithstanding, at the moment no

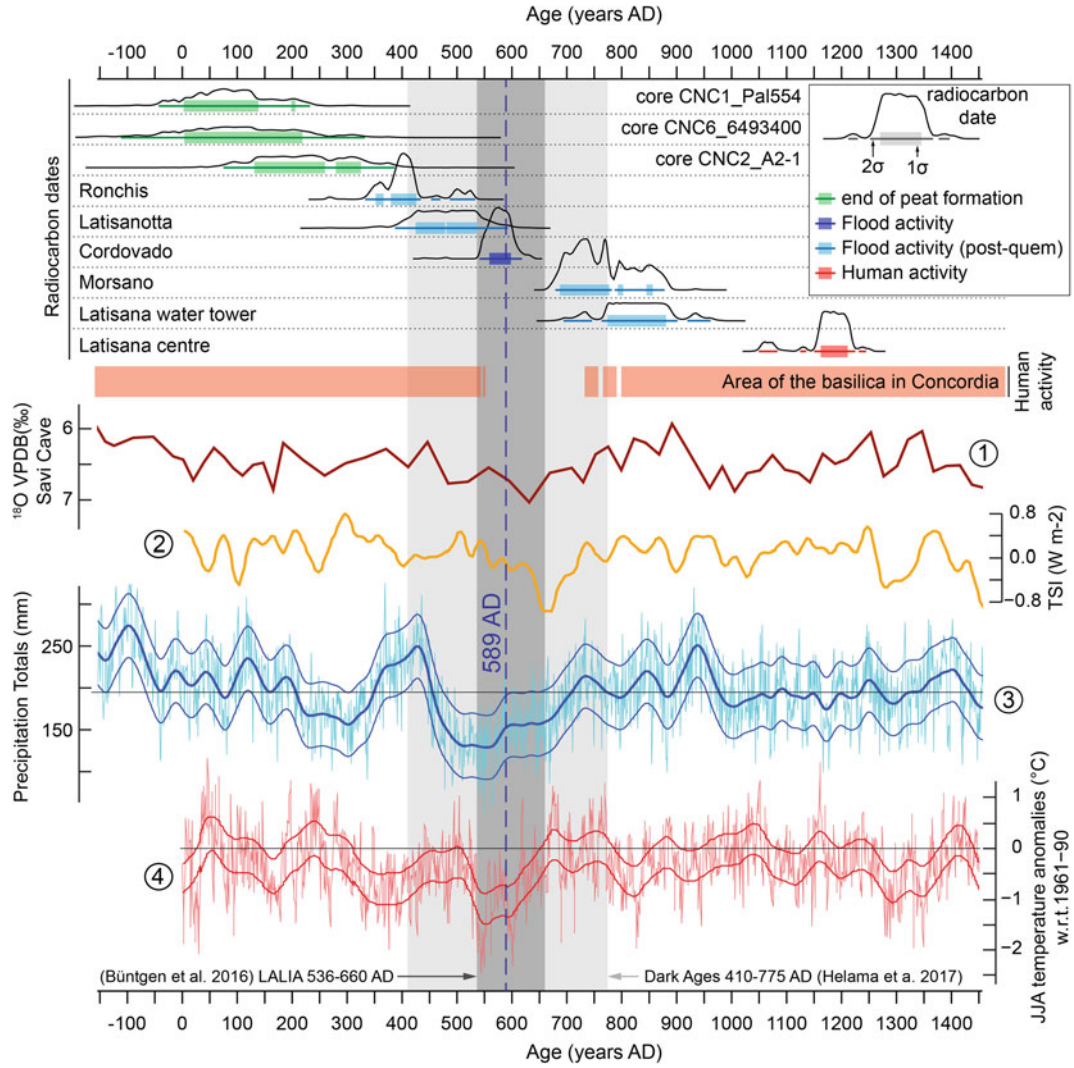

Fig. 5.7 Plot diagram of the available archaeological and geochronological information on the evolution of the Tagliamento River between the Roman period and the Middle Age. A series of climatic proxies are reported. 1 $\delta^{18}O$ concentration at the Savi Cave, after Frisia et al. (2005), 2 ice-core-derived solar forcing as total solar irradiance (ΔTSI), after Steinhilber et al. (2009), 3 April-to-June precipitation in central Europe, after Büntgen et al. (2011), 4 June-to-August (JJA) temperature anomalies with respect to the 1901–2000 period, after Büntgen et al. (2011)

further evidence is available for ascertaining the real absolute age of these events and if the flood documented near Cordovado corresponds to the main one in the area of Concordia or if they are two different episodes, even if separated by a rather short time interval.

The floods of the end of the sixth century and eventually of the first part of the seventh century triggered the formation of a new hydrographic landscape in the lower sector of Tagliamento, but the avulsion process lasted much more, as the direction of *Tiliaventum Maius* has been

definitively abandoned by the river during the twelfth century, as reported by the document of Pope Urbanus III described above. Anyhow, the direction of the Lugugnana River (i.e. the former *Tiliaventum Maius*) has been exceptionally used by the waters of the Tagliamento during some major floods even in rather recent times, as in 1450, 1692 and 1851 (Castellarin 1990), but the sedimentary evidence related to these episodes along Lugugnana River is very poor. This fact testifies the occurrence along the history of high-magnitude floods which did not leave any sedimentary trace, while other events left a marked sedimentary evidence but were not recorded in any written sources and chronicles. Thus, only the combined use of complementary data allows to extend and integrate the record of paleofloods.

Along the direction of Latisana, the activity of Tagliamento has progressively extended the width of the fluvial ridge, as documented by the progressive younger age of the base of the river deposits. In fact, while close to the river channel in Latisanotta the first deposition occurred after 380–600 AD (#1 in Fig. 5.6), almost 1.5 km eastward, in the area of the water tower (#3 in Fig. 5.6), this is dated to 760–900 AD. Notwithstanding, the elevation of the natural levees forming the fluvial ridge has not changed significantly since the end of the twelfth century, when the Tagliamento flowing in Latisana has remained the only active channel and we can consider the avulsion process completed. In the centre of Latisana, few tens of metres from the river channel, the artificial embankment was built only in the seventeenth century (cf. Castellarin 1990), but the alluvial sediments of the eleventh century are in the immediate subsurface, almost only covered by the anthropogenic aggradation (Fig. 5.5f).

Beside the flood of Adige River in Verona in 589 AD, directly described by Paul the Deacon in his manuscript, also the Piave River activated a new channel in that period, as testified by the radiocarbon age of the swamp environment sealed by its deposits and dated to 530–682 AD (Bondesan and Meneghel 2004). Moreover, also Livenza River experienced the activation of a temporary branch in which was found a trunk radiocarbon dated between 430 and 650 AD (Bondesan and Meneghel 2004). Thus, most of the major fluvial systems of NE Italy experienced dramatic changes in a period which is constrained between the end of the sixth century and the seventh century. This interval includes the 589 AD and, at least, generally corresponds to the historical sources describing that period as characterized by severe hydrological disorders.

It is difficult to assess the magnitude of a paleoflood in the distal plain but, in the case of Concordia, we tried to compare the quantity of sediment delivered in the area during the alluvial activity between the sixth and seventh centuries. Considering the dimensions of the incised valley of Concordia in the sector between Gruaro and Franzona (Fig. 5.2a), the sediments deposited during early Middle Age have a volume that is in the order of 1.5×10^6 m^3 for every longitudinal kilometre of the valley. With a rough estimate, along the direction of Concordia in that phase the Tagliamento transported a volume between 1 and 2×10^7 m^3. It is worth noting that this is an underestimation, as it does not consider the sediment deposited in the same period along the *Tiliaventum Maius*, the direction of present Tagliamento and in the delta system. Considering that Tagliamento River currently transports between 0.6 and 1×10^5 m^3/a in its medium tract (cf. Ziliani and Surian 2012), it is evident that the quantity of sediment moved during the activation of Concordia branch, thus mainly during a single event, was two orders of magnitude higher than the modern annual discharge, and thus, it can be defined as a catastrophic situation.

The main flood which buried Concordia was produced in the mountain basin of and, despite the natural origin of the water discharge forming the flood (probably an extreme rainfall event), it is possible that the huge amount of sediment transported by the river has been partly fed by the collapse of the management in the catchment during the decades before the event. As recently demonstrated for the flood that hit some of the major rivers fed by the northern Apennine (Lucía et al. 2015), the role of the living and dead vegetation along the channel and the slopes can

play a very important role, which can be exerted by the abandonment of maintenance interventions and can induce larger damages also in the downstream tract of the river. In this perspective, the abandonment of large portions of the SE Alps and the lack of maintenance works along slopes and main valleys could generate an available wave of sediment that could represent a major threat in the alluvial plain during next floods.

The production of sediments in the mountain catchment could have been also favoured by the occurrence of a significant period of cooling, as documented in many climatic proxy records around Europe between 530 and 660 AD (Fig. 5.7; cf. Büntgen et al 2016; Helama et al. 2017). Despite its low temporal resolution, this situation is also documented in NE Italy by the speleothem collected near Trieste in the Savi Cave, that testify a cool interval between 450 and 750 AD, with the minimum reached at about 630 (Frisia et al. 2005). Also in the Carnic and Julian Alps these climatic conditions could have fostered the activity of slope, weathering and periglacial processes. They could have induced the accumulation of deposits in the valleys until a major meteorological event with the capability of transporting them towards the alluvial plain. In this perspective, we fully support the idea deduced by Cremonini et al (2013) in the southern sector of Po Plain that the alluvial event/phase of the sixth century was not necessarily the result of a prolonged phase of higher precipitations, but could have been also an extreme event, possibly occurred even during a period of general drought.

Acknowledgements This paper benefited from discussions with members of the project "EX-AQUA: Palaeohydrological Extreme Events, Evidence and Archives", sponsored by INQUA (TERPRO, 1623P). The Municipality of Concordia Sagittaria and, in particular, Michelangelo Dal Pos is thanked for facilitating the studying of the area. The authors are indebted with Jürgen Herget for his efforts in sustaining the production of this chapter.

References

Benito G, Macklin MG, Panin A, Rossato S, Fontana A, Jones AF, Machado MJ, Matlakhova E, Mozzi P, Zielhofer C (2015) Recurring flood distribution patterns related to short-term Holocene climatic variability. Sci Rep 5(16398):1–12

Bertolini D (1877) Sepolcreto di Concordia. Notizie di Scavi 21–48

Bianchin Citton E (1996) Breve storia delle ricerche e degli studi. In: AA.VV. (eds) La protostoria tra Sile e Tagliamento. Antiche genti tra Veneto e Friuli, Catalogo della mostra, Concordia, 14 settembre–10 novembre 1996, Esedra, Padova, pp 185–187

Bondesan A, Furlanetto P (2012) Artificial fluvial diversions in the mainland of the Lagoon of Venice during the 16th and 17th centuries inferred by historical cartography analysis. Géomorphologie 2(2012):175–200

Bondesan A, Meneghel M (2004) Geomorfologia della provincia di Venezia. Esedra, Padova

Bondesan A, Meneghel M, Rosselli R, Vitturi A (eds) (2004) Geomorphological map of the province of Venice, scale 1:50,000. LAC, Firenze, 4 sheets

Bronk Ramsey C (2009) Bayesian analysis of radiocarbon dates. Radiocarbon 51:337–360

Brown T (1997) Alluvial geoarcheology. Cambridge Manuals in Archaeology, Cambridge

Büntgen U, Tegel W, Nicolussi K, McCormick M, Frank D, Trouet V, Kaplan JO, Herzig F, Heussner K, Wanner H, Luterbacher J, Esper J (2011) 2500 years of European climate variability and human susceptibility. Science 331:578–582

Büntgen U, Myglan V, Ljungqvist F, McCormick M, Di Cosmo N, Sigl M, Jungclaus J, Wagner S, Krusic P, Esper J, Kaplan J, de Vaan M, Luterbacher J, Wacker L, Tegel W, Kirdyanov A (2016) Cooling and societal change during the Late Antique Little Ice Age from 536 to around 660 AD. Nat Geosci 9:231–237

Calzolari M (1996) Alluvioni e dissesti idrogeologici in Italia settentrionale nel VI e VII sec. D.C.: i dati delle fonti scritte. Ann Benacensi 11:39–75

Castellarin B (1990) Le inondazioni del Tagliamento. In: Altan M, Castellarin B, Fantin E, Foramitti G, Romanin F, Turoldo D (eds) Le alluvioni del Tagliamento a Latisana e nei comuni della Bassa Friulana. La Bassa, collana 12, Latisana

Castiglioni GB (2001) Response of the fluvial system to environmental variations. In: Castiglioni GB, Pellegrini GB (eds) Illustrative notes of the geomorphological map of Po Plain (Italy). Geogr Fis Dinam Quat suppl 4:165–188

Christie N (2006) From Constantine to Charlemagne: an Archaeology of Italy AD 300–800. Ashgate, Aldershot

Cicogna A (ed) (2008) Atlante climatico del Friuli Venezia Giulia. Agenzia Regionale per la Protezione dell'Ambiente del Friuli Venezia Giulia Settore Osservatorio Meteorologico Regionale

Cividini T, Ventura P (2007) Ronchis (UD): impianto produttivo. Notiziario Soprintendenza Beni Archeologici Friuli Venezia Giulia 2:57–62

Cremaschi M, Gasperi G (1989) L'alluvione altomedievale di Mutina (Modena) in rapporto alle variazioni ambientali oloceniche. Mem Soc Geol Ital 42: 179–190

Cremonini S, Labate D, Curina R (2013) The late-antiquity environmental crisis in Emilia region (Po river plain, Northern Italy): geoarchaeological evidence and paleoclimatic considerations. Quatern Int 316:162–178

Croce Da Villa P, Di Filippo Balestrazzi E (a cura di) (2001) Concordia Sagittaria tremila anni di storia. Esedra Editrice, Padova

Dall'Aglio P (1997) Il Diluvium di Paolo Diacono e le modificazioni ambientali tardoantiche: un problema di metodo. Ocnus 5:97–104

Destefanis E (1999) Fonti scritte e toponomastiche per la conoscenza del territorio. In: Cantino Wataghin G (ed) Antichità e Alto Medioevo tra Livenza e Tagliamento, contributo per una lettura della carta archeologica della Provincia di Pordenone. Provincia di Pordenone, Assessorato alla Cultura, Pordenone, pp 25–42

Favaretto S, Sostizzo I (2006) Vegetazione e ambienti del passato nell'area di Concordia Sagittaria (VE). Quaderni del Dottorato Dipartimento di Geografia Università di Padova 1:57–69

Favero V (1991) Concordia Sagittaria. Scavo protostorico. Quaderni Archeologia del Veneto 7:79–85

Fontana A (2006) Evoluzione geomorfologica della bassa pianura friulana e sue relazioni con le dinamiche insediative antiche. Monografie Museo Friulano Storia Naturale 47. Enclosed Geomorphological Map of the Low Friulian Plain scale 1:50,000

Fontana A, Bondesan A, Meneghel M, Toffoletto F, Vitturi A, Bassan V (2012) Note illustrative della Carta Geologica d'Italia alla scala 1:50.000-Foglio 107 "Portogruaro". ISPRA, Regione Veneto, Infocartografica, Piacenza

Fontana A, Mozzi P, Marchetti M (2014) Alluvial fans and megafans along the southern side of the Alps. Sed Geol 301:150–171

Fontana A, Vinci G, Tasca G, Mozzi P, Vacchi M, Bivi G, Salvador S, Rossato S, Antonioli F, Asioli A, Bresolin M, Di Mario F, Hajdas I (2017) Lagoon settlements and relative sea level during Bronze Age in Northern Adriatic: geoarchaeological evidence and paleogeographic constraints. Quatern Int 439:19–36

Frassine M (2017) Alluvioni, bonifiche e viabilità romana nel Friuli occidentale. Nuovi dati per la ricostruzione del paesaggio antico. In: Turchetto J, Asolati M (eds) Paesaggi in movimento. Ricerche dedicate a Guido Rosada, Padova University Press, pp 165–174

Frassine M, Fontana A, Bezzi A (2014) Viabilità romana nel territorio di Morsano al Tagliamento (PN): la direttrice Concordia-Norico dal telerilevamento allo scavo archeologico. J Ancient Topogr 23:107–128

Frisia S, Borsato A, Spötl C, Villa IM, Cucchi F (2005) Climate variability in the SE Alps of Italy over the past 17000 years reconstructed from a stalagmitic record. Boreas 14:445–455

Helama S, Jones P, Briffa K (2017) Dark Ages Cold Period: a literature review and directions for future research. Holocene 27:1600–1606

IPCC (2014) Climate change 2014: synthesis report. Contribution of Working Groups I, II and III to the fifth assessment report of the Intergovernmental Panel on Climate Change [Core Writing Team, Pachauri RK, Meyer LA (eds)]. IPCC, Geneva, 151 pp

Lamb HH (1995) Climate history and the modern world, 2nd edn. Routledge, New York

Lucía A, Comiti F, Borga M, Cavalli M, Marchi L (2015) Dynamics of large wood during a flash flood in two mountain catchments. Nat Hazards Earth Syst Sci 15:1741–1755

Marcello A, Comel A (1963) L'alluvione che seppellì Julian Concordia. Mem Biogeogr Adriat, Ist Stud Adriat 5:139–145

Michelutti G, Zanolla S, Barbieri S (2003) Suoli e Paesaggi del Friuli-Venezia Giulia, 1. Pianura e colline del pordenonese. ERSA, Agenzia Regionale per lo sviluppo agrario, Pozzuolo del Friuli, Udine

Monegato G, Ravazzi C, Donegana M, Pini R, Calderoni G, Wick L (2007) Evidence of a two-fold glacial advance during the last glacial maximum in the Tagliamento end moraine system (eastern Alps). Quatern Res 68: 284–302

Mozzi P, Piovan S, Corrò E (in press) Long-term drivers and impacts of abrupt river changes in managed lowlands of the Adige river and northern Po delta (Northern Italy). Quatern Int. https://doi.org/10.1016/j.quaint.2018.10.024

Paulus Diaconus. Historia Langobardorum. http://www.intratext.com/IXT/LAT0338/PP.htm

Prenc F (2002) Le pianificazioni agrarie di età romana nella pianura aquileiese. Antichità Alto Adriatiche 52

Ragazzi F, Zamarchi P (eds) (2008) Carta dei suoli della Provincia di Venezia, scala 1:50.000. LAC, Firenze

Reimer PJ, Bard E, Bayliss A, Beck JW, Blackwell PG, Bronk Ramsey C, Grootes PM, Guilderson TP, Haflidason H, Hajdas I, Hatté C, Heaton TJ, Hoffmann DL, Hogg AG, Hughen KA, Kaiser KF, Kromer B, Manning SW, Niu M, Reimer RW, Richards DA, Scott EM, Southon JR, Staff RA, Turney C, van der Plicht J (2013) IntCal13 and Marine13 radiocarbon age calibration curves 0–50,000 years cal BP. Radiocarbon 55:1869–1887

Rinaldi F, Vigoni A (eds) (2015) Le necropoli della media e tarda età imperiale (III–IV secolo d.C.) a Iulia Concordia e nell'arco alto adriatico - organizzazione

spaziale, aspetti monumentali e strutture sociali atti del convegno di studio, Concordia Sagittaria, 5–6 giugno 2014. Gr. A.V.O., Album, 20

Rosada G, Frassine M, Ghiotto A (eds) (2013) …via Anniam influentibus palustribus aquis eververatam… Tradizione, mito, storia e katastrophé di una strada romana. Canova, Treviso

Sandron R (2013) Storia di Portogruaro dalle origini ai giorni nostri. Edizioni Biblioteca dell'Immagine, Sartor, Pordenone

Squatriti P (2010) The floods of 589 and climate change at the beginning of the middle ages: an Italian microhistory. Speculum 85:799–826

Stefani M, Vincenzi S (2005) The interplay of eustasy, climate and human activity in the late Quaternary depositional evolution and sedimentary architecture of the Po Delta system. Mar Geol 222–223:19–48

Steinhilber F, Beer J, Fröhlich C (2009) Total solar irradiance during the Holocene. Geophys Res Lett 36: L19704

Surian N, Mao L, Giacomin M, Ziliani L (2009) Morphological effects of different channel-forming discharges in a gravel-bed river. Earth Surf Proc Land 34:1093–1107

Uggeri G (2013) La nuova Via Annia da Roma ad Aquileia (153 a.C.). J Ancient Topogr 22:133–174

Valle G, Vercesi P (1996) Concordia Sagittaria, Sintesi della situazione paleoambientale. In: AA. VV., 1996, La Protostoria tra Sile e Tagliamento, catalogo della mostra. Esedra, Padova

Van Dinter M, Cohen KM, Hoek WZ, Stouthamer E, Jansma E, Middelkoop H (2017) Late Holocene lowland fluvial archives and geoarchaeology: Utrecht's case study of Rhine river abandonment under Roman and Medieval settlement. Quatern Sci Rev 166:227–265

Ventura P, Duiz A, Fontana A, Gaddi D, Gobbato L, Mandruzzato L, Oriolo F (2011) Nuovi dati sulla Via Annia dal territorio del Friuli Venezia Giulia. In: Veronese F (a cura di) Via Annia: Adria, Padova, Altino, Concordia, Aquileia - progetto di recupero e valorizzazione di un'antica strada romana. Atti della II giornata di studio, Padova, 17 giugno 2010. Padova, 17 giugno 2010, Il Poligrafo, Padova, pp 279–305

Ziliani L, Surian N (2012) Evolutionary trajectory of channel morphology and controlling factors in a large gravel-bed river. Geomorphology 173–174:104–117

6 Inverted Channels in the Eastern Sahara—Distribution, Formation, and Interpretation to Enable Reconstruction of Paleodrainage Networks

Abdallah S. Zaki, Robert Giegengack and Sébastien Castelltort

Abstract

During the Cenozoic Era, the Egyptian Sahara was the site of fluvial activity in a succession of at least three main drainage systems, including the Gilf System (40–16 Ma ago), the Qena System (24–6 Ma ago), and the Nile (30 Ma ago to present). These systems developed as a response to wet conditions, the dramatic events of tectonic activity in the Red Sea Region and southwestern Egypt, and changes of sea level in the Tethys Sea in Late Eocene time to sea-level rise in Late Pleistocene time. The modern Nile consists of captured components of ancestral Nile segments. Representatives of those Nile ancestors and lost tributaries of the Nile have been buried beneath dune fields and sand seas, or have been eroded by wind deflation to be topographically inverted. In this chapter, we present the distribution of inverted river channels in the Egyptian Sahara, and a description of the mechanisms that led to the development of those features during several periods of time within the Cenozoic Era. Moreover, we offer some stratigraphic and geomorphic interpretations that enable reconstructions paleodrainage networks and paleoclimates during those periods of time. Further study of the geochronology and paleohydrology of these relics is necessary to reconstruct the fluvial and paleoclimatic history of the eastern Sahara.

Keywords

Nile · Inverted topography · Cenozoic · Quaternary · Sahara · Climate oscillation

6.1 Introduction

Inverted fluvial landforms develop wherever materials deposited on a valley floor are, or become, more resistant to erosion than the adjacent valley slopes (e.g., Pain and Ollier 1995; Pain et al. 2007; Williams et al. 2007, 2011). As the adjacent slopes erode, the valley floor becomes a ridge high in the landscape. Multiple processes can cement, armor, or lithify valley-floor sediments, including cementation by a variety of materials such as calcrete, silcrete, ferricrete, or gypcrete. Inverted topography may result from filling of a valley floor with resistant lava, in which case the inversion may occur without change in regional stream regimen (Williams et al. 2007). Glacial eskers are also involved in the evolution of inverted topographic

A. S. Zaki (✉) · S. Castelltort
Department of Earth Sciences, University of Geneva, Rue des Maraîchers 13, 1205 Geneva, Switzerland
e-mail: Abdallah.zaki@etu.unige.ch

R. Giegengack
Department of Earth and Environmental Science, University of Pennsylvania, Philadelphia, PA 19104-6316, USA

J. Herget and A. Fontana (eds.), *Palaeohydrology*, Geography of the Physical Environment,
https://doi.org/10.1007/978-3-030-23315-0_6

features in different regions such as Ross Island in Antarctica (e.g., Hall et al. 2006). But conversion of a valley fill to a raised topographic feature requires a change in stream regimen, from one of deposition to one of erosion. Formation of sequential generations of inverted valley sediment requires a sequence of alternating stream regimens. Thus, a sequence of stream-inversion episodes can represent proxy evidence of a series of changes in stream regimen, which may be the consequence of regional or global changes in climate.

Inverted fluvial landforms occur over all continents on Earth, including Asia, Australia, Africa, North America, South America, Europe, and Antarctica. Inverted fluvial landforms on Earth range in age from Upper Ordovician, like those in Tassili N'Ajjer (Libya and Algeria), to Late Pleistocene and Holocene, such as those in the southern part of Egypt and the northern part of Sudan, and near Lake Chad (e.g., Giegengack 1968; Bristow et al. 2009; Girard et al. 2012; Zaki et al. 2018). Sediment induration as an essential step in the inversion process has been identified at many sites on Earth, including Arabia, Australia, and the Western Desert of Egypt (e.g., Miller 1937; Holm 1960; Pain and Ollier 1995; Zaki and Giegengack 2016; Zaki 2016; Zaki et al. 2018). Inverted fluvial channels also developed via sediment lithification in different locations, such as Tassili N'Ajjer (Libya and Algeria), Dakhla Depression in Egypt, Utah desert in USA, and Cañadón Asfalto Basin of Argentina (Brookes 2003; Williams et al. 2007; Foix et al. 2012; Girard et al. 2012). Inverted volcanic channels are preserved at many sites in New South Wales and Victoria, Australia; and the Sierra Nevada and Stanislaus Table Mountains in California (e.g., Le Conte 1880, 1886; Rhodes 1980; Pain and Ollier 1995). Glacial eskers and Inversion via surface armoring have also been identified in China, Sahara, North America, and Antarctica (e.g., Banerjee and McDonald 1975; Hall et al. 2006; Wang et al. 2015; Zaki and Giegengack 2016).

Inverted topographic features have also been identified on Mars. Based on planimetric pattern, more than 200 sites of sinuous ridges have been observed from spacecraft imagery, including MOC (0.5/12 m/pixel), THEMIS IR (100 m/pixel), VIS (18–36 m/pixel), CTX (~6 m/pixel), and HiRISE (~0.3 m/pixel), and the list continues to grow (e.g., Williams 2007; Davis et al. 2016; Fawdon et al. 2018). These sites are interpreted to be relics of ancient fluvial activity, but there is less agreement on the source of water and the mechanism of flow (Williams 2007; Williams et al. 2007, 2009; Fawdon et al. 2018). As we mentioned earlier, several processes have led to stream-channel inversion on Earth (e.g., Miller 1937; Pain and Ollier 1995; Pain et al. 2007; Williams et al. 2007). Sinuous ridges on the surface of Mars range from a few hundred meters to several tens of kilometers in length, from 10 m to a few kilometers in width, and rise ~50 m above the surrounding terrain (Burr et al. 2010; Williams 2007; Williams et al. 2007). The different geomorphic characteristics of inverted drainage networks on Mars indicate a range of paleofluvial environments that provide clues to the complicated fluvial history of the Martian surface (Williams et al. 2007, 2009). Williams (2007) determined the age of 175 sites of sinuous ridges based on the age of the host bedrock; a total of 89 sites were assigned to be Noachian (~3.8 Ga), 54 sites were assigned a maximum age of Hesperian (~3.7 Ga), and 32 sites were assigned a maximum age of Amazonian (~3.0 Ga).

Several terms have been used to describe inverted relief: "suspendritic drainage lines" (Miller 1937), "gravel-capped ridges" (King 1942), "inverted courses" (Holm 1960), "perched ridges" or "wadi ridges" (Butzer and Hansen 1968), "suspenparallel drainage" (Reeves 1983), "raised channels systems" (Maizels 1990), "inverted paleochannels" (Williams et al. 2007), "exhumed channels" (e.g., Cuevas et al. 2010; Foix et al. 2012), and "inverted wadis" (Giegengack 1968; Embabi 2004; Zaki and Giegengack 2016). In this chapter, the term "inverted river channels" is used to describe examples from the Egyptian Sahara.

In this chapter, we concisely review the timing of fluvial activity in the eastern Sahara. Subsequently, we present the distribution of

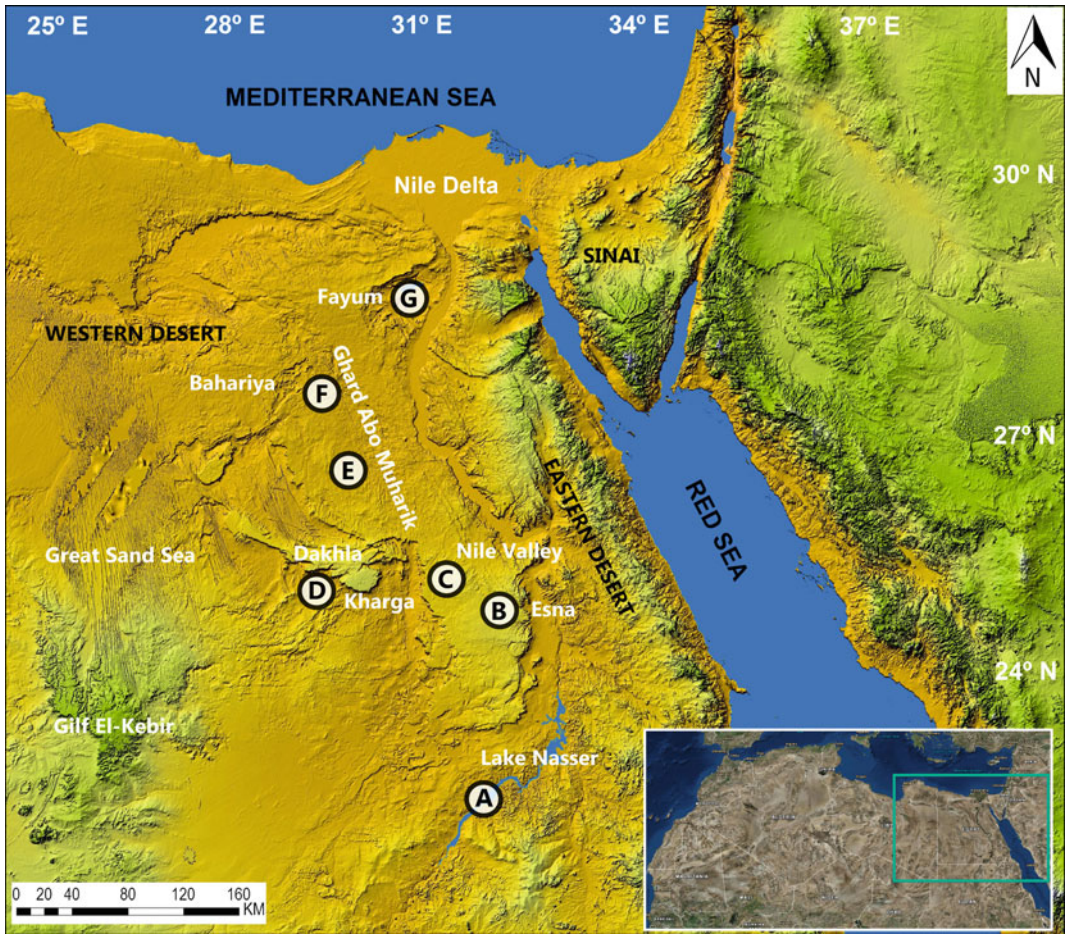

Fig. 6.1 Map of distribution of inverted river channels in the Egyptian Sahara. (**A**) southern Egypt and northern Sudan, (**B**) west of Esna city, (**C**) east of Kharga Depression, (**D**) Dakhla Depression, (**E**) west of Ghard Abo Muharik, (**F**) east of Bahariya Depression, and (**G**) Fayum Depression (Giegengack 1968; Brookes 2003; Zaki and Giegengack 2016; Giegengack and Zaki 2017; Zaki et al. 2018)

inverted channels in the Egyptian Sahara (Fig. 6.1) and the mechanisms of the development of these features (Fig. 6.2). Then, we end with some insights on inverted channels in the context of paleodrainage systems.

6.2 Timing of Fluvial Phases in the Eastern Sahara

During the Cenozoic Era, uplift occurred in two parts of the eastern Sahara (the Tibesti Plateau and Red Sea margin), and wetter conditions enabled large drainage systems to develop; Issawi and McCauley (1993) identified and categorized several stages of Saharan Nile evolution, including the Gilf system, the Qena system, the Nile system, Pliocene flooding, and Late Pleistocene sea-level rise. This reconstruction was based on several recent advances:

(a) Recognition of the relationship between the drop of the Mediterranean sea level during late Miocene time, known as the Messinian Salinity Crisis event, and evolution of the Nile System (e.g., Said 1981, 1990; Embabi 2018).
(b) Detailed work on the nature, origin, and regional setting of the Oligocene fluvial-

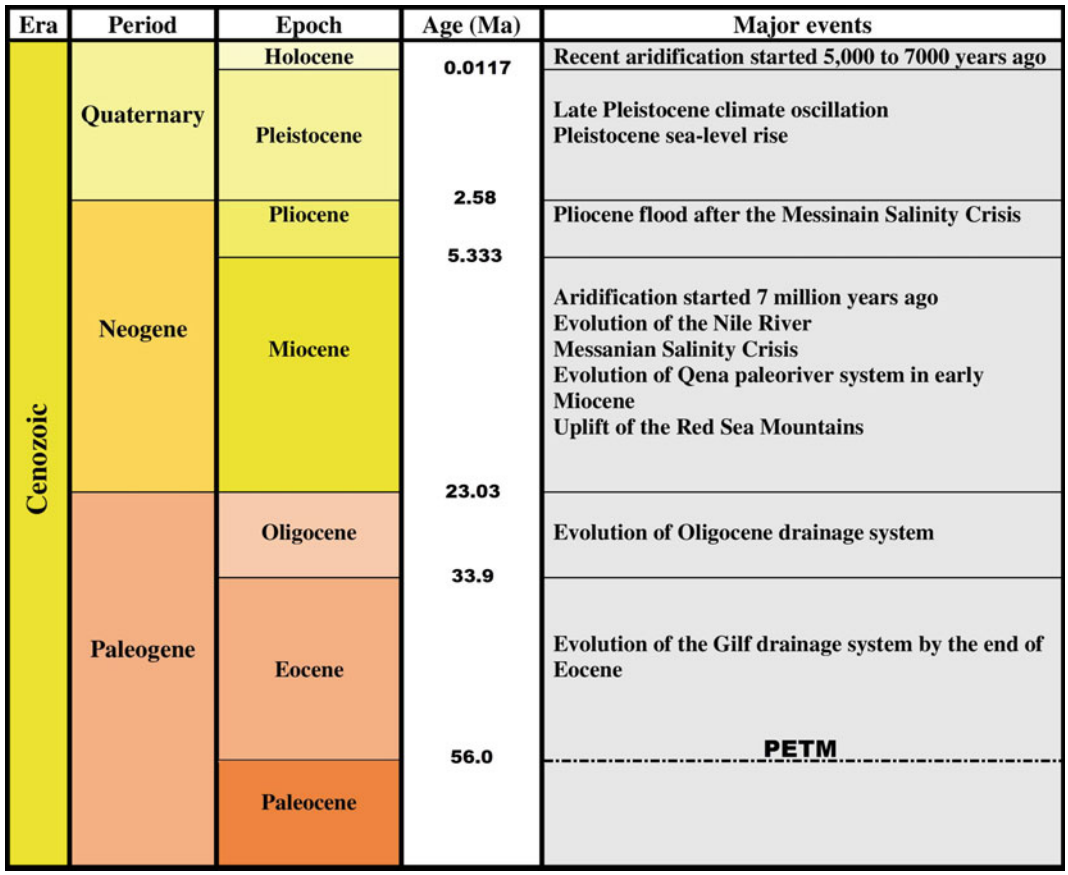

Fig. 6.2 Major fluvial and tectonic events that enabled inverted topographic features to develop in the eastern Sahara (This figure was drawn based on the work of Giegengack 1968; Foucault and Stanley 1989; Issawi and McCauley 1993; Omar and Steckler 1995; Goudie 2005; Hoffmann et al. 2016). PETM is the Paleocene-Eocene Thermal Maximum

deltaic sediments and on polycrystalline gravel in the northern part of Fayum Depression and on the surface of Gallaba plain (e.g., Bown and Kraus 1988; Issawi and Sallam 2017).

(c) Discovery of paleo-channels buried beneath the Selima Sand Sheet in the southern part of Egypt and the northern part of Sudan, known as radar rivers (e.g., McCauley et al. 1986; Ghoneim and El-Baz 2007, 2008; Ghoneim et al. 2012).

(d) Detailed work on the nature and timing of the Red Sea Range uplift (e.g., Omar and Steckler 1995).

6.2.1 Paleogene and Neogene Time

6.2.1.1 The Gilf System

The Gilf System (Issawi and McCauley 1993; Issawi and Sallam 2017) consisted of north-flowing consequent drainage lines that developed in response to retreat of the Tethys Sea, joined by streams that flowed down the flanks of the Red Sea Mountains (Fig. 6.3a). This reconstruction requires that rainfall during Tertiary time generated enough run-off to erode this stream network and to develop karst landforms (e.g., sub-surface streams) in the Eocene limestones of the Western Desert (Goudie 2005;

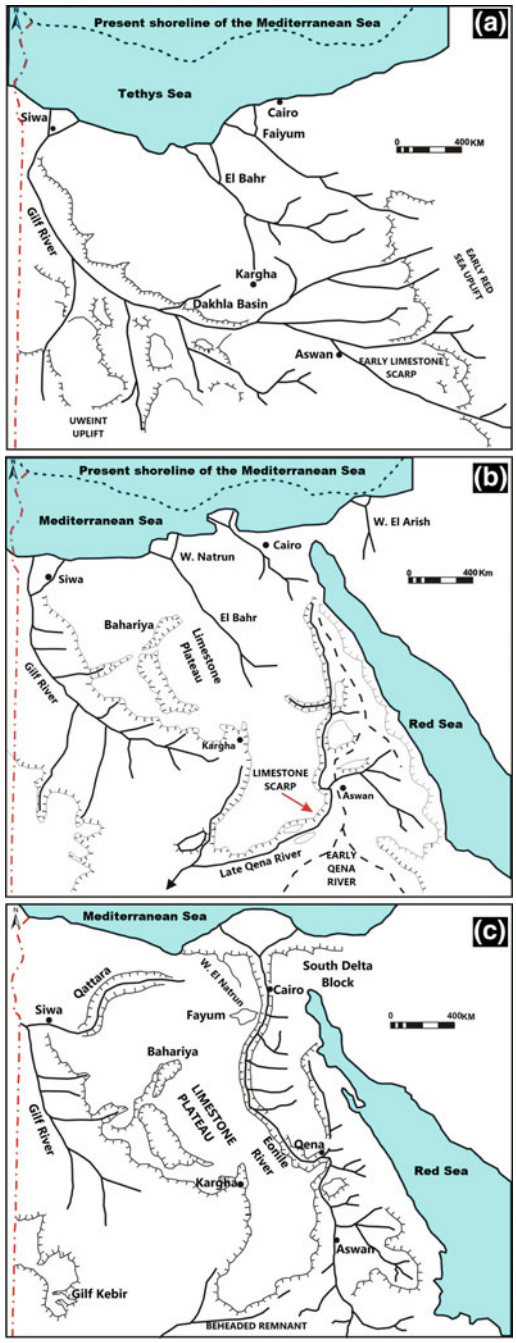

Fig. 6.3 Sequential drainage systems that developed in the eastern Sahara; **a** the Gilf system, **b** Qena system, and **c** Nile system (modified from Issawi and McCauley 1993)

Embabi 2018). This system was sustained from 40 to 24 million years ago (Goudie 2005). Said (1981, 1990) postulated that most of the Gilf System developed during Oligocene time; these studies refer to an "Oligocene System". Said (1981, 1990) and Issawi and McCauley (1993) considered the Oligocene deltaic deposits west of the Fayum Depression to be the best-preserved component of the early Cenozoic Drainage System, labeled the "Gilf System".

6.2.1.2 The Qena System

The Qena System developed in response to tectonic activity that led to the development of an uplift along the west flank of the Red Sea (Fig. 6.3b). This uplift caused a reversal of drainage that diverted the river to the southward Aswan and Sudan. This system operated from 24 to 6 Ma ago.

6.2.1.3 The Nile System

The Nile System, The Messinian Salinity Crisis, at around 6 Ma (Krijgsman et al. 1999), precipitated a fall in Mediterranean sea-level of ~1000 m, which caused incision of the present-day Nile Valley, the "Eonile" of Said (1981). Said (1981) identified a series of stages of Nile evolution and labeled them: Eonile, Paleonile, Protonile, Prenile, and Neonile. The cutting of the Eonile valley formed a canyon larger and deeper than the Grand Canyon of the Colorado River in the USA (Said 1990). The Eonile Canyon ranges from 2 to 3 km in width, with a depth ranging from 190 to 900 m (Said 1990; Embabi 2004). The deposits of the Eonile have been found only in the subsurface of the North Delta Embayment (Embabi 2004; Leila and Moscariello 2019). The steep gradient of the Eonile enabled it to capture the south-flowing Qena system (Fig. 6.3c). Goudie (2005) characterized the Eonile as the first drainage system to extend the length of Egypt. Recent work pointed out that there has been a connection between the Ethiopian highlands and the cone of the Nile

Delta since Oligocene time (30 Ma ago) (Fielding et al. 2018; Williams 2019). This is confirmed by studies of knickpoint propagation due to the Messinian sea-level drop, which suggest that the pre-Messinian drainage area of the Nile was similar to its current one (Babault et al. 2006).

6.2.1.4 The Pliocene Flooding

The Pliocene flooding occurred when the sea level rose to at least 125 m, and a Nile an estuary extended more than 900 km into the Egyptian landmass, reaching Aswan (the "Gulf Phase" of Goudie 2005). During the Paleonile phase, a local drainage system carried sediment to the Gulf (Goudie 2005). A dry period succeeded the Paleonile stage, and was succeeded by the Prenile stage (Goudie 2005).

6.2.2 Quaternary

6.2.2.1 In Mid-Pleistocene Time

In Mid-Pleistocene time, some of the Nile discharge was contributed from Ethiopia when the Atbara River delivered water to the Nile through Nubia and Aswan (Goudie 2005). Goudie (2005) labeled this phase the "Neonile".

6.2.2.2 In Late Pleistocene and into Holocene Time

In Late Pleistocene and into Holocene time climate oscillation across Africa led to the development of shallow lakes in southern Egypt and northern Sudan that expanded and contracted with that oscillation; some of those lake basins are now topographically inverted (e.g., Giegengack 1968; Maxwell et al. 2010).

Most of the stratigraphic evidence of previous drainage systems and/or tributaries of the Nile system lies buried under sand seas and/or dune fields, or has been removed by subsequent erosion. That erosion continues today and has led to topographic inversion of components of the landscape (Said 1990; Issawi and McCauley 1993; Embabi 2004, Zaki and Giegengack 2016; Giegengack and Zaki 2017; Zaki et al. 2018).

6.3 Distribution of Inverted Channels and Other Features

Inverted channels in the eastern Sahara occur over an area of $\sim$40,000 km^2 at seven sites (Fig. 6.1; Giegengack 1968; Brookes 2003; Zaki and Giegengack 2016; Giegengack and Zaki 2017; Zaki et al. 2018).

6.3.1 Southern Egypt and Northern Sudan

Inverted channels, which have also been labeled "inverted wadis" and "wadi conglomerates," in southern Egypt and northern Sudan occur over $\sim$38,000 km^2 (Giegengack 1968; Zaki and Giegengack 2016; Giegengack and Zaki 2017). The Nile Valley divides this location into an eastern part and a western part. Some of these features now are submerged beneath the water of Lake Nasser as a consequence of the construction of the High Dam (Figs. 6.1 (A) and 6.4; Giegengack and Zaki 2017). These inverted channels consist of quartzite cobbles and pebbles originally deposited in wadi channels. These materials, some cemented by iron oxide, represent the most resistant elements of the landscape (Giegengack 1968; Zaki and Giegengack 2016; Giegengack and Zaki 2017). Most of these channels display a dendritic pattern (Fig. 6.4; Zaki and Giegengack 2016). No fossils have been recovered from these deposits to determine their ages. Also, no isotopic technique has been applied successfully to assign an age to these features. A single Acheulean hand axe and several worked flakes, all on quartzite from the Nubia Fm., were recovered from the inverted channel sediments in southern Egypt (Giegengack 1968; Zaki and

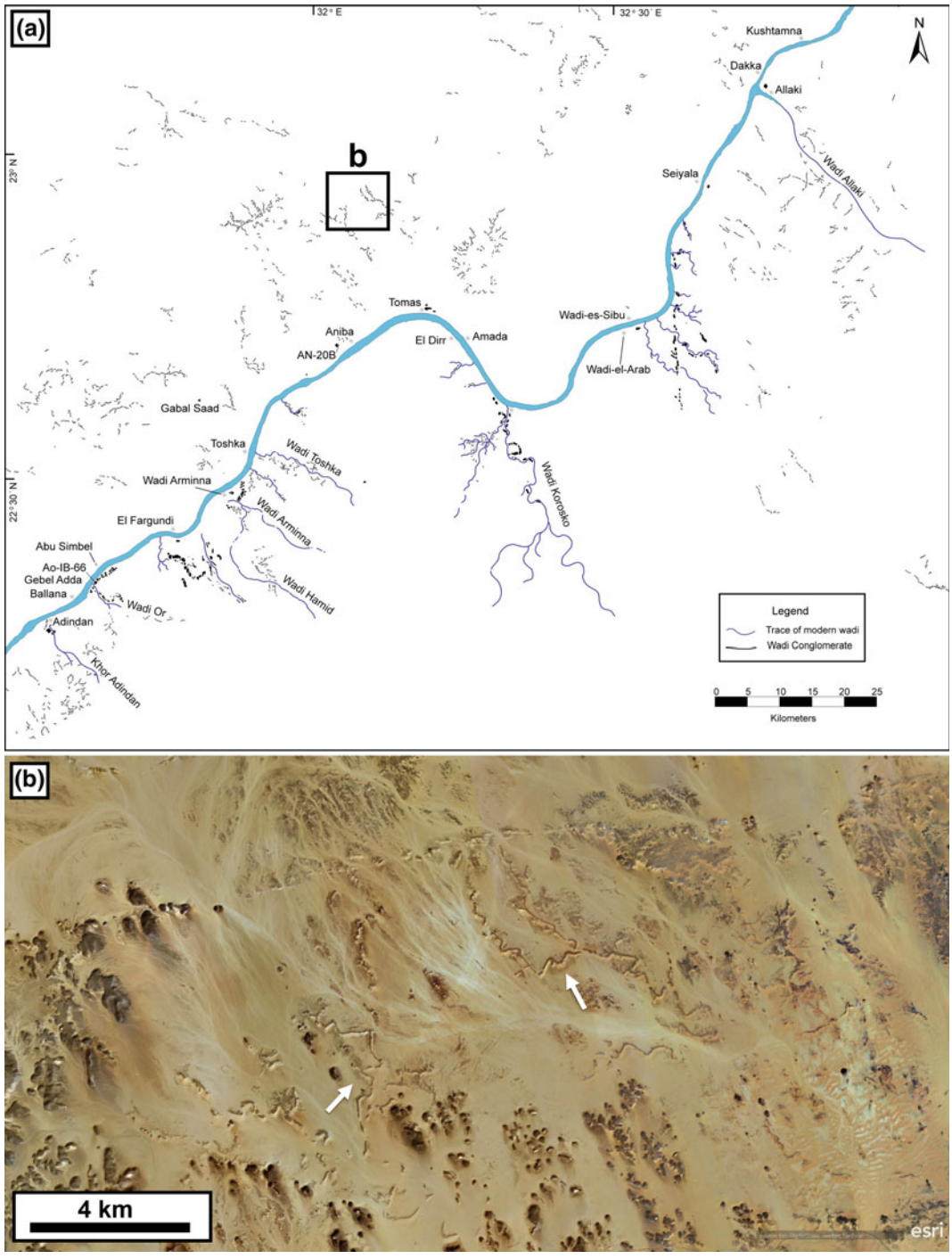

Fig. 6.4 **a** Distribution of inverted river channels in the southern part of the Egyptian Sahara (adapted from Giegengack 1968) and **b** dendritic and rectangular patterns of the inverted channels north of Wadi Tushka (*Image credit* ArcGIS Earth)

Giegengack 2016; Giegengack and Zaki 2017). These artifacts were characterized as "not later than Middle Pleistocene by Maxine Kleindienst from the University of Toronto" (Giegengack 1968, p. 104; Giegengack and Zaki 2017).

6.3.2 West of Esna City

A small site of inverted river channels lies to the west of Esna City (Figs. 6.1 (B) and 6.5; Zaki et al. 2018). Zaki et al. (2018) mapped 55 inverted-channel bodies from remotely-sensed

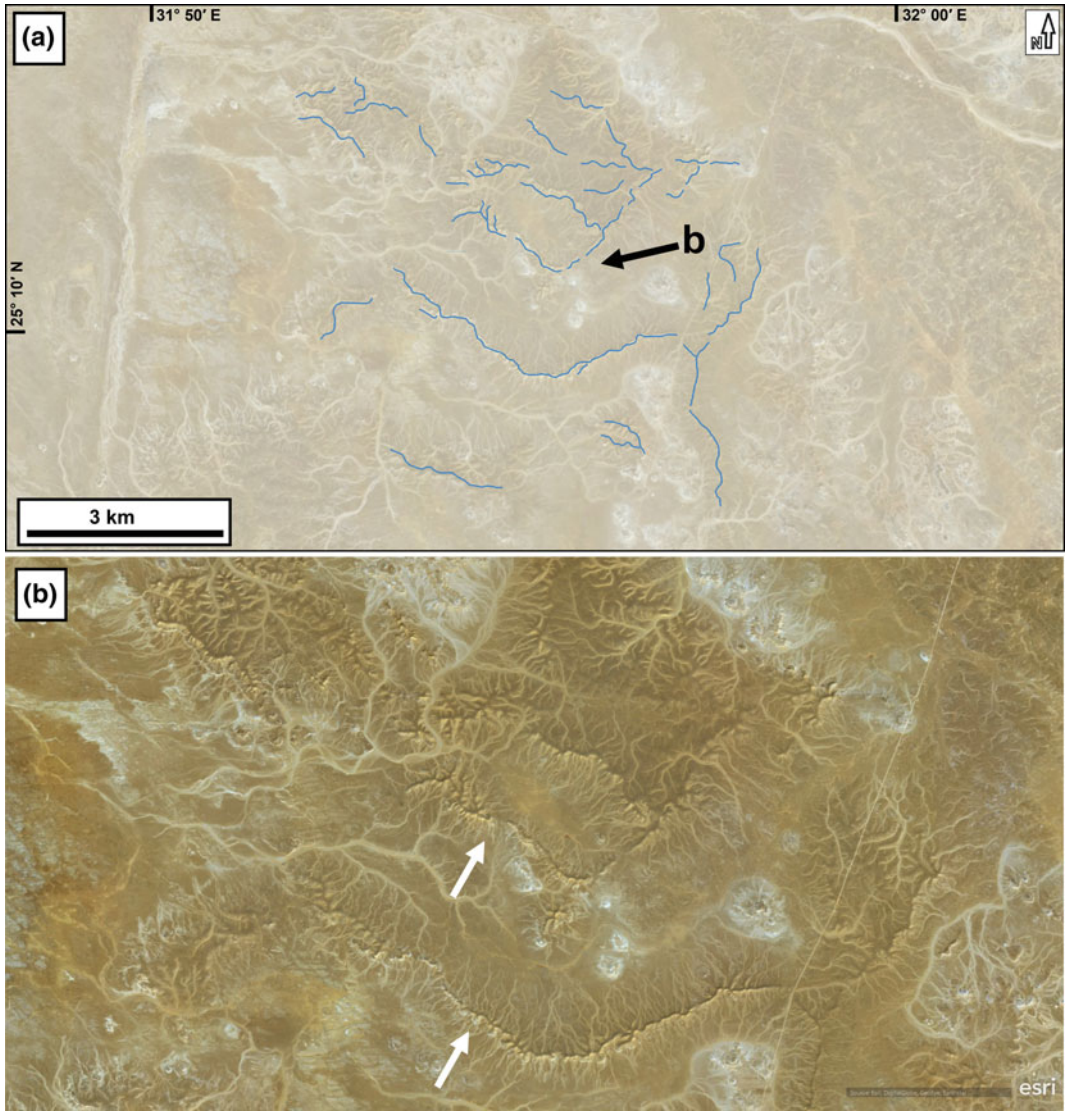

Fig. 6.5 **a** Sketch map of distribution of inverted channels west of Esna city (modified from Zaki et al. 2018) and **b** satellite image of some of the inverted-channel segments in the same site (*Image credit* ArcGIS Earth)

data, distributed over an area of about 160 km^2. These channels display a dendritic pattern. Some bodies of inverted-channel sediment are incised by younger channels.

6.3.3 East of Kharga Depression

Fifty-nine of inverted-channel bodies in this site cover an area of about 2250 km^2 (Figs. 6.1 (C) and 6.6; Zaki et al. 2018). The age of these

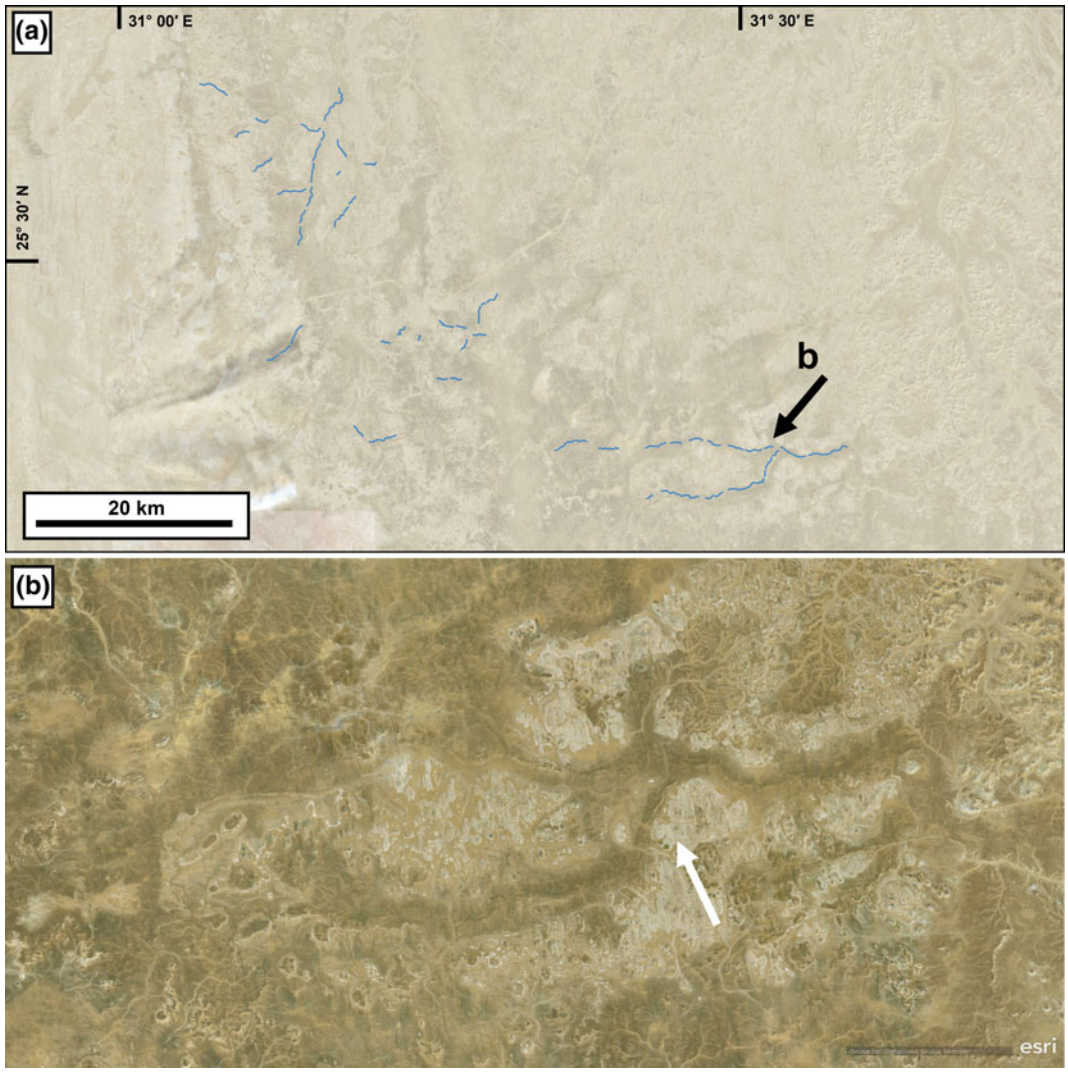

Fig. 6.6 **a** Sketch map of the distribution of inverted channels east of the Kharga Depression (modified from Zaki et al. 2018) and **b** satellite image shows some of the inverted-channel segments at the same site (*Image credit* ArcGIS Earth)

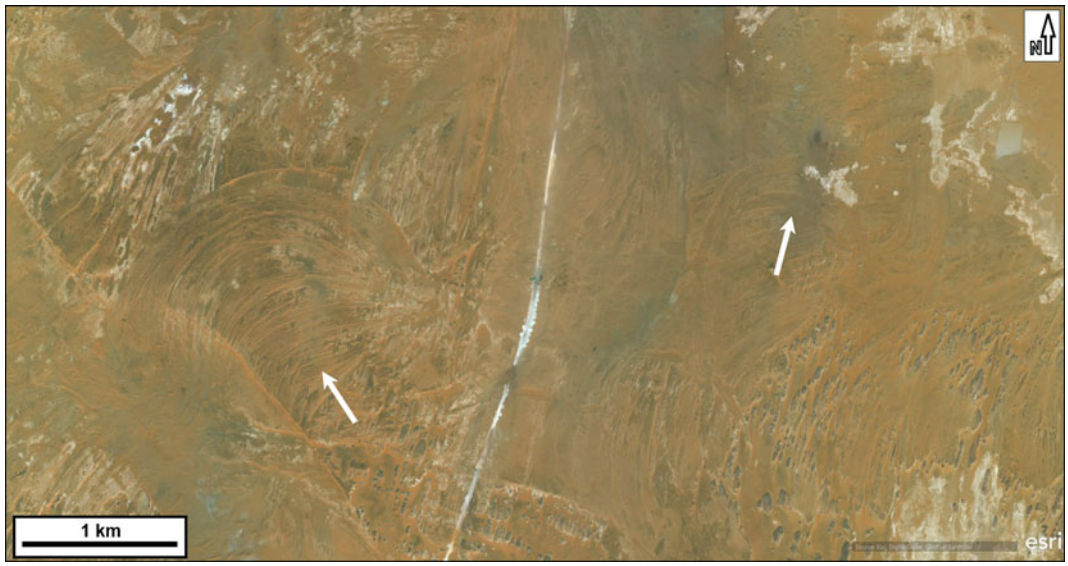

Fig. 6.7 Satellite image shows exhumed meander and channel with strong and weak segments in the Dakhla Depression (25° 27′N, 29° 12′E) (*Image credit* ArcGIS Earth)

features has not been determined, either chronologically or stratigraphically; several studies assert that these relics might be part of an Oligocene drainage system (Said 1981, 1990; Issawi and McCauley 1993). The drainage pattern of these relics is dendritic.

6.3.4 Dakhla Depression

Based on the aerial photographs, Brookes (2003) identified exhumed meander scrolls and channels in the southern part of Dakhla Depression (Figs. 6.1 (D) and 6.7). These features have been found within the Taref Formation, Turonian, Upper Cretaceous (Brookes 2003; Zaki et al. 2018). These features are represented over an area of about 950 km^2 (Zaki et al. 2018). The paleodischarge of the exhumed meanders has been estimated to be $4.4–7.0 \times 10^3$ m^3s^{-1} (Brookes 2003). Through a combination of the paleofluvial estimates and analysis of the sedimentary structures of these features, Brookes (2003) concluded that these meanders were incised, shallow, low in sinuosity, and produced minimal overbank deposition of muds.

6.3.5 West of Ghard Abo Muharik

The longest inverted-channel body in the eastern Sahara has been reported from the surface of the Eocene Plateau (Figs. 6.1 (E) and 6.8; Embabi 2004). High-resolution images from space have captured small and isolated exposures of inverted-channel features around the longest one. Zaki et al. (2018) mapped 53 inverted-channel bodies in an area of $\sim$1130 km^2 (Fig. 6.8). The alluvial sediments in these features have been deposited by a Late Eocene drainage system that flowed from the Red Sea Mountains, a reconstruction suggested by some previous work (Said 1990; Issawi and McCauley 1993; Embabi 2004, 2018). Inverted channels at this site consist of

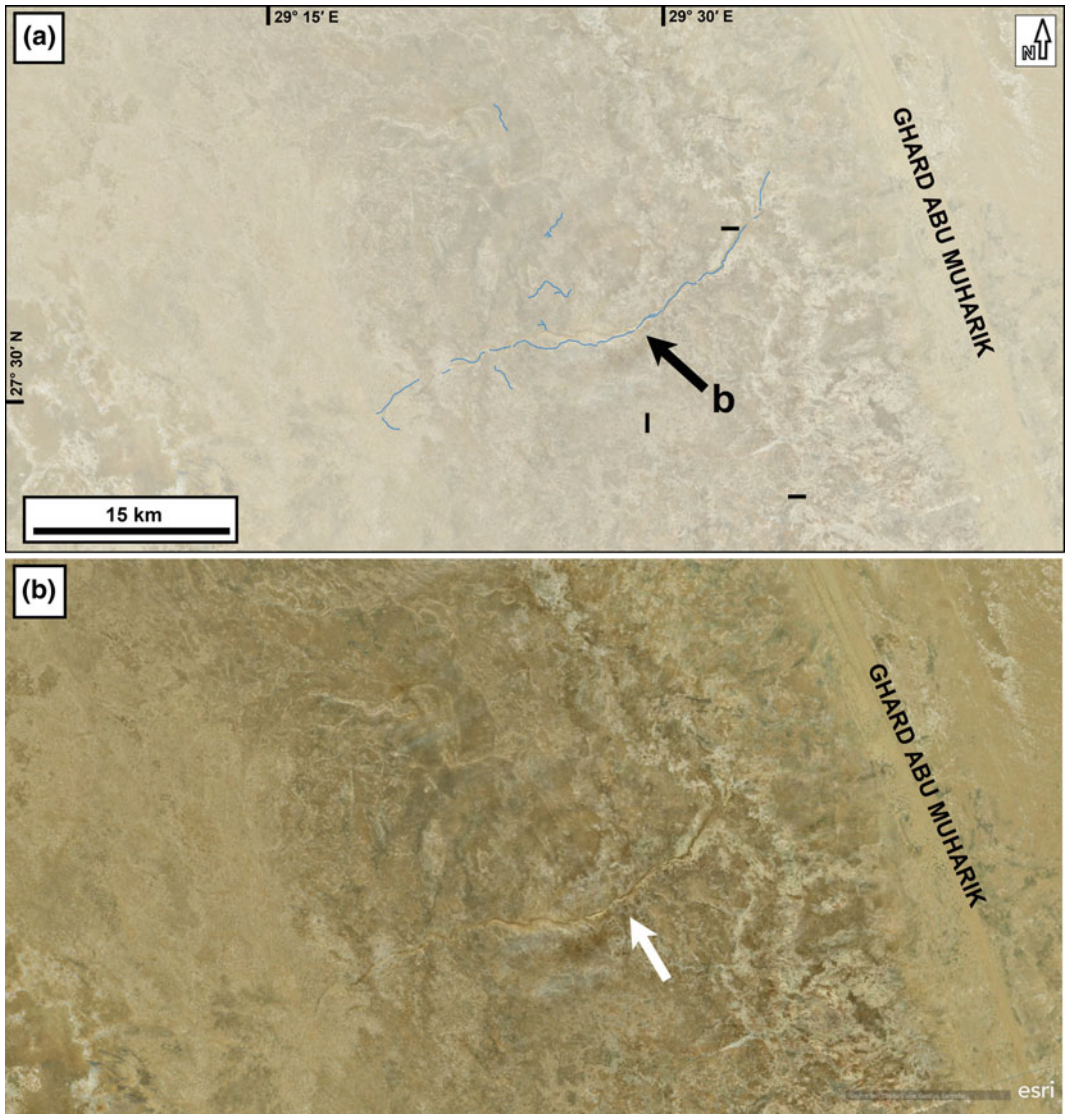

Fig. 6.8 **a** Sketch map of distribution of inverted channels west of Ghard Abo Muharik (modified from Zaki et al. 2018) and **b** satellite image of inverted-channel bodies at the same site (*Image credit* ArcGIS Earth)

consolidated fluvial rounded gravel and finer materials (Fig. 6.9), derived from Cretaceous and Eocene formations, and hence transported from the west flank of the Red Sea Mountains to the Limestone Plateau (Embabi 2004).

6.3.6 East of Bahariya Depression

A small closed drainage basin in the eastern part of Bahariya Depression (Figs. 6.1 (F) and 6.10; Zaki et al. 2018) displays inverted channels over

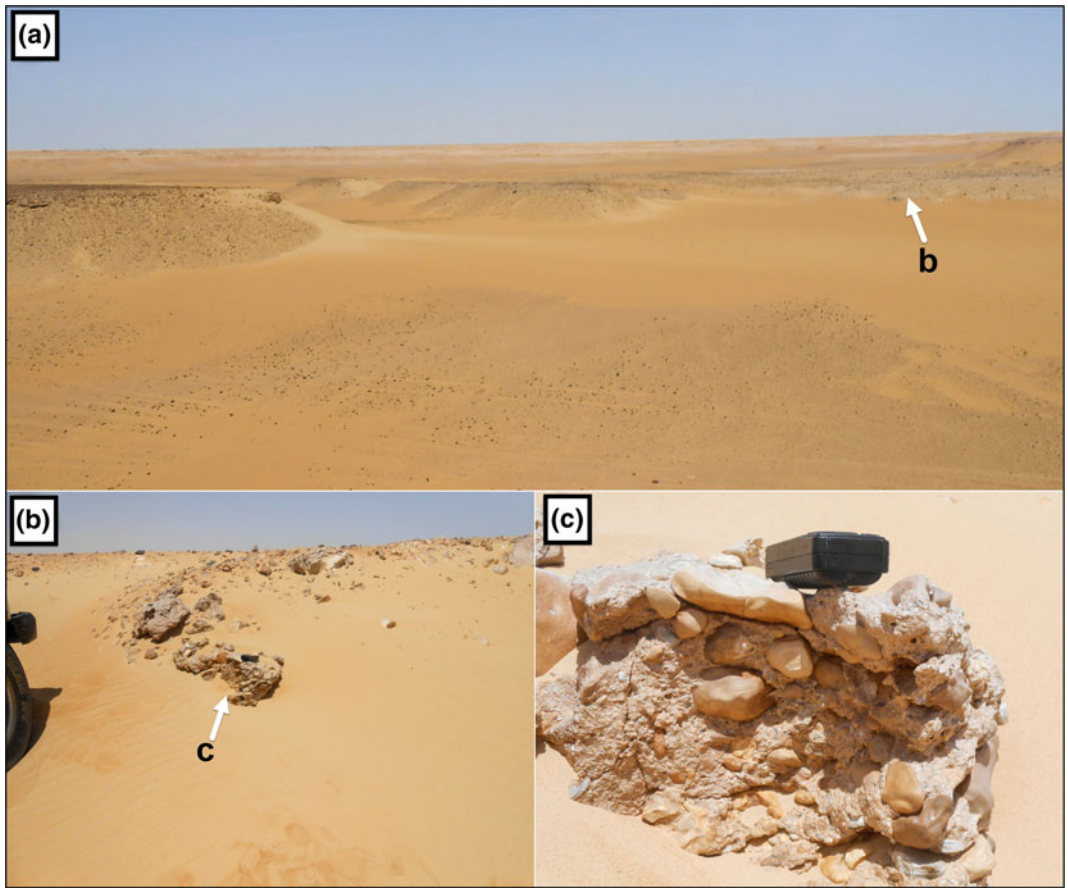

Fig. 6.9 **a–c** Field photographs showing different sections of an Oligocene inverted channel at the site West of Ghard Abo Muharik (27° 33′N, 29° 25′E)

an area of 81 km^2 (Zaki et al. 2018). The inverted stream channels in this site display a dendritic pattern. No stratigraphic or geochronologic evidence is yet available to relate these isolated features to the Nile System (Zaki et al. 2018) (Fig. 6.11).

6.3.7 Fayum Depression Site

Many small and isolated outcrops of inverted channels have been described along the Nile River adjacent to the Fayum Depression (Figs. 6.1 (G) and 6.11; Sandford and Arkell 1929; Embabi 2004, 2018; Zaki et al. 2018). These outcrops are composed of Pliocene fluvial gravels, and cap hills such as Gabal El-Na'aloon and Gabal El-Rus (Embabi 2004, 2018). Inverted channels at this site occur over 49 km^2 (Zaki et al. 2018). Mining and agricultural activities have destroyed some of these inverted landforms (Zaki et al. 2018). These landforms are interpreted to be remnants of a former river, which flowed east toward the Pliocene Nile Gulf (Sandford and Arkell 1929). The source area of the runoff that carved and inverted these features is the Dakhla Depression to the west of these landforms (Sandford and Arkell 1929). Embabi

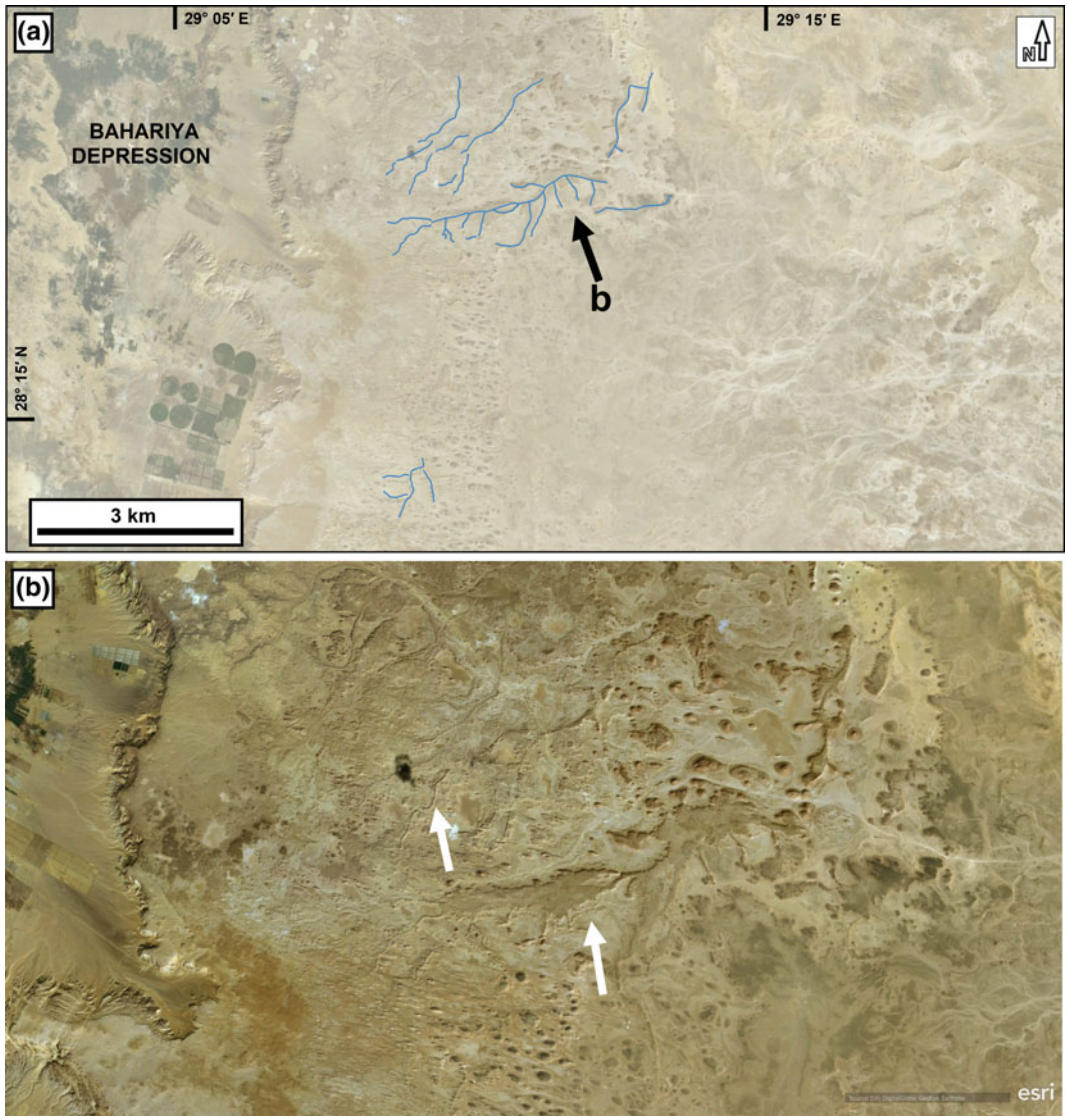

Fig. 6.10 **a** Sketch map showing the distribution of inverted channels east of Bahariya Depression (modified from Zaki et al. 2018) and **b** satellite image shows the dendritic pattern of the inverted-channel bodies at the same site (*Image credit* ArcGIS Earth)

(2004) pointed out that there are two drainage systems in the Dakhla Depression: one flows toward the Fayum Depression, the second toward the Nile Valley. Embabi (2004) also concluded that these channels were incised during Lower Pliocene time, and that these channels were inverted during Early Pleistocene time. The gradient of these ridges ranges from 11° to 18° (Zaki et al. 2018).

6.4 Mechanisms of Inverted River Channels

Several processes can lead to the development of inverted topographic features on Earth and Mars, including sediment induration, sediment lithification, surface armoring, volcanism, and deposition of glacial eskers (e.g., Pain and Ollier

Fig. 6.11 **a**, **b** Satellite images showing inverted topographic features and one inverted delta or maybe the all area represents an eroded delta in the Fayum Depression (29° 17′N, 31° 05′E) (*Image credit* ArcGIS Earth)

1995; Pain et al. 2007; Williams et al. 2007; Zaki et al. 2018). In this section, we briefly explain the mechanisms that led to the evolution of inverted river channels in the eastern Sahara.

6.4.1 Sediment Induration

Through this mechanism, the fluvial sediments in a channel became cemented via formation of gypcrete, ferricrete, calcrete, and/or silcrete (e.g., Pain and Ollier 1995; Pain et al. 2007; Zaki et al. 2018), and thus offered more resistance to post-deposition erosion. This process led to the development of inverted-channel features in six sites: (1) Fayum Depression, (2) west of Ghard Abo Muharik, (3) east of Kargha Depression, (4) west of Esna City, (5) southern Egypt, and (6) east of Bahariya Depression (Giegengack 1968; Aref 2003; Zaki and Giegengack 2016;

Giegengack and Zaki 2017; Zaki et al. 2018). The primary cementing materials in the induration processes were gypcrete in the Fayum Depression (Aref 2003), silcrete and calcrete in west of Ghard Abo Muharik (Zaki et al. 2018), and ferricrete, silcrete, and calcrete in southern Egypt (Giegengack 1968).

6.4.2 Sediment Lithification

Via this mechanism, the fluvial sediments in a channel become lithified by compaction during burial, not only by chemical induration of the sediments (e.g., Williams et al. 2007). These lithified channels may be returned to the surface by subsequent exhumation mobilized by tectonic events (Williams et al. 2007; Zaki et al. 2018). Inverted features in the Dakhla Depression site are developed by sediment lithification (Brookes 2003). No data have been reported on either the depth or duration of burial of these features.

6.4.3 Surface Armoring

When bodies of sediment deposited in channels do not contain cement material, subsequent erosion may remove fine, medium, and some coarse materials (Pain and Ollier 1995). Under those circumstances, larger clasts may accumulate as a lag residue on the surface of such sediment which is resistant to erosion and thus armour the feature; subsequent erosion then leaves the armored body of channel sediment standing in topographic relief (Pain and Ollier 1994; Pain et al. 2007). Some bodies of inverted-channel sediment in southern Egypt are developed by this mechanism (Giegengack 1968; Zaki et al. 2018).

6.5 Evidence to Enable Reconstruction of the Paleodrainage Systems

As we mentioned earlier, the Egyptian landscape, during the Cenozoic Era, was drained not by a single drainage system, but by at least three different drainage systems, described as (1) the Gilf System, that prevailed 40–60 Ma ago; the Qena System, that prevailed 24–6 Ma ago; and the Nile System, that prevailed from 6 Ma ago to the present. Many components of these drainage systems were eroded via wind deflation; others were buried beneath the sand seas and dune fields and subsequently exhumed. Aeolian deposits today cover more than 20% of the total area of the Egyptian Sahara (Embabi 2004, 2018).

6.5.1 Paleogene and Neogene Rivers

Gilf and Qena drainage systems were active before 40–6 Ma (Said 1990; Issawi and McCauley 1993). Inverted river channels on the surface of the Eocene Plateau, west of Esna City, east of Kharga Depression, and west of Ghard Abo Muharik may be attributed to one or another of the Nile ancestors. Embabi (2004) correlated the consolidated gravels on the Eocene Plateau with the Oligocene Nukheil Formation in the Red Sea Region, both fluvial consolidated gravel bodies deposited by Late Eocene and Oligocene drainage systems (Figs. 6.8 and 6.9; Hermina et al. 1989; Said 1990; Issawi and McCauley 1993; Zaki 2015; Embabi 2004, 2018). The sediment of the inverted fluvial channels was carried westward from headwaters on the western side of the newly uplifted Red Sea Mountains (Said 1990; Issawi and McCauley 1993). The conglomerates of the inverted channels are interpreted to have been derived from the Cretaceous and Eocene formations, which covered the Red Sea Mountains (Embabi 2004; Zaki et al. 2018). Further study of the geochronology, geometry, and paleohydrology of these channels at the three sites may offer new insights on the development and evolution of these drainage systems.

6.5.2 Quaternary

Numerous studies have described geologic evidence of climate oscillation in North Africa and southern Europe that documents changes of paleodischarge and sediment loads from the

Atbara, Blue Nile, and White Nile, cave speleothems, and archeological sites during Late Pleistocene time to mid-Holocene (e.g., Foucault and Stanley 1989; Hoffmann et al. 2016; Kuper and Kröpelin 2006). These studies inferred climate oscillation associated with six well-documented wet phases during the period 65–5 ka ago (e.g., Foucault and Stanley 1989; Hoffmann et al. 2016; Kuper and Kröpelin 2006); these oscillations represent temporal extensions of the well-documented pattern of cyclic climate oscillation that has characterized the entire Quaternary period.

Inverted topographic features in the southern part of Egypt and northern part of Sudan document climate oscillation during Late Pleistocene time via several generations of incision and inversion (Giegengack 1968; Haynes 1980; Zaki and Giegengack 2016; Giegengack and Zaki 2017). No geochronological data have been reported from these features; thus, while we know from stratigraphic data that at least 3 generations of cyclical topographic inversion are represented, we do not know the duration of each generation, nor do we know how many generations are represented. Further study of the geochronology and paleohydrology of these features is vital for reconstructing the paleoclimate of the eastern Sahara during Late Quaternary time.

6.6 Summary and Future Work

Inverted river channels in the eastern Sahara occur over ~40,000 km^2 at seven sites, including (1) southern Egypt, (2) west of Esna city, (3) east of Dakhla Depression, (4) west of Ghard Abo Muharik, (5) Dakhla Depression, (6) east of Bahariya Depression, and (7) Fayum Depression. These channels are a result of sequential episodes of incision and inversion extending from Late Eocene to Late Quaternary time. Inverted river channels are developed as bodies of alluvial sediment acquired resistance to erosion via three distinct mechanisms—sediment induration, sediment lithification, and surface armoring—and were then inverted by erosion, either fluvial or Aeolian. Further study of the geochronology and paleohydrology of these relics is necessary for reconstructing the configuration of drainage systems since Late Eocene time. Moreover, study of the geomorphology, sedimentology, and stratigraphy of these features may provide an instructive terrestrial analogue to interpret the environmental significance of similar landforms on the Martian surface.

Acknowledgements Abdallah Zaki gratefully acknowledges the support of the Swiss Confederation excellence fellowships program (fellowship **No: 2017.1006**). Thanks go to Mathieu Schuster for sharing a lot of information on the paleoclimate of Sahara. The authors are grateful to Kenneth Edgett from Malin Space Science Systems and Sanjeev Gupta from the Imperial College of London for sharing information on the evolution of inversion of relief on Earth and Mars. We also would like to thank Rebecca Williams from the Planetary Science Institute for her comments on some ideas in this chapter. We greatly appreciate the constructive comments and edits suggested by the reviewers and the editor.

References

Aref MAM (2003) Classification and depositional environments of Quaternary pedogenic gypsum crusts (gypcrete) from east of the Fayum Depression, Egypt. Sed Geol 155:87–108. https://doi.org/10.1016/S0037-0738(02)00162-8

Babault J, Loget N, Van Den Driessche J et al (2006) Did the Ebro basin connect to the Mediterranean before the Messinian salinity crisis? Geomorphology 81:155–165. https://doi.org/10.1016/j.geomorph.2006.04.004

Banerjee I, McDonald BC (1975) Nature of esker sedimentation. SEPM 23:132–154

Bown TM, Kraus MJ (1988) Geology and palaeoenvironment of the Oligocene Jebel Qatrani Formation and adjacent rocks, Fayum Province, Egypt. US Geol Surv Prof Pap 1452:1–60

Bristow CS, Drake N, Armitage S (2009) Deflation in the dustiest place on Earth: the Bodélé Depression, Chad. Geomorphology 105:50–58

Brookes IA (2003) Palaeofluvial estimates from exhumed meander scrolls, Taref formation (Turonian), Dakhla Region, western desert, Egypt. Cretac Res 24:97–104

Burr DM, Williams RMS, Wendell KD et al (2010) Inverted fluvial features in the Aeolis/Zephyria Plana region, Mars: formation mechanism and initial paleodischarge estimates. J Geophys Res Planets. https://doi.org/10.1029/2009je003496

Butzer KW, Hansen CL (1968) Desert and river in Nubia. University of Wisconsin Press, Madison

Cuevas M, Cabera JL, Marcuello L et al (2010) Exhumed channel sandstone networks within fluvial fan deposits from the Oligo-Miocene Caspe Formation, south-east Ebro Basin (north-east Spain). Sedimentology 57:162–189

Davis JM, Balme M, Grindrod PM et al (2016) Extensive Noachian fluvial systems in Arabia Terra: implications for early Martian climate. Geology. https://doi.org/10.1130/g38247.1

Embabi NS (2004) The geomorphology of Egypt. Landforms and evolution, vol 1. The Nile Valley and the Western Desert. Egyptian Geographical Society, Cairo

Embabi N (2018) Landscapes and landforms of Egypt. Springer, Zug

Fawdon P, Gupta S, Davis J et al (2018) Hypanis Valles delta: the last high stand of an ocean on early Mars? Earth Planet Sci Lett 500:225–241. https://doi.org/10.1016/j.epsl.2018.07.040

Fielding L, Najman Y, Millar I et al (2018) The initiation and evolution of the River Nile. Earth Planet Sci Lett 489:166–178

Foix N, Allard JO, Paredes JM et al (2012) Fluvial styles, palaeohydrology and modern analogues of an exhumed, Cretaceous fluvial system: Cerro Barcino Formation, Cañadón Asfalto Basin, Argentina. Cretac Res 34:298–307

Foucault A, Stanley DJ (1989) Late Quaternary paleoclimatic oscillations in East Africa recorded by heavy minerals in the Nile delta. Nature 339:44–46. https://doi.org/10.1038/339044a0

Ghoneim E, El-Baz F (2007) The application of radar topographic data to mapping of a mega-paleodrainage in the Eastern Sahara. J Arid Environ 69:658–675

Ghoneim E, El-Baz F (2008) Mapping water basins in the eastern Sahara by SRTM data. In: IEEE International Geoscience and Remote Sensing Symposium, 6–11 July, Boston, pp 1–4

Ghoneim E, Benedetti M, El-Baz F (2012) An integrated remote sensing and GIS analysis of Kufrah Paleoriver, Eastern Sahara. Geomorphology 139–140:242–257

Giegengack RF (1968) Late Pleistocene history of the Nile Valley in Egyptian Nubia. Dissertation, Yale University

Giegengack RF, Zaki AS (2017) Inverted topographic features, now submerged beneath the water of Lake Nasser, document a morphostratigraphic sequence of high-amplitude late-Pleistocene climate oscillation in Egyptian Nubia. J Afr Earth Sc. https://doi.org/10.1016/j.jafrearsci.2017.06.027

Girard F, Ghienne JF, Rubino JL (2012) Channelized sandstone bodies ('cordons') in the Tassili N'Ajjer (Algeria & Libya): snapshots of a Late Ordovician proglacial outwash plain. Geol Soc London, Spec Publ. https://doi.org/10.1144/sp368.3

Goudie A (2005) The drainage of Africa since the Cretaceous. Geomorphology 67:437–456. https://doi.org/10.1016/j.geomorph.2004.11.008

Hall BL, Hendy CH, Denton GH (2006) Lake-ice conveyor deposits: geomorphology, sedimentology, and importance in reconstructing the glacial history of the Dry Valleys. Geomorphology 75:143–156

Haynes CV (1980) Geochronology of Wadi Tushka: lost tributary of the Nile. Science 210:68–71

Hermina M, Klitzsch E, List FK (1989) Stratigraphic lexicon and explanatory notes to the geological map of Egypt, scale 1: 500,000. Conco Inc., Cairo

Hoffmann DL, Rogerson M, Spötl C et al (2016) Timing and causes of North African wet phases during the last glacial period and implications for modern human migration. Sci Rep-UK 6:36367. https://doi.org/10.1038/srep36367

Holm DA (1960) Desert geomorphology in the Arabian Peninsula. Science 132:1369–1379. https://doi.org/10.1126/science.132.3437.1369

Issawi B, McCauley JF (1993) The Cenozoic landscape of Egypt and its river systems. Ann Geol Surv Egypt 19:357–384

Issawi B, Sallam E (2017) Rejuvenation of dry paleochannels in arid regions in NE Africa: a geological and geomorphological study. Arab J Geosci. https://doi.org/10.1007/s12517-016-2793-z

King LC (1942) South African scenery. Oliver and Boyd, Edinburgh

Krijgsman W, Raffi FJH, Wilson DS (1999) Chronology, causes and progression of the Messinian salinity crisis. Nature 400:652–655

Kuper R, Kröpelin S (2006) Climate-controlled Holocene occupation in the Sahara: motor of Aftica's evolution. Science 313:803–807

Le Conte J (1880) The old river beds of California. Am J Sci 19:176–190

Le Conte J (1886) A post-Tertiary elevation of the Sierra Nevada shown by the river beds. Am J Sci 32:167–181

Leila M, Moscariello A (2019) Seismic stratigraphy and sedimentary facies analysis of the pre- and syn-Messinain salinity crisis sequences, onshore Nile Delta, Egypt: implications for reservoir quality prediction. Mar Pet Geol 101:303–321

Maizels J (1990) Raised channels as indicators of palaeohydrologic change-a case study from Oman. Palaeogeogr Palaeoclimatol Palaeoecol 76:241–277. https://doi.org/10.1016/0031-0182(90)90115-N

Maxwell TA, Issawi B, Vance Haynes C (2010) Evidence for Pleistocene lakes in the Tushka region, south Egypt. Geology 38:1135–1138

McCauley J, Breed M, Schaber G et al (1986) Palaeodrainages of the eastern Sahara, the radar rivers revisited (SIR-A/B implications for a Mid-Tertiary Trans-African Drainage System). IEEE Trans Geosci Remote Sens GE 24:624–648

Miller RP (1937) Drainage lines in bas-relief. J Geol 45:432–438

Omar GI, Steckler MS (1995) Fission track evidence on the initial rifting of the Red Sea: two pulses, no propagation. Science 270:1341–1344

Pain CF, Clarke JDA, Thomas M (2007) Inversion of relief on Mars. Icarus 190(2):478–491. https://doi.org/10.1016/j.icarus.2007.03.017

Pain CF, Ollier CD (1995) Inversion of relief—a component of landscape evolution. Geomorphology 12 (2):151–165. https://doi.org/10.1016/0169-555X(94)00084-5

Reeves T (1983) Pliocene channel calcrete and suspen-parallel drainage in West Texas and New Mexico. In: Wilson, RCL (ed) Residual deposits-surface related weathering processes and materials. Geol Soc Spec Publ 11:178–183. https://doi.org/10.1144/gsl.sp.1983.011.01.18

Rhodes DD (1980) Exhumed topography—a case study of the Stanislaus Table Mountain, California. Reports of Planetary Geology Program 1980, NASA Technical Memorandum 82835:397–399

Said R (1981) The geological evolution of the River Nile. Springer, New York

Said R (1990) The geology of Egypt. Balkema, Rotterdam

Sandford KS, Arkell WJ (1929) Paleolithic man and the Nile-Fayum divide: a study of the region during Pliocene and Pleistocene times. Oriental Institute Publications 17, University of Chicago Press, Chicago, pp 1–92

Wang ZT, Lai ZP, Qu JJ (2015) Inverted relief landforms in the Kumtagh Desert of northwestern China: a mechanism to estimate wind erosion rates. Geol J. https://doi.org/10.1002/gj.2739

Williams RME (2007) Global spatial distribution of raised curvilinear features on Mars. In: Lunar and Planetary Science Conference 38, Houston, Texas, abstract 1821

Williams M (2019) The Nile basin: quaternary geology, geomorphology and prehistoric environments. Cambridge University Press, Cambridge. https://doi.org/10.1017/9781316831885

Williams RME, Chidsey TC, Eby DE (2007) Exhumed paleochannels in central Utah—analogs for raised curvilinear features on Mars. In: Willis GC, Hylland MD, Clark DL et al (eds) Central Utah—diverse geology of a dynamic landscape. Utah Geol Assoc Publ 36:220–235

Williams RME, Irwin RP, Zimbelman JR (2009) Evaluation of paleohydrologic models for terrestrial inverted channels: implications for application to martian sinuous ridges. Geomorphology 107:300–315. https://doi.org/10.1016/j.geomorph.2008.12.015

Williams RME, Irwin RP, Zimbelman JR et al (2011) Field guide to exhumed paleochannels near Green River, Utah: terrestrial analogs for sinuous ridges on Mars. In: Garry WB, Bleacher JE (eds) Analogs for planetary exploration. Geol Soc Am Spec Pap 483:483–505. https://doi.org/10.1130/2011.2483(29)

Zaki AS (2015) Reconstruction the residuals of the lost drainage systems on the Eocene Plateau of Western Desert of Egypt. 2015 GSA Annual Meeting, Baltimore. https://doi.org/10.13140/rg.2.1.2301.0803

Zaki AS (2016) Inverted channels on Earth: analogs for inverted topography on Mars. 47th LPSC 2466#. https://doi.org/10.13140/rg.2.1.2563.2243

Zaki AS, Giegengack R (2016) Inverted topography in the southeastern part of the Western Desert of Egypt. J Afr Earth Sc 121:56–61. https://doi.org/10.1016/j.jafrearsci.2016.05.020

Zaki AS, Pain C, Edgett KE, Giegengack R (2018) Inverted stream channels in the Western Desert of Egypt: synergistic remote, field observations and laboratory analysis on Earth with application to Mars. Icarus 309:105–124

Noah's Flood—Probing an Ancient Narrative Using Geoscience

7

Helmut Brückner and Max Engel

Abstract

This article sheds new light on the narrative of Noah's Flood (Genesis Flood, Great Deluge) from a geoscientific point of view. It outlines the four most popular hypotheses: (i) the postglacial–early Holocene flooding of the Persian/Arabian Gulf which fell dry during the last glacial lowstand of the sea; (ii) a cosmic impact by a meteorite ca. 10,000 years ago, which triggered tsunami waves worldwide; (iii) the rapid re-filling of the Black Sea basin when the early Holocene rise of the Mediterranean Sea surpassed the Bosphorus sill about 8400 years ago; and (iv) the occurrence of one or several mega-floods in Central and Lower Mesopotamia, which left imprints in and around ancient settlement mounds (tells) such as Ur and Uruk. The pros and cons of these scenarios are discussed. Based on geological and sedimentological evidence the authors argue for the latter theory and describe future research venues.

Keywords

Noah's flood · Great deluge · Epic of Gilgamesh · Persian/Arabian Gulf · Cosmic impact · Black sea · Mesopotamia · Ur · Uruk

7.1 Introduction to the Great Mystery

The Great Flood, the Genesis Flood, Noah's Flood, the Great Deluge—there are several expressions attributed to a mega-catastrophe that affected (the whole or parts of) the Earth. This well-known story is recorded both in the Bible (Genesis 6,5–8,22), and—although much shorter—in the Quran (Surah 11, 37–49). The biblical narrative is attributed to the seventh century BC, while the Quranic version to the seventh century AD. There are, however, much older accounts of a mega-flood including a Sumerian story probably from ca. 3150 BC, and the Akkadian Atrahasis Epic (fourteenth century BC) (Teller et al. 2000). The earliest cuneiform flood stories date back to at least the eighteenth century BC, and many Mesopotamian legends bear indications that they derive from older oral narratives (Finkel 2014).

The most famous "predecessor" of the biblical account is the deluge narrated in the Epic of Gilgamesh. Gilgamesh is the legendary king of the Mesopotamian city-state Uruk (Erech); the erection of its still preserved city wall is

H. Brückner (✉) · M. Engel
Institute of Geography, University of Cologne, Cologne, Germany
e-mail: h.brueckner@uni-koeln.de

M. Engel
e-mail: max.engel@naturalsciences.be; max.engel@uni-koeln.de

M. Engel
Geological Survey of Belgium, Royal Belgian Institute of Natural Science, Brussels, Belgium

J. Herget and A. Fontana (eds.), *Palaeohydrology*, Geography of the Physical Environment,
https://doi.org/10.1007/978-3-030-23315-0_7

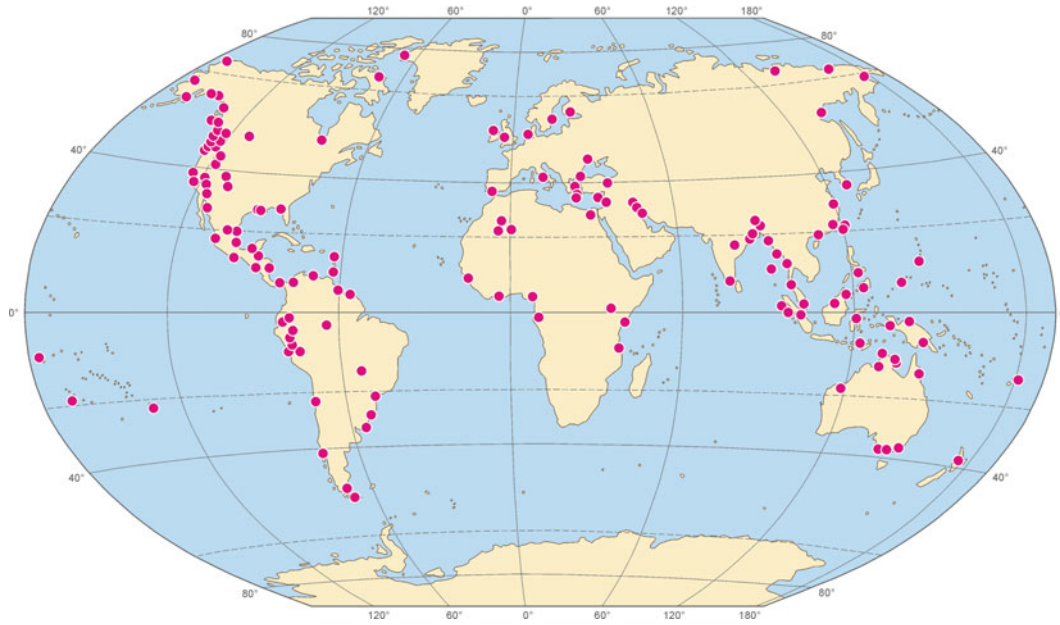

Fig. 7.1 Flood myths in more than 140 ancient societies, based on ethnological and historico-cultural sources. Compiled by Dieter Kelletat, unpublished

attributed to him. The epic, which bears his name, is written in the Akkadian language on twelve tablets, which were discovered in the mid-nineteenth century at Nineveh in the library of the Assyrian king Ashurbanipal (reign: 668–627 BC) (George 2003). The eleventh tablet, the so-called Flood Tablet, which is preserved in the British Museum in London, tells the flood story. The tale of Noah's Flood is closely interwoven with the ark. The many attempts to find it is a story of its own (well summarized by Pleins 2003). It is interesting to note that there are flood myths in more than 140 ancient societies, on all continents, some of which lie far from the coast (Fig. 7.1; see also the compilation by Tollmann and Tollmann 1993).

In this context, it is neither possible nor intended to compare and contrast each of these accounts. The central narrative of all the tales is a mega-catastrophe caused by a flood of an unprecedented magnitude that destroyed an enormous area, if not the whole (then known) world, and nearly all of its inhabitants. It is the aim of this contribution to probe the flood narrative from a scientific standpoint, as many myths and legends are reflections of natural phenomena (cf. Vitaliano 2007; Vött et al. 2017).

Regarding the Genesis Flood, many attempts at an explanation exist (cf. Herget 2019). In the following we concentrate on those which can well be summarized to four geoscience hypotheses (cf. Brückner 2003: 246): (1) the postglacial flooding of the Persian/Arabian Gulf; (2) a cosmic impact ca. 10,000 years ago; (3) the postglacial flooding of the Black Sea; and (4) one or several mega-floods in Central and Lower Mesopotamia around 3000 BC.

7.2 Hypothesis 1: The Postglacial Flooding of the Persian/Arabian Gulf

Sarnthein (1972) was probably the first who linked the flood story to the postglacial flooding of the Persian/Arabian Gulf. During the Last Glacial Maximum (LGM), about 20,000 years ago, global sea level dropped to 120–130 m below its present position. Thus, more than half of the Earth's shelf areas—nowadays reaching

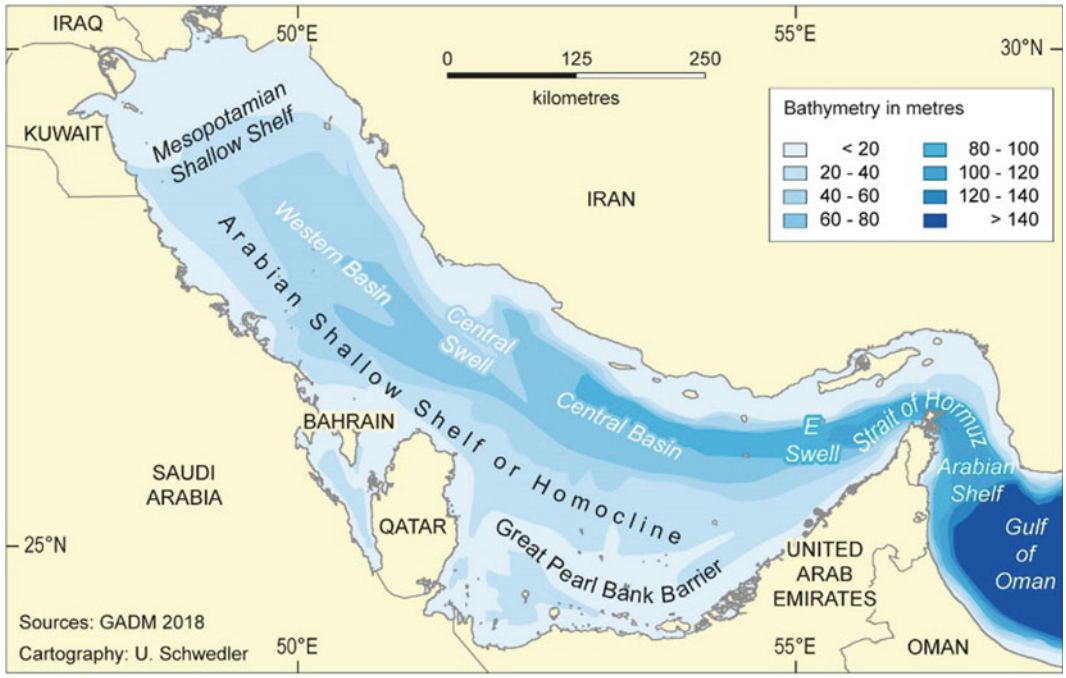

Fig. 7.2 Bathymetric map of the Persian/Arabian Gulf. Note that this marginal sea is a shelf sea with an average depth of just 50 m. After Teller et al. (2000, Fig. 1)

down to roughly minus 200 m—constituted land and was subjected to terrestrial conditions. This was also the case for the Persian/Arabian Gulf, a relatively shallow shelf sea with an average depth of about 50 m (max. depth: 90 m; Fig. 7.2). During the LGM, the sea floor was exposed, and several lakes existed (Sarnthein 1972; Lambeck 1996).

Global warming led to an enormous deglaciation, which caused sea level to rise from the LGM lowstand close to its present position ca. 6 ka BP. The most rapid rise was between 15 and 7 ka BP. This late glacial–early Holocene transgression caused a worldwide flooding of the shelves and enormous landward shifts in the shorelines. Former land bridges were drowned, and areas connected to the mainland became islands (cf. Brückner et al. 2017).

A general confirmation of this scenario comes from Teller et al. (2000): near-coast calcareous dunes of the United Arab Emirates contain up to 70% of bioclastic carbonates; this concentration decreases with an increasing distance from the coast; 50–100 km inland the dunes mainly consist of quartz. The authors presume that the origin of the carbonates was the exposed sea floor of the Persian/Arabian Gulf during low sea levels of the last glacial period (about 100,000–12,000 years ago). Between 12,000–11,500 and 9500–8500 a BP a rapid glacio-eustatic rise occurred.

A detailed scenario of the flooding of the Gulf was presented by Lambeck (1996), who based his glacio-hydro-isostatic model on the then known shifts in the palaeo-shorelines of the Gulf. From the LGM until 14,000 BP, the Gulf was without marine influence up to the edge of the Biaban Shelf, before the Strait of Hormuz opened up as a narrow waterway. Around 12,500 BP, the marine transgression of the Central Basin began, while around 11,500 BP the Western Basin had been flooded. Between 11,300 and 10,500 BP, temporary sea-level plateaus may have occurred (Lambeck 1996). Around 7000 BP the present shoreline was reached. Around 6000–4500 BP, a sea-level highstand meant that relative sea level was between 1 and 2 m above its present

position (Engel and Brückner 2014; Lokier et al. 2015; Parker et al. 2018).

A thick sequence of brackish-marine deposits below the low-lying areas of Lower Mesopotamia provides evidence that flooding of the Shatt-al-Arab region had already occurred around 9000–8000 BP (Aqrawi 2001), associated with extremely rapid landward shifts in the shoreline of up to 1 km/a (Teller et al. 2000). Around 8000 BP, the shoreline reached Basra, while ca. 2000 years later, during the mid-Holocene highstand, it can be traced at least as far as the ancient city of Ur in the west and modern Amara in the east (Sanlaville 1989; Aqrawi 2001; Heyvaert and Baeteman 2007). The spatial extent of the mid-Holocene transgression is corroborated by cuneiform texts indicating that the inland sites of Lagash and Ur were port cities in the third millennium BC (Jacobsen 1960; Pollock 1999).

Both Sarnthein (1972) and Teller et al. (2000) link the extended postglacial to early Holocene flooding to the flood event narrated in the Epic of Gilgamesh and the Bible. Undoubtedly, this transgression must have strongly affected the shallow Gulf and its civilizations. The experience of the permanent landward shift in the shoreline and the flooding of vast areas were later condensed into the legend of a world-devastating flood.

Counter-argument: The postglacial transgression lasted many human generations. Despite the high rate of landward shoreline change, it seems probable that communities shifted their dwelling places accordingly. It is, therefore, unlikely that this is the essence of the Genesis Flood which reflects a unique single event. In fact, archaeological evidence for many drowned dwelling places in the Gulf is as yet missing. Could it be that the postglacial–early Holocene flooding of all the shelves worldwide, which massively affected many Palaeolithic and Mesolithic hunter-gatherer communities (Turney and Brown 2007), is the background of the flood stories of many peoples on Earth (Fig. 7.1)?

7.3 Hypothesis 2: Cosmic Impact About 10,000 Years Ago

The geologic background for this scenario is the cosmic impact at the Cretaceous/Palaeogene (C/Pg) boundary, which terminated the Mesozoic Era. According to the so-called Alvarez hypothesis (Alvarez et al. 1980), an asteroid hit Earth 65—newer dating: 66 (Renne et al. 2013) —Ma ago, which created the 180 km-wide Chicxulub Crater in Yucatán, Mexico. One of the central arguments for this event is that, at the C/Pg boundary, a high concentration of iridium occurs, which is extremely rare on Earth and is suggested to have an extra-terrestrial origin. The ensuing "impact winter" interrupted the food chain resulting, among others, in the extinction of the dinosaurs. This cosmic catastrophe triggered a mega-tsunami, which devastated large areas of the land bordering the Gulf of Mexico, the Caribbean and even far beyond. The tsunami deposits are found in many boreholes and outcrops at the C/Pg boundary (Bourgeois et al. 1988; Claeys et al. 2002).

This is the background for the second hypothesis of the Genesis Flood, published more than 25 years ago by A. Tollmann, formerly professor of Geology at the University of Vienna, together with his wife (Kristan-Tollmann and Tollmann 1992, 1994; Tollmann and Tollmann 1993). Their approach was to collect flood stories worldwide, in different cultural and geographical contexts. They only considered those that were not "contaminated" by the biblical flood account, i.e., that originated directly from the specific populations and had not been transmitted by Christian missionaries. The synopsis of this approach led the authors to postulate that about 9545 years ago (with reference to the year of publication 1992) a comet hit our planet. Shortly before the collision, the Earth's tidal forces caused it to disintegrate into many pieces, of which seven major ones fell into the oceans and triggered huge tsunami waves causing destruction of coastal areas worldwide and reaching far

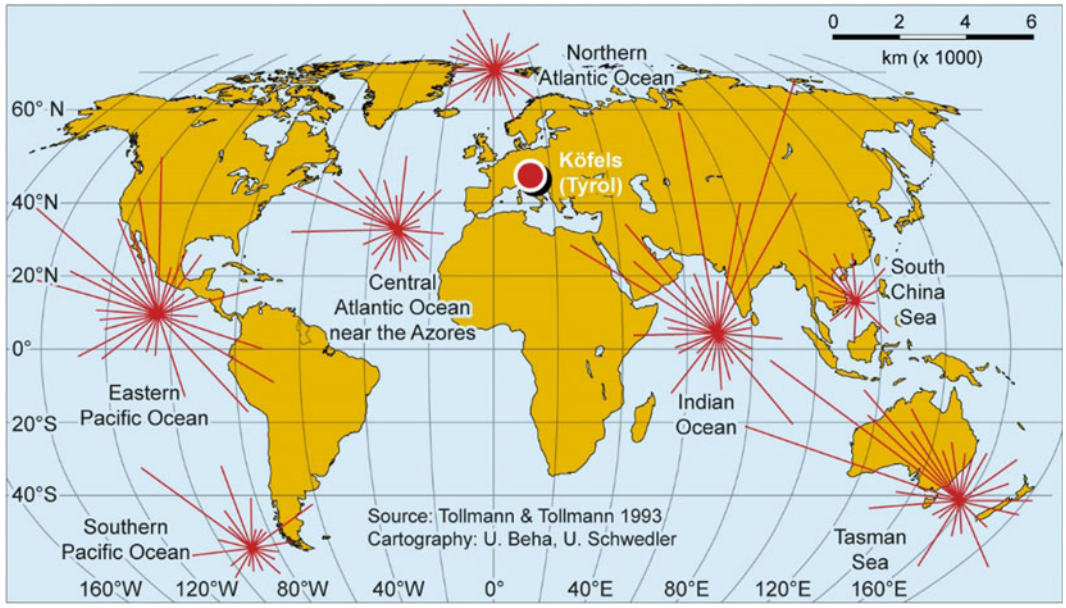

Fig. 7.3 Locations of the impact of the seven main fragments of the Flood Comet that hit the oceans plus the terrestrial impact near Köfels in Austria. This map is based on the synopsis of geological and mythological indications. The authors explain the dispersed pattern with Earth's rotation during the time span between the different impacts. After Tollmann and Tollmann (1993, Fig. 36), modified

inland. From the oral traditions they had collected, Tollmann and Tollmann (1993) even deduced the impact locations (Fig. 7.3). They assumed that this scenario would best explain why so many peoples independently share the myth of a unique world-devastating mega-flood.

Counter-argument: In contrast to the Alvarez hypothesis, geological and palaeoclimatological evidence is missing and age estimates for the environmental effects and tektites associated with the impact are largely asynchronous (Deutsch et al. 1994). It would be almost impossible to detect any potential remains of the comet on the ocean floor, and—even if so—to date synchronous impacts. Furthermore, it would be difficult to trace the tsunami deposits because, at the beginning of the Holocene, sea level was about 40 m lower than today. It is most likely that traces of the tsunami waves on the palaeocoastlines were eroded or totally erased by Holocene sea-level rise. Regarding the terrestrial impact in Tyrol/Austria, which was based on earlier theories (Suess 1936; Surenian 1986), convincing geological evidence is also missing. In fact, the latter has been reinterpreted as a giant landslide ca. 8000 (new dating: 9500) years ago, and the Köfels "pumice" is believed to be a product of the friction during the event (Erismann et al. 1977; Brückl et al. 2001; Nicolussi et al. 2015).

In light of the fact that meteorite-triggered tsunamis have never been directly observed or unequivocally reported in human history (Kelletat 2003), very few scholars have investigated this process in detail. Bryant (2008) and Bryant et al. (2010) identified five impact events, which they correlate with onshore tsunami deposits: Burckle 2807 BC, Akkadian 2200 BC, Keyes AD 535, Celtic AD 1014, and Mahuika AD 1491 (Fig. 7.4). Two of them (Burckle, Mahuika) are supposed to be associated with impact craters on the ocean floor, while the three others are linked with legends and oral traditions about devastating floods in the late Holocene. Furthermore, Bryant et al.'s (2010) tsunami chronology lists four possibly synchronous events (nos. 1–4 in Fig. 7.4: 4200 BC, 3200 BC, 60 BC, AD 790), for which the evidence in more than one ocean

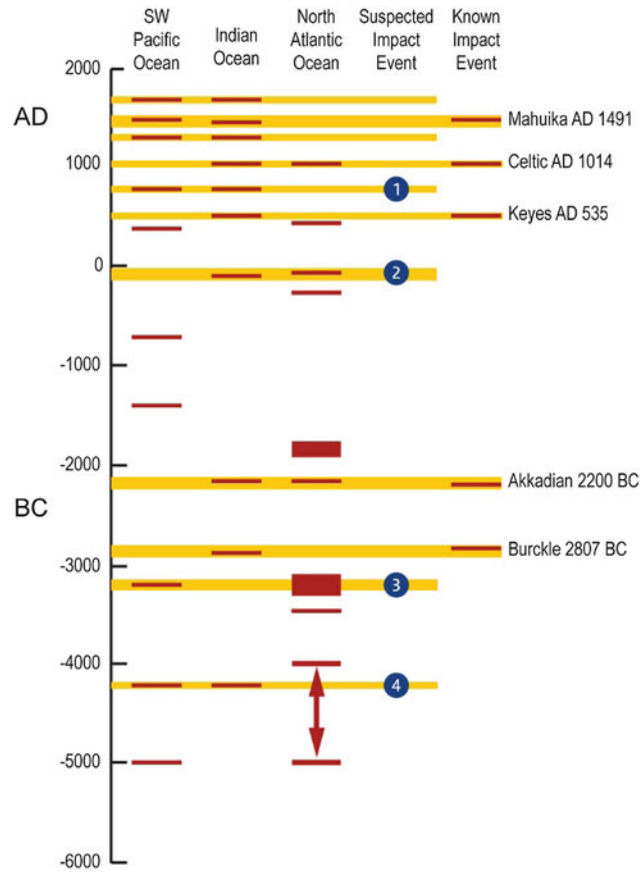

Fig. 7.4 Summary of tsunami events and corresponding impacts. Yellow lines indicate impacts with synchronous evidence in at least two oceans. Five impact events with onshore tsunami deposits have been identified and named, while the four numbered ones are as yet only suspected. After Bryant et al. (2010, Fig. 4), modified

basin is presented (Bryant 2008; Bryant et al. 2010). These have, however, not yet been attributed to identifiable impacts.

However, these meteorite-triggered tsunamis, if they occurred, were local and diachronic and it is unlikely that they constitute the background for the Genesis Flood narrative.

7.4 Hypothesis 3: Postglacial Flooding of the Black (Lake) Sea

This hypothesis is based on the rapid late glacial–early Holocene marine transgression of the Black Sea (cf. Ryan 2007; Ryan and Pitman 1998; Ryan et al. 1997, 2003; Fig. 7.5). The geological evidence on which the authors base their conclusion is the faunal inventory of drill cores. They demonstrate that the late Pleistocene and early Holocene strata show a gradual salinity decrease of the Black Sea until it turned fresh. Above an erosional unconformity the sediment comprises Mediterranean marine molluscs and microfauna. Ryan and Pitman (1998) conclude that in the course of the MIS 2 regression, the Black Sea and the Aegean Sea were disconnected, since the Bosphorus sill is only ca. 40 m deep. While the Aegean Sea, like the Mediterranean, which was still connected with the Atlantic Ocean via the Strait of Gibraltar, regressed up to 120–130 m below its present level during the LGM, the Black Sea was isolated and constituted a giant freshwater lake. At its lowest point, the lake level dropped to minus 150 m. During the early Holocene transgression, the rising level of the Mediterranean Sea surpassed the Bosphorus sill, with the effect of a catastrophic refilling of the Black Sea basin and the rapid drowning of more than 100,000 km^2 of its exposed continental shelf. According to the

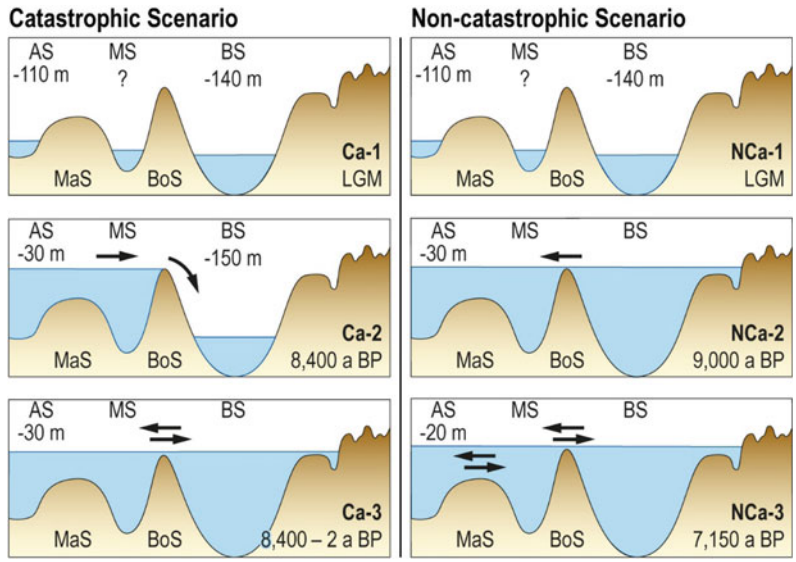

Fig. 7.5 Evolution of the exchange of water masses between the Marmara Sea and the Black Sea in three steps, according to the catastrophic flood model sensu Ryan and Pitman (1998), Ballard et al. (2000), Ryan et al. (2003), and Ryan (2007), as well as the gradual outflow model sensu Aksu et al. (1999, 2002). *AS* Aegean Sea, *MS* Marmara Sea, *BS* Black Sea; *MaS* Maramara sill, *BoS* Bosphorus sill; *LGM* Last Glacial Maximum, ca. 20 ka BP. Compilation from different sources

authors' age estimates, this happened ca. 7150 (later corrected to 8400) years ago. The sudden and catastrophic flooding caused a tremendous rise in the Black Sea level in a very short period of time. Since many populations had used the lake as a freshwater resource, numerous early Neolithic coastal communities are assumed to have drowned during this event. The survivors of the deluge fled in all directions, spreading the memory of this tragic event. According to Ryan and Pitman (1998), this is the reason why so many peoples on Earth have a flood story in their tradition.

Some years later, Ryan et al. (2003) presented geomorphic arguments to substantiate their hypothesis, such as submerged channels, estuaries, coastal dunes, coastal lagoons and barrier islands. They re-dated the catastrophic saltwater intrusion to 8400 a BP. They even extended the time scale to the entire Quaternary, stating that the Black Sea had witnessed at least eight marine flooding events over the past 3 Ma, and that throughout the past 2 Ma the Black Sea was predominantly a freshwater lake, interrupted only briefly by saltwater invasions coinciding with global sea-level highstands during interglacial periods (Ryan et al. 2003; Ryan 2007).

Hypothesis 3 triggered a fierce debate in the scientific community, well summarized in the book "The Black Sea Flood Question" (Yanko-Hombach et al. 2007a). The strongest opposition came from Aksu et al. (1999, 2002), Hiscott et al. (2007), Yanko-Hombach (2007) and Yanko-Hombach et al. (2007b).

According to Aksu et al. (1999, 2002) and Hiscott et al. (2007), who interpreted seismic profiles and dated sediment cores from the Marmara Sea, the Black Sea has been at or above the Bosphorus sill depth and flown into the world ocean more or less continuously since ~10,500 a BP. Their reasoning is based on continuous Holocene water-column stratification (leading to sapropel deposition in the Marmara Sea and the Aegean Sea), proxy indicators of sea-surface salinity, and migration of endemic species across the Bosphorus in both directions whenever appropriate hydrographic conditions existed in the strait. In summary, the proposed flood did not

occur, instead, there was a slow, progressive reconnection of the Black Sea to the world ocean.

Yanko-Hombach (2007) and Yanko-Hombach et al. (2007b) base their arguments against Ryan and Pitman's (1998) Flood theory on geological and palaeontological evidence from the Black Sea shelf. For the purposes of this paper, the following conclusions are noteworthy: during the Younger Dryas, the level of the Late Neoeuxinian lake, the late Pleistocene predecessor stage of the Black Sea, dropped from −20 to about −50 m and later rose again to about −20 m, pouring its excess semi-fresh to brackish water into the Sea of Marmara and from there into the Mediterranean. At ca. 10,000 a BP, the lake level fluctuated slightly, allowing Mediterranean water and organisms to enter the Late Neoeuxinian basin. This re-colonization of the Black Sea occurred in an oscillating manner. It was slow at the beginning, becoming most prominent at about 7000 a BP. The connection between the adjacent basins was probably not through the Bosphorus Strait, but via an alternative route. After ca. 10,000 a BP, the level of the Black Sea never again dropped below the −40 m isobath. On average, sea level rose gradually, but in an oscillating manner, to its present level, averaging 3 cm per 100 years, but certainly not 15 cm per day (almost 55 m per year!) as postulated by Ryan and Pitman (1998). An increase in sea level of 3 cm per 100 years would not have been noticed by the region's inhabitants (Yanko-Hombach 2007).

In the same book (Yanko-Hombach et al. 2007a), Ryan (2007) synthezises the arguments for his hypothesis. In short: sediments with marine fauna occur above the Neoeuxinian layer; they are separated from it by a layer of sand and gravel representing a younger unconformity. There are dune fields between −65 and −80 m, and wave-truncated terraces with beach-like berms at −90 to −100 m, which contain shell material dated between 9500 and 8500 a BP. This suggests that the younger unconformity represents a post-Younger Dryas regression that took the surface of the Black Sea's lake below the level of the global ocean. Strontium isotopes document the first intrusion of saltwater at 8400 BP.

In any case, the controversy has triggered several research programmes, namely the UNESCO-IGCP 521 (*Black Sea-Mediterranean Corridor during the last 30 ky: Sea level change and human adaptation*; 2005–2009), and the INQUA project 501 (*Caspian-Black Sea-Mediterranean Corridor during the last 30,000 years: Sea level change and human adaptive strategies*; 2005–2011). It also stimulated the underwater search by Ballard et al. (2000, 2001) for the Neolithic civilizations that were said to have populated the drowned shorelines of the former freshwater lake. They discovered a beach at a water depth of 550 ft (168 m), with a mixture of freshwater and saltwater molluscs. Their submersible revealed underwater structures, possibly of a house; however, the retrieved wood turned out to be only ca. 250 years old (Ballard et al. 2000, 2001; summary in Pleins 2003). Although the finds were very ambiguous, National Geographic produced a film about Ballard's search in 2001, entitled "The Quest for Noah's Flood".[1]

Until today, the nature of the flooding of the Black Sea basin is a matter of intense scientific research (e.g. Giosan et al. 2009; Goldberg et al. 2016), which includes the archaeological perspective (e.g. Bikoulis 2015). Based on cruises with research vessels, Lericolais and his team studied seafloor deposits and geomorphic features (submerged landscapes: fans, wave-cut terraces, coastal dunes, delta mouth bars) between the Bosphorus and the Danube delta fan. Lately, the author summarized the results as follows (Lericolais 2017): during the LGM, water level was about 120 m deeper than today; at this time, the Black Sea was probably a giant freshwater lake. The scenario of the following water-level fluctuations is complex. For the purposes of this article, it is noteworthy that ca. 9000 years ago, the surface waters of the Black Sea suddenly attained present-day conditions due to an abrupt flooding of the Black Sea by

[1] https://www.imdb.com/title/tt1341253/videoplayer/vi3808732697?ref_=tt_ov_vi.

Mediterranean waters. The flooding rate of about 10 m per century preserved coastal features on the shelf. Prior to its reconnection with the Sea of Marmara the Black Sea was a freshwater lake. The replacement of lacustrine by marine biota took almost 1000 years.

While the flooding scenario of the Black Sea is still being debated, there are several *counter-arguments against this concept*: The mechanisms for the lowering of the water table to −150 m despite the inflow of major freshwater rivers, are not fully understood. A submarine alluvial fan at the exit of the Bosphorus into the Marmara Sea is evidence of a persistent outflow from the Black Sea to the Mediterranean after the reconnection, which occurred much earlier than 8400 a BP (Aksu et al. 2002). There are indeed drowned landscape features on the Black Sea shelves (Lericolais 2017), but the flooding as such was definitely not catastrophic (Yanko-Hombach 2007). Furthermore, unequivocal archaeological finds of drowned Neolithic civilizations are as yet missing. There is no *in situ* evidence on the Black Sea shelves for such an occupation. The idea that after the flooding those humans who survived fled in all directions, which would explain why so many peoples have the flood story in their traditions, must be deemed as "archaeo-fantasy."

7.5 Hypothesis 4: Mega-Flood Catastrophe in Mesopotamia

One specific in the biblical version of the Great Deluge is interesting to note: when Noah builds the ark, he is told to use Earth pitch/bitumen in order to waterproof the vessel (Genesis 6, 14), which is one of *the* characteristic natural resources of Mesopotamia (Schwartz and Hollander 2000). After the ark had landed, Noah sends out a dove which returns with an olive branch (Genesis 8, 11). The olive tree is *the* characteristic element of the Mediterranean cultural sphere (Loumou and Giourga 2003). These two elements may indicate from which region the Flood story originated.

There is a lot of evidence for catastrophic floods in Mesopotamia. This is not surprising since (i) the name as such is derived from the Ancient Greek words for "between" (μέσος, mésos) and "river" (ποταμός, potamós), i.e. the land between Euphrates and Tigris (Finkelstein 1962); and (ii) the middle and lower courses of these rivers have very low gradients, whereby extremely heavy rainfalls and/or a sudden snowmelt in the area of their upper courses may cause catastrophic flooding in Lower Mesopotamia (Verhoeven 1998; Morozova 2005).

The search for the Flood deposits within settlement hills (tells) of Mesopotamia was triggered by Sir C. Leonard Woolley, who excavated Ur in the 1920s (Woolley 1923, 1929, 1955; location of Ur: Fig. 7.7, inserted map). In his book "Ur of the Chaldees", Woolley (1929) ascribed an up to 3.5 m thick homogeneous floodplain deposit void of artefacts to Noah's Flood[2]. It is sandwiched between occupation layers. Below the Flood layer, he found traces of an early civilization (Fig. 7.6). Systematic research has shown that other tells in Central and Lower Mesopotamia, e.g. Kish (Tell al-Uhaymir) and Shuruppak (Tell Fara), also have layers which may be interpreted as deposits of a significant flood (Brückner 2003).

Of special interest in this context is Uruk (also Erech, modern Warka), the city ascribed to the legendary king Gilgamesh, whose epic is an important non-biblical source for the Great Deluge (Figs. 7.7 and 7.8a). According to archaeological evidence, the city was founded in late Chalcolithic times at the end of the fifth millennium BC (Boehmer 1997), in the so-called late Ubaid period. It played a prominent role among

[2]Woolley (1955:68) described the flood layer as follows: "As to the character of the silt there could be no doubt; the analysis … makes it perfectly clear that it is the type of deposit normally left by the Euphrates in flood, collected from the upper reaches of the river; it is fluvial, not marine. The practical absence of stratification shows that it was deposited all at one time and is not the result of repeated minor floodings… Over the greater part of the area… no break in the uniformity of the deposit from top to bottom could be detected; here and there might be a 'pocket' of material of a different character, rubbish such as would be carried along by the swirling waters as they passed over an inhabited site, but such were isolated and discontinuous…"

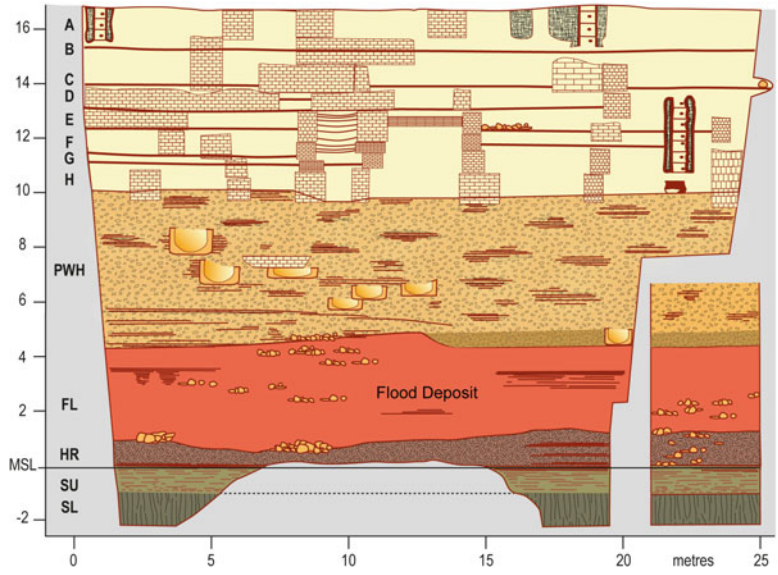

Fig. 7.6 Woolley's excavation pit F in Ur with the Flood layer. **A**–**H** Building strata; *PWH* pottery waste-heap; *FL* Flood layer (water-laid silt of fluvial origin, deposited at one time, average thickness of 3.50 m); *HR* house rubbish with mud floors and all kinds of artefacts; *SU* upper layer of swamp with horizontally layered pottery; *SL* lower layer of swamp, green clay with discolouration due to decay of plant roots, no signs of human occupation; 0 m: sea level. Woolley (Woolley 1955, plate 73 and pp. 56–68), modified

the world's earliest urban societies and can be called one of the cradles of civilization (van Ess et al. 2013). It seems that Uruk was the birthplace of writing, since its earliest written texts date to ca. 3200 BC.

A sediment coring campaign was carried out in March 2002 to test the hypothesis that this city was once traversed by water-bearing canals, fed by a branch of the Euphrates River, which led to Uruk being named "Amsterdam in the sand (Fig. 7.8b)." This interpretation of geophysically detected subsurface structures (Becker and Fassbinder 2001) could be confirmed by comparing drill cores from outside and inside these structures. The stratigraphy demonstrated that they had once been occupied by slowly running water (Brückner 2003, 2013a, b; cf. corings U2 and U3 in Fig. 7.9). The canal strata overlie a sharp, erosional contact. They contain small pieces of rolled ceramics and bricks, as well as a fauna which is indicative of clear running freshwater (bivalves: *Unio tigridis*, *Corbicula fluminalis*; gastropods: *Melanopsis nodosa*, *Theodoxus (Neritaea) doriae*; Brückner 2003; see also coring U4 in Fig. 7.9). *Corbicula fluminalis* is a species typical of the Euphrates (*locus typicus*) and lives predominantly in a river or canal (Plaziat and Younis 2005). Further evidence is that the canal bottom shows a low gradient between the entrance of the waterways into the city and their exit (Brückner 2003, Table 1 therein).

In the present context, it is of special interest that all coring profiles from Uruk (Fig. 7.9) have a very similar bottom stratigraphy: they start with a layer of homogeneous, well sorted sand at the base which is void of any fossils. This facies is interpreted as dune sand, typical of late-glacial times (MIS 2), since dunes are also attested on the then exposed seafloor of the northern (cf. Sarnthein 1972; Uchupi et al. 1996) and southern (cf. Evans et al. 2002) Persian/Arabian Gulf.

Then follows a layer of alluvial loam, reflecting the prograding deltas of the rivers Euphrates, Tigris and Karun. Many flood events —major and minor ones—are recorded in this layer. It is, however, very homogeneous (due to bioturbation?) and does not indicate the presence

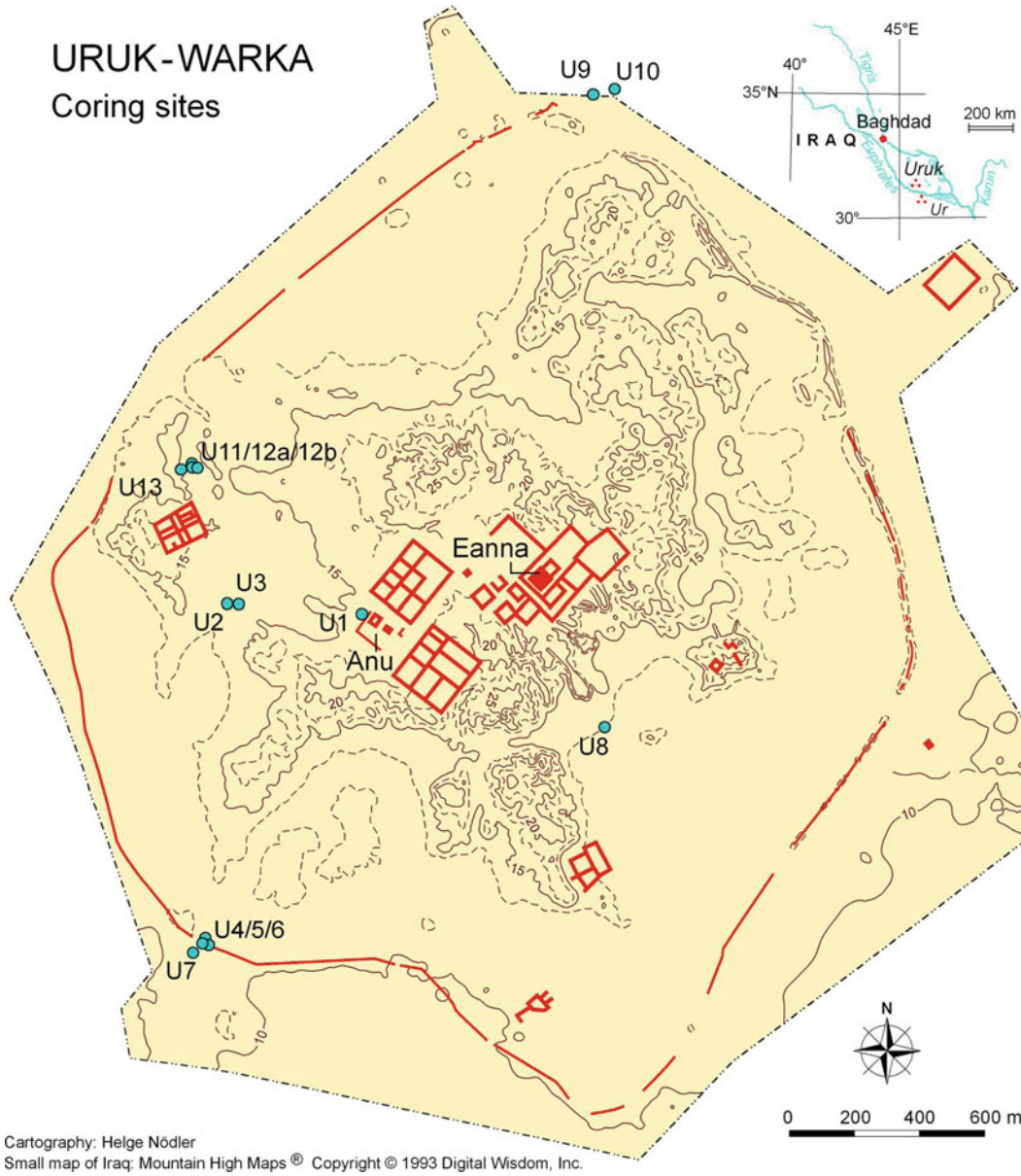

Fig. 7.7 Topographic map of Uruk (modern Warka) with archaeological structures and the coring sites of the 2002 expedition of the Orient Department of the German Archaeological Institute. The area shown is the fenced archaeological zone. Today, the tell (settlement hill) rises ca. 16 m above the extremely flat alluvial plain. Red: city wall, which is ascribed to the legendary king Gilgamesh, and main buildings (among others: Eanna Ziqqurrat and Anu Ziqqurrat). U1–U12b = coring sites. Altitudes in m a.s.l. (above mean sea level) After Brückner (2003, Fig. 1) modified, based on data from Deutsches Archäologisches Institut, Orient-Abteilung, Berlin

of one single catastrophic event. In some of the cores, an organic-rich layer can be identified. There is only proof that the sea was once close to Ur; there is no indication that it ever reached Uruk. Thus, the organic layer can be associated with a high groundwater table and wetland formation on the low-lying distal delta in the Uruk region when the marine transgression reached up to Ur (Brückner 2003; Engel and Brückner 2018).

Fig. 7.8 **a** The settlement hill (tell) of Uruk. In the central background the remains of the Eanna ziqqurrat (twenty-first century BC), the main sanctuary of Inanna (Ishtar), venerated as the goddess of love and war. In the foreground excavations in the area of the Seleucid temple complex for Ishtar (Irigal). In the far background, the extended Mesopotamian lowlands. **b** Inverted channels. They are evidence that the Sumerians had a sophisticated irrigation system; in fact, a channelled branch of the Euphrates River even ran through the city of Uruk. When the area was given up, probably due to increased climatic aridification and salinization of the fields (missing drainage led to efflorescence of salts), the channel fills were harder due to the precipitation of salts (including calcium carbonate) than the surrounding fields, where in the course of the horticulture the soil had always been loosened. Wind erosion caused relief inversion: while the material from the former fields was blown out and partly accumulated in the background as dunes, the former channel fills were more resistant to aeolian erosion. In the foreground, a black pen provides scale

The overlying strata are full of artefacts (anthropogenic layers). Most of the deposits represent debris of former loam bricks, which—step by step, generation by generation—led to the aggradation of the tell above the surrounding plain. In the case of Uruk, the preserved part of the tell is 40 m high. In one of the drill cores (Uruk 2), there is a layer interpreted as a flood layer, possibly deposited by a single event (cf. Figure 7.9). As yet, it has not been dated

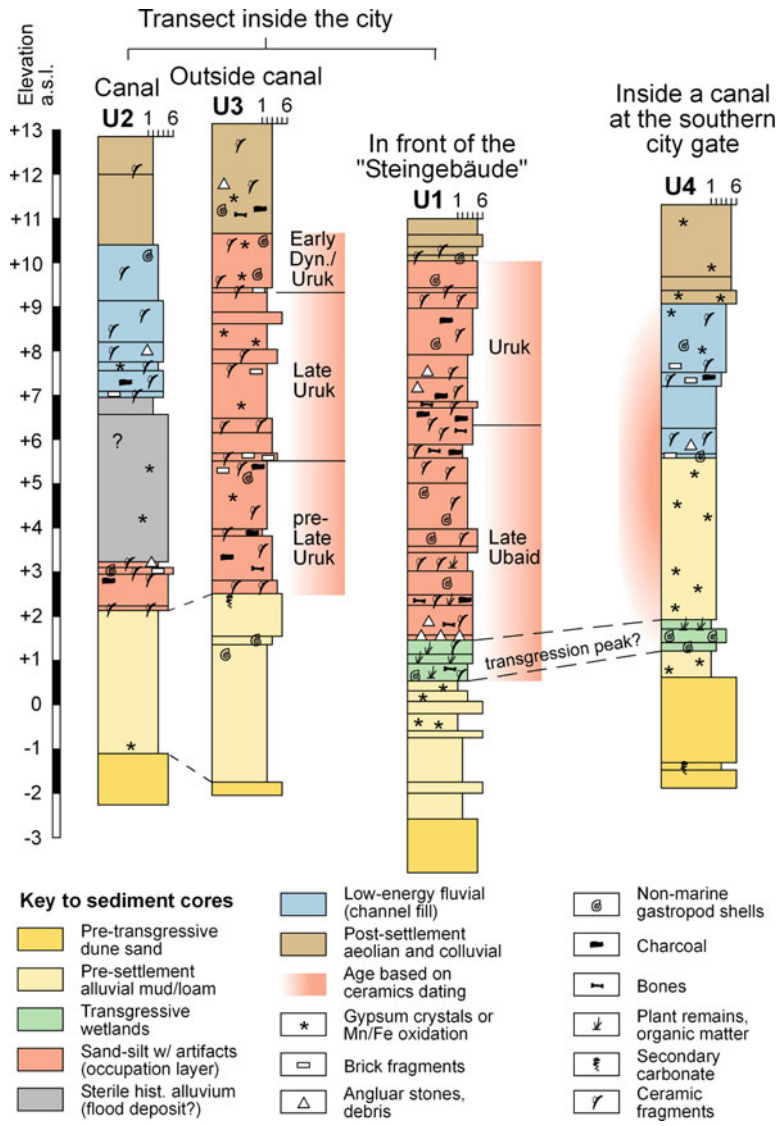

Fig. 7.9 Sediment cores from the city of Uruk. The environment changed from a desert with dunes (Late Pleistocene–Early Holocene) to freshwater marshes due to the early to mid-Holocene sea-level rise, and then alluvial plains shaped by the prograding river deltas. The anthropogenic layers document almost five thousand years of urban history. Note the contrast between the corings inside (U2, U4) and outside (U1, U3) the canal structures. Note the flood deposit in U2. After Engel and Brückner (2018), modified

(Brückner 2003). Therefore, it is unclear if this layer is contemporaneous with the Flood deposit from Ur (first described by Woolley 1923, 1929), Kish, Shuruppak and other tells.

The mid-Holocene sea-level highstand linked with the formation of wetlands around Uruk (organic-rich layer in cores U1 and U4, Fig. 7.9) occurred around 6000 years ago. After 5000 BP, during the highstand plateau and subsequent relative sea-level fall, hypersaline coastal sabkhas developed from salt marshes along the inland coast under an increasingly arid climate. The subsequent initiation of delta formation can be inferred by the capping of the transgressive parasequence by coastal marsh facies, i.e. evaporates dominated by gypsum, dolomite and

palygorskite, as well as fluvial silts and clays (Aqrawi 2001). The fluvial facies results from rapid post-highstand deltaic progradation controlled by river sediment loads, eustasy and isostasy, while the role of vertical tectonic activity seems to be of minor importance (Sanlaville 1989; Aqrawi 2001; Kennett and Kennett 2007).

One can draft several speculative scenarios for a massive flooding of Central and Lower Mesopotamia: i) a millennial event with an enormous, long-lasting rainfall period in the drainage areas of the upper reaches of the Euphrates and the Tigris; ii) a rapid snow-melt event in the same area; iii) the outburst of a temporary lake that had evolved after the damming of a major river course by a landslide. The latter phenomenon has also been observed for tributaries of the Tigris in modern times (Sissakian et al. 2014).

7.6 Conclusion

Out of the four hypotheses discussed above, the fourth one is the most reasonable geoscientific explanation. It seems that Central and Lower Mesopotamia was subject to a mega-flood, possibly before or around 3000 BC. Most probably the Gilgamesh Epic and the biblical flood story draw their essence from the same (written?) source.[3] A unique rise in the water table of the Euphrates and Tigris, e.g. caused by extraordinary and long-lasting rains and/or snow melt in their source areas, in combination with a southern wind blocking the drainage into the Arabian Gulf, may have drowned the extremely flat Central and Lower Mesopotamia completely (Woolley 1955; Brückner 2003; Engel and Brückner 2018)[4].

Further research may also reveal whether Noah's Flood was indeed a single event, or whether this narrative is the condensate of many severe floods that afflicted the inhabitants of Mesopotamia. There are arguments for the latter interpretation. The fact is that many (normal) floods have created the alluvial plains of Mesopotamia, much like other hydraulic civilizations of the Nile and the Indus valleys. It seems that now and then catastrophic flooding had occurred before 3000 BC while, after the rise of the Mesopotamian (Sumerian) high culture, extensive flooding of the entire alluvial plain no longer occurred—at least do the archaeological layers of those epochs not show any sedimentary footprint of such an extreme event. An explanation could be that with the beginning of the urban (high) culture, an irrigation network existed with thousands of kilometres of canals and a sophisticated water management system (Fig. 7.8b). Thus, when river levels were high, the excess water could be dissipated effectively before it created major damage. Due to the irrigation network and the advanced horticulture, an agricultural surplus was generated. This was one of the prerequisites for the emergence of the first cities.

Future palaeogeographic and palaeoecological research should look to furnish more evidence for the described scenarios and assumptions. Due to its geographic position, Uruk and its environs are—besides Ur—a key site for probing the mystery. The next step will be to systematically date the various flood layers in the different tells in order to understand if their deposition was synchronous or diachronous, and to study them as geo-bio-archives.

[3]It is noteworthy that the first prosaic texts are in cuneiform lettering and date from the late fourth millennium BC.

[4]This kind of catastrophic scenario had already been favoured by Woolley. He ends his comment about the Flood layer: …. (a riverine) "flood eight metres deep may well have spread over what was for the farmers of the Mesopotamian valley the whole world" (Woolley 1955:19).

References

Aksu AE, Hiscott RN, Yasar D (1999) Oscillating Quaternary water levels of the Marmara Sea and vigorous outflow into the Aegean Sea from the Marmara Sea–Black Sea drainage corridor. Mar Geol 153: 275–302

Aksu AE, Hiscott RN, Mudie PJ et al (2002) Persistent Holocene outflow from the Black Sea to the Eastern Mediterranean contradicts Noah's flood hypothesis. GSA Today 12(5):4–10

Alvarez LW, Alvarez W, Asaro F et al (1980) Extraterrestrial cause for the Cretaceous-Tertiary extinction. Science 208:1095–1108

Aqrawi A (2001) Stratigraphic signatures of climatic change during the Holocene evolution of the Tigris-Euphrates delta, Lower Mesopotamia. Glob Planet Change 28:267–283

Ballard RD, Coleman DF, Rosenberg GD (2000) Further evidence of abrupt Holocene drowning of the Black Sea shelf. Mar Geol 170:253–261

Ballard RD, Hiebert FT, Coleman DF et al (2001) Deepwater archaeology of the Black Sea: the 2000 season at Sinop, Turkey. Am J Archaeol 105:607–623

Becker H, Fassbinder JWE (2001) Uruk—city of Gilgamesh (Iraq). First tests in 2001 for magnetic prospecting. Monuments Sites 6:93–97

Bikoulis P (2015) Evaluating the impact of Black Sea flooding on the Neolithic of Northern Turkey. World Archaeol 47(5):756–775

Boehmer RM (1997) Uruk—Warka. In: Meyers EM (ed) The Oxford encyclopedia of archaeology in the Near East. Oxford University Press, Oxford, pp 294–298

Bourgeois J, Hansen TA, Wiberg PL et al (1988) A tsunami deposit at the Cretaceous-Tertiary boundary in Texas. Science 241:567–570

Brückl E, Brückl J, Heuberger H (2001) Present structure and prefailure topography of the giant rockslide of Köfels. Z Gletscherk Glazialgeol 37(1):49–79

Brückner H (2003) Uruk—a geographic and palaeo-ecologic perspective on a famous ancient city in Mesopotamia. Geoöko 24:229–248

Brückner H (2013a) Uruk—aus geoarchäologischer Sicht. In: van Ess M, Hilgert M, Salje B (eds) Uruk. 5000 Jahre Megacity. Begleitband zur Ausstellung "Uruk—5000 Jahre Megacity" im Pergamonmuseum. Curt-Engelhorn-Stiftung für die Reiss-Engelhorn-Museen, Deutsches Archäeologischen Institut—Orient-Abteilung, Deutsche Orient-Gesellschaft e. V., Vorderasiatisches Museum Berlin. Imhof Verlag, Petersberg, pp 343–351

Brückner H (2013b) Wasserstraßen im Wüstensand. Uruk aus geoarchäologischer Perspektive. Antike Welt 3:18–24

Brückner H, Herda A, Kerschner M et al (2017) Life cycle of estuarine island-from the formation to the landlocking of former islands in the environs of Miletos and Ephesos in western Asia Minor (Turkey). J Archaeol Sci Rep 12:876–894

Bryant E (2008) Tsunami—The underrated hazard, 2nd edn. Springer, Berlin

Bryant E, Haslett SK, Scheffers S et al (2010) Tsunami chronology supporting late holocene impacts. J Siberian Fed Univ Eng Technol 3(1):63–71

Claeys P, Kiessling W, Alvarez W (2002) Distribution of Chicxulub ejecta at the Cretaceous-Tertiary boundary. Geol Soc Am Spec Paper 356:55–68

Deutsch A, Koeberl C, Blum JD et al (1994) The impact-flood connection: does it exist? Terra Nova 6:644–650

Engel M, Brückner H (2014) The South Qatar survey project (SQSP)—preliminary findings on Holocene coastal changes and geoarchaeological archives. Z Orient-Archäol 7:290–301

Engel M, Brückner H (2018) Holocene climate variability of Mesopotamia and its impact on the history of civilization. EarthArXiv. https://doi.org/10.31223/osf.io/s2aqt

Erismann T, Heuberger H, Preuss E (1977) Der Bimsstein von Köfels (Tirol), ein Bergsturz-"Friktionit". Miner Petrol 24(1–2):67–119

Evans G, Kirkham A, Carter RA (2002) Quaternary development of the United Arab Emirates Coast: new evidence from Marawah Island, Abu Dhabi. GeoArabia 7(3):441–458

Finkel I (2014) The ark before Noah: decoding the story of the flood. Hodder & Stoughton, London

Finkelstein, JJ (1962) Mesopotamia. J Near East Stud 21:73–92

George AR (2003) The Babylonian Gilgamesh epic: introduction, critical edition and cuneiform texts, vol 1. Oxford University Press, Oxford

Giosan L, Filip F, Constatinescu S (2009) Was the Black Sea catastrophically flooded in the early Holocene? Quat Sci Rev 28:1–6

Goldberg SL, Lau HCP, Mitrovica JX et al (2016) The timing of the Black Sea flood event: Insights from modeling of glacial isostatic adjustment. Earth Planet Sci Lett 452:178–184

Herget J (2019) Die Sintflut—Mythos und Realität. Geographische Rundschau (in press)

Heyvaert VMA, Baeteman C (2007) Holocene sedimentary evolution and palaeocoastlines of the Lower Khuzestan plain (southwest Iran). Mar Geol 242:83–108

Hiscott RN, Aksu AE, Mudie PJ et al (2007) The Marmara Sea gateway since ~16 ky BP: non-catastrophic causes of paleoceanographic events in the Black Sea at 8.4 and 7.5 ky BP. In: Yanko-Hombach V, Gilbert AS, Panin N et al (eds) The Black Sea flood question. Springer, Dordrecht, pp 89–118

Jacobsen T (1960) The waters of Ur. Iraq 22:174–185

Kelletat D (2003) Tsunami durch impacts von Meteoriten im Quartär? Essen Geogr Arb 35:27–38

Kennett DJ, Kennett JP (2007) Influence of Holocene marine transgression and climate change on cultural evolution in southern Mesopotamia. In: Anderson DG, Maasch KA, Sandweiss DH (eds) Climate change and cultural dynamics: a global perspective on Mid-Holocene transitions. Elsevier, Amsterdam, pp 229–264

Kristan-Tollmann E, Tollmann A (1992) Der Sintflut-Impakt. The Flood impact. Mitt Österr Geol Ges 84:1–63

Kristan-Tollmann E, Tollmann A (1994) The youngest big impact on Earth deduced from geological and historical evidence. Terra Nova 6(2):209–217

Lambeck K (1996) Shoreline reconstructions for the Persian Gulf since the last glacial maximum. Earth Planet Sci Lett 142:43–57

Lericolais G (2017) Late Pleistocene environmental factors defining the Black Sea, and submerged landscapes on the Western continental Shelf. In:

Flemming NC, Harff J, Moura D et al (eds) Submerged landscapes of the European Continental shelf: Quaternary paleoenvironments. Blackwell-Wiley, Chichester, pp 479–495

Lokier SW, Bateman MD, Larkin NR et al (2015) Late Quaternary sea-level changes of the Persian Gulf. Quat Res 84:69–81

Loumou A, Giourga C (2003) Olive groves: "The life and identity of the Mediterranean". Agr Hum Values 20:87–95

Morozova GS (2005) A review of Holocene avulsions of the Tigris and Euphrates rivers and possible effects on the evolution of civilizations in Lower Mesopotamia. Geoarchaeology 20:401–423

Nicolussi K, Spötl C, Thurner A, Reimer PJ (2015) Precise radiocarbon dating of the giant Köfels landslide (Eastern Alps, Austria). Geomorphology 243:87–91

Parker AG, Armitage SJ, Engel M et al (2018) Geomorphology, geoarchaeology and palaeoenvironments. In: Drechsler P (ed) Dosariyah—an Arabian Neolithic Coastal community in the central Gulf. Archaeopress, Oxford, pp 21–55

Plaziat JC, Younis WR (2005) The modern environments of Molluscs in southern Mesopotamia, Iraq: a guide to paleogeographical reconstructions of Quaternary fluvial, palustrine and marine deposits. Carnets Géol CG2005 (A01), https://doi.org/10.4267/2042/1453

Pleins JD (2003) When the great abyss opened: classic and contemporary readings of Noah's Flood. Oxford University Press, Oxford

Pollock S (1999) Ancient Mesopotamia. Cambridge University Press, Cambridge

Renne PR, Deino AL, Hilgen FJ et al (2013) Time scales of critical events around the Cretaceous-Paleogene boundary. Science 339:684–687

Ryan WBF (2007) Status of the Black Sea flood hypothesis. In: Yanko-Hombach V, Gilbert AS, Panin N et al (eds) The Black Sea flood question. Springer, Dordrecht, pp 63–88

Ryan WBF, Pitman WC (1998) Noah's flood: the new scientific discoveries about the event that changed history. Touchstone, New York

Ryan WBF, Pitman WC, Major CO et al (1997) An abrupt drowning of the Black Sea shelf. Mar Geol 138:119–126

Ryan WBF, Major CO, Lericolais G et al (2003) Catastrophic flooding of the Black Sea. Ann Rev Earth Planet Sci 31:525–554

Sanlaville P (1989) Considérations sur l'évolution de la Basse Mésopotamie au cours des derniers millénaires. Paléorient 15:5–27

Sarnthein M (1972) Sediments and history of the postglacial transgression in the Persian Gulf and Northwest Gulf of Oman. Mar Geol 12:245–266

Schwartz M, Hollander D (2000) Annealing, distilling, reheating and recycling: bitumen processing in the Ancient Near East. Paléorient 26:83–91

Sissakian VK, Abdul Jab'bar MF, Al-Ansari N et al (2014) Meandering of tributaries of the Tigris River due to mass movements within Iraq. Engineering 6:712–730

Suess FE (1936) Der Meteor-Krater von Köfels bei Umhausen im Ötztale, Tirol. Neues Jahrb Mineral Geol Paläontol Abh 72:98–155

Surenian R (1986) Scanning electron microscope study of shock features in pumice and gneiss from Köfels (Tyrol, Austria). Mitt Geol Paläontol Innsbruck 15:135–143

Teller JT, Glennie KW, Lancaster N et al (2000) Calcareous dunes of the United Arab Emirates and Noah's Flood: the postglacial reflooding of the Persian (Arabian) Gulf. Quat Int 68–71:297–308

Tollmann A, Tollmann E (1993) Und die Sintflut gab es doch. Vom Mythos zur historischen Wahrheit. Droemer Knaur, München

Turney CS, Brown H (2007) Catastrophic early Holocene sea level rise, human migration and the Neolithic transition in Europe. Quat Sci Rev 26:2036–2041

Uchupi E, Swift SA, Ross DA (1996) Gas venting and late Quaternary sedimentation in the Persian (Arabian) Gulf. Mar Geol 129:237–269

van Ess M, Hilgert M, Salje B (eds) (2013) Uruk. 5000 Jahre Megacity. Begleitband zur Ausstellung "Uruk—5000 Jahre Megacity" im Pergamonmuseum. Curt-Engelhorn-Stiftung für die Reiss-Engelhorn-Museen, Deutsches Archäeologischen Institut—Orient-Abteilung, Deutsche Orient-Gesellschaft e.V., Vorderasiatisches Museum Berlin. Imhof Verlag, Petersberg

Verhoeven K (1998) Geomorphological research in the Mesopotamian flood plain. In: Gasche H, Tanret M (eds) Changing watercourses in Babylonia. Towards a reconstruction of the ancient environment in Lower Mesopotamia, vol I. University of Chicago Press, Chicago, pp 159–245

Vitaliano DB (2007) Geomythology: geological origins of myths and legends. Geol Soc London Spec Pub 273:1–7

Vött A, Brückner H, Kraft JC (2017) Do mythological traditions reflect past geographies? The Acheloos delta (Greece) and the Artemision (Turkey) case studies. Z Geomorph 61(Suppl 1):203–221

Woolley CL (1923) Excavations at Ur of the Chaldees. Antiq J 3:311–333

Woolley CL (1929) Ur of the Chaldees: a record of seven years of excavation. Reprinted with revisions in 1952 by Harmondsworth, Middlesex, Eng., Penguin Books (German first edition in 1930 as: Ur und die Sintflut. Sieben Jahre Ausgrabungen in Chaldäa, der Heimat Abrahams. F. A. Brockhaus, Leipzig)

Woolley L (1955) Ur Excavations, vol. IV: the early periods. A report on the sites and objects prior in date to the Third Dynasty of Ur discovered in the course of the excavations. Publications of the joint expedition of the British Museum and of the Museum of the

University of Pennsylvania to Mesopotamia. London, Philadelphia

Yanko-Hombach V (2007) Controversy over Noah´s flood in the Black Sea: geological and foraminiferal evidence from the shelf. In: Yanko-Hombach V, Gilbert AS, Panin N et al (eds) The Black Sea flood question. Springer, Dordrecht, pp 149–203

Yanko-Hombach V, Gilbert AS, Panin N et al (eds) (2007a) The Black Sea flood question: changes in coastline, climate, and human settlement. Springer, Dordrecht

Yanko-Hombach V, Gilbert AS, Dolukhanov P (2007b) Controversy over the great flood hypotheses in the Black Sea in light of geological, paleontological, and archaeological evidence. Quat Int 167–168:91–113

Part III

Studies with Methodical and Technical Topics

8 Luminescence Dating in Fluvial Settings: Overcoming the Challenge of Partial Bleaching

Rachel K. Smedley and Grace K. A. Skirrow

Abstract

Optically stimulated luminescence (OSL) dating is a versatile technique that utilises the two most ubiquitous minerals on Earth (quartz or K-feldspar) for constraining the timing of sediment deposition. It has provided accurate ages in agreement with independent age control in many fluvial settings, but is often characterised by partial bleaching of individual grains. Partial bleaching can occur where sunlight exposure is limited and so only a portion of the grains in the sample was exposed to sunlight prior to burial, especially in sediment-laden, turbulent or deep water columns. OSL analysis on multiple grains can provide accurate ages for partially bleached sediments where the OSL signal intensity is dominated by a single brighter grain, but will overestimate the age where the OSL signal intensity is equally as bright (often typical of K-feldspar) or as dim (sometimes typical of quartz). In such settings, it is important to identify partial bleaching and the minimum dose population, preferably by analysing single grains, and applying the appropriate statistical age model to the dose population obtained for each sample. To determine accurate OSL ages using these age models, it is important to quantify the amount of scatter (or overdispersion) in the well-bleached part of the partially bleached dose distribution, which can vary between sediment samples depending upon the bedrock sources and transport histories of grains. Here, we discuss how the effects of partial bleaching can be easily identified and overcome to determine accurate ages. This discussion will therefore focus entirely on the burial dose determination for OSL dating, rather than the dose-rate, as only the burial doses are impacted by the effects of partial bleaching.

Keywords

Optically stimulated luminescence dating · OSL · Partial bleaching · Fluvial · Single grains · Age models

8.1 Introduction

Constraining the timing of sediment deposition in fluvial settings is important for understanding the rates and magnitude of sedimentary processes and events (e.g. floods). A number of geochronological techniques are available to provide ages in fluvial settings, but certain techniques can be restricted by the lack of material preservation and dateable age ranges. Optically stimulated luminescence (OSL) dating is a versatile technique that directly dates the

R. K. Smedley (✉) · G. K. A. Skirrow
Department of Geography and Planning, University of Liverpool, Liverpool, UK
e-mail: rachel.smedley@liverpool.ac.uk

J. Herget and A. Fontana (eds.), *Palaeohydrology*, Geography of the Physical Environment,
https://doi.org/10.1007/978-3-030-23315-0_8

time elapsed since a mineral grain or rock surface was exposed to sunlight and subsequently buried (Huntley et al. 1985) and has often extended age ranges for sediment burial beyond radiocarbon dating (e.g. Burow et al. 2015). OSL dating is performed on the two most ubiquitous minerals in the Earth's crust (either quartz or K-feldspar), which increases the likelihood of finding material for dating. Moreover, grainsizes from silt up to boulder-sized clasts can be used for dating and the dateable age range for OSL dating extends beyond that of radiocarbon dating, typically up to ~100 ka for quartz and ~500 ka for K-feldspar; however, the age range of the technique is highly dependent upon the characteristics of each sample and the luminescence signal used for analysis. OSL dating is therefore well-suited for constraining sediment deposition in a fluvial setting and has been used extensively to determine accurate ages in many different environments (e.g. Burow et al. 2015; Colarossi et al. 2015; Giosan et al. 2012; Kolb and Fuchs 2018; Lyons et al. 2013, 2014; Thomas et al. 2017); this includes the deposition of young (Shen and Mauz 2012) and paleo-deltaic sediments (Shen et al. 2012, 2015), and rapidly deposited sediment during flood events (e.g. He et al. 2019; Medialdea et al. 2014). Novel approaches of the OSL dating technique have also deciphered sediment transport pathways and residence times in fluvial systems (e.g. Chamberlain et al. 2017; Gray et al. 2018; Reimann et al. 2015).

An important consideration for OSL dating in fluvial settings is the extent of sunlight exposure that each individual grain has experienced prior to burial. When grains are exposed to sufficient durations and intensities of sunlight, the OSL signal is reset to zero (or bleached). To determine an accurate age for the deposition of a sedimentary sample, it must contain at least some grains whose OSL signals were fully reset prior to burial. Typically, in depositional setting where there is a greater opportunity for grains to have been exposed to sunlight prior to burial (e.g. aeolian), the OSL signal of all of the individual grains was equally reset; this is often termed well-bleached. In contrast, in depositional settings where there is less opportunity for sunlight exposure to all grains (e.g. fluvial, glaciofluvial), the OSL signal of only a portion of the grains in the sample may have been reset to zero prior to burial; this is often termed partial bleaching. To calculate an accurate OSL age for well-bleached sediments, all of the grains in the population can be used; however, for partially bleached sediments, only those grains in the partially bleached population that were well-bleached prior to burial can be used to prevent overestimation of the true burial age. Here, we will discuss the process of partial bleaching in a fluvial setting, in addition to the approaches that can be used in OSL dating to identify the effects of partial bleaching and calculate accurate ages for sediment burial.

8.2 Luminescence Dating: Basic Principles

A fundamental requirement of OSL dating is that a mineral grain can store and release energy (or electrons), almost like a rechargeable battery (after Duller 2008). The electrons are ionised by the low-level radiation that is all around us due to the emission of alpha and beta particles, and gamma rays during the radioactive decay of K, Rb, U and Th in radionuclide equilibrium in the surrounding environment, in addition to cosmic rays. In the crystal lattice of minerals, electrons become trapped at defects or impurities, which can then be released when the mineral is excited by stimulation of light (OSL), heat or pressure. When the mineral grains are then buried for a period of time and exposed to natural radiation from the surrounding environment, trapped electrons will reaccumulate at the defects within the grain. The long life-times of radioactive elements in the natural environment mean that the accumulation of energy resulting from the environmental dose-rate is typically constant over time. Therefore, we can determine the time elapsed since a mineral grain was last exposed to light and buried by measuring the OSL signal emitted from the mineral grains and comparing it to OSL signals resulting from known radiation

doses delivered in the laboratory to the same sample: this gives the equivalent dose (D_e). To obtain the age, we divide the D_e by the environmental dose-rate (Eq. 8.1), which is determined for the bulk sediment from its geochemical composition or by emission-counting techniques for alpha, beta and gamma radiation.

$$\text{Age (ka)} = \frac{\text{Equivalent dose (Gy)}}{\text{Dose rate (Gy/ka)}} \quad (8.1)$$

8.3 Mineral Choice: Quartz or Feldspar?

The two principle minerals used for OSL dating are quartz and K-feldspar. Since 2000 and the development of the single aliquot regenerative dose (SAR) protocol (Murray and Wintle 2000), quartz has been the preferred mineral for OSL dating. However, in certain settings very few grains of quartz emit an OSL signal and those signals can be very dim, making OSL analysis to determine the D_e value very difficult and inefficient (e.g. Chiverrell et al. 2018). In comparison, for the same sample a large proportion of K-feldspar grains can emit a detectable OSL signal of K-feldspar, which can be relatively brighter than the OSL signal of the quartz; thus, making OSL analysis more efficient and potentially more precise as brighter signals generate better counting statistics and reduce uncertainties on the D_e values. The relative brightness of K-feldspar grains over quartz has meant that in some settings it is advantageous to analyse K-feldspar grains. However, we need to consider the additional complexities of internal dose-rates, anomalous fading and slower inherent bleaching rates for K-feldspar, which are characteristic of K-feldspar but do not pertain to quartz.

Anomalous fading of K-feldspar is the athermal depletion of trapped charge stored within the grain during burial (Wintle 1973). Previous studies have suggested that anomalous fading is ubiquitous to all K-feldspar when the D_e value is measured using the infra-red stimulated luminescence (IRSL) signal at 50 °C (Huntley and Lamothe 2001), and thus, the ages need fading correction to prevent age underestimations. There are methods that can be used to measure and correct for anomalous fading (e.g. Huntley and Lamothe 2001; Kars et al. 2008), but this can often introduce additional uncertainty into age calculations. Therefore, it is advantageous to circumvent anomalous fading by using a more stable signal of K-feldspar. In 2008, Thomsen et al. (2008) developed the use of a new signal of K-feldspar that can circumvent the issue of anomalous fading; this is termed the post-IR IRSL signal and has revolutionised the use of K-feldspar for luminescence dating. The post-IR IRSL protocol is a two-step procedure that uses an initial IRSL measurement at a lower temperature (typically 50 °C) to remove the more unstable IRSL signal followed by an IRSL measurement at a higher temperature, typically 225 °C (the $pIRIR_{225}$ signal; Buylaert et al. 2009) or 290 °C (the $pIRIR_{290}$ signal; Thiel et al. 2011), which is used to determine a D_e value. By accessing the higher temperature, more stable pIRIR signal in K-feldspar, we can circumvent anomalous fading and determine accurate ages, which have been validated against independent age control (e.g. Roberts 2012).

Another consideration for the mineral choice is the relative differences in bleaching rates inherent to the OSL signal of quartz and the IR_{50} and post-IR IRSL signals of K-feldspar, especially when dating sediments deposited during the last few centuries. It has long been known that in air (not within a water column); the OSL signal of quartz typically bleaches faster than the IR_{50} signal of K-feldspar (Godfrey-Smith et al. 1988). Colarossi et al. (2015) then showed using a solar simulator (typically up to $\sim$6.5 times stronger than direct sunlight) that the OSL signal of quartz was reduced to 5% of the original signal after only 10 s of bleaching, while the $pIRIR_{225}$ and $pIRIR_{290}$ signals of K-feldspar took four and 14 days, respectively, to reduce to 5% of the original signal. Slower inherent bleaching rates of the pIRIR signals mean that small residual doses may be incorporated into the

D_e value used for dating because the OSL signal was not fully reset to zero prior to burial. These small residual doses are negligible when dating older samples, but may cause age overestimation for young samples deposited in the last few hundred years, and so lower-temperature signals are often preferred in such cases to minimise the impact upon dating (e.g. Reimann et al. 2011; Reimann and Tsukamoto 2012). It was thought that small residual doses in K-feldspar would also restrict the use of the pIRIR signals for single-grain analysis, and although Smedley et al. (2015) found that the inherent bleaching rates of the pIRIR signals of K-feldspar varied between grains, the bleaching rates of the $pIRIR_{225}$ signals of most of the single grains were similar and would not restrict single-grain analysis. However, the bleaching rates of the higher-temperature $pIRIR_{290}$ signals of the single grains were highly variable, where very few grains bleached at faster rates and so single-grain dating of K-feldspar grains using the $pIRIR_{290}$ signal in a partially bleached setting would likely be characterised by large and variable residual doses in individual grains (Smedley et al. 2015). This is supported by recent findings from modern river systems that showed that some single grains of K-feldspar determined zero dose values using the pIRIR signals (Gliganic et al. 2017).

8.4 Partial Bleaching in Fluvial Settings

Sedimentary samples from fluvial settings can be partially bleached prior to deposition, especially in higher-energy, deeper river channels. Although there is the potential for the OSL signal of fluvial sediments to be partially bleached prior to burial, a surprising proportion of samples were well-bleached, especially in shallow, low-energy fluvial settings (e.g. Durcan et al. in press). For a suite of 72 glaciofluvial samples from the British-Irish Ice Sheet, the single-grain D_e distributions determined using quartz showed that ~30% of them were well-bleached prior to burial (e.g. Smedley et al. 2017a, b). This demonstrates that there is a greater potential for sunlight exposure prior to burial than we might assume in glaciofluvial settings, which are typically expected to have less opportunity for sunlight exposure than fluvial settings. Little is known about the physical processes of OSL signal resetting in fluvial settings in the natural environment, but it is suggested that sunlight attenuation is greater in deeper, sediment-laden, turbulent water columns. Therefore, implying that there may be variability in the bleaching efficiency of different grainsizes, and potentially different minerals due to preferential attenuation of different wavelengths through water columns. Previous studies have shown how shorter wavelengths that are more efficient at bleaching the OSL signal of quartz are attenuated to greater extents in turbid water columns in comparison with the wavelengths that are more efficient at bleaching the IRSL signals of K-feldspar (e.g. Jerlov 1970; Kronborg 1983; Sanderson et al. 2007). However, this still needs to be validated by directly comparing single-grain OSL dating of quartz and K-feldspar of the same sedimentary samples taken from a former river system.

Our understanding of how coarser (sand) and finer (silt) grainsizes bleach in a fluvial setting varies between studies, perhaps reflecting the complex nature of sunlight bleaching in different fluvial settings and processes. Many studies report a difference in the OSL ages obtained from the coarser and finer grainsizes (e.g. Gray and Mahan 2015; Bailey et al. 2003; Fuchs et al. 2005; Olley et al. 1998; Truelsen and Wallinga 2003), but the reasons for this continue to be unresolved. Some studies have repeatedly observed a general depletion of D_e in fluvial sedimentary samples with increasing transport distances (Gray and Mahan 2015; Bailey et al. 2003; Stokes et al. 2001); this is attributed to the fact that coarser grainsizes fall out from suspension first, which restricts the distance that the grains are transported and therefore their potential exposure to sunlight during transportation. This theory is also relevant to vertical grainsize distribution in the water column as a turbid water column with a high suspended load is likely to attenuate the sunlight through the water column and so restrict the bleaching of coarser grainsizes

transported across or close to the river bed via saltation (e.g. Gray and Mahan 2015; Rittenour 2008). Alternatively, other studies have reported that coarser grainsizes are less prone to partial bleaching and are therefore deemed to determine accurate ages in fluvial settings in comparison to finer grainsizes (e.g. He et al. 2019; Kim et al. 2015; Fuchs et al. 2005; Fan et al. 2010; Olley et al. 1998; Thompson et al. 2018; Truelsen and Wallinga 2003). It has been suggested that greater sunlight exposure during shorter periods of deposition prior to transportation (e.g. in mid-channel bars) could preferentially bleach the coarser grainsizes, while the sunlight bleaching of finer grainsizes may be restricted by mud coatings (e.g. Truelsen and Wallinga 2003). It may also be because coarser grainsizes are transported at a slower rate and for longer distance in a river system via traction or saltation and so have greater opportunity for sunlight exposure than finer grainsizes which are transported within the potentially turbulent water column via suspension (He et al. 2019; Thompson et al. 2018). It is likely that the contrasting reports of whether the coarser or finer grainsizes bleach preferentially in a river system are related to the complex sedimentary processes occurring prior to deposition and subsequent burial. Further investigations on the physical processes of OSL signal resetting in river channels in the natural environment are required to understand how partial bleaching in the water column impacts upon different grainsizes and minerals.

8.5 Overcoming Partial Bleaching with OSL Analysis

The effects of partial bleaching in the natural environment may sound challenging for OSL dating in comparison with the well-bleached sediments typical of aeolian settings, but in fact, it can be easily identified and overcome to determine accurate ages by using the appropriate techniques.

8.5.1 Identifying Partial Bleaching

A D_e distribution determined for a well-bleached sediment will form a log-normal distribution around a central D_e value that appears symmetrically distributed when plotted in log-space (e.g. Fig. 8.1a). In contrast, partially bleached D_e distributions are scattered asymmetrically in log-space from a minimum dose population that was well-bleached prior to burial, up to larger doses from grains that may never have been exposed to sunlight and have saturated OSL signals (e.g. Fig. 8.1b). To fully characterise the true nature of a partially bleached D_e distribution, OSL analysis must be performed on single grains as the extent of sunlight exposure and signal resetting varied between grains prior to burial; some grains were well-bleached while the other grains may never have been exposed to sunlight. The easiest method of ensuring that OSL analysis is performed on the OSL signal emitted from an individual grain is to stimulate single grains at a time using a focussed laser system (Duller et al. 1999). Grains are mounted in purpose-built single-grain discs with a 10×10 array of holes drilled at specific diameters so that only a single grain can be in each hole at a time (e.g. Fig. 8.2a). For example, a grainsize of 150–180 and 212–250 μm would be analysed using 200 and 300 μm holes, respectively, to prevent more than one grain being present in each hole (e.g. Fig. 8.2b). Where more than one grain is present in each hole, the analysis should be termed pseudo-single grain or microhole measurements as they are not truly single-grain measurements and it can have an impact upon the D_e value determined (see Arnold and Roberts 2009). Single-grain OSL measurements can also be obtained by integrating the OSL signal emitted by individual grains measured using an electron-multiplying charged coupled device (EMCCD) (Lapp et al. 2015; Thomsen et al. 2015), but typically requires a bespoke EMCCD attachment for equipment and is less sensitive than the photo-multiplier tubes typically used for

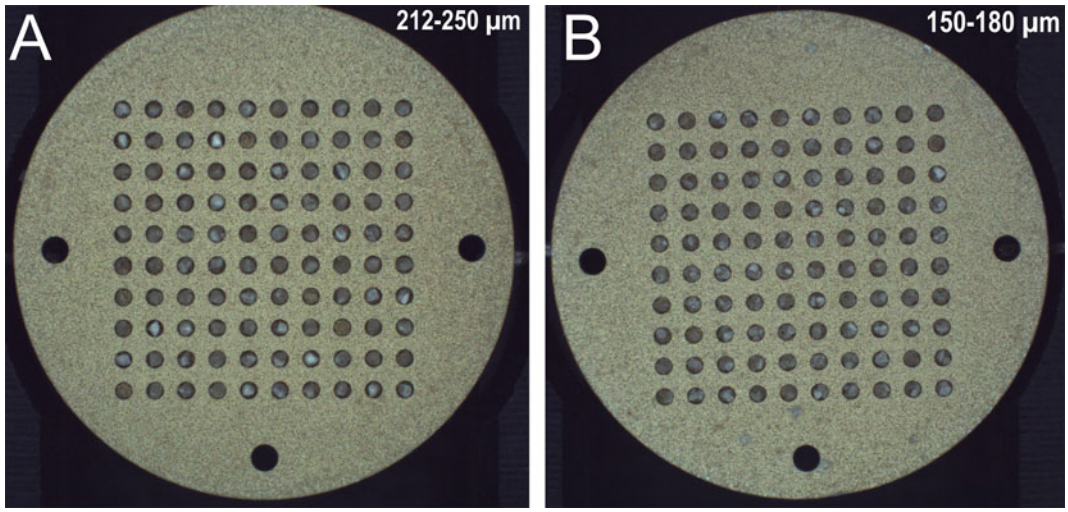

Fig. 8.1 Single-grain discs with hole diameters of 300 µm, but loaded with a grainsize of 212–250 µm so that only a single grain is present in each hole i.e. truly single-grain measurements (**a**), or loaded with a grainsize of 150–180 µm so that up to 4 grains may be present in each hole i.e. microhole measurements (**b**)

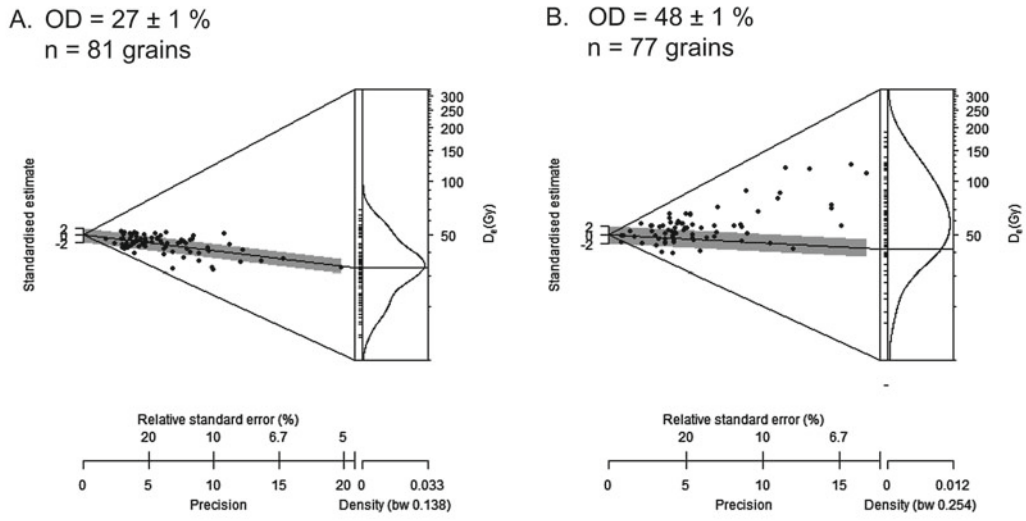

Fig. 8.2 Abanico plots showing example single-grain D_e distributions determined for samples deemed to have been well-bleached (**a**) and partially bleached (**b**) prior to burial in a fluvial setting. Abanico plots (Dietze et al. 2016) are composed of multiple axes and give an indication of the amount of scatter in a D_e distribution. Each datapoint is a D_e value and the value can be read by drawing a line from 0 on the *y*-axis (standardised estimate, $\pm 2\sigma$) through the datapoint to the *z*-axis (D_e). The positioning of the datapoint along the *x*-axis (precision) shows how precisely known the D_e value is (i.e. scale of its uncertainty), where the more precisely known points are towards the right of the graph. The same data is also presented as a probability density function in the plot on the right hand side of the figure. Note that the grey bar shows the D_e value determine for the well-bleached sample using the CAM (**a**) and the partially bleached sample using the MAM (**b**)

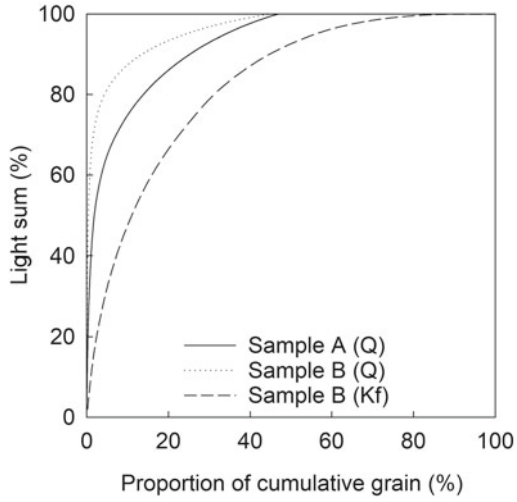

Fig. 8.3 Distribution of luminescence signal intensity emitted by single grains of quartz for samples where the signal intensity distribution between quartz (Q) grains was even (Sample A); where the signal intensity distribution between quartz grains is dominated by a few brighter grains (Sample B). Also shown is the corresponding signal intensity distribution for single grains of K-feldspar for Sample B

OSL analysis (e.g. Thomsen et al. 2015); thus, EMCCDs are not currently used on a routine basis for analysis.

In addition to single-grain analysis, it may also be possible to characterise a partially bleached D_e distribution by analysing multiple-grain aliquots (typically 2 mm in diameter) using light emitting diodes (LEDs), if the OSL signal averaged from all of the grains on the aliquot is dominated by a single grain. This can be the case for some samples (e.g. Fig. 8.3, Sample B), but in certain settings the OSL signal of quartz can be equally distributed across the individual grains (e.g. Fig. 8.3, Sample A) and so more than one grain contributes to the multiple-grain OSL signal. This is often the case during OSL analysis of K-feldspar as the grains are often equally as bright as each other (e.g. Fig. 8.3, Sample B). Where OSL signals are averaged equally across multiple grains and not dominated by a single grain, it can be difficult to characterise the partially bleached D_e distribution (e.g. Trauerstein et al. 2017). This is especially problematic for the minimum dose population as measurements are weighted towards the larger D_e values because they typically emit brighter natural OSL signals than those grains that characterise the minimum dose population. In such cases, many more measurements may be required to characterise the minimum dose population in the partially bleached D_e distribution in comparison with single grains. OSL signal averaging across multiple grains can even be a problem for the pseudo-single-grain measurements where more than one grain is in each hole of a single-grain disc (e.g. Fig. 8.2b), and so microhole measurements should be treated with caution and not assumed to be equivalent to true single-grain measurements (e.g. sample T3DOGM01, Chiverrell et al. 2018).

8.5.2 Calculating Accurate Ages for Partially Bleached Sediments

Sophisticated statistical age models are used to determine OSL ages from partially bleached D_e distributions (see Galbraith and Roberts 2012 for a review). For the majority of partially bleached samples from fluvial settings, an accurate OSL age for the last depositional event will be determined from the well-bleached population in a partially bleached D_e distribution and requires the application of a minimum age model; this includes the minimum age model (MAM; Galbraith and Laslett 1993; Galbraith et al. 1999) or the internal external uncertainty (IEU) model (Thomsen et al. 2007; Smedley 2015). In cases where the D_e distribution contains multiple, distinct populations (e.g. bimodal), the finite mixture model (FMM; Galbraith and Green 1990) would need to be applied to determine ages from those discrete populations (e.g. Rodnight et al. 2006). Bailey and Arnold (2006) provide a decision tree which can be used to determine the most appropriate age model to apply for a given D_e distribution. The number of D_e values needed to fully characterise a partially bleached D_e distribution and calculate an accurate using the

MAM or FMM will depend on the extent of bleaching prior to burial. Rodnight (2006) shows that a minimum of 50 D_e values should be used as a working population. However, this is not fixed and may vary between samples.

Overdispersion quantifies the amount of scatter in a D_e distribution. To determine accurate OSL ages using the MAM, FMM and IEU models, we must be able to quantify the amount of overdispersion that would be expected in the same D_e distribution had the sediment been well-bleached prior to burial, instead of partially bleached. This allows us to identify the well-bleached part of the partially bleached D_e distribution and determine an age based on those grains that were well-bleached prior to burial. For the MAM and FMM, this is quantified by the σ_b parameter, and for the IEU model, it is quantified by the relative values of a and b. Accurately quantifying the values of σ_b (MAM, FMM) and a and b (IEU model) are important for calculating accurate OSL ages, and even small changes can have a large impact upon the age determined (e.g. Fig. 8.4).

The extent of bleaching in nature prior to burial is currently thought to be the most dominant control upon overdispersion in D_e distributions. However, scatter can also be introduced into a D_e distribution from a number of sources, which need to be considered when quantifying σ_b (MAM, FMM) or a and b (IEU model). The most ideal approach to quantify σ_b is to estimate it from the total overdispersion in the D_e distribution of a well-bleached sample from the same site (Galbraith and Roberts 2012) sourced from similar bedrock. However, this is not always possible and so alternatively we can quantify and combine in quadrature the overdispersion arising from the intrinsic and extrinsic sources (after Thomsen et al. 2005). For multiple-grain measurements, sources of overdispersion are limited to the intrinsic luminescence characteristics of the grains, which include a contribution from instrumental reproducibility during OSL analysis (Thomsen et al. 2005). The overdispersion arising from intrinsic luminescence characteristics is typically determined from dose-recovery experiments, which is performed on grains that have fully reset OSL signals and have been given a known beta dose (Murray and Wintle 2000). If the known beta dose can be recovered within ±10%, the protocol used for analysis is appropriate for the sample, and the scatter in the single-grain D_e values determined provides an estimate of the intrinsic overdispersion. Previous studies have shown that the intrinsic overdispersion of single grains of quartz varies between samples, and so sample-specific dose-recovery measurements were performed to quantify the intrinsic overdispersion for σ_b (e.g. Smedley et al. 2017a, b; Chiverrell et al. 2018).

For single-grain measurements, overdispersion in a D_e distribution determined for a natural sample also includes the effects of microdosimetry, but is difficult to quantify. Environmental dose-rates are routinely determined from bulk and homogenous samples taken from the sediment matrix, whereas D_e values are determined from individual grains from a sub-sample of the bulk material. Thus, the bulk estimation of the environmental dose-rate cannot quantify or account for any microscale heterogeneity in the environmental dose-rate to individual grains throughout burial; this is termed microdosimetry. Etching of the grain surface during sample preparation removes the alpha-influenced outer portion of the grain used for analysis, while the

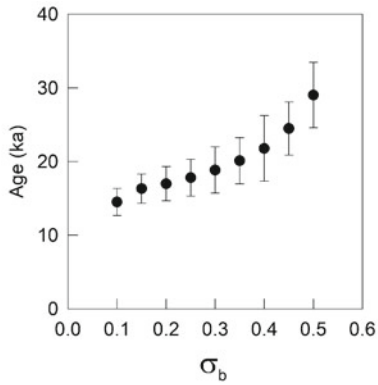

Fig. 8.4 OSL ages calculated using the MAM D_e value plotted as a function of the σ_b used for the D_e calculations for the partially bleached sample shown in Fig. 8.1b, which is an example of a partially bleached sediment from a fluvial setting

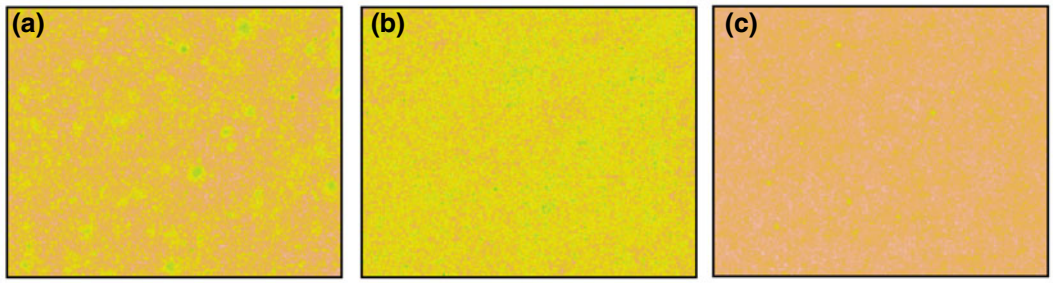

Fig. 8.5 Autoradiography images showing the beta dose heterogeneity in three different samples: **a** high, heterogeneous beta dose-rate; **b** high, homogeneous beta dose-rate; and a **c** low, heterogeneous beta dose-rate. The autoradiographs shown here were corrected for the background signal, normalised to 1 h exposure time and aggregated to 200 μm^2 pixels

effective ranges of gamma and cosmic rays are greater than the size of an individual quartz grain ($\sim$200 µm). Thus, it is only the external beta dose-rate arising from either K, Rb, U and Th that causes microscale heterogeneities in the dose-rate, where beta particles are deposited as a non-linear function of distance from the point source (i.e. a K-feldspar or zircon grain). Autoradiographs of three samples with different extents of beta dose-heterogeneity are shown in Fig. 8.5 as examples. Beta dose-heterogeneity is likely to have a greater influence on single-grain D_e distributions determined from quartz in comparison to K-feldspar as quartz grains are internally inert (e.g. Jacobs et al. 2006). Therefore, all of the environmental dose-rate for quartz is from external sources of K, Rb, U and Th, whereas K-feldspar has an additional internal dose-rate that typically accounts for $\sim$30% of the environmental dose-rate (e.g. Smedley et al. 2012, 2016).

Many studies have suggested that the uneven distribution of K within the sediment matrix can cause heterogeneities in the beta dose-rate and results in scatter in D_e distributions determined using single grains of quartz (Mayya et al. 2006; Nathan et al. 2003; Guerin et al. 2015; Jankowski and Jacobs 2018). Additional overdispersion of 20% was incorporated into the σ_b value when using the MAM for OSL dating of single grain of quartz from glaciofluvial sediments to account for the effects of microdosimetry (Smedley et al. 2017b; Chiverrell et al. 2018; Glasser et al. 2018); this was based on the amount of overdispersion in related well-bleached sediments after the removal of intrinsic luminescence characteristics (Smedley et al. 2017b). The use of an additional overdispersion of 20% incorporated into σ_b for determining accurate OSL ages for these samples was supported by the excellent agreement between the OSL ages and independent age control provided by the cosmogenic nuclide dating (Smedley et al. 2017b).

Single-grain D_e distributions of K-feldspar have two potential sources of overdispersion in addition to intrinsic luminescence characteristics and microdosimetry that are not characteristic of quartz: (1) internal dose-rates and (2) anomalous fading. Studies have used geochemical measurements of single grains of K-feldspar and demonstrated that there is variability between grains in the internal dose-rates of samples caused by internal K-contents (e.g. Smedley et al. 2012; Trauerstein et al. 2012; Gaar et al. 2014), U and Th (Smedley and Pearce 2016). The overdispersion that arises from this variability in the internal dose-rates has been estimated at $\sim$10% (Smedley and Pearce 2016) and should be incorporated into σ_b to account for the scatter that will be in the well-bleached part of the partially bleached D_e distribution. Variability in the anomalous fading rates of single grains of K-feldspar also has the potential to introduce scatter into a single-grain D_e distribution, which is reflected by the larger overdispersion values that are often reported for the IR_{50} signal in

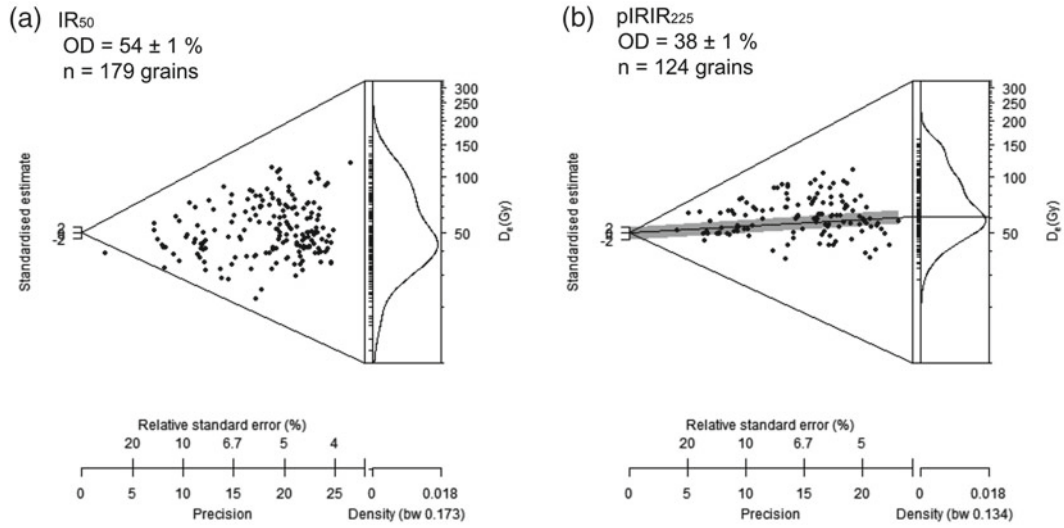

Fig. 8.6 Abanico plots of single-grains of K-feldspar determined using the **a** IR_{50} and **b** $pIRIR_{225}$ signal for the same sample

comparison to the pIRIR signal for the same sample (e.g. Trauerstein et al. 2012; Smedley et al. 2016). Figure 8.6 shows an example of a sample where the single-grain D_e distributions determined using the IR_{50} and $pIRIR_{225}$ signal determined overdispersion values of 54 and 38%, respectively. This suggests that additional overdispersion of 38% (when subtracted in quadrature) is potentially introduced by anomalous fading into single-grain D_e distributions using the IR_{50} signal and should be considered when quantifying σ_b values (MAM, FMM) and a and b values (IEU) when performing single-grain dating of K-feldspars using the IR_{50} signal.

8.6 New Techniques: Luminescence Dating of Rocks

New luminescence dating techniques using rock slices from cobbles and boulders have highlighted the potential for constraining sediment deposition in partially bleached environments such as fluvial systems. Sohbati et al. (2012) developed the use of rock slices taken from boulders for determining surface exposure ages using luminescence dating techniques, which built upon initial research which demonstrated that exposure to sunlight could reset the OSL signal at depths within rocks (e.g. Habermann et al. 2000; Polikreti et al. 2002, 2003; Sohbati et al. 2011; Vafiadou et al. 2007). Depth profiles of the luminescence signal into the rock surface are determined by drilling cores (typically ~2 mm deep) using a water-cooled, diamond-tipped drill bit (typically of diameter ~7–10 mm) and then slicing them at intervals with a diamond-tipped blade (typically ~0.4–1 mm thick); this method has been used to constrain the surface exposure ages of rockfalls (Sohbati et al. 2012; Chapot et al. 2012), glacial boulders (e.g. Lehmann et al. 2018) and archaeological sites (Freiesleben et al. 2015). It was shown that the luminescence depth profiles could record multiple exposure/burial cycles within them (Freiesleben et al. 2015), which led workers to develop the use of rocks for burial dating similar to the approach currently used for dating silt and sand grains (Jenkins et al. 2018; Rades et al. in press). Studies have since provided accurate ages in agreement with independent age control to demonstrate the accuracy of these new techniques (e.g. Jenkins et al. 2018; Lehmann

et al. 2018). Further studies investigating the optical bleaching properties of different lithologies at depth have shown that the light attenuation into the rock is controlled by the mineral opacity (Ou et al. in press; Meyer et al. 2018), where light passes more efficiently through lighter-coloured rocks and should be targeted for OSL dating of rocks (Ou et al. in press). Continued development of this technique has also led to the use of OSL-surface exposure dating paired with cosmogenic nuclide dating for reconstructing erosion rates on centennial to millennial scales which is otherwise not possible with current techniques (e.g. Sohbati et al. 2018). The new luminescence dating techniques using rock slices offer excellent potential for expanding the application of OSL dating in sedimentary environments, especially gravel-bed river systems, but also for constraining novel depositional processes (e.g. erosion rates) via surface exposure dating.

8.7 Conclusion

Optically stimulated luminescence (OSL) dating is a versatile technique that utilises the two most ubiquitous minerals on Earth (quartz or K-feldspar) and is well-suited to constraining the timing of sediment deposition in fluvial settings important for understanding the rates and magnitude of sedimentary processes and events. Continuing technical developments facilitate the determination of accurate and precise ages and provide the potential for analysing new materials, which includes the use of cobbles and boulders for both burial and exposure dating. Although a surprising number of sedimentary samples from fluvial settings are deemed to have been well-bleached prior to burial, OSL dating in fluvial settings can be characterised by partial bleaching of the OSL signal of individual grains. Partial bleaching can occur where the potential for sunlight exposure is limited and so only a portion of the grains in the sedimentary sample were exposed to sunlight prior to burial, especially where grains are transported in sediment-laden, turbulent or deep water columns that have greater attenuation of sunlight. Little is known about the physical processes of OSL signal resetting in water in the natural environment, and there are contrasting reports over whether coarser (sand) or finer (silt) grainsizes bleach preferentially in a fluvial system; this likely reflects the complex sedimentary processes occurring in such settings that may lead to the differential bleaching of grainsizes and minerals.

The effects of partial bleaching in the natural environment may seem challenging for OSL dating in comparison to the well-bleached sediments, but in fact, it can be easily identified and overcome to determine accurate ages. OSL analysis on multiple grains can provide accurate ages for partially bleached sediments where the OSL signal intensity is dominated by a single brighter grain, but will overestimate the age where the OSL signal intensity is equally as bright (often typical of K-feldspar grains) or as dim (sometimes typical of quartz grains). In such settings, it is important to identify partial bleaching and the minimum dose population that was well-bleached during the last depositional cycle; this is possible by analysing single grains and applying an appropriate statistical age models e.g. the MAM, FMM or IEU model. To determine accurate OSL ages using these age models, it is important to quantify the amount of scatter (or overdispersion) in the well-bleached part of the partially bleached D_e distribution, referred to as σ_b for the MAM and FMM, and a and b values for the IEU model. This can be quantified from the total overdispersion in the D_e distribution of a well-bleached sample from the same site sourced from similar bedrock, or where this is not possible, can be combined in quadrature from the overdispersion arising from the intrinsic and extrinsic sources. For quartz grains, these sources are limited to the intrinsic luminescence characteristics, instrument reproducibility and microdosimetry, but for K-feldspar grains, this may also include the overdispersion arising from anomalous fading and internal dose-rates. By using these approaches, OSL dating can provide ages in excellent agreement with independent age control from sedimentary samples across many fluvial settings.

References

Arnold LJ, Roberts RG (2009) Stochastic modelling of multi-grain equivalent dose (D_e) distributions: implications for OSL dating of sediment mixtures. Quat Geochronol 4:204–230

Bailey RM, Arnold LJ (2006) Statistical modelling of single grain quartz D_e distributions and an assessment of procedures for estimating burial dose. Quatern Sci Rev 25:2475–2502

Bailey RM, Singarayer JS, Ward S et al (2003) Identification of partial resetting using D_e as a function of illumination time. Radiat Meas 37:511–518

Burow C, Kehl M, Hilgers A et al (2015) Luminescence dating of fluvial deposits in the rock shelter of Cueva Antón, Spain. Geochronometria 42:107–125

Buylaert JP, Murray AS, Thomsen KJ et al (2009) Testing the potential of an elevated temperature IRSL signal from K-feldspar. Radiat Meas 44:560–565

Chamberlain EL, Wallinga J, Reimann T et al (2017) Luminescence dating of delta sediments: novel approaches explored for the Ganges-Brahmaputra-Meghna delta. Quat Geochronol 41:97–111

Chapot MS, Sohbati R, Murray AS et al (2012) Constraining the age of rock art by dating a rockfall event using sediment and rock-surface luminescence dating techniques. Quat Geochronol 13:18–25

Chiverrell RC, Smedley RK, Small D et al (2018) Ice margin oscillations during deglaciation of the Northern Irish Sea Basin. J Quat Sci 33:739–762

Colarossi D, Duller GAT, Roberts HM et al (2015) Comparison of paired quartz OSL and feldspar post-IR IRSL dose distributions in poorly bleached fluvial sediments from South Africa. Quat Geochronol 30:233–238

Dietze M, Kreutzer S, Burow C et al (2016) The abanico plot: visualising chronometric data with individual standard errors. Quat Geochronol 31:12–18

Duller GAT (2008) Luminescence dating: guidelines on luminescence dating in archaeology. English Heritage report, Swindon

Duller GAT, Bøtter-Jensen L, Murray AS et al (1999) Single grain laser luminescence (SGLL) measurements using a novel automated reader. Nucl Instrum Methods Phys Res, Sect B 155:506–514

Durcan JA, Thomas DSG, Gupta S et al (in press) Holocene landscape dynamics in the Ghaggar-Hakra palaeochannel region at the northern edge of the Thar Desert, northwest India. Quat Int. https://doi.org/10.1016/j.quaint.2017.10.012

Fan YX, Zhao H, Chen FH (2010) The equivalent dose of different grain size quartz fractions from lakeshore sediments in the arid region of north China. Quat Geochronol 5(2–3):205–211

Freiesleben T, Sohbati R, Murray AS et al (2015) Mathematical model quantifies multiple daylight exposure and burial events for rock surfaces using luminescence dating. Radiat Meas 81:16–22

Fuchs M, Straub J, Zöller L (2005) Residual luminescence signals of recent river flood sediments: a comparison between quartz and feldspar of fine-and coarse-grain sediments. Ancient Tl 23(1):25–30

Gaar D, Lowick SE, Preusser F (2014) Performance of different luminescence approaches for the dating of known-age glaciofluvial deposits from northern Switzerland. Geochronometria 41:65–80

Galbraith RF, Green PF (1990) Estimating the component ages in a finite mixture. Nucl Tracks Radiat Meas 17:197–206

Galbraith RF, Laslett GM (1993) Statistical models for mixed fission track ages. Int J Radiat Appl Instrum Part D Nucl Tracks Radiat Meas 21:459–470

Galbraith RF, Roberts RG (2012) Statistical aspects of equivalent dose and error calculation and display in OSL dating: an overview and some recommendations. Quat Geochronol 11(1):27

Galbraith RF, Roberts RG, Laslett GM et al (1999) Optical dating of single and multiple grains of quartz from Jinmium rock shelter, northern Australia: part I, experimental design and statistical models. Archaeometry 41:339–364

Giosan L, Clift PD, Macklin MG et al (2012) Fluvial landscapes of the Harappan civilization. Proc Natl Acad Sci 109:E1688–E1694

Glasser NF, Davies JR, Hambrey MJ et al (2018) Late Devensian deglaciation of south-west Wales from luminescence and cosmogenic isotope dating. J Quat Sci 33(7):804–818

Gliganic LA, Cohen TJ, Meyer M et al (2017) Variations in luminescence properties of quartz and feldspar from modern fluvial sediments in three rivers. Quat Geochronol 41:70–82

Godfrey-Smith DI, Huntley DJ, Chen WH (1988) Optical dating studies of quartz and feldspar sediment extracts. Quatern Sci Rev 7:373–380

Gray HJ, Mahan SA (2015) Variables and potential models for the bleaching of luminescence signals in fluvial environments. Quatern Int 362:42–49

Gray HJ, Tucker GE, Mahan SA (2018) Application of a luminescence-based sediment transport model. Geophys Res Lett 45:6071–6080

Guerin G, Jain M, Thomsen KJ et al (2015) Modelling dose rate to single grains of quartz in well-sorted sand samples: the dispersion arising from the presence of potassium feldspars and implications for single grain OSL dating. Quat Geochronol 27:52–65

Habermann J, Schilles T, Kalchgruber R et al (2000) Steps towards surface dating using luminescence. Radiat Meas 32:847–851

He Z, Long H, Yang L et al (2019) Luminescence dating of a fluvial sequence using different grain size fractions and implications on Holocene flooding activities in Weihe Basin, central China. Quat Geochronol 49:123–130

Huntley DJ, Lamothe M (2001) Ubiquity of anomalous fading in K-feldspars and the measurement and correction for it in optical dating. Can J Earth Sci 38:1093–1106

Huntley DJ, Godfrey-Smith DI, Thewalt MLW (1985) Optical dating of sediments. Nature 313:105–107
Jacobs Z, Duller GAT, Wintle AG et al (2006) Extending the chronology of deposits at Blombos Cave, South Africa, back to 140 ka using optical dating of single and multiple grains of quartz. J Hum Evol 51:255–273
Jankowski NR, Jacobs Z (2018) Beta dose variability and its spatial contextualisation in samples used for optical dating: an empirical approach to examining beta microdosimetry. Quat Geochronol 44:23–37
Jenkins GTH, Duller GAT, Roberts HM et al (2018) A new approach for luminescence dating glaciofluvial deposits—high precision optical dating of cobbles. Quatern Sci Rev 192:263–273
Jerlov NG (1970) Light: general introduction. In: Kinne O (ed) Marine ecology. Wiley, New York, pp 95–102
Kars RH, Wallinga J, Cohen KM (2008) A new approach towards anomalous fading correction for feldspar IRSL dating—tests on samples in field saturation. Radiat Meas 43:786–790
Kim JC, Chang TS, Ti S, Hong SS, Nahm WH (2015) OSL dating of coastal sediments from the southwestern Korean Peninsula: a comparison of different size fractions of quartz. Quatern Int 384:82–90
Kolb T, Fuchs M (2018) Luminescence dating of pre-Eemian (pre-MIS 5e) fluvial terraces in Northern Bavaria (Germany)—benefits and limitations of applying a pIRIR225-approach. Geomorphology 321:16–32
Kronborg C (1983) Preliminary results of age determination by TL of interglacial and interstadial sediments. PACT 9:595–606
Lapp T, Kook M, Murray AS et al (2015) A new luminescence detection and stimulation head for the Risø TL/OSL reader. Radiat Meas 81:178–184
Lehmann B, Valla P, King GE et al (2018) Investigation of OSL surface exposure dating to reconstruct post-LIA glacier fluctuations in the French Alps (Mer de Glace, Mont Blanc massif). Quat Geochronol 44:63–74
Lyons R, Tooth S, Duller GAT (2013) Chronology and controls of donga (gully) formation in the upper Blood River catchment, KwaZulu-Natal, South Africa: evidence for a climatic driver of erosion. The Holocene 23:1875–1887
Lyons R, Tooth S, Duller GAT (2014) Late Quaternary climatic changes revealed by luminescence dating, mineral magnetism and diffuse reflectance spectroscopy of river terrace palaeosols: a new form of geoproxy data for the southern African interior. Quatern Sci Rev 95:43–59
Mayya YS, Morthekai P, Murari MK et al (2006) Towards quantifying beta microdosimetric effects in single-grain quartz dose distribution. Radiat Meas 41:1032–1039
Medialdea A, Thomsen KJ, Murray AS et al (2014) Reliability of equivalent-dose determination and age-models in the OSL dating of historical and modern palaeoflood sediments. Quat Geochronol 22:11–24
Meyer MC, Gliganic LA, Jain M et al (2018) Lithological controls on light penetration into rock surfaces—implications for OSL and IRSL surface exposure dating. Radiat Meas. https://doi.org/10.1016/j.radmeas.2018.03.004
Murray AS, Wintle AG (2000) Luminescence dating of quartz using an improved single-aliquot regenerative-dose protocol. Radiat Meas 32:57–73
Nathan RP, Thomas PJ, Jain M et al (2003) Environmental dose rate heterogeneity of beta radiation and its implications for luminescence dating: Monte Carlo modelling and experimental validation. Radiat Meas 37:305–313
Olley J, Caitcheon G, Murray AS (1998) The distribution of apparent dose as determined by optically stimulated luminescence in small aliquots of fluvial quartz: implications for dating young sediments. Quatern Sci Rev 17:1033–1040
Ou XJ, Roberts HM, Duller GAT et al (in press) Attenuation of light in different rock types and implications for rock surface luminescence dating. Radiat Meas. https://doi.org/10.1016/j.radmeas.2018.06.027
Polikreti K, Michael CT, Maniatis Y (2002) Authenticating marble sculpture with thermoluminescence. Ancient TL 20:11–18
Polikreti K, Michael CT, Maniatis Y (2003) Thermoluminescence characteristics of marble and dating of freshly excavated marble objects. Radiat Meas 37:87–94
Rades EF, Sohbati E, Luthgens C et al (in press) First luminescence-depth pro files from boulders from moraine deposits: insights into glaciation chronology and transport dynamics in Malta valley, Austria. Radiat Meas. https://doi.org/10.1016/j.radmeas.2018.08.011
Reimann T, Tsukamoto S (2012) Dating the recent past (<500 years) by post-IR IRSL feldspar—examples from the North Sea and Baltic Sea coast. Quat Geochronol 10:180–187
Reimann T, Tsukamoto S, Naumann M et al (2011) The potential of using K-rich feldspars for optical dating of young coastal sediments—a test case from Darss-Zingst peninsula (southern Baltic Sea coast). Quat Geochronol 6:207–222
Reimann T, Notenboom PD, De Schipper MA et al (2015) Testing for sufficient signal resetting during sediment transport using a polymineral multiple-signal luminescence approach. Quat Geochronol 25:26–36
Rittenour TM (2008) Luminescence dating of fluvial deposits: applications to geomorphic, palaeoseismic and archaeological research. Boreas 37(4):613–635
Roberts HM (2012) Testing post-IR IRSL protocols for minimising fading in feldspars, using Alaskan loess with independent chronological control. Radiat Meas 47:716–724
Rodnight H (2006) How many equivalent dose values are needed to obtain a reproducible distribution? Ancient TL 26:3–8

Rodnight H, Duller GAT, Wintle AG et al (2006) Assessing the reproducibility and accuracy of optical dating of fluvial deposits. Quat Geochronol 1:109–120

Sanderson DCW, Bishop P, Stark M et al (2007) Luminescence dating of canal sediments from Angkor Borei, Mekong Delta, Southern Cambodia. Quat Geochronol 2:322–329

Shen Z, Mauz B (2012) Optical dating of young deltaic deposits on a decadal time scale. Quat Geochronol 10:110–116

Shen Z, Törnqvist TE, Autin WJ et al (2012) Rapid and widespread response of the Lower Mississippi River to eustatic forcing during the last glacial-interglacial cycle. GSA Bull 124(5–6):690–704

Shen Z, Törnqvist TE, Mauz B et al (2015) Episodic overbank deposition as a dominant mechanism of floodplain and delta-plain aggradation. Geology 43 (10):875–878

Smedley RK (2015) A new R function for the Internal External Uncertainty (IEU) model. Ancient TL 33: 16–21

Smedley RK, Pearce NJG (2016) Internal U and Th concentrations of K-feldspar grains: implications for luminescence dating. Quat Geochronol 35:16–25

Smedley RK, Duller GAT, Pearce NJG et al (2012) Determining the K-content of single grains of K-feldspar for luminescence dating. Radiat Meas 47:790–796

Smedley RK, Duller GAT, Roberts HM (2015) Assessing the bleaching potential of the post-IR IRSL signal for individual K-feldspar grains: implications for single-grain dating. Radiat Meas 79:33–42

Smedley RK, Glasser NF, Duller GAT (2016) Luminescence dating of glacial advances at Lago Buenos Aires (~46°S), Patagonia. Quatern Sci Rev 134:59–73

Smedley RK, Chiverrell RC, Burke MJ et al (2017a) Internal dynamics condition millennial-scale oscillations of a retreating ice stream margin. Geology 45:787–790

Smedley RK, Scourse J, Small D et al (2017b) New ages constraints for the southern limit of the British-Irish ice sheet on the Isles of Scilly. J Quat Sci 32:48–62

Sohbati R, Murray AS, Jain M et al (2011) Investigating the resetting of OSL signals in rock surfaces. Geochronometria 38:249–258

Sohbati R, Murray AS, Chapot MS et al (2012) Optically stimulated luminescence (OSL) as a chronometer for surface exposure dating. J Geophys Res Solid Earth 117(B9). https://doi.org/10.1029/2012jb009383

Sohbati R, Liu J, Jain M et al (2018) Centennial-to millennial-scale hard rock erosion rates deduced from luminescence-depth profiles. Earth Planet Sci Lett 493:218–230

Stokes S, Bray HE, Blum MD (2001) Optical resetting in large drainage basins: tests of zeroing assumptions using single-aliquot procedures. Quatern Sci Rev 20 (5–9):879–885

Thiel C, Buylaert JP, Murray A et al (2011) Luminescence dating of the Stratzing loess profile (Austria)—testing the potential of an elevated temperature post-IR IRSL protocol. Quatern Int 234:23–31

Thomas DSG, Durcan JA, Dansie A et al (2017) Holocene fluvial valley fill sources of atmospheric mineral dust in the Skeleton Coast, Namibia. Earth Surf Proc Land 42:1884–1894

Thompson JA, Chen J, Yang H et al (2018) Coarse-versus fine-grain quartz OSL and cosmogenic 10Be dating of deformed fluvial terraces on the northeast Pamir margin, northwest China. Quat Geochronol 46:1–15

Thomsen KJ, Murray AS, Bøtter-Jensen L (2005) Sources of variability in OSL dose measurements using single grains of quartz. Radiat Meas 39:47–61

Thomsen KJ, Murray AS, Bøtter-Jensen L et al (2007) Determination of burial dose in incompletely bleached fluvial samples using single grains of quartz. Radiat Meas 42:370–379

Thomsen KJ, Murray AS, Jain M et al (2008) Laboratory fading rates of various luminescence signals from feldspar-rich sediment extracts. Radiat Meas 43: 1474–1486

Thomsen KJ, Kook TM, Murray AS et al (2015) Single-grain results from an EMCCD-based imaging system. Radiat Meas 81:185–191

Trauerstein M, Lowick S, Presser F et al (2012) Exploring fading in singlegrain feldspar IRSL measurements. Quat Geochronol 10:327–333

Trauerstein M, Lowick S, Preusser F et al (2017) Testing the suitability of dim sedimentary quartz from northern Switzerland for OSL burial dose estimation. Geochronometria 44:66–76

Truelsen JL, Wallinga J (2003) Zeroing of the OSL signal as a function of grain size: investigating bleaching and thermal transfer for a young fluvial sample. Geochronometria 22(1):e8

Vafiadou A, Murray AS, Liritzis I (2007) Optically stimulated luminescence (OSL) dating investigations of rock and underlying soil from three case studies. J Archaeol Sci 34(10):1659–1669. https://doi.org/10.1016/j.jas.2006.12.004

Wintle AG (1973) Anomalous fading of thermoluminescence in mineral samples. Nature 245:143–144

9 Large Palaeomeanders in Europe: Distribution, Formation Process, Age, Environments and Significance

Jef Vandenberghe and Aleksey Sidorchuk

Abstract

Large palaeomeanders represent a characteristic morphological aspect of many valley floors worldwide. Although the present overview is limited to the European territory, a review of extent, age, geometry and significance in terms of former discharge conditions of large palaeomeanders is timely. Their large size was a function of unusually high river run-off that resulted from specific climate, topography, vegetation and frozen soil conditions. Therefore, their ages and appearances may be variable as a function of geographical position. In addition, the factors that caused the large size of these meanders are discussed. The dimensions of palaeomeanders may be used for discharge reconstructions, but this should be applied with caution, taking into account the different factors that caused the large size of these meanders.

Keywords

Large palaeomeanders · River discharge · Late Pleniglacial · Lateglacial

9.1 Introduction

Inherited fluvial landscapes are often dominated by patterns of large-meandering palaeochannels (including, for instance, large-sized oxbow lakes and point bar series) extending over a great variety of regions and environments. The remnants of large-meandering palaeochannels in modern river valleys are globally a typical characteristic of fluvial morphology. These palaeomeanders often show a well-defined relief and spatial pattern that is clearly visible on remote-sensing images or detailed topographic maps. Apparently, they are not adapted to modern conditions of river discharge. Nevertheless, they have still a significant function in water and sediment transport at high discharges.

Dokuchaev (1878) was one of the first who indicated a discrepancy between the size of present-day rivers and their floodplains. In several cases, the present-day rivers are flowing as narrow bands with smaller-sized meanders within the large-meander belt of former floodplains. These small meanders were called 'underfit' by Davis (1913) and Dury (1954, 1965). Examples are represented in Figs. 9.1, 9.2 and

J. Vandenberghe (✉)
Department of Earth Sciences, Vrije Universiteit, De Boelelaan 1085, 1081HV Amsterdam, The Netherlands
e-mail: jef.vandenberghe@vu.nl

A. Sidorchuk
Geographical Faculty, Moscow State University, Leninskiye Gory 1, 199899 Moscow, Russia
e-mail: aleksey.sidorchuk@geogr.msu.ru

J. Herget and A. Fontana (eds.), *Palaeohydrology*, Geography of the Physical Environment,
https://doi.org/10.1007/978-3-030-23315-0_9

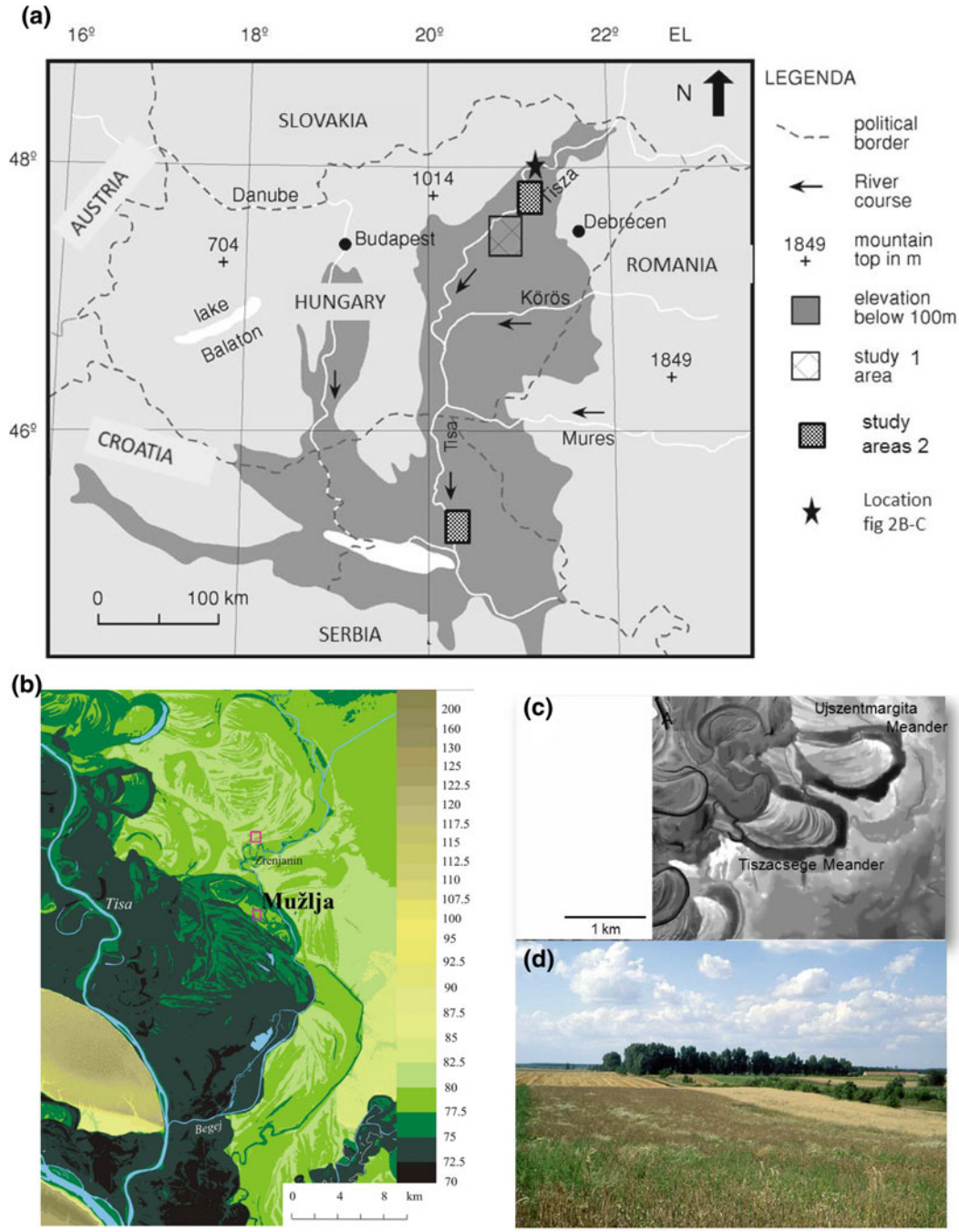

Fig. 9.1 **a** Situation map of the Tis(z)a catchment in the Pannonian Basin (study area 1 refers to Kasse et al. 2010, study area 2 to Vandenberghe et al. 2018); **b** topographic map of the lower Tisa valley near its confluence with the Danube (area 2, Vojvodina, Serbia); **c** air photo from the study areas in the middle Tisza; **d** photo showing ridge and swale topography in the meander bend of Tiszacsege (the middle Tisza; modified after Vandenberghe et al. 2018)

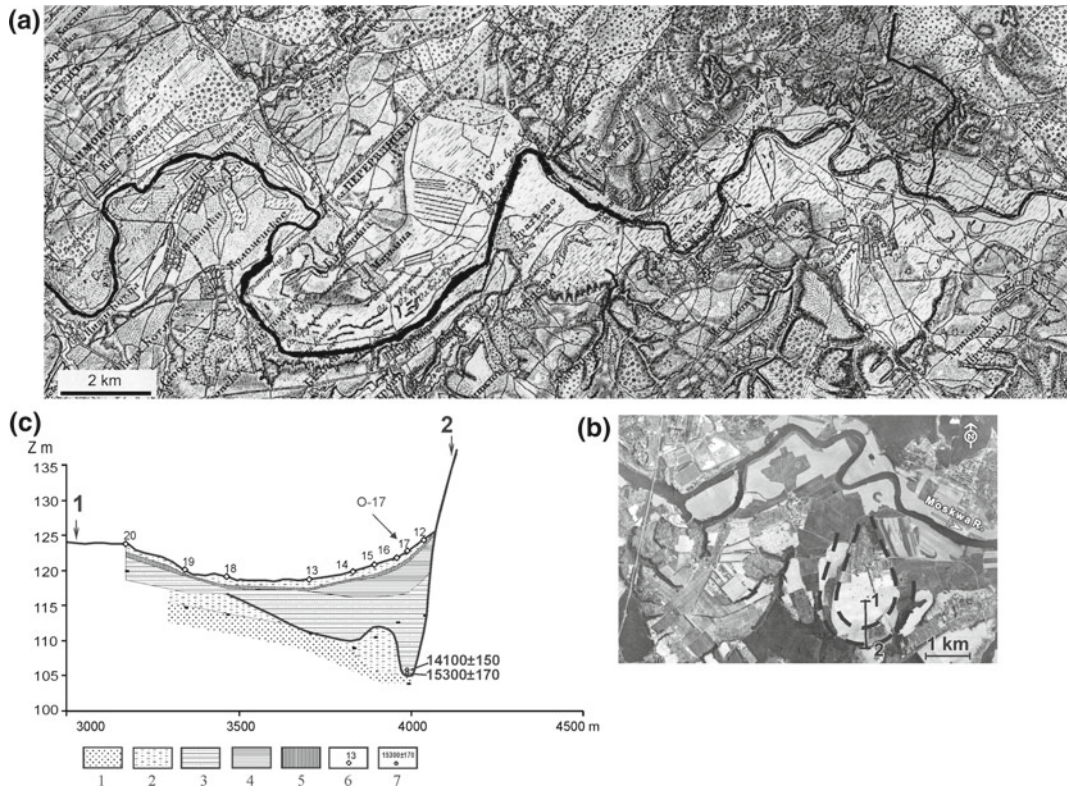

Fig. 9.2 Sequence of macromeanders of the Moskva River as seen on the map of the mid-nineteenth century (**a**) the cored palaeochannel fragment on a satellite image (**b**) and cross-section 1–2 of this palaeochannel (**c**). Keys: (1) sand with gravel; (2) silty sand; (3) silt; (4) clay; (5) loam with peat; (6) core locations with numbers; (7) ^{14}C samples and uncalibrated ^{14}C dates (modified after Sidorchuk et al. 2009)

9.3. Palaeomeander channels are called 'large' since their dimensions are several times larger than their modern equivalents. These characteristics already point to the pre-modern age of most of the large meanders, while their morphological expression suggests a relatively young geological age.

In this contribution, we describe the geometry and age of palaeomeanders by means of a (non-exhaustive) selected number of European cases, from the Atlantic coast to the Ural Mountains. It is striking that large palaeomeanders typically occur in specific periods of the geological history. Some information is added about the environmental conditions in those regions, such as climate, snow and vegetation cover and frozen ground that played a role in the establishment of large-sized meander patterns. We focus further on the potential to derive former palaeohydrological conditions, in particular, by evaluating the relation between meander dimensions and water discharges. We evaluate a number of, mostly empirical, relations which were proposed in the past century for such palaeohydrological reconstructions. We conclude with a discussion on the factors that were responsible for or contributed to the large size of the meander palaeochannels.

9.2 Occurrence and Age of Large Palaeomeanders in Europe

The age of large palaeomeanders has mainly been determined by radiocarbon analyses and pollen stratigraphy of fill deposits in abandoned

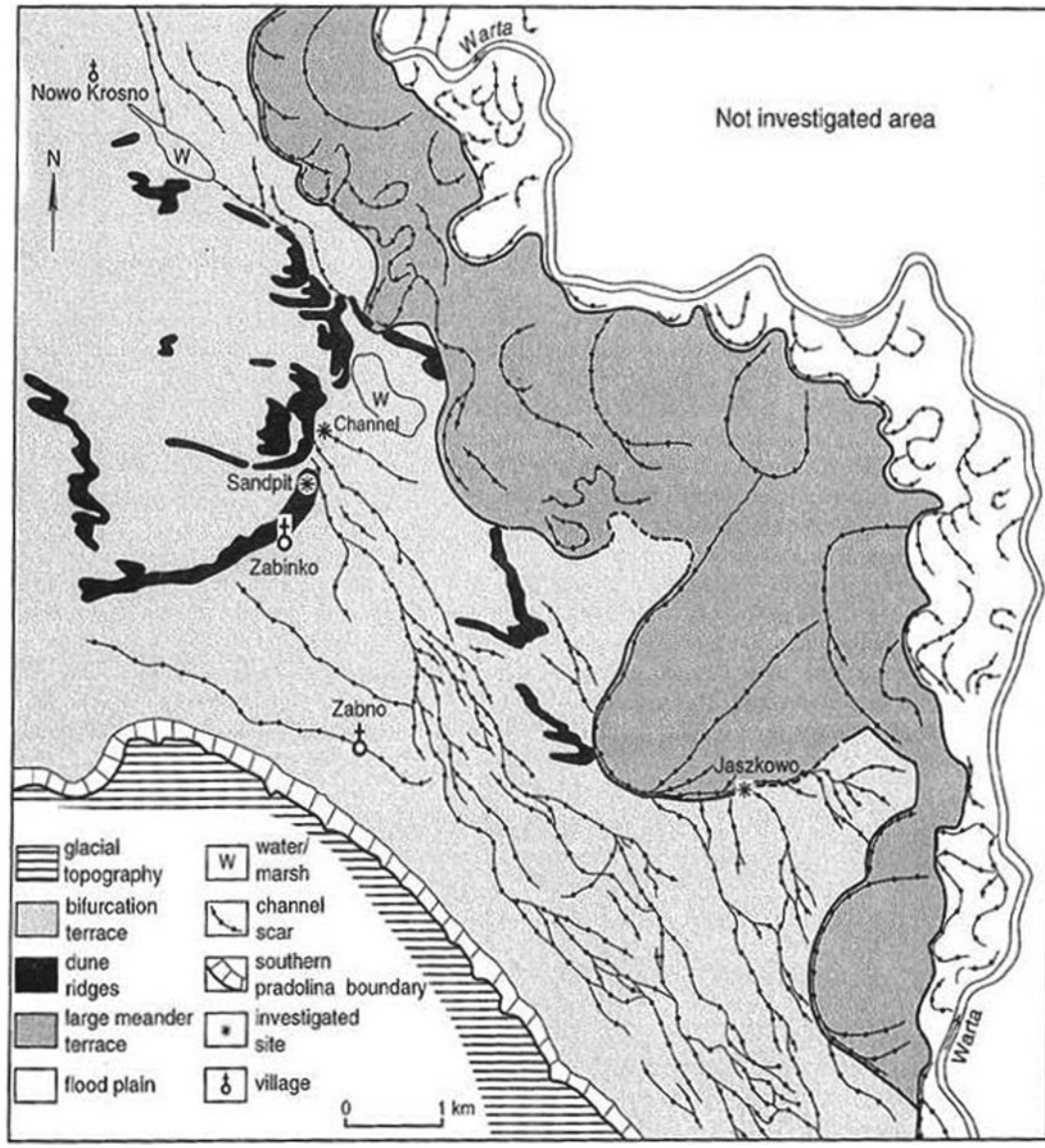

Fig. 9.3 Geomorphology of part of the middle Warta Valley in Poland with the Late Pleniglacial braided (so-called bifurcation) terrace, the Lateglacial large paleomeanders and the small Holocene meanders (modified after Bohncke et al. 1995)

channels, later on supplemented with luminescence dating of sandy point bar deposits. However, it has to be noticed that dating meander formation by the infill of abandoned channels experiences many pitfalls especially in the past studies because of the conventional radiocarbon dating of bulk samples, hard water effect and potential reworking of older deposits. In addition, dating the palaeochannel fill provides minimum ages since hiatuses may be present between the last channel activity and the start of the infill. See a detailed discussion in Kasse et al.

(2000, 2010) and Toonen et al. (2012). All radiocarbon ages in the following text are calibrated unless otherwise reported, or OSL ages.

In the East European Plain, large meanders have been described from the upper Neman and Pripyat Rivers in the west (Byelorussia) to the Ural Mountains in the east (Sidorchuk et al. 2001). This region has not been covered by the last Scandinavian ice sheet (Fig. 9.4). Large palaeomeanders are absent in the Arctic Russia which is situated in the modern permafrost zone. Many palaeorivers had well developed, often omega-like shaped, large meanders which formation lasted at least 1–2,000 years. The age of the large palaeorivers on the East European Plain has only been determined within a few river valleys. A large palaeochannel near Povorino in the Khoper River Valley (Fig. 9.5a, b, nr 1 in Fig. 9.4) was abandoned more than 17 ka ago (Panin et al. 2013). The palaeomeanders on the floodplains of the Seim River (near L'gov, nr. 2 in Fig. 9.4) and Svapa River near its mouth (nr. 3 in Fig. 9.4) were also cut-off from the main channels at about 17 ka ago (Borisova et al. 2006). A large palaeochannel in the Protva Valley (near Borovsk, nr. 4 in Fig. 9.4) was abandoned c. 15–16 ka ago and the palaeochannels of the Samara River (nr. 5 in Fig. 9.4) became inactive at c. 16 ka ago, while a large meander of the Moskva River near Ostrov (Fig. 9.2 and nr. 6 in Fig. 9.4) was cut-off more than 18 ka ago (Sidorchuk et al. 2009). Thus, the formation of large meanders on the East European Plain may be referred to a period between c. 16 and 19 ka calBP, i.e. shortly after LGM and towards the end of the last glacial (end of Pleniglacial).

Large palaeomeanders are also characteristic for Central Europe. They were, for instance, frequently reported from the Polish lowlands and uplands (Szumański 1983; Starkel 1983; Turkowska 1990; Kozarski 1991; Starkel and Gebica 1995; Kalicki 2006; Krupa 2015, and references therein). It was described that a braided pattern existed before the large meanders were formed, until the end of the Pleniglacial as the organic infill of the large meanders has been dated at the beginning of the Bölling. Detailed reconstructions have been made for the Warta by Kozarski (1983), Kozarski et al. (1988) and Bohncke et al. (1995). In the Pannonian Basin (Hungary-Serbia), the wide floodplains of the Danube River and its main tributary, the Tis(z)a River show an intriguing pattern of successive meandering systems with impressive fluvial deposits dating from the last glacial up to the Holocene (Gabris and Nador 2007; Popov et al. 2008; Kasse et al. 2010; Gabris et al. 2012; Vandenberghe et al. 2018). The morphology of a series of large palaeomeanders in a belt along the present-day Tis(z)a is characterized by well-developed point bars with ridge and swale topography and clear sinuous erosive scars, pointing to lateral migration which has often led to neck-cut-offs (Kasse et al. 2010) (Fig. 9.1c). Based on the age of meander fills of this Tis(z)a catchment continuous activity was inferred from at least c. 33–32 ka until 22–17 ka (OSL) while river activity transformed into younger series of progressively smaller (but still large) meanders in the same river belt from c. 19 ka onward until the Lateglacial (Vandenberghe et al. 2018). A similar meandering to anastomosing pattern as in the Tis(z)a catchment was observed by Nowaczinski et al. (2015) in SW Slovakia.

As in the other parts of Europe, the study of large palaeomeanders has a long tradition in the lowlands of N and NW Europe, from Northern Germany to Central France. Both small and large river systems show that braided channels became inactive at the very beginning of the Bölling and were replaced by large-meandering systems (Mol et al. 2000). Examples from small catchments are fluvial systems in Germany (Lipps and Caspers 1990; Urz 2003; Kaiser et al. 2012; Turner et al. 2013) and Northern France (Antoine et al. 2003), the Vecht (Huisink 2000), Dinkel (Van Huissteden 1990) and Mark systems (Vandenberghe et al. 1984, 1987; Vandenberghe and Bohncke 1985) in the Netherlands and its border regions, and the Dijle Valley (De Smedt 1973; Vandenberghe and Woo 2002; Verstraeten et al. 2018) in Belgium. As concerns larger catchments, the Maas and tributaries were synthesized by Kasse et al. (1995, 2005), the Scheldt Valley by Kiden (1991) and Deschodt et al. (2004), while the Seine and Loire systems with

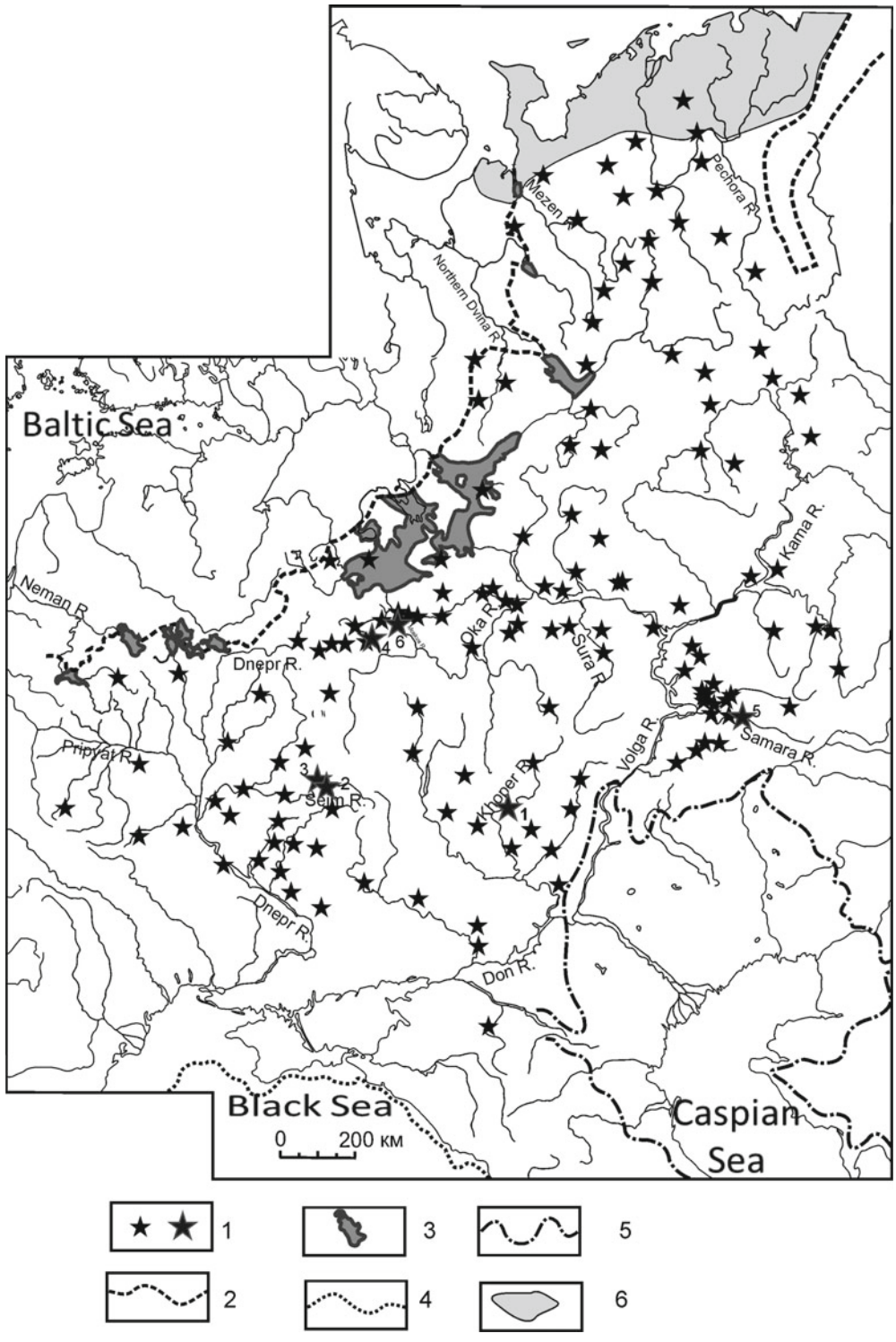

Fig. 9.4 Distribution of the large palaeochannels on the East European Plain about 16–19,000 years ago. Keys: 1: position of the fragments of large paleochannels; 2: southern edge of the last Scandinavian ice sheet; 3: glacial lakes at the edge of the last Scandinavian ice sheet; 4: coastline of the Black Sea at a level of −62 to 67 m; 5: coastline of the Caspian Sea at the maximum of the Khvalynian transgression (shortly after LGM) at a level of +50 m; 6: tundra regions with rare large palaeochannels Numbers on the map refer to the sites described in the text (modified after Sidorchuk et al. 2001)

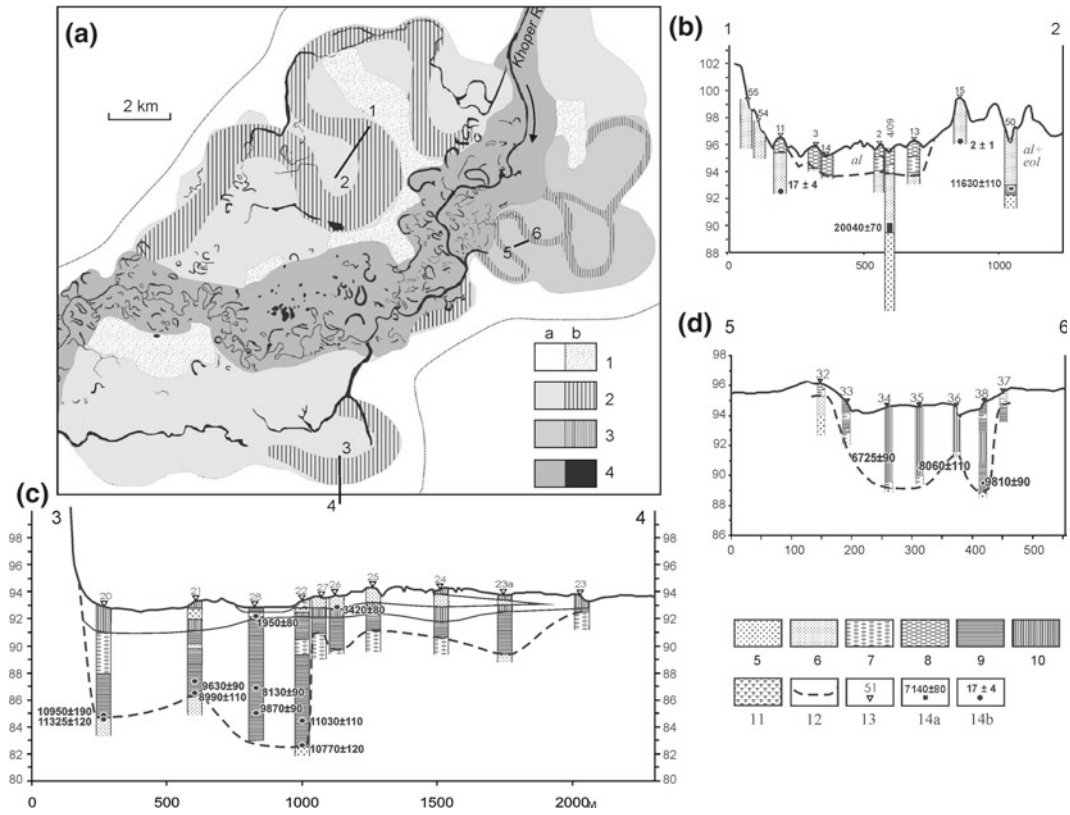

Fig. 9.5 Geomorphological map (**a**) and geological sections (**b**–**d**) across the large-meandering channels of the paleo-Khoper River near Povorino. Keys: 1a—high terraces; 1b—the first terrace above the floodplain; 2a—Late Weichselian floodplain of the first generation; 2b—first generation of large palaeochannels; 3a—Late Weichselian floodplain of the second generation; 3b—second generation of large palaeochannels; 4a—Holocene floodplain; 4b—modern Khoper river channel. Lithology: (5) medium sand, (6) fine sand, (7) silty sand and sandy silt, (8) loam, (9) clay, (10) gyttja, (11) peat; (12) palaeochannel bed; (13) cores, (14a) uncalibrated radiocarbon dates, (14a) TL dates (modified after Panin et al. 2013)

their tributaries in the Paris Basin were studied, for instance, by Pastre et al. (2002, 2003), Castanet (2008) and Morin et al. (2011).

Thus, the age of the beginning of large-meander formation in Central and Western Europe contrasts with the age of that same event in Eastern European and Pannonian catchments which was considerably older. In some cases, the transition from braided to large meandering appeared to be sudden; in other cases, a distinct transitional pattern was observed in contrast to the corresponding abrupt climatic warming. It was demonstrated at first for the Maas River (Vandenberghe et al. 1994; Huisink 1997; Kasse et al. 1995, 2005; Janssens et al. 2012) and confirmed, for instance, for the Warta River (Vandenberghe et al. 1994), the Somme River (Antoine 1997) and the Rhine River (Erkens et al. 2011). This transitional phase developed during the Bölling towards the large-meandering pattern that was generally occurring during the Alleröd and was mostly persisting up to the Younger Dryas. It was considered as a delayed response of the fluvial system to external forcing (i.e. the climate) (Vandenberghe et al. 1994). However, the timing of this transitional phase could also have been earlier: a transitional phase of anabranching between the braided and the single-meandering system occurred already several millennia before the Bölling in catchments

more to the south as, for instance, the Dordogne Valley in Southern France (Bertran et al. 2013). This transitional phase was also recorded in some East European rivers, as in the Khoper River where the cross section of the large palaeochannel bears a similar signal of transformation presumably at the Pleniglacial-Bölling transition before subsequent infilling (Fig. 9.5c; Panin et al. 2013).

Although we restrict our overview to Europe, it is worth mentioning that also in other continents large palaeomeanders were reported at the time of climate warming shortly after LGM, e.g. at 15–16 ka (OSL and cal C^{14}) in relatively low-latitude regions (southeastern USA: Leigh 2006; Suther et al. 2018) but also at LGM and pre-LGM time, i.e. meanders in Australia (Page et al. 1996; Kemp et al. 2017; Müller et al. 2018).

9.3 Climatic Conditions and Vegetation Cover in the Large-Meander Catchments

Apart from climate (precipitation, frost conditions, snow cover), discharge is also a function of the vegetation cover. Vegetation cover is also of utmost importance as a main climatic indicator influencing evapotranspiration and sediment supply to the rivers. Mostly, the archives for vegetation reconstruction consist of palaeobotanical data from the channel fills or floodplains.

Within the East European Plain, palaeobotanical data proved to be sufficient to locate modern geographical analogues to several fossil floras (Borisova et al. 2006; Sidorchuk et al. 2009, 2011). This enabled to estimate climatic characteristics for the period c. 21–16 ka ago at the concerned locations (Table 9.1). The first fossil flora is characteristic for mountain tundra with permafrost. The climate at that time (close to LGM) was cold and dry, while surface run-off was rather high. The second flora association with an age of c. 18.5 ka (which is at the beginning of the so-called Raunis interval, after Savvaitov and Straume 1963) is characterized by sub-alpine and alpine meadows of grass, sedge and forbs, existing next to mountain tundra and open forest with larch and Siberian pine. The climate was cold and humid with high surface run-off at that time. The third palaeoflora, from the optimum of the Raunis interval (c. 17.2 ka ago), corresponds with sparse mountain taiga (pine, birch and Siberian pine forest) which occurred along with wet meadows. The Raunis interval (which is the first relatively mild period shortly after LGM) had a major significance in hydrologic and geomorphologic evolution of the East European Plain. The climatic conditions were relatively mild and wet, with permafrost and high surface run-off. That was the optimum period of large-meander formation on the East European Plain. The fourth fossil flora (end of Raunis interval, c. 16.9 ka ago) is similar to the landscape of present-day south Siberian meadow steppes with patches of larch and pine forest and spruce forest in the river valleys. The climate was cold and semi-arid, but the surface run-off was still rather high. The ancient large lowland rivers developed their channels in the landscapes with periglacial vegetation (mostly tundra with sparse or patchy forest, Velichko 1973), which coincided in general with the area of permafrost occurrence at LGM.

In the Pannonian Basin (Hungary, Slovakia), the Pleniglacial climate was generally somewhat warmer than in NW Europe as suggested by palynological investigations of Willis et al. (1995). The latter authors mention open coniferous forests in refugial areas at the very end of the Pleniglacial (<16 ka). Pollen analyses from an abandoned channel fill of the Tisza river point to a steppe-type vegetation with the local presence of pine trees in the Late Pleniglacial (Kasse et al. 2010). The Lateglacial started with a *Betula* and *Juniperus* phase spreading into a boreal coniferous forest (birch followed by pine) with small amounts of deciduous trees (temperate refugial populations) (Willis et al. 1995; Kasse et al. 2010), an evolution which was very similar to that in northern regions.

A rich literature exists on the reconstruction of the vegetation cover from the late Pleniglacial to Lateglacial in Western Europe reflecting the general temperature and precipitation increase at

Table 9.1 Main climatic indexes in the East European Plain during the period 21–16 ka call BP based on climatic characteristics in the region-analogues, estimated according to the composition of fossil floras (after Borisova et al. 2006; Sidorchuk et al. 2009, 2011)

Ages of fossil floras Ka cal BP	Site names and position of fossil floras in the East European Plain	Region-analogue position and site name	Temperature January (°C)	Δ temperature January (°C)	Temperature July (°C)	Δ temperature July (°C)	Precipitation (mm per year)	Δ precipitation (mm per year)	Runoff depth (mm per year)	Δ Runoff depth (mm per year)
21	Sloboda/ Drichaluki Zapadnaya Dvina River 55° 25′ 41.89″N 30° 44′ 42.63″E	52° 25′ 43.91″N 100° 33′ 45.40″E River Oka valley at headwaters (East Sayany)	−21 to −22	−13 to −14	8 to 10	−7 to −9	400 to 600	−200 to 0	350 to 500	140 to 290
18.5	Moscow Moskwa River 55° 34′ 46.80″N 37° 49′ 24.72″E	51° 5′ 17.27″N 88° 5′ 37.32″E Chulcha-Chylyshman interfluve	−18 to −20	−7 to −9	11 to 13	−5 to −7	850 to 950	350 to 450	440 to 500	210 to 370
17.2	Yudinovo Desna River 52° 40′ 3.78″N 33° 16′ 14.78″E	51° 30′ 12.39″N 87° 30′ 2.24″E Slopes to the west of Teletskoye lake, Altay Mountains	−14 to −18	−5.5 to −9.5	16 to 17	−1.5 to −2.5	700 to 800	125 to 225	500 to 550	350 to 400
16.9	Kudintsevo Seim River 51° 43′ 44.73″N 35° 8′ 45.15″E	51° 47′ 10.37″N 102° 34′ 2.45″E Tunkinskaya lowland	−22 to −26	−14 to −18	15.5 to 16.5	−3.5 to −2.5	425 to 475	−125 to −75	350 to 400	225 to 275

The absolute values of climatic characteristics were taken from climatic maps of the region-analogues, the deviations Δ are the difference between values in the region-analogue and the site with fossil flora

that time. Overviews of the palaeobotany of NW Europe were made, for instance, by Van Geel et al. (1989), Hoek (1997), Bohncke and Vandenberghe (1991) and Pastre et al. (2002) and by Feurdean et al. (2014) for Central and Eastern Europe. Bare surfaces at the end of the Pleniglacial in NW and N Europe were subsequently colonized by herb and shrub tundra from the Bölling onward, and ultimately taiga forest during the Alleröd. Similarly, Tobolski (1988) reported from Poland the immigration of very scarcely distributed plants at the very end of the Pleniglacial (c. 14.7 ka), the establishment of park tundra during the Bölling and forest expansion at the beginning of the Holocene.

9.4 Geometry

Large meanders of the Late Valdaian (∼Weichselian) age (with dimensions up to 15 times the recent ones) occur in the East European Plain (Sidorchuk et al. 2001, 2009). The recent meandering channel of the Khoper River near Povorino is 30–100 m wide with a meander wavelength of 200–1000 m (Fig. 9.5a). The river floodplain is 10–13 km wide here while the youngest floodplain belt, formed by the modern river, is only 1.0–2.5 km wide and follows the recent river channel (Panin et al. 2013; Panin and Matlakhova 2015). The surface of the latter floodplain shows numerous curved natural levees and oxbow lakes. The mean floodplain height is 3–4 m above the low river water level with natural levee tops at 5–5.5 m. The main part of the Khoper River floodplain is formed by much larger meandering channels than the recent ones. The palaeochannel width varies between 200 and 800 m with meander wavelength of 5–7 km. The depth of one palaeochannel, abandoned c. 17–19 ka ago, does not exceed 1.5–3.0 m (Fig. 9.5b); it has rarely been flooded after abandonment so that its former bottom is locally exposed. Another palaeochannel, dating from c. 13 ka onward, is 9–11 m deep (Fig. 9.5c); its pools are now represented by shallow wide troughs and are hardly visible in the floodplain relief. A system of palaeochannels of intermediate size (width of c. 200 m, meander wavelength of c. 2400 m) between Lateglacial and modern channels is preserved (Fig. 9.5d). Macromeanders are very distinct in specific reaches of the Moskva River. Within the reach of Moscow city, a sequence of 18 such macrobends with a mean wavelength of 4400 m was distinguished (Sidorchuk et al. 2009). They are partly transformed by modern river flow. The ratio between the macromeander wavelength and the recent channel width (L/W) is 28 within this reach (see Fig. 9.2), which is significantly larger than the ratio of recent small-meander wavelength to channel width ($L/W = 10$). One more example is the Seim River with palaeomeander wavelengths of 5–6 km and an amplitude of 4 km (Borisova et al. 2006).

The oldest and largest meanders in the Tis(z)a Valley belt have a remarkably large wavelength, although exact determination is difficult. In the Hungarian sector, it is estimated at c. 6–10 km, and in the Serbian sector at c. 10 km, while the palaeochannel is up to 600 m wide and locally more than 14 m deep in Hungary and up to 2 km wide in Serbia (Fig. 9.1). Different generations may be distinguished morphologically in this belt by the successive lateral erosion of previous meander remnants and by progressively decreasing meander wave length (Kasse et al. 2010; Gabris et al. 2012; Vandenberghe et al. 2018). All these palaeomeanders occur approximately at the same topographic level while the younger and considerably smaller Holocene meanders are slightly incised into that level.

In almost all lowland rivers in Western and Northern Europe, there is a similar general decrease in meander dimensions from the Lateglacial to the Holocene. The Warta River in Poland shows large-meander wavelengths of up to 2.5 km, radius of curvature 247 m and width 59 m, while the small (Holocene) meanders have a wavelength of 0.5–0.7 km, radius of curvature of 141 m and width of 45 m (Kozarski 1983; Vandenberghe et al. 1994). The Lateglacial Czarna Nida River in the Polish uplands has a radius of curvature of c. 120 m and a width of 40 m for their large palaeomeanders in comparison with several tens of m wavelength and c. 10–20 m width for the Holocene rivers (Krupa

2015). In the Netherlands, the large palaeomeanders of the Maas River have a wavelength of 2.2–5 km, depth up to 7.5 m and width of c. 125 m (Kasse et al. 1995).

9.5 Relationships Between River Plan Geometry and Discharge

The relationships between river channel plan geometry and flow discharge have been used traditionally for palaeohydrological reconstruction. This widely applied approach dates from the middle of the twentieth century. A most simple equation relates channel width W and flow discharge Q:

$$W = kQ^b. \tag{9.1}$$

Leopold and Maddock (1953) found that channel width increases down the channel in proportion to the square root of discharge, thus $b = 0.5$ in Eq. 9.1. This equation was used in palaeohydrological investigations by Volkov (1960) and Dury (1954, 1965) who replaced channel width by meander wavelength. Their investigations led to discouraging results: palaeodischarges of former large rivers were calculated to be 80–100 times larger than those of the corresponding recent rivers. Such estimates were not supported by any other corresponding precipitation reconstruction.

From the mapping of preserved parts of the incised palaeomeanders of the Mark, a small river in the Belgian-Dutch border region, Vandenberghe (1987) found that the Lateglacial wavelengths were c. 4 times larger than their late Holocene equivalents. Using a relation between wavelength (or channel width) and discharge, as for instance in Eq. 9.1 (Leopold and Wolman 1957, 1960), and the ratio of Lateglacial/Holocene wavelengths or river widths enabled Vandenberghe (1987) to reconstruct Lateglacial formative discharges of 10–15 times the Holocene ones. No exact values of modern discharges were calculated as those discharges are artificial now due to river management. This approach included the (bold) assumption that the parameter k in Eq. 9.1 was identical in both periods.

In this respect, we mention also discharge reconstructions for the Tis(z)a river for palaeomeanders with an average wavelength of 6880–7000 m (Popov et al. 2008). Using those values, average discharges calculated by a slightly modified version of Eq. 9.1 (Timár et al. 2005) point to a three to fourfold higher average discharge during post-LGM and Lateglacial times in comparison with Holocene and present-day values (Popov et al. 2008). Such values of a four–fivefold higher discharges were reported by Page et al. (1996) and Kemp et al. (2017) for large palaeomeanders in Australia, although these authors stress also the temporary and brief character of those discharges.

It was recognized by the previous and other examples that Eq. (9.1), which is an empirical formula, is only valid in a specific catchment and for specific periods (Williams 1988; Huang and Nanson 1997). The relations between hydraulic geometry and discharges cannot be generalized as they are in fact also affected by other factors which are specific for each basin as, for instance, the amount and grain size of the transported material (Schumm 1960; Ackers 1982; Suther et al. 2018), bedrock, bank stability and vegetation (Huang et al. 1997 and references therein) and river gradient (Petrovszki et al. 2014; Vandenberghe et al. 2018), and thus reflect a multivariate relationship (Huang et al. 1997). In other words, the parameter k in Eq. 9.1 is regionally and temporarily highly variable. The recognition of the impact of a multitude of regionally dependent variables had the consequence that local conditions of the catchment have to be taken into account (Sidorchuk and Borisova 2000). In other words, palaeohydrological reconstructions have to be limited to temporal comparisons in one specific catchment rather than to intercomparison of catchment discharges. This reduces at least some of the catchment variables. Alternatively, the coefficient k in Formula 9.1 should regionally be specified.

Furthermore, it appears that seasonality plays a major role in the formation of the river's

Table 9.2 Annual water flow from the main river basins in the East European Plain (location see Fig. 9.3) at the last glacial terminus (=LGT), i.e. 19–16 ka

The river basin	Modern characteristics		LGT (calculated)		The ratio V_p/V_m
	Basin area, 10^3 km^2	Flow volume V_m, km^3 a^{-1}	Basin area, 10^3 km^2	Flow volume V_p, km^3 a^{-1}	
The Northern Dvina	357	110	260	115	1.05
Mezen'	78	28	78	45	1.6
Pechora	322	126	322	220	1.7
Upper Volga	291	59	105	77	1.3
Oka and Sura	312	49	312	161	3.3
Kama	507	119	507	225	1.9
Volga mouth	1360	254	1174	500	2.0
Don	422	29	422	110	3.8
Dnepr	504	54	504	166	3.1

geometry. The Lateglacial rivers had certainly larger discharges during spring than at present. It means channel dimensions may have been related to discharges larger than the average ones (Gregory 1976). In this respect, the bankfull width W_b of the Lateglacial meanders has been introduced to reflect the spring discharges Q_{max} rather than the mean annual discharges Q_a applied by Leopold and Maddock (1953) and Dury (1976) in their equations. Therefore, the mean maximum discharge ratio, i.e. the discharge variability within one year, has been initiated in discharge reconstructions. For example, about 700 river sections in drainage basins situated in a variety of landscapes from steppe to tundra from Northern Eurasia were used as modern analogues (Sidorchuk et al. 2001, 2003, 2008). Based on those data, the next empirical relationship has been established:

$$Q_a = 0.012 y^{0.73} W_b^{1.36}, \quad (9.2)$$

$$\text{in which } y = 100 \frac{Q_a}{Q_{max}}. \quad (9.3)$$

Equations (9.2)–(9.3) were used to calculate the mean annual discharges (Q_a) for about 200 sites in large periglacial rivers in the East European Plain, where well-preserved fragments of palaeochannels still persist. These discharges were used to estimate the annual water yields of the main rivers (Table 9.2).

Further, it is often rather difficult to determine accurately the width and meander length of palaeochannels (Rotnicki 1983; Toonen et al. 2012) and also meander radius as suggested by Williams (1988). Together with the limitations described above, equations based on hydraulic geometry resulted in large scatter between predictions and observations. This scatter is ±20% when Formulas (9.2)–(9.3) are used (Sidorchuk et al. 2008). A different method of reconstruction of bankfull discharge was applied by Dury (1965) and later on by Rotnicki (1983, 1991), Gonera and Kozarski (1987) and Sidorchuk and Borisova (2000). It is based on the Chézy-Manning formula and is essentially depending on a derivation of the flow velocity which requires, apart from the hydraulic radius (or bankfull depth), the definition of the Manning roughness coefficient and the river gradient. It should be noted that this approach is also used to estimate bankfull discharges which were considered as 'formative discharges'. The result for the Prosna and Warta Rivers in Poland is a c. fivefold larger bankfull discharge during the formation of the large palaeomeanders in comparison with present-day or Holocene meanders. The same approach for the Khoper River palaeochannel

showed 6.2-fold larger bankfull discharge in comparison with the modern discharge (Sidorchuk and Borisova 2000). It has to be stressed that the use of such flow formulae suffers from a similar problem as the use of empirical relations of hydraulic geometry, namely the exact determination of channel cross section geometry, river gradient and roughness coefficient.

9.6 Discussion

With regard to the importance of local factors in the change of river morphology, it should be emphasized that already in the first studies of underfit rivers, the significance of local factors was put forward. Dokuchaev (1878) argued that the modern underfit rivers of Southern Russia and Ukraine were flowing within ancient lake basins, while Davis (1913) argued that the most probable cause for the underfit Maas River was river piracy. Dury (1954, 1965, 1976) and Volkov (1960) opened the way for the climatic hypothesis of large hydrological changes at global scale, which led to the formation of large meanders during certain periods. But, in this respect we should reject, for instance, the hypothesis that waters from the melting Scandinavian ice sheet should have been the source of the reconstructed high water volumes in the European palaeochannels (Fig. 9.4). The recent reconstruction of the Last Scandinavian ice sheet margin shows that in the East European Plain the Pechora River flow was open to the sea at the time of the maximum ice extent. The ice dam lakes at the Mezen River and the Northern Dvina River mouths were rather small (Zaretskaya et al. 2014). The level of ice dam lakes at the upper Volga River basin was low, and the flow of meltwater flow here was only partly (if any) to the Volga River basin (Sidorchuk et al. 2009). The Don River basin was completely beyond the influence of meltwater flow (Sidorchuk et al. 2011). Only the Upper Dnepr valley received meltwater from the lakes near to the ice sheet, but this flow lasted only until c. 18.5 ka and terminated before the main period of large river activity (Sidorchuk et al. 2011).

Higher annual discharges at the end of the Weichselian Pleniglacial in comparison with the present may have resulted from lower mean temperatures and evapotranspiration. In addition, evaporation was not very high due to the short thawing period, while the annual precipitation at the East European Plain was not less (and may have been higher) at that time than at present (Panin and Sidorchuk 2006; Panin et al. 2011; Sidorchuk 2003; Sidorchuk et al. 2008). The precipitation consisted mostly of snow that accumulated in the river basins during long winters. Higher radiation at that time caused rapid snow melt during spring and subsequent meltwater drainage towards the river network in accordance with the topography. The impact of the latter factor is complex as low relief may have favoured snow melt in short time, but steep slopes may also have favoured relatively high run-off due to the limited time for infiltration. Further, soil infiltration was limited due to annually long-lasting frozen ground or even permafrost. In general, during the summer, water supply to the rivers was relatively small (Sidorchuk et al. 2008) as is also apparent in present-day arctic river hydrographs (Woo 1986). Thus, surface run-off was comparable to that in recent permafrost regions with very high maximum flood discharges and rather low annual/maximum discharge ratio. Consequently, flood volume and maximum discharges in the large palaeomeanders of the East European Plain were up to 6–7 times higher than in the same recent rivers while floods formed channels with width and meander wavelength 4–15 times larger than the recent ones. When air temperature and evaporation increased towards the end of the Weichselian and/or the transition to the Holocene, the subsequent increase of soil permeability resulted in decreased surface run-off, and meander dimensions globally reduced due to lower and more steady discharges (Kasse 1997).

Another important factor that influenced river activity and its related morphology was the vegetation cover and its density. The re-initiation of a vegetation cover after a period of bare conditions at the transition from Pleniglacial to Lateglacial in Northwest and North Europe but earlier in other

European regions (see above) resulted in increased slope stability and reduction in sediment supply to the rivers, corresponding to the change from a braided to a meandering river pattern. However, due to the slow re-establishment of a fully developed forest and the short thawing period during the Bölling evaporation was limited thus increasing run-off (Vandenberghe et al. 1984; Vandenberghe 1995). Together with similar high amounts of snowfall and melt on top of long-lasting frozen ground (although not permafrost), these combined effects resulted, as in East Europe, in temporary very high run-off (Vandenberghe and Woo 2002). The prevalence of a braided pattern in otherwise dry conditions until the end of the Pleniglacial in Northwest and Northern Europe, as is evidenced by the intense aeolian activity in those regions (Van der Hammen and Wijmstra 1971; Schwan 1988; Vandenberghe 1991; Kasse 1997, 2002) contrasts with other, more humid regions in Europe where vegetation was more abundant. Consequently, also the timing of large-meander initiation was different, it means already during the (Late) Pleniglacial in more southern parts of West Europe (Bertran et al. 2013) and in Central and Eastern Europe (see above), although all mentioned regions had a permanently or long seasonally frozen ground and thus limited water infiltration in common.

Finally, it has to be stressed that, apart from vegetation cover, snow supply and frozen soils, factors of local to regional significance may influence river pattern development (Kasse 1998). This has, for instance, been illustrated for the Tisza basin in Central Europe where the low longitudinal river gradient, caused by tectonic subsidence during the Pleistocene, favoured the establishment of large-meandering patterns throughout the Pleniglacial (Vandenberghe et al. 2018). The tectonic impact is not only relevant on large scale (e.g. the Pannonian Basin) but also at a smaller regional scale as in the lower Maas Valley (Woolderink et al. 2018).

9.7 Conclusions

The establishment of large meanders, with channel width up to 5–15 times larger than the modern ones, is inventoried for the European territory. The main causes for large-meander formation were very high discharges during the spring snowmelt, when high and rapid surface run-off was due to a combination of long winters with considerable snowfall and a short thaw period, low evaporation, reduced infiltration as a result of long-lasting frozen soil (or permafrost) and scarce vegetation.

The initiation time and duration of large-meander formation was regionally different as a result of temporal and spatial variations of local factors and environmental conditions. Large-meander formation started already before the LGM in the Pannonian Plain and, later on, at c. 19–16 ka (around the Raunis warm interval) on the East European Plain, while it typically occurred since c. 14.7 ka, i.e. during the Late-glacial, often after a transitional phase, in Western and Northcentral Europe.

The transition to the Holocene led to a general transformation of large-meandering channels into relatively smaller sizes of modern meanders in accordance with overall reduction of river discharge due to higher evapotranspiration and soil infiltration.

Acknowledgements Many thanks go to Dr. C. Kasse for critical comments to this paper.

References

Ackers P (1982) Meandering channels and the influence of bed material. In: Hey RD, Bathurst JS, Thorne RC (eds) Gravel bed rivers. Wiley, Chichester, pp 389–415

Antoine P (1997) Modifications des systèmes fluviatiles à la transition Pléniglaciaire-Tardiglaciaire et à l'Holocène: l'exemple du bassin de la Somme (Nord de la France). Géogr Phys Quat 51:93–106

Antoine P, Munaut AV, Limondin-Lozouet N et al (2003) Response of the Selle River to climatic modifications during the Lateglacial and early Holocene (Somme basin-northern France). Quat Sci Rev 22:2061–2076

Bertran P, Frouin M, Mercier N et al (2013) Architecture of the lower terraces and evolution of the Dordogne River at Bergerac (south-west France) during the last glacial–interglacial cycle. J Quat Sci 28(6):605–616

Bohncke S, Vandenberghe J (1991) Palaeohydrological development in the Southern Netherlands during the last 15000 years. In: Starkel L, Gregory K, Thornes J (eds) Temperate palaeohydrology. Wiley, Chichester, pp 253–281

Bohncke S, Kasse C, Vandenberghe J (1995) Climate induced environmental changes during the Vistulian Lateglacial at Zabinko, Poland. Quaest Geogr 4:43–64

Borisova O, Sidorchuk A, Panin A (2006) Palaeohydrology of the Seim River basin, Mid-Russian Upland, based on palaeochannel morphology and palynological data. CATENA 66:53–73

Castanet C (2008) La Loire en Val d'Orléans. Dynamiques fluviales et socio-environnementales durant les derniers 30000 ans: de l'hydrosystème à l'anthroposystème. Ph.D. Thesis, Université Paris 1

Davis WM (1913) Meandering Valleys and Underfit Rivers. Ann Ass Am Geogr 3:3–28

De Smedt P (1973) Paleogeografie en Kwartair-geologie van het confluentiegebied Dijle-Demer. Acta Geograph Lovan 11:1–141

Deschodt L, Salvador PG, Boulen M (2004) Formations sédimentaires et évolution de la vallée de la Deûle depuis le Pléniglaciaire supérieur à Houplin-Ancoisne (Nord de la France). Quaternaire 15:269–298

Dokuchaev VV (1878) The Ways of the River Valleys Formation at the European Russia. Dermakov Publ, St.-Petersburg (in Russian)

Dury GH (1954) Contribution to a general theory of meandering valleys. Am J Sci 252(4):193–224

Dury GH (1965) Theoretical implications of underfit streams. US Geological Survey Professional Paper 452-C

Dury GH (1976) Discharge prediction, present and former, from channel dimensions. J Hydrol 30:219–245

Erkens G, Hoffmann T, Gerlach R et al (2011) Complex fluvial response to Lateglacial and Holocene allogenic forcing in the Lower Rhine Valley (Germany). Quat Sci Rev 30:611–627

Feurdean A et al (2014) Climate variability and associated vegetation response throughout Central and Eastern Europe (CEE) between 60 and 8 ka. Quat Sc Rev 106:206–224

Gabris G, Nador A (2007) Long-term fluvial archives in Hungary: response of the Danube and Tisza rivers to tectonic movements and climatic changes during the Quaternary: a review and new synthesis. Quat Sci Rev 26:2758–2782

Gabris G, Horvath E, Novothny A et al (2012) Fluvial and Aeolian landscape evolution in Hungary-results of the last 20 years research. Neth J Geosci 91:111–128

Gonera P, Kozarski S (1987) River channel changes and rough paleodischarge estimates for the Warta river, West-Central Poland. Geogr Ann 69A:163–171

Gregory KJ (1976) Drainage networks and climate. In: Derbyshire E (ed) Geomorphology and climate. Wiley, London, pp 289–318

Hoek WZ (1997) Late-Glacial and early Holocene climatic events and chronology of vegetation development in the Netherlands. Veg Hist Archaeobot 6:197–213

Huang HQ, Nanson GC (1997) Vegetation and channel variation; a case study of four small streams in southeastern Australia. Geomorphology 18:237–249

Huisink M (1997) Late Glacial sedimentological and morphological changes in a lowland river as a response to climatic change: the Maas, The Netherlands. J Quat Sci 12:209–223

Huisink M (2000) Changing river styles in response to Weichselian climate changes in the Vecht valley, eastern Netherlands. Sed Geol 133:115–134

Janssens MM, Kasse C, Bohncke SJP et al (2012) Climate-driven fluvial development and valley abandonment at the last glacial-interglacial transition (Oude Ijssel-Rhine, Germany). Neth J Geosci 91:37–62

Kaiser K, Lorenz S, Germer S et al (2012) Late Quaternary evolution of rivers, lakes and peatlands in northeast Germany reflecting past climatic and human impact—an overview. E&G Quat Sci J 61 (2):104–132

Kalicki T (2006) Reflection of climatic changes and human activity and their role in the Holocene evolution of Central European valleys. Prace Geogr 204:5–348

Kasse C (1997) Cold-climate aeolian sand-sheet formation in north-western Europe (c. 14–12.4 ka): a response to permafrost degradation and increased aridity. Permafr Perigl Proc 8:295–311

Kasse C (1998) Depositional model for cold-climate tundra rivers. In: Benito G, Baker VR, Gregory KJ (eds) Palaeohydrology and environmental change. Wiley, Chichester, pp 83–97

Kasse C (2002) Sandy aeolian deposits and environments and their relation to climate during the Last Glacial Maximum and Lateglacial in northwest and central Europe. Prog Phys Geog 26:507–532

Kasse C, Vandenberghe J, Bohncke S (1995) Climatic change and fluvial dynamics of the Maas during the Late Weichselian and Early Holocene. In: Frenzel B, Vandenberghe J, Kasse C et al (eds) European river activity and climatic change during the Lateglacial and early Holocene. Paläoklimaforschung 14: 123–150

Kasse C, Huisink M, Hoek WZ et al (2000) Comment: Fluvial incision and channel downcutting as a

response to Late-glacial and Early Holocene climate change: the lower reach of the River Meuse (Maas), The Netherlands. J Quat Sci 15:91–94

Kasse C, Hoek WZ, Bohncke SJP et al (2005) Lateglacial fluvial response of the Niers-Rhine (western Germany) to climate and vegetation change. J Quat Sci 20:377–394

Kasse C, Bohncke SJP, Vandenberghe J et al (2010) Fluvial style changes during the last glacial—interglacial transition in the middle Tisza valley (Hungary). Proc Geol Assoc 121:180–194

Kemp J, Pietsch T, Gontz A et al (2017) Lacustrine-fluvial interactions in Australia's Riverine Plains. Quat Sci Rev 166:352–362

Kiden P (1991) The Lateglacial and Holocene evolution of the Middle and Lower River Scheldt, Belgium. In: Starkel L, Gregory K, Thornes J (eds) Temperate palaeohydrology. Wiley, Chichester, pp 283–299

Kozarski S (1983) River channel changes in the middle reach of the Warta valley, Great Poland Lowland. Quat Stud Poland 4:159–169

Kozarski S (1991) Warta—a case study of a lowland river. In: Starkel L, Gregory KJ, Thornes JB (eds) Temperate palaeohydrology. Wiley, New York, pp 189–215

Kozarski S, Gonera P, Antczak B (1988) Valley floor development and palaeohydrological changes: the Late Vistulian and Holocene history of the Warta River (Poland). In: Lang C, Schlüchter C (eds) Lake, mire and river environments. Balkema, Rotterdam, pp 185–203

Krupa J (2015) Natural and anthropogenic channel pattern changes in the mid-mountain valley during the Late Glacial and Holocene, Polish Uplands. Quat Int 370:55–65

Leigh DS (2006) Terminal Pleistocene braided to meandering transition in rivers of the Southeastern USA. CATENA 66:155–160

Leopold LB, Maddock T (1953) The Hydraulic Geometry of Stream Channels and Some Physiographic Implications. US Geological Survey Professional Paper 252

Leopold LB, Wolman MG (1957) River channel patterns: braided, meandering and straight. US Geological Survey Professional Paper 282-B

Leopold LB, Wolman MG (1960) River meanders. Bull Geol Soc Amer 71:769–794

Lipps S, Caspers G (1990) Spätglazial und Holozän auf der Stolzenauer Terrasse im Mittelwesertal. Eiszeitalter u Gegenwart 40:111–119

Mol J, Vandenberghe J, Kasse C (2000) River response to variations of periglacial climate. Geomorphology 33:131–148

Morin E, Macaire JJ, Hinschberger F et al (2011) Spatio-temporal evolution of the Choisille River (southern Parisian Basin, France) during the Weichselian and the Holocene as a record of climate trend and human activity in north-western Europe. Quat Sci Rev 30:347–363

Müller D, Jacobs Z, Cohen TJ et al (2018) Revisiting an arid LGM using fluvial archives: a luminescence chronology for palaeochannels of the Murrumbidgee River, south-eastern Australia, J Quat Sci. https://doi.org/10.1002/jqs.3059

Nowaczinski E, Schukraft G, Keller C et al (2015) Fluvial dynamics of the Žitava River, SW Slovakia during the last 45 ka BP and their influence on Early Bronze Age human occupation. Quat Int 370:113–126

Page KJ, Nanson GC, Price DM (1996) Chronology of Murrumbidgee River palaeochannels on the Riverine Plain, southeastern Australia. J Quat Sci 11:111–126

Panin AV, Matlakhova E (2015) Fluvial chronology in the East European Plain over the last 20 ka and its palaeohydrological implications. CATENA 130:46–61

Panin AV, Sidorchuk AY (2006) Macromeanders: the problem of origin and interpretation. Vestnik MGU Series 5. Geografiya 6:14–22 (in Russian)

Panin AV, Sidorchuk AY, Chernov AV (2011) Main stages of floodplain formation in North Eurasian Rivers. Geomorfologiya 3:20–31 (in Russian)

Panin AV, Sidorchuk AY, Vlasov MV (2013) Large Late Valdai discharge in the Don River basin. Izvestiya Akad. Nauk. Ser. Geogr. 1:118–129 (in Russian)

Pastre JF, Leroyer C, Limondin-Lozouet N et al (2002) Variations paléoenvironnementales et paléohydrologiques durant les 15 derniers millénaires: les réponses morphosédimentaires des vallées du Bassin Parisien (France). In: Bravard JP, Magny M (eds) Histoire des rivières et des lacs de Lascaux à nos jours. Errance, Paris, pp 45–62

Pastre JF, Limondin-Lozouet N, Leroyer C et al (2003) River system evolution and environmental changes during the Lateglacial in the Paris Basin (France). Quat Sci Rev 22:2177–2188

Petrovszki J, Timar G, Molnar G (2014) Is sinuosity a function of slope and bankfull discharge?—A case study of the meandering rivers in the Pannonian Basin. Hydrol Earth Syst Sci Discuss 11:12271–12290

Popov D, Markovic SB, Strbac D (2008) Generations of meanders in Serbian part of Tisa valley. J. Geogr. Inst. Jovan Cvijic SASA 58:29–41

Rotnicki K (1983) Modelling past discharges of meandering rivers. In: Gregory KJ (ed) Background to Palaeohydrology. Wiley, Chichester, pp 321–354

Rotnicki K (1991) Retrodiction of palaeodischarges of meandering and sinuous alluvial rivers and its palaeohydroclimatic implications. In: Starkel L, Gregory K, Thornes J (eds) Temperate palaeohydrology. Wiley, Chichester, pp 431–471

Savvaitov AS, Straume JA (1963) On question of stratigraphic subdivision of till of Valday glaciation in the area of lower reaches of the rivers Daugava and Gauja. Proc Inst Geol Acad Sc Latvian SSR 2:71–86. Riga (in Russian)

Schumm SA (1960) The shape of alluvial channels in relation to sediment type. US Geological Survey Professional Paper 353 B: 17–30

Schwan J (1988) The structure and genesis of Weichselian to early Holocene aeolian sand sheets in western Europe. Sed Geol 55:197–232

Sidorchuk AY (2003) Floodplain sedimentation: inherited memories. Glob Planet Change 39(1–2):13–29
Sidorchuk AY, Borisova OK (2000) Method of paleogeographical analogues in paleohydrological reconstructions. Quat Int 72(1):95–106
Sidorchuk AY, Borisova OK, Panin A (2001) Fluvial response to the Late Valdai/Holocene environmental change on the East European Plain. Glob Planet Change 28:303–318
Sidorchuk AY, Panin A, Borisova O (2003) The Late Glacial and the Holocene palaeohydrology of the Northern Eurasia. In: Gregory KJ, Benito G (eds) Palaeohydrology: understanding global change. Wiley, Chichester, pp 61–76
Sidorchuk AY, Panin AV, Borisova OK (2008) Climate-induced changes in surface run-off on the north-Eurasian plains during the Late Glacial and Holocene. Water Resour 35(4):386–396
Sidorchuk AY, Panin AV, Borisova OK (2009) Morphology of river channels and surface run-off in the Volga River basin (East European Plain) during the Late Glacial period. Geomorphology 113:137–157
Sidorchuk AY, Panin AV, Borisova OK (2011) Surface run-off to the Black Sea from the East European Plain during Last Glacial Maximum–Late Glacial time. In: Buynevich I, Yanko-Hombach V, Gilbert AS et al (eds) Geology and geoarchaeology of the Black Sea Region: beyond the flood hypothesis. Geol Soc Am Spec Paper 473:1–25
Starkel L (1983) The reflection of hydrologic changes in the fluvial environment of the temperate zone during the last 15 000 years. In: Gregory KJ (ed) Background in palaeohydrology. Wiley, Chichester, pp 213–235
Starkel L, Gebica P (1995) Evolution of river valleys in southern Poland during the Pleistocene-Holocene transition. Biul Perygl 34:177–190
Suther BE, Leigh DS, Brook GA et al (2018) Mega-meander paleochannels of the southeastern Atlantic Coastal Plain, USA. Palaeogeogr Palaeoclim Palaeoecol 511:52–79
Szumański A (1983) Palaeochannels of large meanders in the river valleys of the Polish Lowland. Quat Stud Poland 4:207–216
Timár G, Sümegi P, Horváth F (2005) Late Quaternary dynamics of the Tisza river: evidence of climatic and tectonic controls, Hungary. Tectonophysics 410:97–110
Tobolski K (1988) Palaeobotanical study of Bölling sediments at Zabinko in the vicinity of Poznan. Pol Quaest Geogr 10:119–124
Toonen WHJ, Kleinhans MG, Cohen KM (2012) Sedimentary architecture of abandoned channel fills. Earth Surf Proc Landforms 37:459–472
Turkowska K (1990) Main fluvial episodes in the Ner valley in the last 22000 years; a detailed study at Lublinek near Lodz, Central Poland. Quat Stud Pol 9:85–99
Turner F, Tolksdorf JF, Viehberg F et al (2013) Lateglacial/early Holocene fluvial reactions of the Jeetzel river (Elbe valley, northern Germany) to abrupt climatic and environmental changes. Quat Sci Rev 60:91–109
Urz R (2003) Die jungpleistozäne Talfüllung der mittleren Lahn - ein Spiegel der kaltzeitlichen Klimaschwankungen in hessischen Mittelgebirge. Zeitschr f Geomorph NF 47:1–27
Van der Hammen T, Wijmstra TA (1971) The Upper Quaternary of the Dinkel valley. Med Rijks Geol Dienst 22:59–72
Van Geel B, Coope GR, Van der Hammen T (1989) Palaeoecology and stratigraphy of the Lateglacial type section at Usselo (The Netherlands). Rev Palaeobot Palyn 60:25–129
Van Huissteden J (1990) Tundra rivers of the Last Glacial: sedimentation and geomorphological processes during the Middle Pleniglacial in the Dinkel Valley (eastern Netherlands). Med Rijks Geol Dienst 44:3–138
Vandenberghe J (1987) Changing fluvial processes in a small lowland valley at the end of the Weichselian Pleniglacial and during the Late Glacial. In: Gardiner V (ed) International geomorphology I. Wiley, Chichester, pp 731–744
Vandenberghe J (1991) Changing conditions of aeolian sand deposition during the last deglaciation period. Z. Geom NF Suppl Bd 90:193–207
Vandenberghe J (1995) Timescales, climate and river development. Quat Sci Rev 14:631–638
Vandenberghe J, Bohncke S (1985) The Weichselian Late Glacial in a small lowland valley (Mark river, Belgium and The Netherlands). Bull Ass franç et Quat 2–3:167–175
Vandenberghe J, Woo MK (2002) Modern and ancient periglacial river types. Progr Phys Geogr 26:479–506
Vandenberghe J, Beyens L, Paris P et al (1984) Palaeomorphological and -botanical evolution of small lowland valleys (Mark valley). CATENA 11: 229–238
Vandenberghe J, Bohncke S, Lammers W et al (1987) Geomorphology and palaeoecology of the Mark valley (southern Netherlands). I Geomorphological valley development during the Weichselian and Holocene. Boreas 16:55–67
Vandenberghe J, Kasse C, Bohncke S et al (1994) Climate-related river activity at the Weichselian-Holocene transition: a comparative study of the Warta and Maas rivers. Terra Nova 6:476–485
Vandenberghe J, Kasse C, Popov D et al (2018) Specifying the external impact on Fluvial Lowland evolution: the Last Glacial Tisza (Tisa) Catchment in Hungary and Serbia. Quaternary 1, 14; https://doi.org/10.3390/quat1020014
Velichko AA (1973) Natural processes in the Pleistocene. Nauka, Moscow (in Russian)

Verstraeten G, Notebaert B, Broothaerts N et al (2018) River landscapes in the Dijle catchment: From natural to anthropogenic meandering rivers In: Demoulin (ed) Landscapes and landforms of Belgium and Luxembourg. Springer, pp 269–280

Volkov IA (1960) On the recent past of the rivers Ishim and Nura. Proceedings of the Laboratory of Aeromethods, USSR Academy of Sciences 9:15–19 (in Russian)

Williams G (1988) Paleofluvial estimates from dimensions of former channels and meanders. In: Baker V, Kochel R, Patton P (eds) Flood geomorphology. Wiley, New York, pp 321–334

Willis KJ, Sümegi P, Braun M et al (1995) The late Quaternary environmental history of Bàtorliget, NE Hungary. Palaeogeogr Palaeoclim Palaeoecol 118:25–47

Woo MK (1986) Permafrost hydrology in North America. Atmos Ocean 24:201–234

Woolderink HAG, Kasse C, Cohen KM et al (2018) Spatial and temporal variations in river terrace formation, preservation, and morphology in the Lower Meuse Valley, The Netherlands. Quat Res. https://doi.org/10.1017/qua.2018.49

Zaretskaya NE, Panin AV, Golubeva YV et al (2014) Sedimentation settings and the late Pleistocene-Holocene geochronology in the Vychegda River valley. Dokl Earth Sci 455(1):223–228

Palaeostage Indicators in Rivers—An Illustrated Review

10

Jürgen Herget

Abstract

Palaeostage indicators mark previous water levels. Knowledge about their characteristics and formation is of significant importance for a qualified interpretation. They might indicate the minimum or maximum values for the previous water level which might have been a low level during a drought, mean level or most frequently a high flood-level indicator. They can be divided into natural and man-made types with the first consisting of sedimentary and geomorphological structures, soils and jetsam consisting of vegetation and other debris. Man-made palaeostage indicators are marks on buildings, texts, illustrations and archaeological features like irrigation systems and bridges including technical infrastructure like sewage water systems from historic times. Due to uncertainties as to the accuracy of the reconstructed water levels each palaeostage might indicate, it is useful to carry out plausibility analyses and use more than only one indicator for interpretations—if available.

Keywords

Flood reconstruction · Drought reconstruction · Palaeohydrology · Water level

J. Herget (✉)
Department of Geography, Bonn University,
Meckenheimer Allee 166, 53115 Bonn, Germany
e-mail: jherget@uni-bonn.de

10.1 Palaeostage Indicators—What Are They, What Do They Mean and Where Do They Come from?

For all kinds of hydrological events, the water level is of dominant interest: will we get wet or even inundated, or are we running dry? For the estimation of potential future extremes, frequently a first view is taken on water levels associated with previous events by palaeostage indicators. Palaeostage indicators (PSIs) indicate the elevation of previous water levels. "Previous" in this context might mean any time scale dating back from recent fluctuations of the water surface of a river, lake or even ocean via historic times back into the geologic past (e.g. Jarrett and England 2002, p. 92). The prefix "palaeo" in palaeohydrology (based on the similar Greek root word meaning old with a tendency towards ancient) in this context is applied in a less strict sense than in other disciplines, e.g. climatology or historical hydrology where usually recent, historic and prehistoric (=palaeo) times are carefully differentiated (e.g. Baker 2014, p. 1; Brázdil et al. 2006, Fig. 7; Glaser 2008, p. 4; Jarrett and England 2002, p. 91f). An occasionally additional or alternative distinction is made between an instrumental and a pre-instrumental period, without further differentiating the earlier stage into historic times with documentary evidence before more or less systematic measurements of the hydrological cycle began that

J. Herget and A. Fontana (eds.), *Palaeohydrology*, Geography of the Physical Environment,
https://doi.org/10.1007/978-3-030-23315-0_10

Fig. 10.1 Palaeostage indicators of previous lake levels: shorelines resulting from wave action and currents along the shore of the Pleistocene ice-dammed lake in Chuya Basin, Altai Mountains/Siberia (Fig. 10.1a) and different levels within a small delta at Upper Ikhnach Lake, Tian Shan Mountains, Uzbekistan (Fig. 10.1b). *Photographs* Herget

continue until nowadays. Note, that the application of methods typically also includes palaeoflood studies applied to recent flood events (e.g. hydraulic interpretation of a PSI instead of gauge data analysis) should not lead to the labelling the recent event as a "palaeoflood" as this is beyond any logic of the meaning of words (cf., e.g. House and Pearthree 1995, 3062). Consequently, one might think about erasing the prefix "palaeo" but this is not done herein.

Previous water levels are of specific interest for studies in a variety of hydrological environments. Due to the related extended inundations, lake and sea level changes are of specific interest, but typically are related to longer time intervals in the context of changes of the hydrological balance or even tectonic movements (cf., e.g. Baker 2014; Murray-Wallace and Woodroffe 2014). On the other hand, features like shorelines of ice-dammed lakes (Fig. 10.1a) or different levels of a recent river delta surface (Fig. 10.1b) provide valuable to determine the volume of lakes that later experienced outburst floods and therefore are of interest also for river flood studies taking place in significantly shorter time periods.

Palaeostage indicators may relate to different water levels: floods, low water and even mean levels. Most frequently, PSI is used to estimate the level of previous floods. Especially, indicators of extreme flood events are located high above others and therefore remain preserved

during the more frequent smaller events. Consequently, it is not surprising that PSIs of low water levels are less frequently documented, as they might be washed out, get reworked or are simply not visible as they are inundated most of the time. For the reconstruction of previous environments including the rehabilitation of river environments, natural mean water levels are of interest, too. Especially in intensively modified environments with dense networks of settlements and channel modifications, e.g. for navigation or flood protection, the original natural level can be difficult to estimate.

In the context of palaeoflood studies, PSI is used as proxies for the water level in cases where measurements could not be carried out directly due to floods in prehistoric or even geological times or simply the absence of suitable gauges, e.g. in the case of local flash floods (e.g. Gaume and Borga 2008). They are preserved in a different form:

Due to a missing or rather short historic record in combination with a short time instrumental period, palaeoflood studies are frequently carried out in North America (e.g. Wolman 1971; Baker et al. 1988; House and Pearthree 1995; House et al. 2002; Baker 2014). Here, natural PSIs like sedimentary deposits, botanical evidence, erosional features respectively specific landforms are interpreted frequently (e.g. Baker 1976; Williams and Costa 1988; Jarrett 1990; Jarrett and England 2002).

In addition to earth scientists interpreting natural PSI, historians carried out investigations on the magnitude of previous floods with their specific qualifications. By the analysis and interpretation of historic sources like written flood reports, drawings of inundated cities, photographs and flood markers on buildings, previous water levels during specific events are recorded. Especially, investigations on extreme low water levels during droughts, whose traces are either reworked later on or are inundated most of the time, can benefit from historical source texts. While in many cases the level of detail or accuracy in historic documents is not sufficient to determine water levels, at least the identification of events that did not leave specific individual traces in the environment is possible. Additionally, historic texts not dealing explicitly with (semi-)quantified water levels but being related to it like reports of a ship that ran aground due to a low water level of a river can also be the source for the quantification of the water level and even discharge from a period of time when no alternative data sources are available. Argumentation by plausibility becomes an important clue as will be illustrated below by selected examples.

Archaeological evidence is probably less obvious to be considered as a palaeostage indicator. On the other hand, e.g. bridges are designed considering the width and depth of a river channel to cross. As will be illustrated below in further details, also technical infrastructure like irrigation and wastewater systems from historic times provide information on the water levels of the rivers they drained into.

In this summary, an illustrated review of the variety of palaeostage indicators is presented. As is visualized below, the range of features is much broader than previously reviewed as especially historical sources were under-represented in this context before. As mentioned in the title, the focus is limited to PSIs in the fluvial environment. A preliminary review table is provided, and a call for further additions to complete it closes this review in addition to a view on further (and future) systematic application of quantified palaeostage indicators. References given in the text focus on texts of specific value, rich in references to additional case and key studies, and more detailed explanations.

10.2 Natural Palaeostage Indicators

A view on an ordinary creek (Fig. 10.2) illustrates several PSIs: e.g. sedimentary deposits like bars within the channel respectively along the shores, layers of fine-grained deposits on the floodplain or driftwood in front of obstacles.

Already on a first glance, specific water levels related to the different PSIs are evident: driftwood at the obstacles and fine-grained deposits on the floodplain indicate a minimum flood

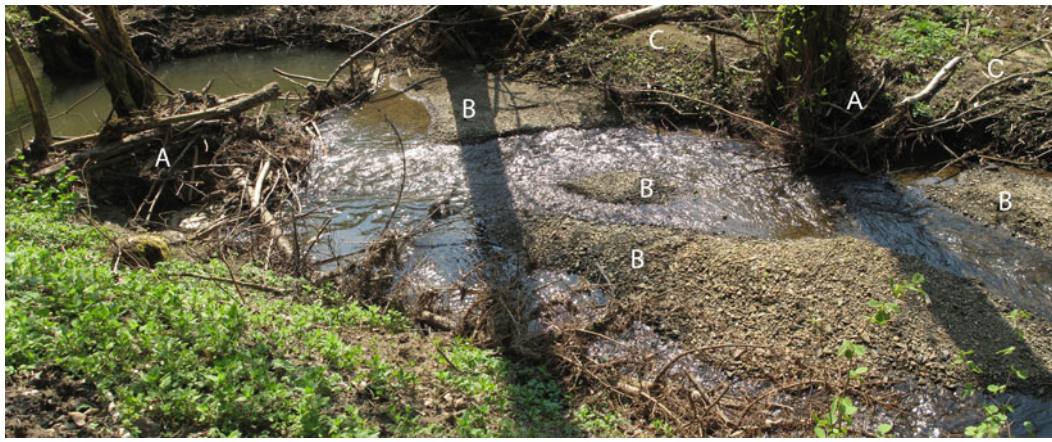

Fig. 10.2 Natural palaeostage indicators in a creek in Eifel Mountains, Germany: A—driftwood, B—bars in the channel, C—fine-grained deposits in the floodplain (direction of flow is right to left). *Photograph* Herget

stage, while the missing vegetation cover on the lower surface of the bars illustrates repeated inundation, probably even frequent reworking of the bar. Also, different transport modes have to be considered: while driftwood might be assumed to be transported floating near the surface of the water, the bars might be resulting from bedload transport. Typically, fine-grained deposits on a floodplain were transported in suspension, but also reworking of sediments within the floodplain should be taken into consideration. Consequently, the character as a minimum flood-level indicator is based on the post-flood settling of the driftwood and the minimum water level of suspension load for the floodplain sediments. The bar surfaces also indicate a minimum water level, which is already significantly lower than the stage indicated by the other PSIs. Further on, it is less certain whether the PSI is related to the same water level or not—their individual formation is also possible. Consequently, an individual view on the nature and formation of the different natural PSIs has to be taken.

Previous reviews illustrated the variety of natural palaeoflood features and investigated their formation, significance and reliability (e.g. Baker and Kochel 1988; House and Pearthree 1995; Jarrett and England 2002; Benito et al. 2004; Herget 2012). By the example of a hypothetic flood event, the different natural palaeostage indicators can best be illustrated schematically (Fig. 10.3) and will be explained in further detail below.

10.2.1 Sedimentary and Geomorphological PSI

Fluvial sedimentary deposits are rather frequent along any river channel. Preserved deposits are usually related to flood stage as deposits generated during low water stages usually get reworked soon during a rising again water level. As illustrated by the equation of continuity ($Q = v * A$, with Q for discharge, v for mean flow velocity and A for cross-sectional area), flow velocity as the component responsible for sediment transport gets reduced due to increasing cross-sectional area. Any kind of channel widening e.g. due to changes in bedrock lithology or at tributary mouths has a potential to act as a trap for sediments in transport.

Based on hydraulic theory derived by Komar (1970), for deposited sediments >7 mm previously transported as bedload and clear water in straight homogenous channels, depth of flow can be derived from known representative grain size of sediments in the channel beds as shown by

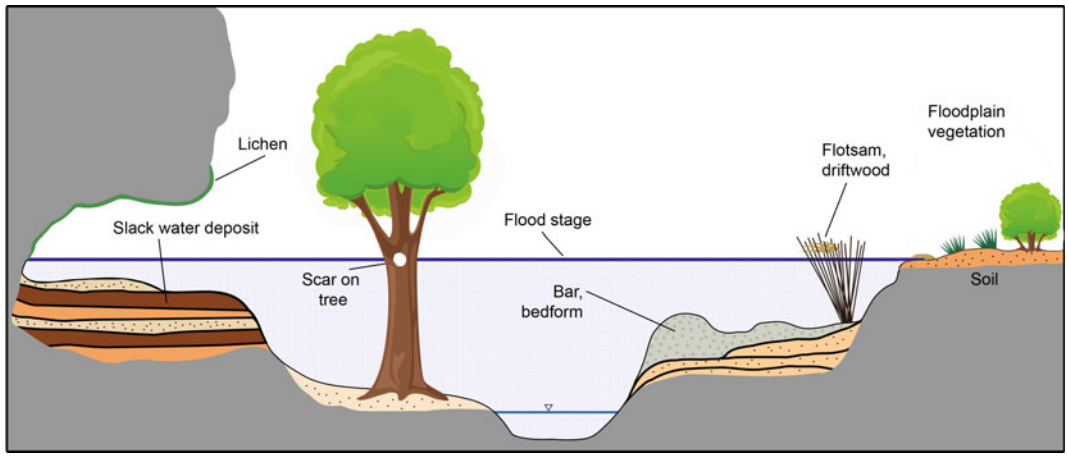

Fig. 10.3 Scheme of natural palaeostage indicators exemplified on a flood stage. Modified from Jarrett and England (2002)

Baker (1974): $D = 0.099\ d/S$ with D = depth of flow [m], S = energy slope [−] (approximately equal to water surface slope) and d = intermediate grain size [m].

Further, increased turbulence, e.g. in the wake of any kind of obstacle in the pathway of the current or at flow separation points like gates to embayments with eddy formation, might trigger sediment deposition (e.g. Baker and Kochel 1988; Benito et al. 2004) (Fig. 10.4).

Bars are rather frequent sedimentary features and can be classified into different types, e.g. point bars at the inner bend of a meander, alternate bars along at the lateral margins along straight sections, mid-channel bars and tributary bars as illustrated and discussed intensively in numerous textbooks on fluvial geomorphology and sedimentology (e.g. Bridge 2003; Knighton 1998). A systematic mapping of the locations and survey of the heights of bars was carried out by Herget (2005) in the context of the reconstruction of the water level of the outburst flood released from Pleistocene ice-dammed lakes in the Altai Mountains, Siberia. Due to their height of up to 300 m above the recent valley bottom, they are characterized as giant bars (Fig. 10.5), which blocked the mouths of tributary valley by the deposition of sediments transported in suspension during the repeated outburst flood events (Carling et al. 2009).

Frequently applied is the interpretation of slack water deposits for palaeoflood estimations (e.g. Kochel and Baker 1988; Smith 1993; Jarrett and England 2002; Benito et al. 2015; Lam et al. 2017). Specific for slack water deposits is the fine-grained composition characteristically consisting of fine sand and coarse silt. Transported in suspension, such fine sediments are rapidly deposited in the floodplain areas that are sheltered from high-velocity flows and remain there as the energy of the current was just sufficient to transport them in the protected location but is even during the following event not sufficient to rework or erode them again. Consequently, a pile of sediments useful for flood–chronological studies becomes accumulated (Fig. 10.6). They indicate a minimum water level of the related flood event which could be quantified by a difference of 10% between the elevation of the deposits and the water surface at Pecos River, Texas (Kochel in Greenbaum et al. 2000, 955). Typical locations for slack water deposits are any location of slack water conditions (cf. Fig. 10.4) like tributary mouths, shallow caves along bedrock channel walls, downstream from obstructions, areas of significant channel widening

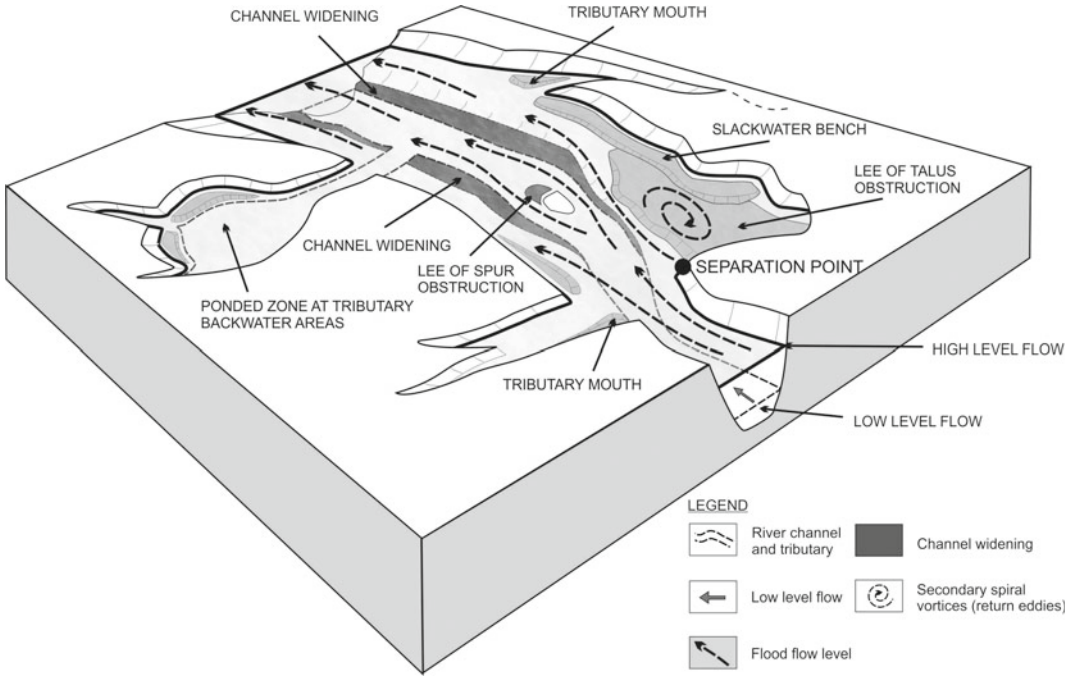

Fig. 10.4 Block diagram illustrating the location of sediment deposition during flood events (Benito et al. 2004, Fig. 2.2, reprinted with kind permission by publisher)

Fig. 10.5 Giant bar related to Pleistocene outburst floods at the village of Inya in the Russian Altai Mountains. *Photograph* Herget

Fig. 10.6 Slack water deposits accumulated in an alcove in French Creek at Black Hills of South Dakota, USA. *Photographs* Herget

including overbank accumulation on high terraces (cf. "C" in Fig. 10.2) (Kochel and Baker 1988, 358).

A less frequently considered kind of flood deposits acting as PSI are run-up sediments. They are located in front of large obstacles like bedrock ridges or valley slopes and represent the locally risen water surface level in front of the obstruction due to the transfer of kinetic energy into potential energy. In everyday life the effect is visible in front of bridge piers or tree trunks on a floodplain, where the water level rises due to this effect (Fig. 10.7). Flood currents loaded with sediments transported in suspension are found to deposit this load in front of the obstacle in higher locations than, e.g., along the lateral shores (Fig. 10.8), and consequently by the difference in height (=run-up) flow velocity can be estimated (Herget 2005). For debris flows, systematic analysis of the involved fluid mechanics by Iverson et al. (2016) concluded that the adverse slope angle, Froude number and degree of liquefaction are of influence on the run-up height. Herget (2005) and later on more advanced flood flow modellers could benefit from the surveyed height of run-up sediments as they limit the maximum water level above the surface of neighbouring bars in the context of the reconstruction of the Pleistocene megafloods in the Altai Mountains, Siberia. Lumbroso and Gaume (2012) used the run-up magnitude visible in videos of recent flash flood events for the verification of flow velocities estimated by other approaches.

There is a large variety of bedforms generated at specific water depths on the surface of a river channel bed (e.g. Allen 1984; Knighton 1998; Bridge 2003; Dey 2014). As water depth is neither the only nor the most significant parameter in comparison with flow velocity, shear stress,

Fig. 10.7 Locally risen water level in front of a tree trunk on a floodplain (direction of flow is right to left). *Photograph* Herget

grain size and time for the formation of a bedform up to the steady state, the relationship between bedform geometry and size and water depth is rather complex and specific for the different bedforms. Another challenge is the relation of the dimension and other characteristics of a bedform to a specific stage of an unsteady flow, e.g. a passing-through flood wave. Background for this problem is the relationship of the time required for the bedform formation—especially up to the steady state—and the duration of the related discharge conditions. Proportional parameters of the bedform geometry—e.g. dune height to length or obstacle mark width to depth—indicate their maturity. On the other hand, bedforms ease estimations of related discharges as, e.g., water depth must have been larger than bedform height (for most bedforms except, e.g., antidunes). Also, water depth is limited to bedform formation due to the hyperbolic rise of flow velocity and shear stress resulting in a shear stress below the threshold to mobilize sediments if the water depth is too high. Exact values are hard to be determined due to complex turbulent current pattern in reality and idealized laminar current pattern in the modelled explanations. Consequently, bedforms typically indicate a range of related water depth. Due to the complex interpretation, bedforms are less frequently interpreted as PSI even though analytical and empirical relations are developed as might be illustrated by the examples of obstacle marks and fluvial dunes.

Fluvial obstacle marks are composite morphological structures, which consist of an upstream conical scour hole, wrapping laterally around an obstacle and a contiguous depositional region in the wake of the obstruction. Obstacle marks have been reported at a variety of spatial scales (e.g. Karcz 1968; Herget 2005) and have

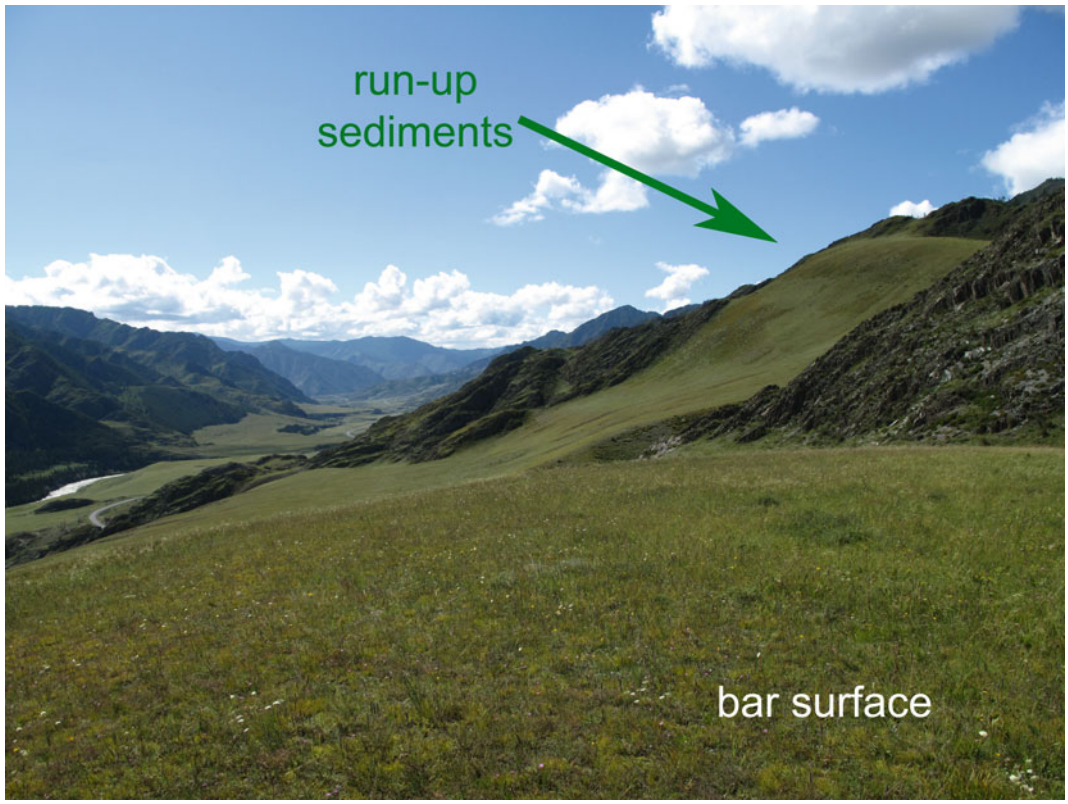

Fig. 10.8 Run-up sediments deposited in front of bedrock ridge in relation to bar surface in Chuya Valley and Altai Mountains, Siberia (view in direction of flow). *Photograph* Herget

been used for palaeohydraulic reconstructions (Herget et al. 2013). Nevertheless, their utility as an indicator for past flood stages remains ambiguous. However, preliminary experimental results exhibit a relationship between the geometrical size of the scour hole and the submergence ratio, defined as ratio of flow depth to obstacle height. Thus, for a given flow velocity and constant obstacle dimensions, normalized scour hole volumes are maximized at a submergence ratio of 0.7–1.0, so that the magnitude of flow depth is approximately equal to obstacle size (Fig. 10.9a; Schloemer et al. 2019). Increasing water depth beyond this value will cause a decrease in scour hole volume, due to the fact that a large portion of the approaching boundary layer flows is atop the obstacle with no significant impact on the morphodynamic processes at the streambed (Euler and Herget 2012; Euler et al. 2017; Schloemer et al. 2019). Beyond a submergence ratio of 3.0–4.0, the formation of obstacle marks eases nearly completely (Fig. 10.9b). Experimental results in a flume reveal that the presence of large scour holes indicates flow depths that are related to the obstacle dimensions; thus, obstacle marks are supposed to indicate the minimum values of flow depth during a flood event.

Fluvial gravel dunes formed during the Pleistocene outburst floods from ice-dammed lakes in the Russian Altai Mountains (Fig. 10.10) were analysed by Carling (1996a, b) and Herget (2005) for their characteristics, origin and palaeohydraulic indication.

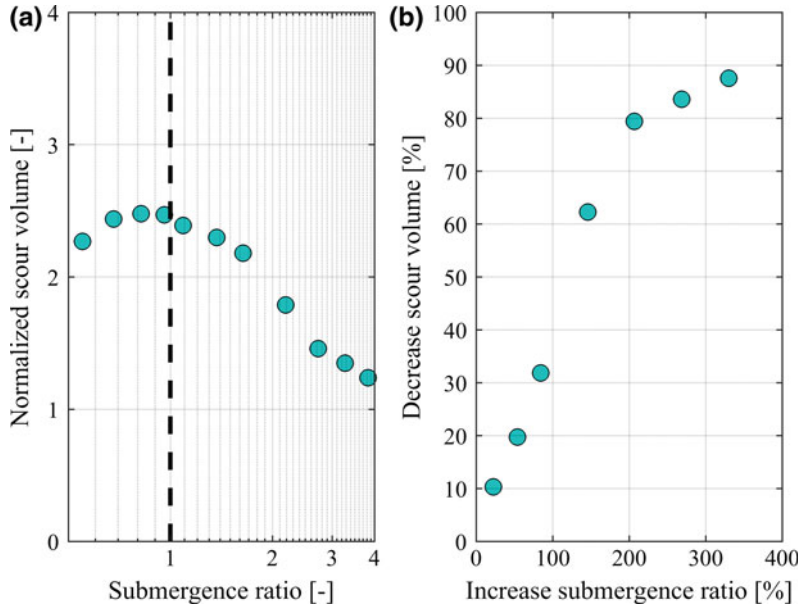

Fig. 10.9 Relation between submergence ratio and scour hole volume based on experimental results (Schloemer et al. 2019). **a** Threshold of submergence ratio where scour holes were maximized is indicated by the dashed line. **b** Rising submergence ratio above threshold value leads to decreasing scour hole volumes

Fig. 10.10 Fluvial gravel dunes in Kuray Basin and Russian Altai Mountains (direction of flow was right to left, note the coarse grain size exposed in front). *Photograph* Herget

For the estimation of depth of flow during their formation, empirical relationships compiled from different sources by Raudkivi (1982, 34f) were applied:

$$0.15 < \frac{h_d}{y} < 0.29 \quad 4 < \frac{l_d}{y} < 8 \quad l_d = 2\pi y$$

where h_d represents the height of a dune, l_d the length of a dune and y the depth of flow. The maximum height of 16 m and length of 200 m of the dunes indicate a depth of flow in the range of 25–106 m. On the first view, the factor of 4 of the range of the uncertainty might seem to be less satisfying. Also considering that the empirical relations were developed for fine-grained sediments smaller than gravels might create doubt. On the other hand, the estimation indicates that the rather large dunes were

Fig. 10.11 Erosional levels in construction gravel stored in the floodplain of the River Rhine at Cologne; temporary flood levels are indicated by both erosional levels and deposited jetsam. *Photograph* Herget

formed during relatively shallow flow conditions in the final stages of the lake drainage with a previous maximum depth of 550 m at the location of the gravel dunes.

Currents of flowing water might cause erosional scars, during both flood events and mean water levels. In bedrock channels, transported sediments act to abrade and dominate the large variety of sculpted forms partly indicating flow patterns (e.g. Richardson and Carling 2005). Similarly, erosional levels in loose sediments like gravels and sands develop much faster and might even develop towards staircases indicating different temporary levels of a passing-through flood wave (Fig. 10.11).

10.2.2 Soils and Flotsam

Soils and their evolution in the floodplains are driven by repeated periodic or episodic inundation (Cain and Beatty 1968; Baker 1976; Brown 1997, 96f; Blume and Stahr 2002). The dominant related process is the deposition of transported suspension load as colluvium. In contradiction to gley soils, redoximorphic indicators are missing, at least for the upper 40 cm. As inundations last only for relatively short periods, redoximorphic process like bleaching does not occur in the upper horizons. These fluvisols according to FAO/WRB classification experience repeated accumulation of solid and liquid deposits, occasionally also eluviation during flood events; hence, soil development is repeatedly interrupted. Typically, the topsoil consists of different layers with variable humic content resulting in differences of dark topsoil colours. Exceptional low water conditions lasting for a longer period might lead to the lowering of the groundwater level in the proximal parts of the floodplain and an exposure of the characteristically bleached horizons of the subsoil. Soil chemistry is typically characterized by enriched nutrient content, but also contaminations and pollutions are frequently observed. Occasionally, historic flood events and levels can be identified by layers of a specific chemical composition or tracers, e.g. from mining activities in the headwaters (e.g. Brown 1997; Kleszen and Chrobok 1989). In contradiction to sedimentary units like slack water deposits or bars, soils form a more or less continuous layer within the floodplain. By their characteristics, they might be a useful tool to determine the extension of a natural floodplain if no morphological indicators like terraces can be identified, e.g. due to human relief modifications in urbanized areas.

Flotsam is transported by floating close to the surface of the water. It gets deposited as jetsam when either the water becomes too shallow, e.g. on the distal parts of a floodplain, or the material

Fig. 10.12 Branches accumulated in front of obstacles in a usually dry valley bottom near Bonn/Germany after a thunderstorm-related cloudburst (view downstream). Note the sorted bedload deposits with grain sizes up to pebbles in front. *Photograph* Herget

got stuck, e.g. at bushes. Flotsam consists of both natural material like leaves and branches up to tree trunks (Figs. 10.11 and 10.12) and also artificial material like plastic and any kind of floatable rubbish located in the pathway of a flood. Even sediments up to the size of boulders can be transported as ice-rafted debris or trapped in tree root masses.

Floating close to the water surface, flotsam once deposited indicates the elevation of the water level. Note that this might not be the maximum level of a passing-through flood wave, hence peak discharge. Theoretically, it can be assumed that the water level of peak discharge is rarely indicated by jetsam as already during the early rising stage of a flood, floatable deposits within the floodplain became mobilized. Consequently, they are no longer available when a flood reaches its maximum level. For ice-rafted debris, observations were made by Bjornstad (2014) that the maximum flood level cannot be indicated due to the deep inundation of icebergs (typically 90% submerged). Icebergs ground before reaching the shore, and the transported debris melts out at elevations below the maximum water level which leads to its systematic underestimation. Calculations by De Brue et al. (2015) indicate that even if the necessary ice volume or water depth to raft coarse sediments is not available a limited ice layer might result in a reduced effective density of boulders and a decreased bed friction, hence an increased transport competence (Carling and Tinkler 1998).

10.2.3 Vegetation

Different aspects of the vegetation cover of river channels, the related banks and floodplains provide a rich variety of water level indicators (e.g. Baker 1976; Hupp 1988). Due to rather long time required for growing, plants indicate mean and repeated water levels for all low, mean and flood conditions. On the other hand and as it will be explained below, both scars in tree rings and growth of new sprouts on a tree are related to distinct events archived when, e.g., flotsam hits a tree growing in the floodplain or sediments buried parts of it.

It is obvious that aquatic plants including algae indicate a minimum water level in a river channel that usually is not any lower. On the opposite, river banks that are frequently flooded and even reworked do not show any vegetation cover (Figs. 10.2 and 10.13). Consequently, the elevation of the different vegetation patterns indicates these levels.

On a global scale it has to be considered that vegetation patterns including the species and their distributions vary by ecological zones. For the temperate zone, a characteristic vegetation pattern from the channel towards the distal respectively highest parts of the floodplain is frequently developed reflecting typical inundation depth and especially frequency with closely related duration (e.g. Baker 1976; Hupp 1988; Ellenberg and Leuschner 2010, 416f). The proximal parts near the channel typically consist of gravels and are free of vegetation or might be settled by annual plants, grasses and reeds for example. This level is frequently fully inundated. The following softwood vegetation in the floodplain is represented by willow species in the

Fig. 10.13 Channel and floodplain of River Landwasser downstream Davos/Switzerland with algae growing within the channel while the shores are without vegetation cover. *Photograph* Herget

Fig. 10.14 Lichen cover on the sandstone walls of Canyon de Chelly, Arizona, down to the marked level (the dark line indicates the elevation of the valley bottom, locally eroded recently). *Photograph* Herget

lower parts growing as bushes up to short trees on sandy deposits. The upper parts are represented by species such as grey alder. This gallery forest is typically inundated annually but usually is not fully submerged. The uppermost part of the floodplain is reached only by extreme flood magnitudes leaving loamy sediments and is characterized by species such as elm and oak growing as tall trees.

Lichen cover rock surfaces but cannot resist the corrosive and erosive forces of flowing water. Consequently, they are found only above the water level of floods (Fig. 10.14). Based on investigations in eastern Australia, Gregory (1976) found that annually reached flood levels are without lichen cover and lichen density increases towards higher levels where flood frequency is reduced. Further, the grow rates in the magnitude of <1 mm/a of lichen allow additional chronological estimations for floods of specific levels (e.g. Foulds et al. 2014).

Scars in trees mark both the water level when the obstacle hit the tree and the time this event took place by the damage of tree rings (e.g. Sigafoss 1964; Hupp 1988; George 2010). Most flood scars seem to be formed by floating logs, while ice and saltating cobbles were also observed (Gottesfeld 1996, 319). As the triggers of the scars mostly are floating close to the surface of the water, the minimum values for the maximum water level are indicated. In contrast, in a key study in Western Canada, Gottesfeld (1996) found that a regression line of the flood-scar top elevations runs within a distance of 20 cm below roughly parallel to the peak discharge elevations along the shoreline and concluded, that maximum flood stages were indicated. In a similar study in Spain, Ballesteros et al. (2011) found a similar pattern comparing

Table 10.1 Sources of information for historic water levels

Concrete sources	Flood marks, hunger stones, memorials, inscriptions, etc.
Printed sources	Chronicles, monographs on events, newspapers, journals, leaflets, etc.
Handwritten sources	Diaries, letters, chronicles, financial and economic-administrative records, etc.
Maps and plans	Inundation maps, plans of dam systems, etc.
Illustrations	Paintings of rivers and inundations, engravings, photographs, etc.

Modified from Herget (2012, 16) and Brázdil et al. (2018, 1917f)

scar elevations with gauge data but question the relationship about the timing of the scar infliction within the flood hydrograph and discuss different findings without final conclusion (Ballesteros-Cánovas et al. 2016). Considering the large amount of driftwood being transported under natural conditions in near-natural catchments (e.g. Rickenmann 1997) and missing alternative information, tree scars are also considered for flood frequency studies (e.g. Ballesteros-Cánovas et al. 2016), especially in combination with additional plant anatomical flood signatures (e.g. George and Nielsen 2002).

In addition to scars on trees, the occurrence of palaeofloods can be indicated by additional botanical evidence but with less distinct palaeostage indication like adventitious sprouts respectively adventitious shoot formation by growing from broken or inclined stems or eccentric ring growth after tilting the stem (e.g. Sigafoss 1964; Hupp 1988). As the depth of flow in this latter case is less distinct, they are considered in this context but should be mentioned as a perspective for future studies.

Ancient natural PSI are typically not preserved in cultivated river channels and floodplains, especially in the settled area due to more or less intensive and even repeated artificial modifications. Under such conditions, alternative anthropogenic sources replace them.

10.3 Historical Marks and Documents

Frequently as component of studies on historical climatology and related natural hazards (e.g. Alexandre 1987; Bradley and Jones 1992; Buisman 1995; Pfister 1999; Glaser 2008; Sangster et al. 2018; Brázdil et al. 2018), reports on flood and drought levels in historic times are archived. The different ways and styles of tradition (Table 10.1) can be generalized into concrete sources like water level marks on buildings, text documents and illustrations.

All the information require specific quality and reliability analysis with some individual aspects exemplified below.

10.3.1 Water Level Marks

Flood level marks (Fig. 10.15) are the most frequent palaeostage indicators in the group of concrete sources. They are found at buildings and constructions like bridges at numerous historic cities. Most prominent are settlements of administrative, economic respectively religious significance in historic times. A first classification of their different characters is based on given temporal resolution (e.g. year only or exact date), physical characteristics (e.g. coloured mark or metal plate) and actors who installed the mark (e.g. individual volunteer or governmental organization) (Deutsch and Pörtge 2019, 13ff). Probably, the oldest ones are from ancient Egypt and date back to 3018 BC (Popper 1951).

Among critical aspects on the reliability of recorded flood levels on buildings is the correct transfer of the height throughout time, e.g. on renewed buildings like the one in Fig. 10.15 built in 1934. Occasionally, the level markers are preserved for decoration instead of accurate documentation. Plausibility can be checked by, e.g., searching for additional text information, by comparing the level of distinct events in

Fig. 10.15 Compilation of 20 historic flood levels of the River Main at Randersacker/Germany dating back up to AD 1552. *Photograph* Herget

longitudinal profiles along the river or by comparison with other events of known relationship to the dubious one. Typically, the flood marks were drawn or engraved when the flood level already was receded. Due to capillary action, an overestimation of the flood level might be obtained if the uppermost wet part of the stone got marked. Also, it had to be observed that stones are reused for construction after the damage of the building without consideration of the flood mark given on it. Consequently, the given level has no further meaning, which is occasionally less obvious than in Fig. 10.16, where the stone was turned over during reuse.

In comparison with flood level marks, those of low water levels are rather rare. Due to the indication of drought and resulting bad harvest or even famines, they are called hunger stone (German: Hungerstein) (Brázdil et al. 2018, p. 1922). Luckily, the chance to see them (Fig. 10.17) is pretty rare as most of the time they remain inundated.

Catalogues of historic water level marks are rather rare. Typically, only in local publications of regional history, reviews are available, which might be an important additional source in cases were buildings where demolished or destroyed in the meantime, e.g. due to war actions.

Fig. 10.16 Reused stone with turned over flood level mark at the foundation of a railway bridge in Koblenz/River Rhine. *Photograph* Herget

Compilations for larger regions require enthusiasts with sufficient time (e.g. Deutsch and Pörtge 2019; LUBW 2006).

10.3.2 Text Documents on Historic Water Levels

There is a large variety of text sources on historic water levels. Typically, they divide into primary and secondary sources indicating whether the author observed the event personally (Fig. 10.18) or is compiling a chronicle from different sources —the first one is usually thought to be more reliable. Anyhow, due to loss through time caused by archivists disposing of documents (of seemingly no value), bookworm, fires and not least flooding frequently contemporary text sources might not be available any more.

Quantifications of water levels like the different water depths in different churches during the Magdalena Flood in July 1342 in Frankfurt are relatively rare: "The floors of all churches were inundated, St. Nicolaus 6 Fuß, St. Jakob 3 Fuß, Franciscan Church 4 Fuß, St. Elisabeth at Sachsenhausen 6 Fuß, …" (own analogous translation after Latomus in Weikinn 1958, 206).

Fig. 10.17 Hunger stone with low water marks of the River Elbe at Decin/Czech Republic. *Photograph* Elleder

More frequent are relative level descriptions like that a part of town or specific building was reached. Based on modern survey data or archaeological investigations, the quantitative water level can be derived, at least by magnitude. "The water in the River Rhine was that low at several places, that it could be crossed by horse" (Wetter et al. 2014, attachment) illustrates that frequently quantitative information is given indirectly only and has to be derived as a plausible magnitude. In this example, the depth of water in the river channel was less than 1 m according to personal comments from different equestrians.

By careful analysis and plausibility checks, information given in other contexts than water level can provide quantitative information. Roggenkamp and Herget (2015a) interpreted a historic text by Tacitus about a loaded ship that run aground due to a low water level of the River Rhine and a finally successful raid of German tribes conquering the ship from the Roman military roughly 2000 years ago. By archaeological and historical investigations, the kind of ship and especially its draught is known and a maximum depth of water can be derived. The mentioned fight must have occurred near the ship instead of celebrating a formal battle between two regular armies which limits maximum water depth in the main channel, too. In combination with geomorphological evidence, the historic channel geometry could be reconstructed and discharge estimated: considering full ranges of the uncertainty of different parameters, the discharge was only half the value ever recorded during the entire instrumental period.

Search for regional information of historic water levels during floods and droughts is eased by previous research and compilations. Reviews are given in the previously listed studies on historical climatology, for floods by the bibliography on source texts, data lists and chronologies in, e.g., Herget (2012, 58) and for droughts by the extended reference list in Brázdil et al. (2018). Recently, published reviews become supplemented by online databases:

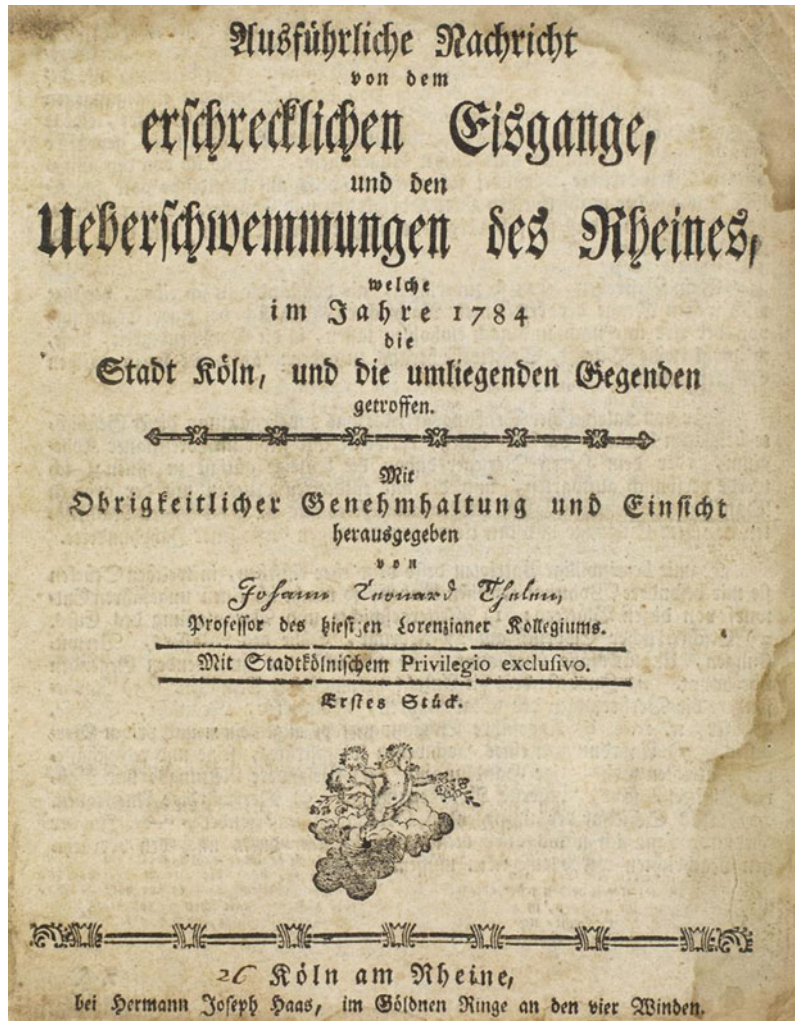
Ausführliche Nachricht
von dem
erschrecklichen Eisgange,
und den
Ueberschwemmungen des Rheines,
welche
im Jahre 1784
die
Stadt Köln, und die umliegenden Gegenden
getroffen.
Mit
Obrigkeitlicher Genehmhaltung und Einsicht
herausgegeben
von
Johann Leonard Thelen,
Professor des hiesigen Lorenzianer Kollegiums.
Mit Stadtkölnischem Privilegio exclusivo.
Erstes Stück.
Köln am Rheine,
bei Hermann Joseph Haas, im Göldnen Ringe an den vier Winden.

Fig. 10.18 Book cover of Thelen (1784) on the ice-jam flood of the River Rhine at Cologne in February 1784

- "Historical climatology from all man-made sources" (www.tambora.org)
- "Chronology of British Hydrological Events" (www.cbhe.hydrology.org.uk)
- "Euro-Climhist database" (https://www.euroclimhist.unibe.ch/de)
- "Le répertoire des repères de crues" (www.reperesdecrues.developpement-durable.gouv.fr)
- "Observatoire Régional des Risques d'inondation" (https://orrion.fr/#).

Note, that all information and texts including those from databases and other compilations require careful analysis about reliability and context, so-called source criticism (e.g. Barriendos and Coeur 2004; Glaser and Stangl 2004, 492f). As illustrated above, already units of given water depth have to be transferred into the metric system carefully considering the regional and temporal variability of, e.g., "Fuß". For the context, the intention of the historical

Fig. 10.19 Flood level in the city of Meißen located at River Elbe/Germany on 24 February 1799 (Deutsch et al. 2010, with kind permission by the publisher)

document should be taken into consideration. Note a potential tendency to exaggerate, e.g. flood magnitudes in the case of a letter asking the local lord for compensation for experienced damage.

10.3.3 Illustrations of Historic Water Levels

Illustrations like paintings and photographs are a promising but also challenging source for water level information. In historic times, when the majority of the population was illiterate, illustrations, of e.g., flood events were mainly for illustration rather than documentation and might tend to exaggeration for effect. Consequently, the documentary value of the water level is rather low. Later on, it changed towards a documentary character that provides a more detailed indication of flood levels, e.g. in relation to windowsills of probably still remaining buildings for geodetic survey and calculation of the historic water level (Fig. 10.19).

Except in case of retouching—in the beginning of the twentieth century, postcards with exaggerated water levels from recent flood events have been popular (Deutsch et al. 2012)—photographs are a more objective source for information on water levels. Beyond the geodetic survey of remaining buildings, under lucky conditions it might be even possible to reconstruct flood hydrographs, e.g. if a clock is visible in the historic photographs like Roggenkamp and Herget (2015b) found during studies on historic floods of the River Ahr, Germany.

10.4 Archaeology and Technical Infrastructure

The altitudes of ancient buildings provide valuable information about previous water levels, by the simple assumption that the builders were clever enough to avoid frequent inundations. Several further interpretations are based on plausibility and therefore provide ranges of reasonable water levels.

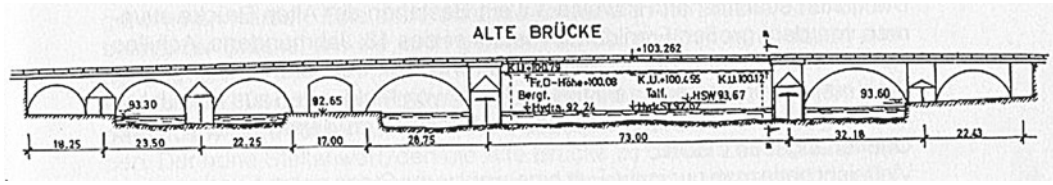

Fig. 10.20 Reconstruction of the Roman bridge across the River Rhine at Cologne, AD 310, and conclusions on channel depth and water level (after Kraus from Roggenkamp and Herget 2016)

For water-related facilities like harbours, mills and irrigation systems, the relationship to a mean range of water levels is evident (e.g. Scarborough 2003; Viollet 2007). Additionally, based on archaeological findings including the gauge facilities "nilometer" from ancient Egypt, the flood chronology of the lower Nile River could be reconstructed (Popper 1951; Seidlmayer 2001).

Beyond such highlights, remnants of ancient bridges respectively of their foundations can be used to reconstruct the range of water levels while they have been in use (Fig. 10.20) (e.g. BGU 2011). By location and height of the bridge pillars, width and depth of the channel can be determined. It might be assumed that only during exceptional flood levels the bridge deck might be inundated, hence, during mean water levels both sides remain dry and the bridge was not overflowed. By plausibility, it might be assumed that the bridge pillars have been high enough to allow navigation below the bridge most of the time. Consequently, both low water levels can be estimated considering the draught of passing vessels, while the height of the ships above the water level indicates a typical upper range of the mean water level, probably even up to an average flood level.

In the context of the reconstruction of the hydrology and water levels of the River Rhine in Roman times approximately 2000 years ago, Roggenkamp (2016; summary in Roggenkamp and Herget 2016) also interpreted the elevation of the ancient sewage water system of the city of Cologne for water level estimations. Background is the idea that the system could only work if the sewage duct was above the level of the River Rhine, even during rather frequent mean high water stage, which thereby can be quantified.

10.5 Conclusion and Perspectives

Trying to summarize the explanations and comments above a review compilation of the main characteristics of the variety of PSI might be useful (Table 10.2).

Many more details might be discussed and additional perspectives illustrated, but for the review character aimed to present here, space is limited. Anyhow, it is already obvious that not all variants of PSI are available at any location but one has to apply and interpret whatever is handed down.

For all aspects, specific knowledge and experience are required about how far and into which spatial resolution an indicator can be interpreted. Anyhow, in case of doubts an uncertainty analysis considering the maximum and minimum values might be useful. Palaeostage indicators always provide components of the uncertainty, and it should be avoided to argue with values calculated up to decimal places.

Due to both natural and anthropogenic changes in channel capacity and modifications on flood plains since the event of interest took place, palaeostage indicators cannot be related to modern levels without further reconstructions. This includes the reference levels—e.g. the elevation of an inundated floor of a church due to changes within the building in the meantime.

Additionally, and as already commented by Baker (1976) and Williams and Costa (1988), it is useful to use the entire range of available data on palaeostages. Basing a story on a single indicator at one location only is weak argumentation, especially as the uncertainty typically is challenging to be quantified. Combinations with

Tab. 10.2 Characteristics of palaeostage indicators

Palaeostage indicator	Formation		Water level			Relationship	
	Erosive	Accumulative	Minimal	Mean	Maximal	Distinct event/stage	Repeated water level
Bar		X	X			X	
Slack water deposit		X	X			X	
Run-up sediment		X			X	X	
Bedform, e.g. dune		X	X		(X)	X	
Bedform, e.g. obstacle mark	X	(X)	X		(X)	X	
Erosional scar (loose sediments)	X		X			X	
Erosional scar (bedrock)	X		X				X
Soil		X	X			(X)	X
Flotsam, ice-rafted debris		X	X			X	
Floodplain vegetation		X	X		X		X
Lichen	X				X		X
Tree scar	X		X		(X)	X	
Historic mark and text			X		X	X	
Archaeological evidence			X	X	X	(X)	X

additional points—even though of different characteristics—upstream and downstream will result in more reliable data sets.

Acknowledgements Comments and materials from several colleagues improved the manuscript and provided inspiration in the context recently and in previous years. Support in this context is appreciated from Gerardo Benito, Paul Carling, Libor Elleder, Renate Gerlach, Oliver Schlömer and Willem Tonen. The topic was discussed during the workshops EX-AQUA 2017 and 2018 "Palaeohydrological extreme events—evidence and archives" in Noida/India and Szeged/Hungary which both were kindly supported by the INQUA Commission on Terrestrial Processes, Deposits and History (TERPRO).

References

Alexandre P (1987) Le climat en Europe au Moyen Âge. Ecole de Haute Etudes en Sciences Sociales, Paris

Allen JRL (1984) Sedimentary structures—their character and physical basis. Elsevier, Amsterdam

Baker VR (1974) Paleohydraulic interpretation of Quaternary alluvium near Golden, Colorado. Quatern Res 4:94–112

Baker VR (1976) Hydrogeomorphic methods for the regional evaluation of flood hazards. Environ Geol 1:261–281

Baker VR (2014) Palaeohydrology—introduction. In: Baker VR (ed) Palaeohydrology. International Association of Hydrological Science, Wallingford, pp 1–13

Baker VR, Kochel RC, Patton PC (eds) (1988) Flood geomorphology. Wiley, New York

Baker VR, Kochel RC (1988) Flood sedimentation in bedrock fluvial systems. In: Baker VR, Kochel RC, Patton PC (eds) Flood geomorphology. Wiley, New York, pp 123–137

Ballesteros JA, Bodoque JM, Díez-Herrero A, Sanchez-Silva M, Stoffel M (2011) Calibration of floodplain roughness and estimation of flood discharge based on tree-ring evidence and hydraulic modelling. J Hydrol 403:102–115

Ballesteros-Cánovas JA, Stoffel M, Spyt B, Janecka K, Kaczka RJ, Lempa M (2016) Paleoflood discharge reconstruction in Tatra Mountain streams. Geomorphology 272:92–101

Barriendos M, Coeur D (2004) Flood data reconstruction in historical times from non-instrumental sources in Spain and France. In: Benito G, Thorndycraft VR (eds) Systematic, palaeoflood and historical data for the improvement of flood risk estimation—methodological guidelines. Centro de Ciencias Medioambientales, Madrid, pp 29–42

BGU (2011) Bayerische Gesellschaft für Unterwasserarchäologie (ed) Archäologie der Brücken/Archaeology of Bridges. Pustet, Regensburg

Benito G, Macklin MG, Zielhofer C, Jones AF, Machado MJ (2015) Holocene flooding and climate change in the Mediterranean. CATENA 130:13–33

Benito G, Thorndycraft VR, Enzel Y et al (2004) Palaeoflood data collection and analysis. In: Benito G, Thorndycraft VR (eds) Systematic, palaeoflood and historical data for the improvement of flood risk estimation—methodological guidelines. Centro de Ciencias Medioambientales, Madrid, pp 15–27

Bjornstad BN (2014) Ice-rafted erratics and bergmounds from Pleistocene outburst floods, Rattlesnake Mountain, Washington, USA. E&G Quatern Sci J 63:44–59

Blume HP, Stahr K (2002) Auenböden. In: Blume HP, Brümmer GW, Schwertmann U et al (eds) Scheffer/Schachtschabel Lehrbuch der Bodenkunde, 15th edn. Spektrum, Heidelberg, pp 509–510

Bradley RS, Jones PD (eds) (1992) Climate since AD 1500. Routledge, London

Brázdil R, Kundzewicz ZW, Benito G (2006) Historical hydrology for studying flood risk in Europe. Hydrol Sci J 51(5):739–764

Brázdil R, Kiss A, Luterbacher J et al (2018) Documentary data and the study of past droughts—a global state of the art. Clim Past 14:1915–1960

Bridge JS (2003) Rivers and floodplains—forms, processes and sedimentary record. Blackwell, Oxford

Brown AG (1997) Alluvial geoarchaeology—floodplain archaeology and environmental change. Cambridge University Press, Cambridge

Buisman J (1995) Duizend jaar weer, weind en water in de Lage Landen. Van Wijnen, Franeker

Cain JM, Beatty MT (1968) The use of soil maps in the delineation of floodplain. Water Resour Res 4:173–182

Carling PA (1996a) A preliminary palaeohydraulic model applied to late Quaternary gravel dunes: Altai Mountains, Siberia. In: Branson J, Brown AG, Gregory KJ (eds) Global continental changes: the context of palaeohydrology, vol 115. Geological Society Special Publication, pp 165–179

Carling PA (1996b) Morphology, sedimentology and palaeohydraulic significance of large gravel dunes, Altai Mountains, Siberia. Sedimentology 43:647–664

Carling PA, Tinkler K (1998) Conditions for the entrainment of cuboid boulders in bedrock streams—an historical review of literature with respect to recent investigations. In: Tinkler KJ, Wohl EE (eds) Rivers over rock—fluvial processes in bedrock channels. American Geophysical Union, Washington, pp 19–34

Carling PA, Martini P, Herget J et al (2009) Megaflood sedimentary valley fill—Altai Mountains, Siberia. In: Burr D, Carling P, Baker V (eds) Megaflooding on earth and mars. Cambridge University Press, Cambridge, pp 243–264

De Brue H, Poesen J, Notebaert B (2015) What was the transport mode of large boulders in the Campine Plateau and the lower Meuse valley during the mid-Pleistocene? Geomorphology 228:568–578

Deutsch M., Pörtge KH (2019) Hochwasser in Thüringen – Hochwassermarken und Hochwassergedenksteine. Thüringer Landesanstalt für Umwelt und Geologie Schriffenreihe 117:1–224

Deutsch M, Glaser R, Pörtge KH et al (2010) Historische Hochwasserereignisse in Mitteleuropa. Geographische Rundschau 2010(3):18–24

Deutsch M, Pörtge KH, Börngen M (2012) Bilder von der Flut - Anmerkungen zu Hochwasser- und Sturmflutdarstellungen auf historischen Ansichtskarten. Schriftenreihe der Deutschen Wasserhistorischen Gesellschaft 20:519–530

Dey S (2014) Fluvial hydrodynamics—hydrodynamic and sediment transport phenomena. Springer, Berlin

Ellenberg H, Leuschner C (2010) Vegetation Mitteleuropas mit den Alpen in ökologischer, dynamischer und historischer Sicht, 6th edn. Ulmer, Stuttgart

Euler T, Herget J (2012) Controls on local scour and deposition induced by obstacles in fluvial environments. CATENA 91:35–46

Euler T, Herget J, Schlömer O et al (2017) Hydromorphological processes at submerged solitary boulder obstacles in streams. CATENA 157:250–267

Foulds SA, Griffiths HM, Macklin MG et al (2014) Geomorphological records of extreme floods and their relationship to decadal-scale climate change. Geomorphology 216:193–207

Gaume E, Borga M (2008) Post-flood field investigations in upland catchments after major flash floods—proposal of a methodology and illustrations. J Flood Risk Manag 1:175–189

George SS (2010) Tree rings as paleoflood and paleostage indicators. In: Stoffel M, Bollschweiler M, Butler D et al (eds) Tree rings and natural hazards. Springer, Dortrecht, pp 233–239

George SS, Nielsen E (2002) Flood ring evidence and its application to paleoflood hydrology of the Red River and Assiniboine River in Manitoba. Géog Phys Quatern 56:181–190

Glaser R (2008) Klimageschichte Mitteleuropas - 1200 Jahre Wetter, Klima, Katastrophen. Theiss, Darmstadt

Glaser R, Stangl H (2004) Climate and floods in Central Europe since AD 1000—data, methods, results and consequences. Surv Geophys 25:485–510

Gottesfeld AS (1996) British Columbia flood scars—maximum flood-stage indicators. Geomorphology 14:319–325

Greenbaum N, Schick AP, Baker VR (2000) The palaeoflood record of a hyperarid catchment, Nahal Zin, Negev Desert, Israel. Earth Surf Proc Land 25:951–971

Gregory KJ (1976) Lichens and the determination of river channel capacity. Earth Surf Proc 1:273–285

Herget J (2005) Reconstruction of ice-dammed lake outburst floods in the Altai-Mountains, Siberia. Geol Soc Am Spec Publ 386:1–118

Herget J (2012) Am Anfang war die Sintflut - Hochwasserkatastrophen in der Geschichte. Wissenschaftliche Buchgesellschaft, Darmstadt

Herget J, Euler T, Roggenkamp T et al (2013) Obstacle marks as palaeohydraulic indicators of Pleistocene megafloods. Hydrol Res 44:300–317

House PK, Pearthree PA (1995) A geomorphological and hydrologic evaluation of an extraordinary flood discharge estimate—Bronco Creek, Arizona. Water Resour Res 31:3059–3073

House PK, Webb RH, Baker VR et al (eds) (2002) Ancient floods, modern hazards—principles and applications of paleoflood hydrology. American Geophysical Union, Washington

Hupp CR (1988) Plant ecological aspects of flood geomorphology and paleoflood history. In: Baker VR, Kochel RC, Patton PC (eds) Flood geomorphology. Wiley, New York, pp 335–356

Iverson RM, George DL, Logan M (2016) Debris flow runup on vertical barriers and adverse slopes. J Geophys Res Earth Surf 121:2333–2357

Jarrett RD, England JF (2002) Reliability of paleostage indicators for paleoflood studies. In: House PK, Webb RH, Baker VR et al (eds) Ancient floods, modern hazards—principles and applications of paleoflood hydrology. American Geophysical Union, Washington, pp 91–109

Jarrett RD (1990) Paleohydrologic techniques used to define the spatial occurrence of floods. Geomorphology 3:181–195

Karcz I (1968) Fluviatile obstacle marks from the Wadis of the Negev (southern Israel). J Sediment Res 38:1000–1012

Kleszen R, Chrobok SM (1989) Historische Hüttenstandorte im Mittelharz und ihre fluvial transportierbaren technogenen Gesteine. Z Angew Geol 35:24–31

Knighton D (1998) Fluvial forms and processes—a new perspective. Arnold, London

Kochel RC, Baker VR (1988) Paleoflood analysis using slackwater deposits. In: Baker VR, Kochel RC, Patton PC (eds) Flood geomorphology. Wiley, New York, pp 357–376

Komar PD (1970) The competence of turbidity current flow. Geol Soc Am Bull 81:1555–1562

Lam D, Croke J, Thompson C et al (2017) Beyond the gorge—paleoflood reconstruction from slackwater deposits in a range of physiographic settings in subtropical Australia. Geomorphology 292:164–177

LUBW (2006) Landesanstalt für Umwelt, Messungen und Naturschutz Baden-Württemberg (ed): Historische Hochwassermarken in Baden-Württemberg. CD-ROM

Lumbroso D, Gaume E (2012) Reducing the uncertainty in indirect estimates of extreme flash flood discharges. J Hydrol 414(415):16–30

Murray-Wallace CV, Woodroffe CD (2014) Quaternary sea-level changes—a global perspective. Cambridge University Press, Cambridge

Pfister C (1999) Wetternachhersage - 500 Jahre Klimavariationen und Naturkatastrophen.Haupt, Bern

Popper W (1951) The Cairo Nilometer. University of California Press, Berkeley

Raudkivi AJ (1982) Grundlagen des Sedimenttransportes. Springer, Berlin

Richardson K, Carling PA (2005) A typology of sculpted forms in open bedrock channels. Geol Soc Am Spec Pap 392:1–112

Rickenmann D (1997) Schwemmholz und Hochwasser. Wasser Energie Luft 89(5–6):115–119

Roggenkamp T (2016) Der Rhein zur Römerzeit - Wasserstände und Abflüsse des Mittel- und Niederrheins. Forschungen Geographie und Landeskunde 264:1–208

Roggenkamp T, Herget J (2015a) An extreme drought in the year 69 AD on Lower Rhine—a quantitative reconstruction. Zeitschrift für Geomorphologie 59 (Suppl 3):99–109

Roggenkamp T, Herget J (2015b) Historische Hochwasser der Ahr. Heimatkalender Kreis Ahrweiler 2015:150–154

Roggenkamp T, Herget, J (2016) Middle and Lower Rhine in Roman times—a reconstruction of hydrological data based on historical sources. Environ Earth Sci 75:1–12

Sangster H, Jones C, Macdonald N (2018) The co-evolution of historical source materials in the geophysical, hydrological and meteorological sciences: learning from the past moving forward. Prog Phys Geogr 42:61–82

Scarborough VL (2003) Flow of power—ancient water systems and landscapes. School of American Research, Santa Fe

Schloemer O, Herget J, Euler T (2019) Boundary condition control of fluvial obstacle mark formation —a framework from geoscientific perspective. Earth Surf Proc Land (in print)

Seidlmayer S (2001) Historische und moderne Nilstände - Untersuchungen zu den Pegelablesungen des Nils von der Frühzeit bis zur Gegenwart. Achet, Berlin

Sigafoss RS (1964) Botanical evidence of floods and flood-plain deposition. US Geological Survey Professional Paper 485-A:1–41

Smith GA (1993) Missoula flood dynamics and magnitudes inferred from sedimentology of slack-water deposits on the Columbia Plateau, Washington. Geol Soc Am Bull 105:77–100

Thelen JL (1784) Ausführliche Nachricht von dem erschrecklichen Eisgange, und den Überschwemmungen des Rheines, welche im Jahre 1784 die Stadt Köln, und die umliegenden Gegenden getroffen. Haas, Köln

Viollet PL (2007) Water engineering in ancient civilisations—5000 years of history. International Association of Hydraulic Engineering and Research, Madrid

Weikinn C (1958) Quellentexte zur Witterungsgeschichte Europas von der Zeitwende bis zum Jahre 1850 - Teil 1 Zeitwende bis 1500. Akademie Verlag, Berlin

Wetter O, Pfister C, Werner JP et al (2014) The year-long unprecedented European heat and drought of 1540—a worst case. Clim Change 125:349–363

Williams GP, Costa JE (1988) Geomorphic measurements after a flood. In: Baker VR, Kochel RC, Patton PC (eds) Flood geomorphology. Wiley, New York, pp 65–77

Wolman MG (1971) Evaluating alternative techniques of floodplain mapping. Water Resour Res 7:1383–1392

11 High-Resolution Sedimentary Paleoflood Records in Alluvial River Environments: A Review of Recent Methodological Advances and Application to Flood Hazard Assessment

Willem H. J. Toonen, Samuel E. Munoz, Kim M. Cohen and Mark G. Macklin

Abstract

In this chapter, we discuss recent developments in paleoflood hydrology that are specific to the collection of high-resolution records from alluvial settings. We describe how to develop and analyze alluvial paleoflood records, including (i) the identification of suitable depositional niches in valley environments and the mechanisms of overbank deposition that lead to flood deposit accumulation at those locations, (ii) approaches for sample material collection and methods to measure the coarseness of individual flood units, (iii) data assessment and reconstruction of absolute and relative flood magnitudes from sedimentary information, and (iv) developing flood chronologies with a discussion of available dating techniques. We argue that alluvial paleoflood archives hold enormous potential for flood hazard assessments in densely populated low-lying areas despite the challenge of quantitative discharge reconstructions in dynamic floodplain settings.

Keywords

Extreme events · Natural hazard · Climate change · Holocene · Fluvial archive

W. H. J. Toonen (✉)
Egyptology Unit, Faculty of Arts, KU Leuven, Louvain, Belgium
e-mail: w.h.j.toonen@gmail.com

S. E. Munoz
Department of Marine and Environmental Sciences, Northeastern University, Nahant, USA

Department of Civil and Environmental Engineering, Northeastern University, Boston, USA

K. M. Cohen
Department of Physical Geography, Utrecht University, Utrecht, The Netherlands

Department of Applied Geology and Geophysics, Deltares, Utrecht, The Netherlands

M. G. Macklin
School of Geography and Lincoln Centre for Water and Planetary Health, University of Lincoln, Lincoln, UK

Innovative River Solutions, Institute of Agriculture and Environment, Massey University, Palmerston North, New Zealand

Centre for the Study of the Inland, La Trobe University, Melbourne, Australia

11.1 Introduction

Riverine floods are among the costliest and most frequently occurring type of natural hazard (Wallemarq et al. 2018). Often they affect densely populated valleys, where the economic and humanitarian consequences of flooding are significant. In just 2018, flood catastrophes hit Japan, East Africa, the USA, India, and many

J. Herget and A. Fontana (eds.), *Palaeohydrology*, Geography of the Physical Environment,
https://doi.org/10.1007/978-3-030-23315-0_11

other places, with damage totaling over $100 billion USD (NOAA/NCEI 2018; EM-DAT 2019) and highlighting the scale and persistence of riverine flood hazard.

The diversity of regions that were recently affected by severe flooding illustrates that flood hazard is geographically widespread. A range of hydroclimatic mechanisms can trigger flooding, from spring snowmelt in mid- and high-latitude regions to heavy rainfall from tropical cyclones and the monsoon in low latitudes. Over the last two centuries, many of the world's rivers have seen shifts in land cover together with intensified land use and river management for flood mitigation (e.g., channelization and the construction of dykes) and water resources planning (e.g., reservoirs). These human impacts are known to alter flood hazard (Hall et al. 2014; Best 2019). The size and physiography of a catchment influence its susceptibility to different hydroclimatic mechanisms. Therefore, the flood regimes of downstream river reaches and those of larger river systems that traverse and connect heterogeneous terrains and climate zones become complex (i.e., for the Mississippi River; Knox 2007; Smith and Baeck 2015). Due to the basin-specific interactions between hydroclimatic and geomorphic processes that modulate flood occurrence, aggregated projections of flood hazard under greenhouse forcing bear considerable uncertainty (Kundzewicz et al. 2006; IPCC 2012, 2018; Best 2019). To improve such projections, independent analysis of the influence of climatic-physiographic factors on the recurrence times and size of extreme events that occur in downstream river valleys is pivotal as this allows to relate past climatic variability and ongoing shifts related to greenhouse forcing to changes in flooding hazard.

While the magnitude of several recent catastrophic floods has been referred to as unprecedented, it remains challenging to establish historical precedent and causality of these events —especially in light of the brevity of instrumental discharge records (Naylor et al. 2017; St. George and Mudelsee 2018). One strategy to improve assessment of current and future flood hazard involves extending the length of instrumental discharge records via paleoflood hydrology. Paleoflood hydrology makes use of geomorphological and sedimentary records adjacent to a river and was formalized as a discipline in the 1980s to improve flood hazard assessments for the design of hydraulic structures (e.g., dams, nuclear power plants) built to withstand high-magnitude flood events (Kochel and Baker 1982; Baker 2008). These studies mainly targeted bedrock canyons, where a stable valley and channel morphology allowed a direct comparison of past reconstructed peak discharges with modern monitored data (Kochel and Baker 1982). Besides methods to identify maximum paleoflood levels (Enzel et al. 1993) and calculation of their respective peak discharges, researchers developed approaches to establish chronological control on the paleoflood deposits and began to assess the timing and recurrence of extreme events. Paleoflood hydrology has continued to contribute to flood hazard assessments and has also been used to understand long-term variations in regional hydroclimate (Gregory and Benito 2003).

In the last decade, paleoflood hydrology has expanded outside the bedrock-valley reaches to reconstruct flood magnitudes and their chronologies in other regions and settings (Wilhelm et al. 2018; 2019), including alluvial valley reaches (Jones et al. 2010). Paleoflood hydrology in alluvial settings focuses on the identification of characteristic sedimentary event beds related to the passage of large floods and establishing their ages. Unlike bedrock-canyon reaches, alluvial valleys exist in many river systems, and these are the same reaches where human populations and infrastructure are concentrated. In this chapter, we review current advancement in alluvial paleoflood hydrology, focusing on fluviolacustrine archives from which high-resolution and quantitative paleoflood records can be developed. Such records can supplement and confirm the often short instrumental and sometimes patchy historical records from the same valleys. We discuss how these paleoflood records are generated and used to identify and attribute variability in flood regimes and to improve flood hazard assessment of low-lying regions.

11.2 High-Resolution Alluvial Paleoflood Archives—Site Selection

When rivers overtop their banks in alluvial reaches, sediment is conveyed to floodplain zones adjacent to channels, where it may settle due to reduced flow velocities. This way, each discharge wave that exceeds bank-full stage has the potential to produce a distinct sedimentary unit over some part of the floodplain. Paleoflood hydrological studies wanting to use sedimentary archives from fluvial environments preferentially do so from depositional niches that capture and preserve flood sediments repeatedly and semi-regularly, so that a record forms that can be considered complete. The main depositional niches used are low-lying flood basins and fluvio-lacustrine environments such as abandoned channel depressions (Fig. 11.1). However, also less commonly used niche environments exist (see overview in Wilhelm et al. 2019), including accretional deposits adjacent to the main channel, overflow basins, and archeological contexts.

Rivers with a mixed bed load can supply a range of sediment fractions to their floodplains when they flood, so resulting deposition tends to be heterolithic and changing in style and composition with distance from the channel (Fig. 11.2). Proximal depositional environments, close to the active channel, generally receive larger volumes of sediments during floods compared to more distal locations. The mean grain size of flood deposits generally decreases with the distance the sediment is carried across the floodplain, away from its source. Overbank deposition is also affected by the flow paths of waters across the floodplain and the height above the active channel and mean valley elevation.

Decelerating flow across the floodplain at proximal locations results in deposition of relatively coarse material (muds with an admixed portion of coarser grains otherwise found as channel bed load), while the more distal locations predominantly receive finer material (Fig. 11.2). As a result of these depositional patterns across the floodplain, sedimentary flood records at proximal locations receive material during most flood events and thus have the potential to provide the highest resolution records. Yet, deposit preservation potential in these proximal locations is low, as they are located close to the active channel and hence susceptible to erosion by lateral channel movement (Lewin and Macklin 2003). Preservation potential is generally higher at more distal sites, but sediment conveyance to these locations is lower and limited to rare

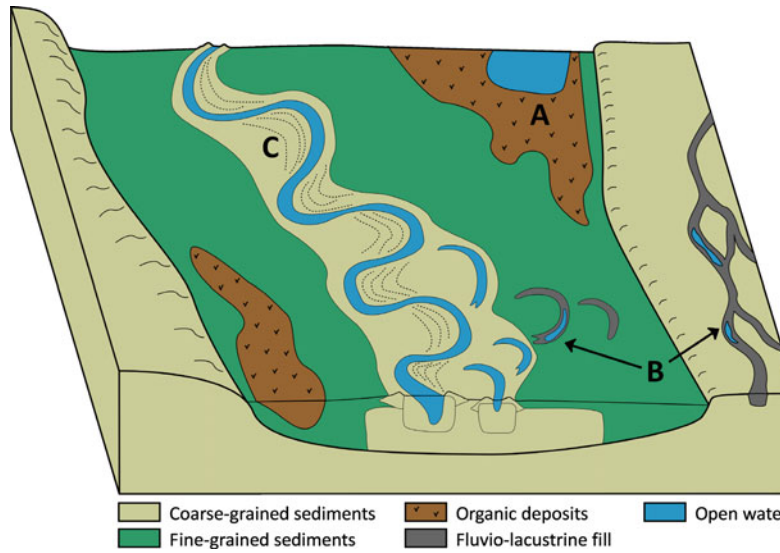

Fig. 11.1 Depositional niches in alluvial river valleys that form and preserve high-resolution paleoflood records; A = floodplains and flood basins (backswamps), B = abandoned channel depressions, C = accretional deposits (e.g. natural levees, bars, and ridge-and-swales)

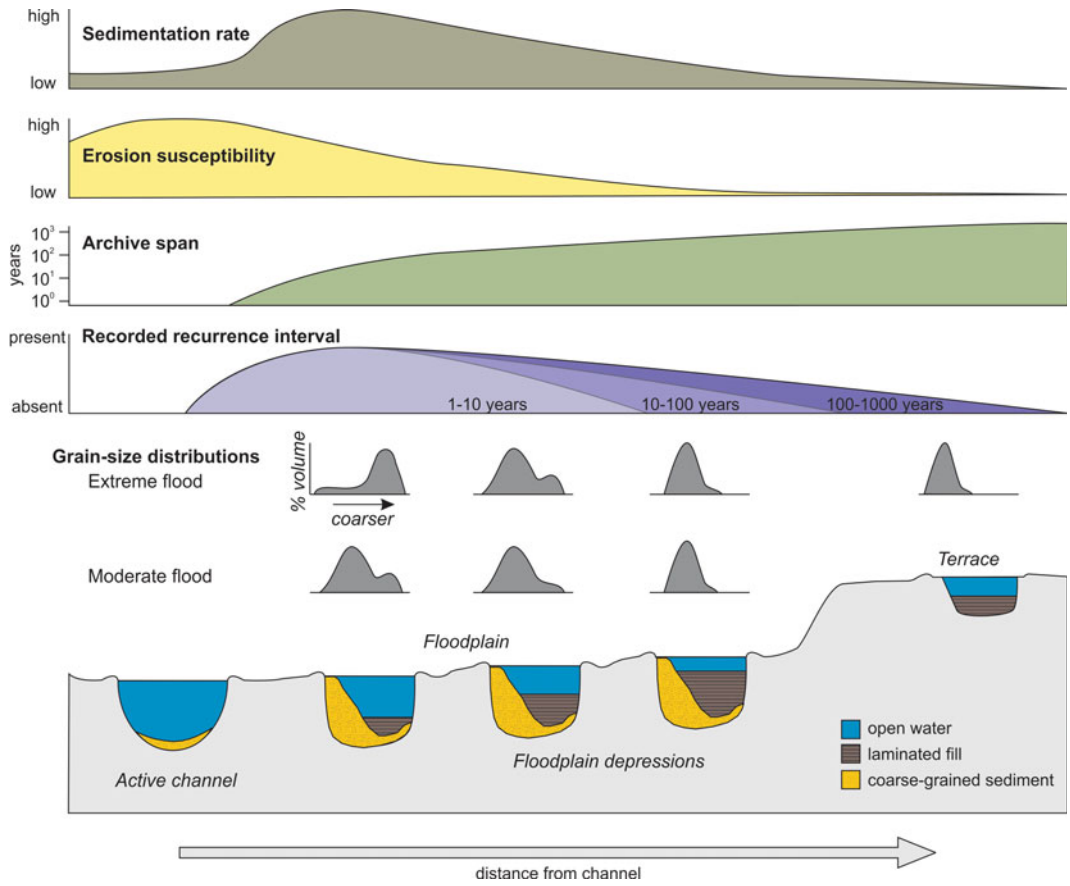

Fig. 11.2 Schematic diagram showing paleoflood record resolution, record length, and preservation potential in relation to the distance of the depositional niche from the active river channel. The characteristic texture (grain-size distribution) of flood deposition and its fining with increasing distality is shown for extreme and moderately sized events at depositional niches across the river valley (cf. Fig. 11.1)

high-magnitude flood events (Lewin and Ashworth 2014). At floodplain margins, one thus may still be able to identify individual highest-magnitude flood events (recurrence 10^2–10^3 years), but not record of individual events below that registration limit. Proximal sites provide shorter records, generally up to a few centuries long, and capture all events that exceeded bank-full stage. One should be conscious of this when selecting research locations for the development of alluvial paleoflood records; studies looking for a high-resolution record of the last few centuries to compare with historical records (e.g., Toonen et al. 2015) or to investigate the impacts of human river management on flood magnitudes (e.g., Munoz et al. 2018) should target different sites than a study that investigates the timing, extent, and magnitude of most extreme floods through the entire Holocene (Toonen 2013).

The development and interpretation of alluvial paleoflood records must consider how the dynamic nature of alluvial rivers can imprint on patterns of deposition and erosion (Fig. 11.3). In addition to being influenced by flood magnitude, the volume and texture of overbank deposits are controlled by the relative positions of the channel and depositional environment, as well as in-channel sediment availability, the shape of the event's hydrograph, flood seasonality, and upstream sediment source area (Asselman 1999; Morehead et al. 2003). As alluvial river systems

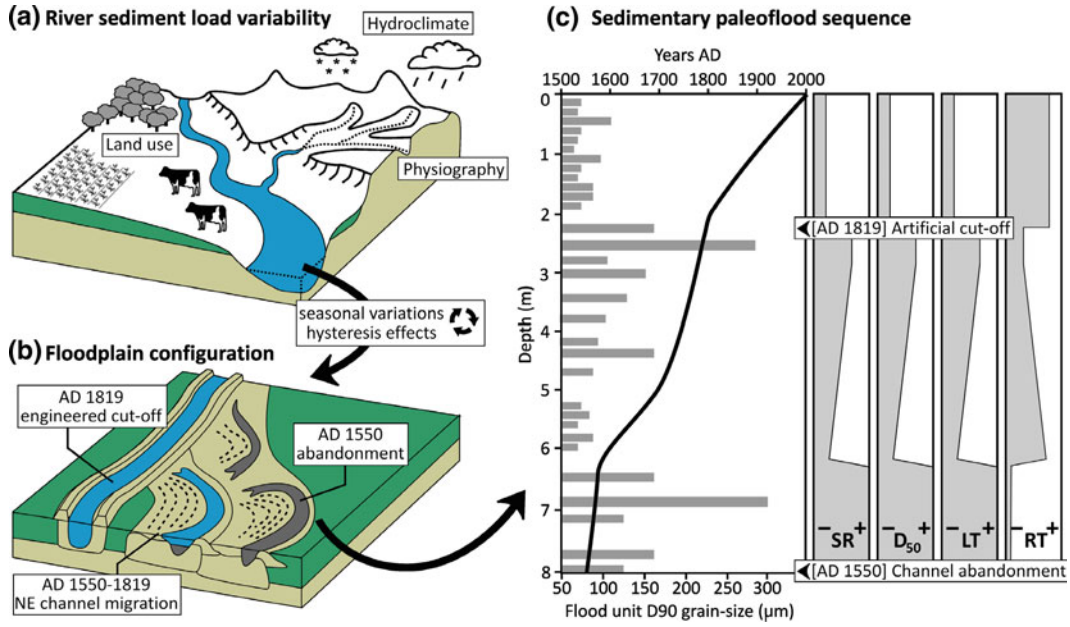

Fig. 11.3 Catchment-wide trends (**a**) in sediment supply and local factors (**b**) that influence (or overprint) sedimentary paleoflood series (**c**); SR = sedimentation rates, D_{50} = relative coarseness of sedimentary fill, LT = thickness of laminae, RT = recording threshold for flood events. Panels B and C are styled after a case study for the Lower Rhine (Toonen et al. 2015)

are sensitive to climate change, anthropogenic alteration of land cover, and human intervention to reduce floods risk and increase navigability (Blöschl et al. 2007; Bronstert et al. 2007; Hall et al. 2014), they respond to these changes by altering their gradient, discharge, sediment load, and channel morphology. Such shifts in the behavior of an alluvial river system and changes in floodplain configuration are reflected in the deposits of overbank sequences (Fig. 11.3). This complicates the development and interpretation of paleoflood records in these environments. Hence, careful consideration of the study location and its broader geomorphic context is critical for improving flood hazard assessments in heavily populated low-lying regions.

11.3 Developing Paleoflood Data Series: Approaches and Processing Steps

11.3.1 Site Selection and Sample Core Extraction

Overbank deposition can be traced across inundated sections of the floodplain, and recovering these deposits use many of the same techniques as those used in soil and/or geological mapping. Remotely sensed imagery, elevation data from topographic and geodetic surveys (including airborne laser altimetry), and hydrographic data can be used to establish a minimal horizontal

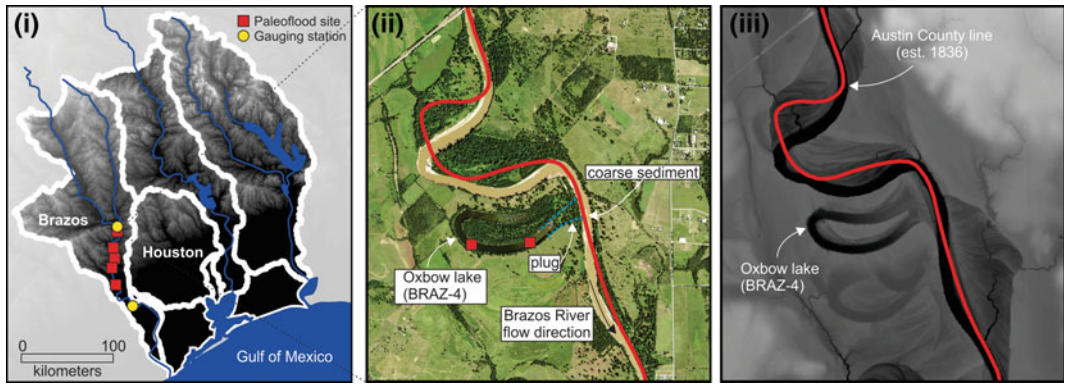

Fig. 11.4 Surveying for potential paleoflood archives—an example from Southeastern Texas, USA (courtesy of S. Munoz); (**i**) identification of alluvial valley reaches in the vicinity of gauging stations, and interpretation of the local fluvial geomorphology, its dynamics (e.g., river channel migration), and identification of depositional niches for paleoflood recording using LandSat imagery (**ii**) and airborne laser altimetry technology (**iii**)

extent of where floodwaters have regularly reached and deposited sediments (Fig. 11.4). Such information allows comparison with the instrumental recording of flood heights from nearby gauging stations and hydraulic simulations of floods. With this information, an expectation on the frequency of flood deposition and the resolution of the sedimentary archive in a particular location can be formed. After a potential paleoflood recording site has been targeted, with the use of topographic and geomorphologic information to locate a suitable depositional niche (Fig. 11.4), a variety of coring techniques is available to collect sample material. Several studies have made use of piston corers that are either mechanically or manually operated (Fig. 11.5). Mechanical systems, include a rod-driven vibracore or Begemann device, are primarily suitable for retrieving densely compacted and long sedimentary sequences. They require a stable setup position on firm ground or a (floating) platform and good access to the research site due to being heavy to transport. Hand-operated systems, such as a Livingstone piston corer (Fig. 11.5), are labor-intensive in operation and can only be deployed in relatively soft sediments.

Prior to the step of sample core collection, it is recommended to survey the internal architecture of the larger geomorphologic element one aims to extract a sample from. The sedimentary infill of cutoff meanders, for example, can have lateral and longitudinal trends with coarse-grained deposits at the places where the channel was initially plugged and relatively fine-grained deposits at the apex of the meander bend (Toonen et al. 2012). Prospecting the character of the infill allows one to pinpoint the best location for sample extraction while avoiding zones that are susceptible to erosion and redeposition (e.g., plug bars) and fitted to the specific aim of the study; i.e., targeting either the highest recording resolution or the longest available period of paleoflood registration at a site. In addition, few studies working in complex sedimentary environments have collected multiple sample cores for local cross-verification (Munoz et al. 2018). Such investigations, despite being costly and time-consuming, however, considerably improve the quality of paleoflood records, as local disturbances and anomalies can be identified and assessed.

11.3.2 Grain-Size Measurements and Data Processing

The magnitude of a paleoflood can be estimated by its peak flood level (Herget, this volume) or from the textural properties of flood deposits as a

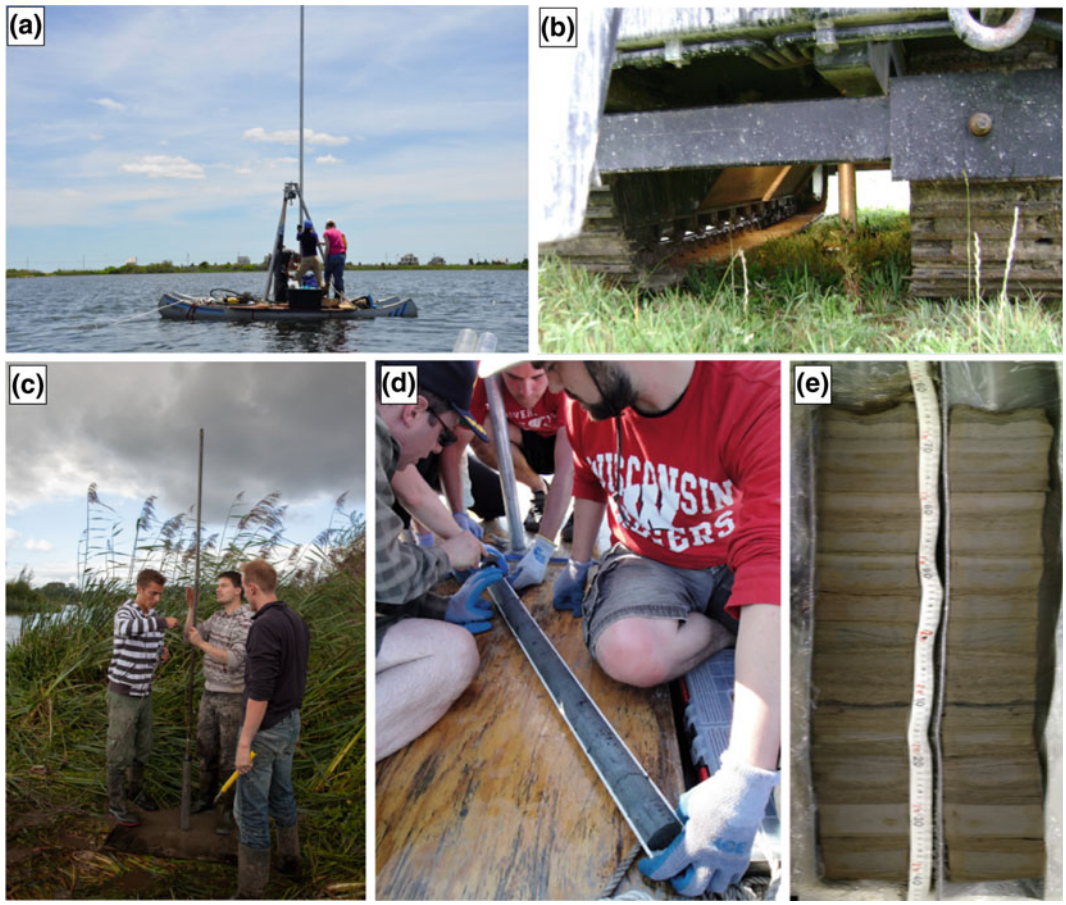

Fig. 11.5 Mechanically operated coring devices: **a** rod-driven vibracoring; and **b** Begemann; **c** a hand-operated Livingstone Piston corer (picture courtesy of W. Nijland); **d** a fresh core segment extruded from a Livingstone corer; and **e** an opened Begemann core segment—split in the laboratory for logging and further analysis

proxy for the energy (i.e., flow velocity) that was required to entrain the deposited material. In upland and bedrock-confined settings, the local relief favors the use of stage indicators (Baker 2008). In low-relief and alluvial settings, however, the only threshold levels for extra-channel deposition are the heights of levees and fluvial terraces (Fig. 11.1). There, variations in the texture of flood-derived deposition can be used as a proxy for flood magnitude (Jones et al. 2012). Toonen et al. (2015) demonstrated for the Lower Rhine River that peak discharge magnitudes as gauged at a nearby station correlated with the coarseness of flood beds contained in abandoned channel fill deposits. Work on other alluvial rivers has confirmed this relationship for proximal floodplain settings (Munoz et al. 2018; Leigh 2018). Estimating flood magnitudes via sediment texture has limitations, which are discussed below, but the approach provides a means to develop continuous and quantitative paleoflood records in alluvial settings.

A number of techniques are available to measure or infer the texture of a flood deposit, i.e., the mix of grain sizes constituting the sediment. Direct measurements of sediment texture include traditional dry- and/or wet-sieving and laser diffraction analysis. One drawback involved with physically measuring grain-size data is that it is time-consuming (and sometimes costly).

These measurements require the pretreatment of samples to ensure that organic materials, flocculates, and pedogenic nodules are removed prior to measurement (Konert and Vandenbergh 1997; Peng et al., 2019). A major advantage of this approach is that it produces an observed grain-size distribution for each individual flood deposit such that precise quantitative metrics may be employed to describe texture (e.g., mean, mode, D_{90}, End Member modeling). It is these quantitative metrics, particularly those that describe the coarse tail of a flood unit grain-size distribution, that exhibit the strongest correlation to gauged peak discharges (Toonen et al. 2015).

Indirect measurements of grain size, for example using magnetic susceptibility, organic content, and X-ray fluorescence (XRF) core scanning, are typically faster obtained than direct grain-size measuring techniques. Fluvial sediments transported to extra-channel locations are typically minerogenic, and depending on the geology and lithology of the catchment, flood units may be detectable using magnetic susceptibility (Oldfield et al. 1979) and/or loss-on-ignition (LOI; Heiri et al. 2001) measurements—the latter only if there is a significant autogenic organic production at the research site. Paleoflood studies increasingly use XRF core scanning to identify flood units and infer their grain size (Jones et al. 2012; Fuller et al. 2018). XRF measurements can be obtained at resolutions <1 mm, so at a higher resolution than what is possible using other direct and indirect techniques. In the application of XRF to paleoflood analysis, commonly used elements that reflect trends in grain size include Zr, Fe, Rb, Ti, Al, Ca, and Si; the XRF counts of these elements are often normalized and expressed as a ratio to assess variations in water and organic content (Jones et al. 2012). Selecting appropriate elemental ratios requires calibration of the XRF data to independent grain-size measurements, as local and regional geology will influence the suitability of a given elemental ratio to infer grain size. The use of multiple elemental XRF ratios is recommended based on the observation of Jones et al. (2018) that a single elemental ratio may not reflect (the magnitude of) all flood units properly in a given paleoflood record.

The properties of relatively finer grained textures can be interpreted as a background signal to which the relative coarseness of marked flood units can be expressed against to produce a normalized Z-scored data series (Fig. 11.6). For high-resolution data, most studies use a moving window to filter for the main trends and develop a normalized record of sediment coarseness. Caution has to be exercised with regard to the choice of moving-window size and the effect this can have on the preservation of short-term periodic trends contained in the data. The latter might reflect hydroclimatic variability, which for most applications should be kept in the processed record.

Inspection of raw data series often reveals overprinted trends in the coarseness of deposits that are not directly related to flood magnitudes (Fig. 11.3). If clear sedimentary breaks or transitions are observed, with markedly shifts in sedimentation rates and the frequency of flood deposition, a data series can be split and sections assessed and normalized separately (Fig. 11.6). If possible, the step of data normalization should be followed by an initial comparison with independent flood records from gauged series, historical records, or established paleoflood series in verification of trends and events observed in the most recent part of the sedimentary sequence (see also Sect. 11.5).

11.4 Dating Methods and Age Interference

The sedimentary units of flood events can be dated individually or in sequence by interpolation of known ages obtained elsewhere in the same sedimentary sequence. Usually, the direct dating of specific flood beds is challenging. Optically stimulated luminescence (OSL) dating requires sample volumes that often exceed the volume that can be retrieved from single flood

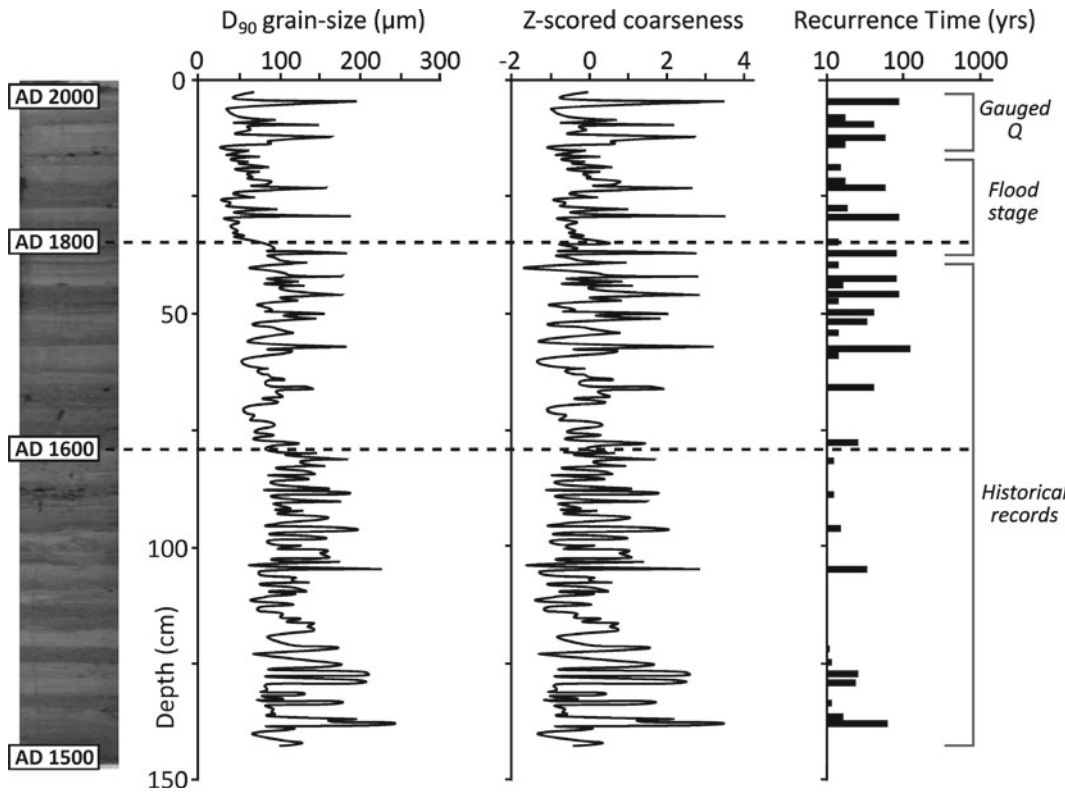

Fig. 11.6 Conceptual example of core data normalization with the conversion of grain-size data into relative coarseness by Z-scoring data per section (indicated with dashed lines) and calculation of statistical recurrence times based on age-depth information. An indicative time span of alternative flood data series and records, suitable for magnitude comparison and verification, is indicated on the far right

units with standard coring techniques. In addition, flood beds must contain either grains of quartz or feldspar that fall within the fine to medium sand grain-size range that is most suitable for dating (90–250 µm). Further complications in age determination from OSL samples can arise when samples have not been fully bleached (their age reset to zero at the time of deposition) or when they have been permanently waterlogged (Aitken 1985; Duller 2004; Cordier 2010). Organic macrofossils can be rare in clastic deposits, and those that are present carry the risk to have been eroded from older deposits, especially when found in deposits relating to high-magnitude events. Hence, radiocarbon dating of flood units often relies on interpolation of dates obtained from relatively organic bracketing levels (e.g., Minderhoud et al. 2016). For paleoflood sequences, cross-correlation with alternative, well-dated flood chronologies from historical records or gauging stations, has proven a reliable approach for establishing dates (Toonen et al. 2015; Fuller et al. 2018). This requires a matching of relative magnitudes (e.g., damage extent with flood unit coarseness) that is only reliable when deployed on few extreme events that are distinguishable in all records. Matching candidates for events of lesser magnitude are generally more numerous and will increase the risk of erroneous age assignment. Other proxy records, including existing paleoflood records in the same catchment, with a well-developed chronology can also be used for comparison and correlation. Munoz et al. (2018), for example, demonstrated that years of water stress as indicated by dendrochronological data derived

from trees in the floodplains of the Mississippi could be used to precisely date sedimentary flood units found in the same region.

In addition to spot ages at irregularly distributed depths (Fig. 11.6) using traditional dating techniques and/or cross-correlation, more-diffuse dating information can be obtained from the sampled material that can further constrain the chronology of the sequence. Fossil pollen can be analyzed to identify changes in vegetation of the region and may reveal the introduction of disappearance of certain species (e.g., introduction of agriculture or certain crops, extirpation of a native taxon) of which the dating is known historically or has been established at other sites nearby. Major changes in land use, as for example observed in New Zealand after European colonization (Fuller et al. 2018), are therefore useful to constrain or inform age-depth models. The same applies to the presence and concentration of (e.g., contaminant metal) pollutants, which may relate to the onset of industrialization in the catchment or documented waste spill events (Macklin et al. 2006).

To infer the date of each flood unit, advanced age-depth modeling tools can be deployed. Openly available tools, such as Bacon or Oxcal (Bronk Ramsey 2009; Blaauw and Christen 2011), use linear interpolated age-depth models in their simplest mode with breaks at depths with independent dating control. In more advanced modes, they allow to use the Bayesian theorem to combine multiple dates in sequence to reduce uncertainty and to identify outliers. Most standard modeling tools have options to define boundaries to mirror abrupt sedimentological changes or a hiatus. Continuous sedimentary information (from grain-size analysis or other proxies; Sect. 11.3) can also be used to infer variations in accumulation rates between known spot ages and make the depth-interpolations non-linear. Minderhoud et al. (2016) demonstrated that inclusion of such information may produce significant offsets in age-depth relations in poorly constrained intervals.

Advancing age-depth models for alluvial paleoflood records is particularly important when stacked records are to be compiled from multiple research locations. It is also of importance for hydroclimatic analysis, because the quantitative assessment of return frequencies and analysis of cyclic variability (through wavelet analysis) relies heavily on dating accuracy. For individual sites, the simplest way to estimate a recurrence time of a bed of given Z-scored coarseness is to divide the number of similar magnitude events in the record through the total record span. However, such inverted frequency–magnitude estimation should be regarded as yielding minimum recurrence times, especially for the few largest events-of-records, as the accuracy of the estimate is highly dependent on the total record length. Therefore, recurrence times of those rarest events are most reliably derived from within series obtained at distal sites, which preserved long time span records (Fig. 11.2).

11.5 Record Compilation

Absolute paleoflood discharges have been estimated, at reasonable accuracy, at places where the paleo-stage of events could be established and used in paleo-hydrologic calculations (Benito et al. 2004; Herget and Meurs 2010; Toonen et al. 2013). For the most recent period, it is also possible to convert sedimentary information from alluvial valley settings into absolute discharge estimates. Where gauged series from nearby gauging stations overlap with sedimentary flood data, the coarseness of flood deposits can be compared to peak discharge information and used in a regression analysis to establish the statistical relationship between deposit coarseness and peak discharge. This regression can then be used to estimate the peak discharges associated with older pre-instrumental flood units in the deeper parts of the core (cf. Toonen et al. 2015). This assumes that limited changes in environmental setting occurred between the

gauged reference period and the preceding centuries on which the established correlation is deployed. As this is rarely the case for alluvial environments with human occupation (Macklin and Lewin 2018), the results of this approach become increasingly uncertain when progressing further back in time.

An alternative approach for estimating flood magnitudes is to calculate their associated recurrence time. With sufficient dating control on the sedimentary sequence, the amount of time that is present in the entire sedimentary sequence, or in subsections, can be estimated. It is then possible to establish the period of recurrence for each relative flood unit coarseness by dividing the elapsed period of time by the number of events exceeding a certain relative magnitude (Z-score) over the same interval (Fig. 11.4). This is a site-independent measure, which allows a direct comparison between different research locations, whereas the coarseness of flood deposits is site specific and controlled by local factors (Fig. 11.2). A recurrence time is not simply translatable into a modern discharge, as it describes a probability at the time of occurrence and is sensitive to hydroclimatic variability and landscape change (Munoz et al. 2018; Best 2019). Nonetheless, such records have considerable use in flood hazard assessments and the study of hydroclimatic change (Sect. 11.6).

For the compilation of a multi-century to millennia-long paleoflood record from an alluvial setting, it is often necessary to combine data from multiple sites. Sites should be selected along the same stretch of river to ensure that the compiled records represent the same flood regime (i.e., not receiving pulses of discharge from additional tributaries). A combination of proximal and distal sampling sites from the same reach (Fig. 11.2) can be used to generate a composite record that includes both high- and low-resolution records to examine multiple scales of hydroclimate variability (Toonen et al. 2017). Record compilation from multiple research locations limits the risk of having gaps in paleoflood registration (e.g., due to erosion on non-deposition) and including anomalous conditions (e.g., caused by ice or log jamming, levee breaching, and crevasse splay formation) that can affect the local coarseness of a flood deposit. Information from multiple locations also offers a way to reproduce and cross-verify individual-site flood magnitude reconstructions.

11.6 Application to Flood Hazard Assessment

Paleoflood records developed for an alluvial river reach can be used to examine the sensitivity of flooding to a range of natural and anthropogenic factors and reduce the uncertainty of flood hazard assessments. Alluvial river systems are highly sensitive to changing climatic conditions and land use and land cover change (Knox 1993; Blöschl et al. 2007; Macklin and Lewin 2008; Hall et al. 2014; Best 2019). Yet, identifying and quantifying the specific effects of each factor separately with the use of only short instrumental records can be challenging because observed variability can arise through the complex interaction of multiple factors. By extending the length of a hydrologic record, paleoflood series can be used to examine the response of flood frequency and magnitude to changes that occurred prior to instrumental measurements (e.g., land clearance) or to evaluate the influence of natural modes of climate variability; e.g., the El Niño-Southern Oscillation (Harden et al. 2010; Richardson et al. 2013) and the North Atlantic Oscillation (Wirth et al. 2013; Schulte et al. 2015; Foulds and Macklin 2016).

Identifying connections between shifts in flood regime and environmental change is an exercise in hypothesis testing that is ideally accomplished using appropriate statistical tools. One common observation in paleoflood series is strong variability in flood occurrence over time, with phasing between ‘active’ and ‘inactive’ flood intervals (Merz et al. 2016) that is often attributed to major modes of climate variability (Czymzik et al. 2013; Foulds et al. 2014; Toonen et al. 2017; Fig. 11.7). Determining the causes of such phasing is of interest for flood hazard assessment, as it may represent a source of variability that is not well represented in the

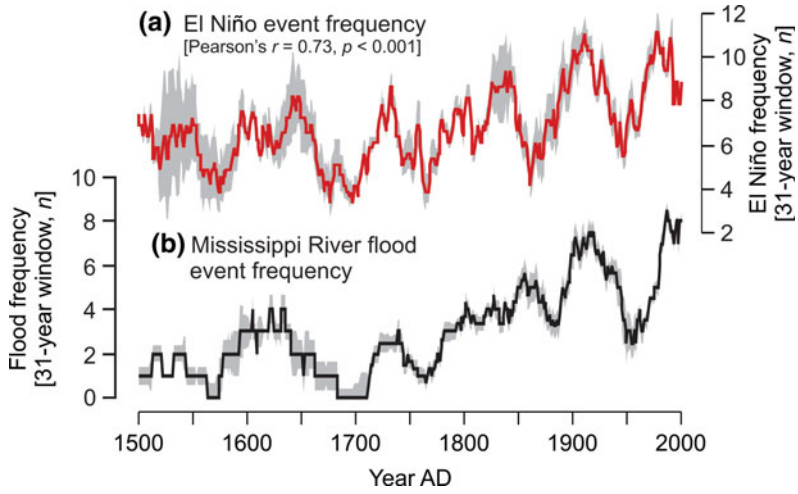

Fig. 11.7 Relationship between **a** the frequency of El Niño events (derived from historical and paleoclimate records) and **b** Mississippi River flood event frequency (derived from alluvial paleoflood records), modified from Munoz et al. (2018). Phasing between active and inactive flood periods (i.e., periods of relatively high and low flood event frequency) corresponds to variations in the El Niño-Southern Oscillation, which modulates the delivery of precipitation to the Mississippi River basin (Munoz and Dee 2017)

instrumental record—particularly if it occurs over multi-decadal or longer timescales (Toonen et al. 2016). Measures of covariance between a paleoflood event series and a climate index or variable are a common means to evaluate the potential role of climate variability on flood activity (Czymzik et al. 2016; Toonen et al. 2016; Munoz and Dee 2017), but significance tests must be corrected for serial autocorrelation (Hu et al. 2017). Additional analysis of instrumental and/or modeled climate data focusing on historic trends or individual events is useful for establishing a mechanistic connection between flood activity and a climate index (Mudelsee et al. 2004; Smith and Baeck 2015). Together, these analyses of paleoflood series can identify the causes of phasing in flood activity and establish sensitivity of an alluvial river reach to climate variability. Current flood hazard assessments generally assume a stationary flood regime despite significant evidence for non-stationary conditions (Milly et al. 2008), though recently developed statistical methods allow flood hazard assessments to include climatically driven non-stationarities (Condon et al. 2015; Machado et al. 2015). Incorporation of paleoflood information into frequency analysis can also constrain the statistical recurrence times of extreme events, which are often poorly represented in short data series (St. George and Mudelsee 2018)—despite their critical importance to flood hazard assessment.

Alluvial rivers also exhibit sensitivity to human modifications to the channel and basin, including land cover change (e.g., agricultural clearance) and river engineering (e.g., dams, artificial levees), that can alter sediment loads and/or flood activity. In paleoflood records, these modifications can exhibit themselves as changes in flood frequency and/or magnitude (Knox 2006; Vorogushyn and Merz 2013; Munoz et al. 2018). The timing and significance of these (stepwise) changes can be identified via change-point analysis or similar tests of non-stationarity in a time series of extreme values. The attribution of changes to a specific action is often based on the temporal correspondence between an observed shift in flood activity and human activity, although it must be noted that rivers can exhibit lagged responses to environmental change. In one example of an abrupt shift in flood regime, Fuller et al. (2018) showed that flood magnitudes on the Manawatu River of New Zealand increased during the

mid-nineteenth century, contemporaneous with large-scale land clearance. The use of statistical or hydrologic models offers another means to perform attribution studies, where flood activity or changes in flood regimes are predicted under different modeling scenarios (e.g., no land cover change) and compared to observed changes (e.g., Beighley and Moglen 2003). Following this approach, Munoz et al. (2018) showed that for the Lower Mississippi River, increases in flood magnitudes during the nineteenth and twentieth centuries were partly triggered by human activities as natural climate variability could not explain the observed changes.

Alluvial paleoflood records with quantitative flood magnitude reconstructions can be integrated into flood frequency analyses following the procedures initially developed in headwater environments (Stedinger and Cohn 1986; Frances et al. 1994). In practice, paleoflood magnitudes in a flood frequency analysis are treated as non-systematic measurements under the assumption that all events above a given threshold are registered. The inclusion of paleoflood data in frequency analysis can improve confidence in estimated magnitudes of low-frequency events—even considering the uncertainty of paleoflood estimates as independent data in the domain of extreme events is scarce (Hosking and Wallis 1986; Klemeš 2000; Kidson and Richards 2005). Several recent studies demonstrated that design flood estimates could change significantly when incorporating historical and paleoflood information (Toonen et al. 2016; Evin et al. 2019). Hence, the ability to develop quantitative and event-scale records of past extreme alluvial floods has opened the door to the integration of paleoflood data into flood hazard assessments of low-lying regions.

11.7 Outlook and Conclusions

Alluvial paleoflood hydrology is a relatively young field and is still developing, and no single standardized methodology exists. Given the range of geographic settings targeted and variable aims of paleoflood studies, it is unclear whether a standardized approach is a realistic or desirable outcome. It is clear, however, that our current understanding of the geomorphic dynamics that control depositional processes at paleoflood sites often rely on relatively underdeveloped post hoc analysis. Similarly, our understanding of how the composition and volume of a river's sediment load can change and how these shifts can imprint on a paleoflood record is limited. Addressing these and related challenges will be key to reduce the uncertainties in paleoflood magnitude reconstructions, which will further facilitate the use of alluvial paleoflood records in flood hazard and risk assessments. Rigorous attribution of stepwise and transient changes in flood regime to specific factors, including climate variability and human activity, remains challenging, but the integration of hydrologic, hydraulic, and Earth system models in the interpretation of sedimentary flood records offers a promising way forward. The continued development and improvement of alluvial paleoflood records are of critical importance for flood hazard and risk assessments, as this approach can significantly reduce the large uncertainties present in likelihood estimates of extreme and extraordinary floods. Riverine floods are a persistent and widespread hazard, particularly in low-lying regions, and alluvial paleoflood hydrology provides a relatively inexpensive and straightforward approach to improve the resilience and preparedness of communities and critical infrastructure to catastrophic floods.

Acknowledgements We thank the INQUA (EX-AQUA) and PAGES floods working groups for stimulating research and discussion on the subject of paleoflood hydrology. Jürgen Herget and Alessandro Fontana are cordially thanked for the invitation to write this chapter and for editing this volume.

References

Aitken MJ (1985) Thermoluminescence dating. Academic Press, London

Asselman NEM (1999) Grain-size trends used to assess the effective discharge for floodplain sedimentation, River Waal, the Netherlands. J Sediment Res 69 (1):51–61. https://doi.org/10.2110/jsr.69.51

Baker VR (2008) Paleoflood hydrology: origin, progress, prospects. Geomorphology 101(1):1–13. https://doi.org/10.1016/j.geomorph.2008.05.016

Beighley RE, Moglen GE (2003) Adjusting measured peak discharges from an urbanizing watershed to reflect a stationary land use signal. Water Resour Res 39(4). https://doi.org/10.1029/2002wr001846

Benito G, Lang M, Barriendos M et al (2004) Use of systematic, palaeoflood and historical data for the improvement of flood risk estimation: review of scientific methods. Nat Hazards 31(3):623–643. https://doi.org/10.1023/B:NHAZ.0000024895.48463.eb

Best J (2019) Anthropogenic stresses on the world's big rivers. Nat Geosci 12(1):7–21. https://doi.org/10.1038/s41561-018-0262-x

Blaauw M, Christen JA (2011) Flexible paleoclimate age-depth models using an autoregressive gamma process. Bayesian Anal 6(3):457–474. https://doi.org/10.1214/11-BA618

Blöschl G, Ardoin-Bardin S, Bonell M et al (2007) At what scales do climatic variability and land cover change impact on flooding and low flows? Hydrol Process 21(9):1241–1247. https://doi.org/10.1002/hyp.6669

Bronk Ramsey CB (2009) Bayesian analysis of radiocarbon dates. Radiocarbon 51(1):337–360. https://doi.org/10.1017/S0033822200033865

Bronstert A, Bárdossy A, Bismuth C et al (2007) Multi-scale modelling of land-use change and river training effects on floods in the Rhine basin. River Res Appl 23(10):1102–1125. https://doi.org/10.1002/rra.1036

Condon LE, Gangopadhyay S, Pruitt T (2015) Climate change and non-stationary flood risk for the upper Truckee River basin. Hydrol Earth Syst Sci 19(1):159–175. https://doi.org/10.5194/hess-19-159-2015

Cordier S (2010) Optically stimulated luminescence dating: procedures and applications to geomorphological research in France. Géomorphologie 16(1):21–40. https://doi.org/10.4000/geomorphologie.7785

Czymzik M, Brauer A, Dulski P et al (2013) Orbital and solar forcing of shifts in Mid- to Late Holocene flood intensity from varved sediments of pre-Alpine Lake Ammersee (southern Germany). Quat Sci Rev 61:96–110. https://doi.org/10.1016/j.quascirev.2012.11.010

Czymzik M, Muscheler R, Brauer A (2016) Solar modulation of flood frequency in central Europe during spring and summer on interannual to multi-centennial timescales. Clim Past 12:799–805. https://doi.org/10.5194/cp-12-799-2016

Duller GAT (2004) Luminescence dating of Quaternary sediments: recent advances. J Quat Sci 19(2):183–192. https://doi.org/10.1002/jqs.809

EM-DAT (2019) The International Disaster Database, Centre for Research on the Epidemiology of Disasters (CRED). www.emdat.be. Accessed 18 Apr 2019

Enzel Y, Ely LL, House PK et al (1993) Paleoflood evidence for a natural upper bound to flood magnitudes in the Colorado River basin. Water Resour Res 29(7):2287–2297. https://doi.org/10.1029/93WR00411

Evin G, Wilhelm B, Jenny JP (2019) Flood hazard assessment of the Rhone River revisited with reconstructed discharges from lake sediments. Glob Planet Change 172:114–123. https://doi.org/10.1016/j.glopacha.2018.09.010

Frances F, Salas JD, Boes DC (1994) Flood frequency analysis with systematic and historical or paleoflood data based on the two-parameter general extreme value models. Water Resour Res 30(6):1653–1664. https://doi.org/10.1029/94WR00154

Foulds SA, Griffiths HM, Macklin MG et al (2014) Geomorphological records of extreme floods and their relationship to decadal-scale climate change. Geomorphology 216:193–207. https://doi.org/10.1016/j.geomorph.2014.04.003

Foulds SA, Macklin MG (2016) A hydrogeomorphic assessment of twenty-first century floods in the UK. Earth Surf Process Landf 41(2):256–270. https://doi.org/10.1002/esp.3853

Fuller IC, Macklin MG, Toonen WHJ et al (2018) Storm-generated Holocene and historical floods in the Manawatu River, New Zealand. Geomorphology 310:102–124. https://doi.org/10.1016/j.geomorph.2018.03.010

Gregory KJ, Benito G (2003) Palaeohydrology: understanding global change. Wiley, Chichester

Hall J, Arheimer B, Borga M et al (2014) Understanding flood regime changes in Europe: a state-of-the-art assessment. Hydrol Earth Syst Sci 18(7):2735–2772. https://doi.org/10.5194/hess-18-2735-2014

Harden T, Macklin MG, Baker VR (2010) Holocene flood histories in south-western USA. Earth Surf Process Landf 35(6):707–716. https://doi.org/10.1002/esp.1983

Heiri O, Lotter AF, Lemcke G (2001) Loss on ignition as a method for estimating organic and carbonate content in sediments: reproducibility and comparability of results. J Palaeolimnol 25(1):101–110. https://doi.org/10.1023/A:1008119611481

Herget J, Meurs H (2010) Reconstructing peak discharge for historic flood levels in the city of Cologne, Germany. Glob Planet Change 70(1–4):108–116. https://doi.org/10.1016/j.glopacha.2009.11.011

Herget J (2019—this volume) Palaeostage indicators in rivers—an illustrated review. In: Herget J, Fontana A (eds) Palaeohydrology—traces, tracks and trails of extreme events. Springer, Heidelberg

Hosking JRM, Wallis JR (1986) Paleoflood hydrology and flood frequency analysis. Water Resour Res 22(4):543–550. https://doi.org/10.1029/WR022i004p00543

Hu J, Emile-Geay J, Partin J (2017) Correlation-based interpretations of paleoclimate data–where statistics meet past climates. Earth Planet Sci Let 459:362–371. https://doi.org/10.1016/j.epsl.2016.11.048

IPCC (2012) Managing the risks of extreme events and disasters to advance climate change adaptation. A special report of working groups I and II of the

Intergovernmental Panel on Climate Change. Cambridge University Press, Cambridge and New York
IPCC (2018) Global warming of 1.5 °C. An IPCC Special Report on the impacts of global warming of 1.5 °C above pre-industrial levels and related global greenhouse gas emission pathways, in the context of strengthening the global response to the threat of climate change, sustainable development, and efforts to eradicate poverty (in press)
Jones AF, Macklin MG, Lewin J (2010) Flood series data for the later Holocene: available approaches, potential and limitations from UK alluvial sediments. The Holocene 20(7):1123–1135. https://doi.org/10.1177/0959683610369501
Jones AF, Macklin MG, Brewer PA (2012) A geochemical record of flooding on the upper River Severn, UK, during the last 3750 years. Geomorphology 179:89–105. https://doi.org/10.1016/j.geomorph.2012.08.003
Jones AF, Turner JN, Daly JS et al (2018) Late Holocene sedimentary flood records in UK and Irish river catchments. In: Proceedings of the FLAG meeting, University of Liège, Liège, 3–4 Sept 2018
Kidson R, Richards KS (2005) Flood frequency analysis: assumptions and alternatives. Prog Phys Geogr 29 (3):392–410. https://doi.org/10.1191/0309133305pp454ra
Klemeš V (2000) Tall tales about tails of hydrological distributions. I. J Hydrol Eng 5(3):227–231. https://doi.org/10.1061/(ASCE)1084-0699(2000)5:3(227)
Knox JC (1993) Large increases in flood magnitude in response to modest changes in climate. Nature 361:430–432. https://doi.org/10.1038/361430a0DO
Knox JC (2006) Floodplain sedimentation in the Upper Mississippi Valley: natural versus human accelerated. Geomorphology 79:286–310. https://doi.org/10.1016/j.geomorph.2006.06.031
Knox JC (2007) The Mississippi river system. In: Gupta A (ed) Large rivers: geomorphology and management. Wiley, pp 145–182
Kochel RC, Baker VR (1982) Paleoflood hydrology. Science 215:353–361. https://doi.org/10.1126/science.215.4531.353
Konert M, Vandenbergh J (1997) Comparison of laser grain size analysis with pipette and sieve analysis: a solution for the under-estimation of the clay fraction. Sedimentology 44(3):523–535. https://doi.org/10.1046/j.1365-3091.1997.d01-38.x
Kundzewicz ZW, Radziejewski M, Piñskwar I (2006) Precipitation extremes in the changing climate of Europe. Clim Res 31:51–58. https://doi.org/10.3354/cr031051
Leigh DS (2018) Vertical accretion sand proxies of gaged floods along the upper Little Tennessee River, Blue Ridge Mountains, USA. Sediment Geol 364:342–350. https://doi.org/10.1016/j.sedgeo.2017.09.007
Lewin J, Macklin MG (2003) Preservation potential for Late Quaternary river alluvium. J Quat Sci 18(2):107–120. https://doi.org/10.1002/jqs.738
Lewin J, Ashworth PJ (2014) The negative relief of large river floodplains. Earth Sci Rev 129:1–23. https://doi.org/10.1016/j.earscirev.2013.10.014
Machado MJ, Botero BA, Lopez J et al (2015) Flood frequency analysis of historical data under stationary and non-stationary modelling. Hydrol Earth Syst Sci 19(6):2561–2576. https://doi.org/10.5194/hess-19-2561-2015
Macklin MG, Brewer PA, Hudson-Edwards KA et al (2006) A geomorphological approach to the management of rivers contaminated by metal mining. Geomorphology 79(3–4):423–447. https://doi.org/10.1016/j.gemorph.2006.06.024
Macklin MG, Lewin J (2008) Alluvial responses to the changing Earth system. Earth Surf Process Landf 33 (9):1374–1395. https://doi.org/10.1002/esp.1714
Macklin MG, Lewin J (2018) River stresses in anthropogenic times: large-scale global patterns and extended environmental timelines. Prog Phys Geog 43(1):3–23. https://doi.org/10.1177/0309133318803013
Merz B, Nguyen VD, Vorogushyn S (2016) Temporal clustering of floods in Germany: do flood-rich and flood-poor periods exist? J Hydrol 541(B):824–838. https://doi.org/10.1016/j.jhydrol.2016.07.041
Minderhoud PSJ, Cohen KM, Toonen WHJ et al (2016) Improving age-depth models of fluvio-lacustrine deposits using sedimentary proxies for accumulation rates. Quat Geochronol 33:35–45. https://doi.org/10.1016/j.quageo.2016.01.001
Milly PCD, Betancourt J, Falkenmark M et al (2008) Stationarity is dead: whither water management? Science 319(5863):573–574. https://doi.org/10.1126/science.1151915
Morehead MD, Syvitski JP, Hutton EWH et al (2003) Modeling the temporal variability in the flux of sediment from ungauged river basins. Glob Planet Change 39(1–2):95–110. https://doi.org/10.1016/S0921-8181(03)00019-5
Mudelsee M, Börngen M, Tetzlaff G et al (2004) Extreme floods in central Europe over the past 5000 years: role of cyclone pathway 'Zugstrasse Vb'. J Geophys Res: Atmos 109(D23). https://doi.org/10.1029/2004jd005034.d23101
Munoz S, Dee S (2017) El Nino increases the risk of lower Mississippi River flooding. Sci Rep 7:1772. https://doi.org/10.1038/s41598-017-01919-6DO
Munoz SE, Giosan L, Therell MD et al (2018) Climatic control of Mississippi River flood hazard amplified by river engineering. Nature 556:95–98. https://doi.org/10.1038/nature26145
Naylor LA, Spencer T, Lane SN et al (2017) Stormy geomorphology: geomorphic contributions in an age of climate extremes. Earth Surf Process Landf 42 (1):166–190. https://doi.org/10.1002/esp.4062
NOAA/NCEI (2018) U.S. Billion-Dollar weather and climate disasters. National Oceanic and Atmospheric Administration / National Centers for Environmental

Information. www.ncdc.noaa.gov/billions/overview. Accessed 30 Dec 2018

Oldfield F, Rummery TA, Thompson R et al (1979) Identification of suspended sediment sources by means of magnetic measurements: some preliminary results. Water Resour Res 15(2):211–218. https://doi.org/10.1029/WR015i002p00211

Peng F, Prins MA, Kasse C et al (2019) An improved method for paleoflood reconstruction and flooding phase identification, applied to the Meuse River in the Netherlands. Glob Planet Change 177:213–224. https://doi.org/10.1016/j.gloplacha.2019.04.006

Richardson JM, Fuller IC, Macklin MG et al (2013) Holocene river behaviour in New Zealand: response to regional centennial-scale climate forcing. Quat Sci Rev 69:8–27. https://doi.org/10.1016/j.quascirev.2013.02.021

Schulte L, Pena JC, Carvalho F et al (2015) A 2600-year history of floods in the Bernese Alps, Switzerland: frequencies, mechanisms and climate forcing. Hydrol Earth Syst Sci 19(7):3047–3072. https://doi.org/10.5194/hess-19-3047-2015

Smith JA, Baeck ML (2015) Prophetic vision, vivid imagination: the 1927 Mississippi River flood. Water Resour Res 51(12):9964–9994. https://doi.org/10.1002/2015WR017927

Stedinger JR, Cohn TA (1986) Flood frequency analysis with historical and paleoflood information. Water Resour Res 22(5):785–793. https://doi.org/10.1029/WR022i005p00785

St. George S, Mudelsee M (2018) The weight of the flood-of-record in flood frequency analysis. J Flood Risk Manag. https://doi.org/10.1111/jfr3.12512 (in press)

Toonen WHJ, Kleinhans MG, Cohen KM (2012) Sedimentary architecture of abandoned channel fills. Earth Surf Process Landf 37(4):459–472. https://doi.org/10.1002/esp.3189

Toonen WHJ (2013) A Holocene flood record of the Lower Rhine. Utrecht Studies in Earth Sciences 41

Toonen WHJ, de Molenaar MM, Bunnik FPM et al (2013) Middle Holocene palaeoflood extremes of the Lower Rhine. Hydrol Res 44(2):248–263. https://doi.org/10.2166/nh.2012.162

Toonen WHJ, Winkels TG, Cohen KM et al (2015) Lower Rhine historical flood magnitudes of the last 450 years reproduced from grain-size measurements of flood deposits using end member modelling. CATENA 130:69–81. https://doi.org/10.1016/j.catena.2014.12.004

Toonen WHJ, Middelkoop H, Konijnendijk TYM et al (2016) The influence of hydroclimatic variability of flood frequency in the Lower Rhine. Earth Surf Process Landf 41(9):1266–1275. https://doi.org/10.1002/esp.3953

Toonen WHJ, Foulds SA, Macklin MG et al (2017) Events, episodes, and phases: signal from noise in flood-sediment archives. Geology 45(4):331–334. https://doi.org/10.1130/G38540.1

Vorogushyn S, Merz B (2013) Flood trends along the Rhine: the role of river training. Hydrol Earth Syst Sci 17(10):3871–3884. https://doi.org/10.5194/hess-17-3871-2013

Wallemarq P, Below R, McLean D (2018) UNISDR and CRED report: Economic Losses, Poverty & Disasters (1998–2017). https://www.emdat.be/publications. Accessed 30 Dec 2018

Wilhelm B, Ballesteros Cánovas JA, Corella Aznar JP et al (2018) Recent advances in paleoflood hydrology: from new archives to data compilation and analysis. Water Secur 3:1–8. https://doi.org/10.1016/j.wasec.2018.07.001

Wilhelm B, Ballesteros Cánovas JA, Macdonald N et al (2019) Interpreting historical, botanical, and geological evidence to aid preparations for future floods. WIREs Water 6(1):e1318. https://doi.org/10.1002/wat2.1318

Wirth SB, Glur L, Gilli A et al (2013) Holocene flood frequency across the Central Alps: solar forcing and evidence for variations in North Atlantic atmospheric circulation. Quat Sci Rev 80:112–128. https://doi.org/10.1016/j.quascirev.2013.09.002

Index

J. Herget and A. Fontana (eds.), *Palaeohydrology*, Geography of the Physical Environment,
https://doi.org/10.1007/978-3-030-23315-0